ION EXCHANGER BASED ION GENERATION AND REMOVAL DEVICES. BEHAVIOR AND APPLICATIONS

by

YONGJING CHEN

Presented to the Faculty of the Graduate School of

The University of Texas at Arlington in Partial Fulfillment

of the Requirements

for the Degree of

DOCTOR OF PHILOSOPHY

THE UNIVERSITY OF TEXAS AT ARLINGTON

DECEMBER 2011

ACKNOWLEDGEMENTS

I would like to express my deepest appreciation to my mentor, Professor Purnendu K. Dasgupta, for his guidance and support during the course of my doctoral program. His tremendous knowledge and authority over the subject have always inspired me to achieve higher goals, and many of my achievements would not have been possible without his support. I would also like to thank my committee members, Dr. Krishnan Rajeshwar and Dr. Brad S. Pierce for their valuable comments with my dissertation manuscript.

I would like to express my very deep appreciation to Dr. Maather Sawalha for her encouragement and support during my most difficult times. I would like to thank Dr. Jason Dyke, Dr. Shin-Ichi Ohira and Dr. Abul K. Azad for their technical advice and assistance with my research. I also would like to thank the staff of Department of Chemistry and Biochemistry for their assistance during the course of my study.

I would like to acknowledge Dionex Corporation (now Thermofisher Scientific) for their support with equipment and consumables and the American Chemical Society Division of Analytical Chemistry Graduate Fellowship program for a summer fellowship. The National Science Foundation Chemistry Division supported my research. I thank the Department of Chemistry and Biochemistry for providing the facilities. I am very grateful to the University of Texas at Arlington for my teaching assistantship support as well as Dean's Excellence Scholarship.

I am thankful to my parents and my grandfather for their love and support over the years.

November 1, 2011

ABSTRACT

ION EXCHANGER BASED ION GENERATION AND REMOVAL DEVICES.

BEHAVIOR AND APPLICATIONS

Yongjing Chen, PhD

The University of Texas at Arlington, 2011

Supervising Professor: Purnendu K. Dasgupta

Ion exchangers have many important applications. In Ion chromatography (IC), ion exchangers are used as stationary phase and used in some of the key components. The innovations that make the modern IC the most popular techniques for ion analysis are closely related to ion exchangers.

Using the ion exchangers and inspired by some of the innovations in electrolytic devices of IC, the research in this dissertation mainly consists of four parts:

A charge detector (ChD) is a flow-through device where a cation exchange membrane (CEM) and anion exchange membrane (AEM) separating three channels. One electrode is disposed in each of the outer channels. A constant electric field is applied to the electrodes with the one on CEM side is positive relative to the one on AEM side, and the current is monitored. Any injected ions in the water carrier passing through the device produce a current signal that is directly related to the charge the ions carry, regardless of their electrochemical properties. The ChD provides a new technique for measurement of ionic solutes in solution phase.

Essentially ChD is a “deionizer”, which removes ions from the central channel into the outer channels. Based on the same principle, a capillary-scale salt remover (SR) was developed to desalt the proteins prior to their entering into ESI-MS. The SR effectively removes

salt ions but not the proteins, which have poorer electrophoretic mobility relative to the salts, guaranteeing the good quality of ESI-MS spectra of the salt-free proteins. Three common proteins were tested, and > 99.8% salt removal in 154 mM NaCl continuous flow at 1 μL/min with > 80% of concurrently present 20 μM proteins transmission was achieved.

The Self-Regenerating Suppressors (SRS) in IC were first time demonstrated to be used as electrodialytical buffer generator (EBG). Buffers of constant concentration but variable pH can be generated by feeding the salts of weak acids or salts of weak bases into the central channels of Anion Self-Regenerating Suppressor (ASRS) and Cation Self-Regenerating Suppressor (CSRS). Linear pH gradients with excellent linearity and reproducibility are produced by feeding the buffer reagent mixture and varying the current applied to the device.

A three-electrode EBG was developed in a configuration similar to ChD, except that a electrode is introduced into the central channel to constitute the ground while the electrode in CEM side outer channel is positive and the electrode in AEM side outer channel is negative. With chosen feed in the outer channels, the device is operated in “additive mode”, where buffers of variable composition can be generated in the central channel with both controllable concentration and pH. When the polarity is reversed, the device can be operated in a “subtractive mode”, where buffer components are removed from the central channel. The device can be operated in a mixed mode which incorporates both additive and subtractive mode, providing a better versatility of generating buffer pH gradients.

TABLE OF CONTENTS

LIST OF ILLUSTRATIONS

Figure Page

CHAPTER 1

INTRODUCTION

1.1 Introduction to Ion Exchange

1.1.1 Ion Exchanger

An ion exchanger comprises of three important elements: (1) an insoluble matrix, which may be organic or inorganic; (2) fixed ionic sites, these are either attached to or are an integral part of the matrix; (3) counter-ions, which are equivalent amount of ions of charge opposite to that of the fixed sites, to maintain electroneutrality. In aqueous solution, the counter-ions are mobile throughout the ion exchanger and most importantly have the ability to be exchanged for ions of like charge from the external solution.

A variety of materials have been used as matrices on which to anchor the ionic sties of an ion exchanger. Ion exchangers made of organic polymers such as poly(styrene-divinylbenzene) (PS-DVB) or polyacrylate have been used as stationary phases, and used in other accessory components associated with modern ion chromatography (IC). These materials are characterized by their excellent chemical and physical stabilities. The PSDVB-based ion exchangers are made by copolymerizing styrene and/or ethylvinylbenzene (EVB) with varying amounts of divinylbenzene (DVB) for crosslinking, followed by chemically introducing suitable functional groups into the polymer matrix.

Ion exchangers are classified as cation exchangers when the fixed ion carries a negative charge, and as anion exchangers when the fixed ion carries a positive charge. Cation exchangers are classified into strong acid and weak acid types. The former retain the negative charge on the fixed ion over a wide pH range, whereas the latter type are ionized only over a much narrower pH range. Strong acid exchangers are functionalized with sulfonic acid groups (Figure 1.1). Weak acid exchangers are functionalized with carboxylic acid or a mixture of

carboxylic and phosphonic acid groups. Similarly, anion exchangers are classified as strong base and weak base exchangers. Quaternary amine functional groups form strong base exchangers, while less substituted amines form weak base exchangers (Figure 1.2).

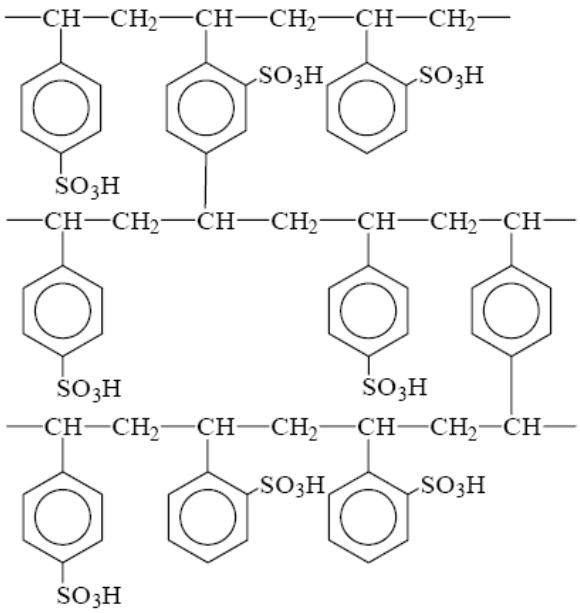

Figure 1.1 A strongly acidic sulfonated PSDVB based cation exchange resin.

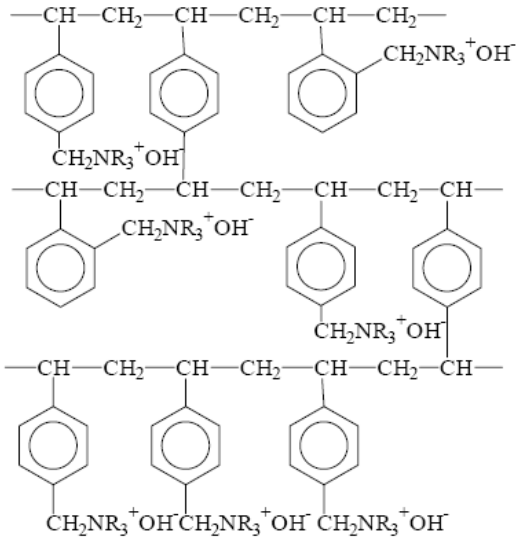

Figure 1.2 A strongly basic quaternary ammonium anion exchange resin.

1.1.1.1 Ion Exchange Resins

An ion exchange resin is an insoluble matrix normally in the form of small (<1 mm diameter) beads, fabricated from an organic polymer substrate. Most typical ion exchange resins are based on crosslinked polystyrenes. The functional groups are introduced after polymerization. Alternatively, substituted monomers can be used.

1.1.1.2 Ion Exchange Membranes

Besides spherical forms, ion exchangers can also be produced as membranes that have a composition similar to ion exchange resin beads. Ion exchange membranes are widely used for electrodialysis.[1,2]

1.1.2 Principles of Ion Exchange

When placed in aqueous solution, the counter-ions of an ion exchanger may move through the matrix either by diffusion (because of a concentration gradient) or under the influence of an electric field. In the ion-exchange process, the mobile counter-ions are replaced by ions of the same charge from the external solution.

The ion exchange process can be illustrated by taking an anion exchanger, for which the counter-ion is A^-, as an example. The exchanger can therefore be represented as M^+A^-, where M^+ denotes the matrix material containing the fixed ionic sites (positive). When a solution containing a different anion B^-, is brought into contact with the anion exchanger, an equilibrium is established between the two mobile ions A^- and B^- as follows:

$$M^+A^- + B^- \leftrightarrow M^+B^- + A^- \qquad (1.1)$$

The ion exchange is stoichiometric since the electroneutrality of the solution and the resin must be maintained during the ion exchange process; therefore a single monovalent anion B^- displaces a single monovalent counter-anion A^-. Eqn. (1.1) can be generalized for y moles of B^{x-} exchanging with x moles (i.e. the stoichiometric amount) of A^{y-} to give:

$$xA_s^{y-} + yB_m^{x-} \leftrightarrow yB_s^{x-} + xA_m^{y-} \qquad (1.2)$$

where the subscript *s* denotes the stationary phase and *m* denotes the mobile phase. The solution phase contains cations of the same charge as the fixed ion, but the cations play no part in the anion exchange process, and are therefore not shown.

The equilibrium constant for the reaction shown in eqn. (1.2) is called the selectivity coefficient, and is given by:

$$K_A^B = \frac{[B_s^{x-}]^y[A_m^{y-}]^x}{[A_s^{y-}]^x[B_m^{x-}]^y} \qquad (1.3)$$

where the parentheses indicate the activities of the specific species. Since the ion activity in the resin phase cannot be determined, K_A^B is not a thermodynamic constant but a coefficient useful for practical requirements.

Selectivity coefficients provide a means for determining the relative affinities of different ion exchangers for different ions. Some general rules can be used to predict the affinity order. They are based on a number of properties of the solute and the ion exchanger and include:[3]

(1) The charge on the solute ion

(2) The solvated size of the solute ion

(3) The degree of cross-linking of the ion exchange resin

(4) The polarizability of the solute ion

(5) The ion exchange capacity of the ion exchanger

(6) The functional group on the ion exchanger

(7) The degree to which the solute ion interacts with the ion exchange matrix

An increase in the charge on the solute ion increases its affinity for an ion exchanger through increased coulombic interactions. The size of the solvated solute ion also exerts a significant effect, with ions of smaller solvated size showing greater binding affinity than larger ions. The affinity is also related to swelling of the resin, since a smaller ion is more easily accommodated in the resin pores. Thus, the higher the degree of cross-linking, the greater is the preference of the resin for smaller solute ions. Ion exchange selectivity coefficients increase with the degree of polarizability of the solute ion. Sulfonic acid fixed sites show greater affinity

for the more polarizable Ag^+ and Tl^+ ions than the harder alkali metal ions. Similarly, the softer I^- is more strongly retained on an anion-exchanger than Br^- or Cl^- even though the charge density is smaller on I^-.

In practice, the relative affinities may vary with the type of ion exchanger and the conditions under which it is used. In some cases, simple ion exchange may not be the sole operative sorption mechanism. For example, partitioning of solute ions between the eluent and the pores of the stationary phase may occur, or the solute ion could be adsorbed onto the ion exchange matrix itself, not associated with an exchange site.

1.2 Ion Exchangers and Ion Chromatography

Ion chromatography (IC) was first introduced in 1975 by Small et al.[4] and since that time, the use of the technique has grown exponentially. IC offers simple, reliable and inexpensive means for the simultaneous separation and determination of inorganic and many organic ions in complex mixtures. The growth of IC has been accompanied by a blurring of the original definition of the technique, some of which is closely related to ion exchangers.

1.2.1 Ion Exchangers used as Stationary Phase in Current IC Practice

The separation of cations and anions on ion exchange resins goes back many years before IC became widely accepted as an analytical tool.[5] Ion exchange resin phases can be based on silica particles (and original high efficiency ion exchange columns were indeed based on derivatized silica) but today they are overwhelmingly composed of organic polymers. Organic polymer materials generally show a much higher stability toward extreme pH conditions while most silica based columns can only be used within a pH range between 2 and 8. The stationary-phase substrate has evolved from non-porous particles in the early columns to porous and later substrates in various other forms. The stationary phase architecture has also evolved into a great variety of designs that cater to different applications. Early IC stationary phases were not organic solvent compatible due to their relatively low crosslinking; most present-generation columns are fully compatible with common organic solvents used in HPLC.[6] Another important

development has been variations in selectivity, brought about by introducing different functionalities to the ion exchange site. For example, early IC columns were based on PS-DVB with strong base functionalities such as $-N(CH_3)_3^+$ that were strongly hydrophobic. Addition of alkanol groups, such as $-CH_2OH$, to the ion exchange site increases the hydrophilicity of the stationary phase, making OH^- a much more effective eluent. Detailed discussion of the development of ion exchange stationary phases can be found in several review papers.[7-9]

1.2.2 Ion Exchangers used in Suppressors in IC

The concept of suppression was first described by Small et al. in 1975.[4] It is a predetection/postcolumn chemical manipulation step that eliminates the background eluent conductivity contribution while enhancing the conductance of the analyte ion (for all but very weakly acidic analytes). As a result detection limits are greatly improved. The first suppressors were packed-bed columns; the suppression reactions for anion analysis can be summarized by the following equations:

$$R\text{-}SO_3H + NaOH\ (eluent) \rightarrow R\text{-}SO_3Na + H_2O\ (suppressed\ eluent) \qquad (1.4)$$

$$R\text{-}SO_3H + NaX\ (analyte) \rightarrow R\text{-}SO_3Na + HX\ (suppressed\ analyte) \qquad (1.5)$$

where R represents an ion exchange resin surface.

A suppressor is placed between the ion exchange separation column and the detector. Take suppressed anion chromatography for instance: after separation, the column effluent passes through a suppressor where Na^+ or K^+ from the eluent is exchanged with H^+, neutralizing the eluent hydroxide, producing lower conductivity background with lower noise levels. The suppression also changes the analyte from the Na^+ or K^+ salt form to the corresponding acid form. For strong acid analyte anions, the conversions result in a significant increase in response since the proton is by far more conductive than the eluent cation (typically sodium or potassium). For weakly dissociated analytes, the relative increase in response is dependent on pK_a and the concentration of the analyte.

Early packed-column suppressors required frequent offline regeneration,[4] caused considerable peak dispersion and broadening,[4] and variation in retention times of weak acid analytes.[10]

Since then, suppressors have undergone many refinements. Hollow fiber suppressor were introduced in 1981.[11] Basically, the eluent flowed through a tubular ion exchange membrane while the regenerant flowed on the outside continuously. Though these devices did not require offline regeneration, they caused substantial band spreading. In 1982, Stevens et al.[12] packed the lumen of the suppressor hollow fiber with inert beads. This reduced band dispersion and improved resolution. However, its performance deteriorated with use, especially in terms of band broadening and dead volume. The beads were reportedly packed by suction, without pressure. Under use, pressure expanded the elastomeric membrane allowing the mobile beads to pack down densely and less uniformly, leaving large voids in the tube. Additionally, the mobility of the beads contributed to pressure-induced rupture of the membrane at lower pressures, presumably by creating local pressure points. In 1984 Dasgupta[13,14] introduced the annular helical suppressor, where a nylon monofilament was inserted in to a Nafion® perfluorosulfonate cation exchange membrane (CEM) tube and the whole was then coiled to a small diameter coil and thermoset. This functioned as an efficient suppressor of low dispersion and dead volume for anion chromatography. With the helical configuration,[13] efficiency of mass transfer to the walls of a tube was greatly enhanced. In 1985, a dual membrane annular helical configuration was described by Dasgupta et al.[15] as a high capacity low dispersion suppressor for ion chromatography. The device contained one filament-filled membrane tube inserted inside another closely fitting membrane tube of the same type. The dual membrane assembly was coiled as a small diameter helix, the shape being retained by the filament. The column effluent flowed in the annular space between the two membranes; regenerant flowed through the two separate channels, inside the inner membrane and through a jacket which surrounded the entire device. Compared to simple filament-filled membrane

helices, these devices exhibited a substantially larger available membrane surface area per unit dispersion of an injected band.

Planar membrane suppressors were introduced in 1985 by Stillian.[16] By replacing the ion exchange tubing with flat sheets of membrane, the surface area available for exchange between eluent and regenerant ions was thereby increased greatly for a given device length, and so was the ion exchange capacity. The continuously regenerated flat membrane suppressors, referred commercially as the MicroMembrane™ Suppressors (MMS), were introduced commercially in 1991.[17] Although these suppressors had minimal dead volume (< 50 µL) and thus results in minimal loss of peak efficiency, as in previous suppressors the limitations include the need to supply chemical regenerant, added costs of dispensing and disposing of the chemical regenerant, and leakage of the chemical regenerant across the ion exchange membrane into the eluent, which raises the background and affects the sensitivity of some analytes.

In 1989, Dasgupta et al.[18] developed a dual membrane helical electrodialytic eluent suppressor. A platinum-wire-filled tube made of Nafion® perfluorosulfonate membrane, inserted in another perfluorosulfonate membrane tube, was coiled into a helix. The helical assembly was inserted within an outer jacket packed with granular conductive carbon. An alkaline eluent, e.g., NaOH or Na_2CO_3, flowed in the annular channel between the two membranes and pure water flows through the inner membrane and the outer jacket, countercurrent to the eluent flow. A DC voltage (typically 3-8 V) was applied across the carbon bed and the platinum wire. The column effluent containing the eluent NaOH and analytes flowed in the middle channel between the membranes. At the anode side, water flowed between the anode and the CEM generating hydrogen ion and oxygen gas,

$$2H_2O - 4e^- \rightarrow 4H^+ + 2O_2(g) \qquad (1.6)$$

the H^+ ions are transported through the CEM into the middle channel and replaced the eluent cations Na^+, thus neutralizing OH^- and changing the analytes from the salt to the acid form,

which were then measured by conductivity in a neutral medium. The Na^+ ions permeated through the other CEM into the cathode channel, where the water flowing between the cathode and the membrane generates hydrogen gas and hydroxide ion.

$$2H_2O + 2e^- \rightarrow 2\ OH^- + H_2(g) \qquad (1.7)$$

Based on the same principle, in 1992 Dionex Corp introduced the Self Regenerating Suppressor (SRS).[19] Figure 1.3 shows a schematic of the mechanism of an Anion Self Regenerating Suppressor (ASRS) suppressor. Basically the ASRS is composed of a cathode and an anode separated by two CEMs, thus, forming three compartments for liquid flow. The column effluent is fed into the middle channel between the membranes, while water from an external reservoir or the suppressed eluent itself is fed into the regenerant channels in the countercurrent direction to carry the formed base along with the electrolytic gases out of the

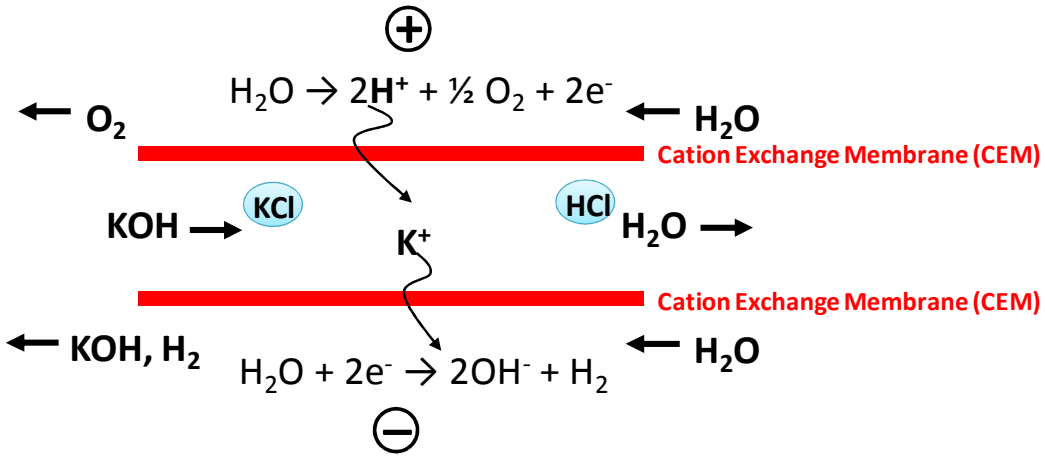

Figure 1.3 An Anion Self Regenerating Suppressor (ASRS) schematic. Eluent KOH is converted to H_2O and analyte KCl is converted to HCl.

ASRS suppressor to waste. The SRS suppressors address the limitations of the chemical suppressor and suppressors from prior years, and operate on the principles of the electrolytic water-splitting reactions outlined in Eqns (1.6) and (1.7). An ASRS consists of two CEMs in hydronium form (Figure 1.3), a Cation Self Regenerating Suppressor (CSRS) consists of two

AEMs in hydroxide form. The “recycle mode”, where the suppressed eluent is fed back into the regenerant channels as the water source for water splitting, is very commonly used as it considerably simplifies the operation. However, the sensitivity here is compromised due to the fact that the quantitatitve removal of eluent counter-ions and electrolysis products may become limited by the flow rate dictated by the analytical separation. The use of “gas assisted recycle mode”[20] allow rapid removal of the eluent counter-ions and electrolysis products assisted by inert gas, offering sensitivity even better than using the external water mode. In an ASRS, the transport of hydronium ions to the cathode determines the current efficiency. The ion exchange capacity of the eluent screen plays an important role in determining the current efficiency of a given electrolytic suppressor device. The lower the ion exchange capacity of the eluent screen, the greater the current efficiency.[21]

In 1998, Small et al.[22] described “ion reflux”, this can withstand high pressures like packed columns but can be operated continuously like membrane suppressors. An “ion reflux” suppressor device comprised a small bed of high capacity, cation exchange resin confined between two electrodes in a rigid polymer body. Water passed through the electrically polarized resin bead and electrolysis reactions were used to generate the eluent and also provide the means of suppression.

After SRS suppressors, Dionex Corporation introduced a new type of continuous electrolytically regenerated packed-bed suppressor,[23] which was made commercially available as the Atlas electrolytic suppressor (AES®) in 2001. The suppression bed consists of six cation exchange monolith disks and five flow distributor disks. The monolith disks and flow distributor disks are alternately sandwiched between the CEMs that separate the eluent chamber from the anode and cathode chambers of the suppressor. The placement of these disks is such that a serpentine flow pathway is created to increase the effective residence time of the eluent in the suppression bed. As a consequence, the current efficiency and the dynamic suppression capacity of the suppressor are increased.

1.2.3 Ion Exchangers used in Eluent Generators in IC

In the pioneering work on IC with suppressed conductometric detection, the most successful eluent used for anion analysis was a CO_3^{2-}/HCO_3^- solution. Despite several literature articles[24-26] as well as manufacturer's notes[27,28] indicating the superior performance that can be obtained with an alkali hydroxide (typically NaOH) eluent, the CO_3^{2-}/HCO_3^- still remains the commonly used eluent in suppressed anion chromatography. Briefly, the following points can be made concerning hydroxide versus carbonate eluents: (1) at eluent concentrations typically required for the analysis of common anions the suppressed conductance is an order of magnitude lower with hydroxide, resulting in better detection limits; (2) unlike carbonate, hydroxide does not produce a weak acid upon neutralization and analyte response nonlinearity due to the change in the extent of the background carbonic acid dissociation[29] is not a problem; (3) hydroxide is unquestionably superior for gradient elution because of the relatively stable and flat baseline which results because of its complete suppression to water.

There are several inconveniences in the preparation and use of hydroxide eluents. Hydroxide eluents are more difficult to prepare in exactly known concentrations because commercially available standard solutions are certified only with respect to total alkalinity, which is unaffected by dissolved CO_2. While relatively pure NaOH solutions can be made by diluting the supernatant from a centrifuged, $Ba(OH)_2$-treated 50% NaOH solution, the necessary operations must be performed in the absence of CO_2, e.g., under He,[30] and it is still necessary to perform an alkalimetric titration to determine the exact alkalinity. Additionally, after an eluent is purified with great care, it still requires considerable further care to keep CO_2 from reentering the eluent through the plastics often used in the storage and transmission of the eluent. Even a small amount of dissolved CO_2 can have a major influence on retention behavior since CO_3^{2-} is a strong eluting anion, its presence in variable concentrations in the eluent can lead to poor separation, poor reproducibility and high detection limits.[31]

While there is no question that hydroxide is superior to carbonate for gradient elution, the expectation that the suppressed background will be pure water and that the background conductance will not change during a gradient run is not ordinarily realized in practice. Even with prepurified NaOH eluents, impurities remain and are trapped on the column during the initial, low strength, portion of the run to be eluted later as artifact peaks as the eluent strength increases throughout the gradient. To some degree this can be ameliorated by placing an impurity trapping column between the pump and the injection valve or by storage of a blank background and subtracting it from the sample run. Both methods have their limitations and it is clear that it is desirable to have as pure an eluent as possible from the start.

The introduction of the electrodialytic generator for eluents has been a milestone in IC. In 1991, Dasgupta et al.[32-34] pioneered the use of electrochemical methods to purify/generate hydroxide eluents in situ and to electrically control the eluent concentration for use in IC. They developed electrodialytic membrane devices to generate high-purity NaOH eluents on-line using NaOH feed solutions. Two basic types of electrodialytic devices were studied. The first type of device consisted of two flow-through electrode chambers separated by a CEM. The anode chamber was continuously fed with the source NaOH solution while deionized water was pumped into the cathode chamber. With sufficient applied voltage, Na^+ migrated across the CEM and formed NaOH at the cathode channel:

$$(Na^+ +)\ H_2O + e^- = (Na^+ +)\ OH^- + \tfrac{1}{2}\ H_2 \qquad (1.8)$$

At the anode, O_2 was evolved and OH^- was electrolytically neutralized:

$$2\ OH^- - 2\ e^- = H_2O + \tfrac{1}{2}\ O_2 \qquad (1.9)$$

This type of NaOH generator had essentially faradaic current efficiency; however, the hydrogen gas generated along with NaOH had to be removed by a membrane-based degasser before it entered the chromatographic pump.

The second type of device utilized multiple layers of ion exchange membranes to separate the NaOH product channel and source channel so that the high-purity NaOH solution

generated was free of electrolysis gas (Figure 1.4). However, this type of device did not offer faradaic current efficiency.

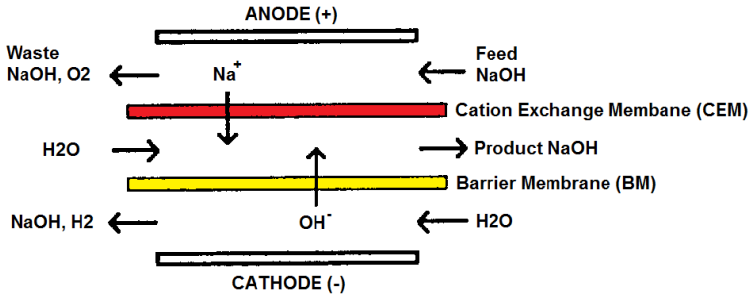

Figure 1.4 Two-membrane NaOH generator schematic.[32]

In 1997, Dasgupta et al.[35] demonstrated a capillary-scale electrodialytic NaOH eluent generator. It was a device with two flow-through electrode chambers separated by a cation CEM. Because of the miniaturization of device components, the NaOH generator was able to withstand higher pressure, so it was deployed on the high-pressure side of the pump and required no special measure for electrolytic gas removal. The NaOH concentration was generated linearly with applied current with near-Faradaic efficiency. Later, Dasgupta et al.[36] demonstrated the use of another microelectrodialytic NaOH generator, which incorporated after the conductivity detector in a suppressed anion chromatography system, to convert the suppressed analytes from the acid form to sodium salts and thus improve the detection of weak acid anions.

In 1998, an automated electrolytic eluent generator was introduced commercially.[37] The device produces high-purity acid or base eluents on-line using ionized water as the carrier stream for either isocratic or gradient ion chromatographic separations. Later, large-capacity eluent generators capable of generating high-purity acid and base solutions over an extended period were developed.[38] The commercial large-capacity KOH generator consists of a high-pressure KOH generation chamber and a large-capacity K^+ electrolyte reservoir filled with 4.0 M KOH as the source of K^+ ions connected together through an ion exchange connector, which is

fabricated by stacking multiple layers of CEMs together. A platinum cathode is placed in the generation chamber and a platinum anode is placed inside the K^+ ion source reservoir. It is placed at the outlet of the chromatographic pump, and only on flowing stream of deionized water is required to generate the KOH solution. The same concept for generation of KOH is applied to the generation of acids, such as methanesulfonic acid (MSA), a typical eluent for cation analysis.

In 2008, Dasgupta et al.[39] developed a new configuration for electrodialytic eluent generator. Both low- and high-pressure, capillary-scale electrodialytic generators were demonstrated. While the low-pressure devices rely on planar or tubular membranes, the high-pressure devices rely on ion exchange resin beads. The dual ion exchanger configuration ensures the production of gas-free eluent, obviating the need of a gas removal device used with single ion exchanger eluent generators. The schematic is shown in Figure 1.5.

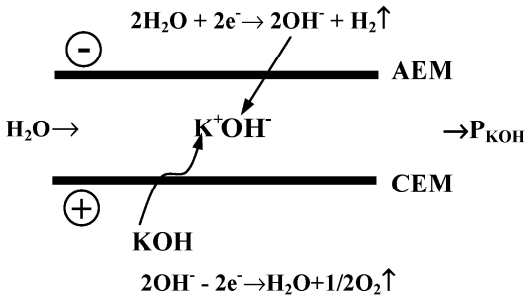

Figure 1.5 Electrodialytic generator designs, schematically shown.[39]

One CEM and one AEM separate three flow-through chambers. A platinum anode is placed in the outer chamber on CEM side and a stainless steel (SS) cathode is placed in the outer chamber on AEM side (referred to as “forward biased”). 4 M KOH is fed into both of the outer chambers, and water is used as the carrier in the central chamber. Under the electric field, K^+ and OH^- are transported from outer chambers through CEM and AEM respectively, producing high-purity KOH eluent for capillary IC. The authors also studied the behavior of the device

when the polarity was reversed (referred to as “reverse-biased”). And they found the current-voltage behavior of “forward biased” and “reverse-biased” fully corresponds to that of a semiconductor diode. Since the generation of the eluents is governed solely by the choice of the respective feed solutions, based on the same principle, diverse eluents such as Na_2CO_3/$NaHCO_3$, CH_3SO_3H, and KNO_3 can be produced, as demonstrated in both isocratic and gradient operations in capillary IC.[40]

CHAPTER 2

CHARGE DETECTOR FOR THE MEASUREMENT OF IONIC SOLUTES

2.1 Introduction

Electrical conductivity is the most common solution phase detection method for ions; this derives from the field induced mobility of a charge carrier. Cavendish first measured solution electrical conductivity in 1776 with static electricity, substantially before Volta invented his "pile".[41] Details of Cavendish's remarkable feat remained undisclosed until Maxwell's perusal of the Cavendish archives in 1921.[42] Kohlrausch pioneered AC conductometry.[43] This was mostly limited to conductometric titrations and estimating dissolved solids content in water until the advent of suppressed conductometric IC; Small *et al*.[4] separated ions chromatographically and detected them as corresponding acids or bases atop a poorly conducting "suppressed" eluent background. Conductometric detection is mobility-based rather than charge-based; individual calibrations must be conducted for individual analytes. In suppressed anion chromatography the detector sees the analytes as the corresponding acids; the difference among various strong acid analyte anions is minimized because the highly mobile H^+ dominates the conductivity. If the still-elusive goal of pure water eluent IC[44-46] is ever realized, there would be marked difference between different electrolytes. Pure standard-based calibration is burdensome when such standards are unavailable or unstable. A detector that responds to all ions in a near-equivalent manner will obviate the need for standards.

For analytes that undergo well-defined redox processes at accessible potentials, coulometry provides a sensitive means of charge transfer based quantitation. To measure the quantity of electric charge, Faraday devised *Voltameters*. Faraday relied on gas volume measurement; Matteucci introduced a gravimetric approach that proved superior.[47] Edison's first utility meters were copper-based gravimetric Voltameters; electricity was sold by weight.

Richards coined the term *Coulometer* and perfected high precision coulometry; his Nobel laurel, first for an American Chemist, credited his exactitude.[48] Coulometry entered analytical practice;[49] titrimetric applications extended that applicability.[50] Despite its superb precision and accuracy, coulometry remains inapplicable for the majority of ionic analytes e.g., Na^+ or SO_4^{2-} whose redox potentials lie beyond the solvent breakdown potentials or e.g., with dilute Cl^-, where such oxidation competes with water breakdown and is faradaically inefficient.

We have previously described three-compartmented devices where cation/anion exchangers (resin beads or membranes) formed three flow-through channels with water flowing through the central channel.[39] In one embodiment, high concentrations of KOH solutions (4 M) were used in both outer channels. With the CEM/AEM side held positive/negative, respectively, K^+ and OH^- migrated to the central channel to produce gas-free KOH that we used as an IC eluent. However, even at zero applied voltage (V_{app}), some KOH penetrated into the central channel as the large osmotic potential difference between the outer and the central channels overcame the Donnan barrier. We noted that when V_{app} was reversed, current flowed in the opposite direction and the KOH concentration in the central channel decreased as K^+/ OH^- present in the central channel were removed by the electric field, respectively through the CEM/AEM. Further, the relationship between what was removed and the coulombs consumed was essentially Faradaic. We reasoned that under "reverse bias", the device is acting as a deionizer and the deionization process involves the respective transport of the cation/anion from the central channel to the negative/positive electrode via the CEM/AEM.

We have now studied in detail similar three channel "charge detector" (ChD) devices, fabricated either with ion exchanger beads or larger area membranes, with varied design and experimental parameters. We studied the effects of varying V_{app}, the central channel flow rate (CCFR), electrode placement, outer channel solution composition, and outer channel flow rates on the current signal (hereinafter we call the integrated value the measured charge signal, Q_m) elicited upon injecting an electrolyte into the central channel. We found that while Q_m may not

always precisely equal the injected charge (Q_i), Q_m always monotonically varies with Q_i. The device thus behaves as a pseudo-coulometer, and allows detection of injected charge regardless of the ability to undergo redox transformation in aqueous solution. The ChD responds to weak electrolytes in a unique manner because the undissociated analyte continues to dissociate as the ions are removed. This paper presents the first account of the ChD.

2.2 Experimental Section

2.2.1. Bead-Based Device

This ChD device (ChD-B) was identical to that used previously as a resin bead-based eluent generator[39] shown schematically in Figure 2.1. The cation exchanger side contained the negative electrode. Flow-through tubular platinum electrodes were used. The through-channels of both arms of a 10-32 4-way cross fitting (P-730, Upchurch) were bored out for 1.6 mm o.d. PEEK tubing to just pass through. For each of two segments of 0.5 mm i.d., 1.6 mm o.d. PEEK tubing, the terminal bore at one end was widened to 0.9 mm to a depth of ~1 mm. Ion exchange resin beads (Rexyn 101 H^+-type for the cation exchange resin (CER) and Dowex AG-2X8 Cl^- form for the anion exchange resin (AER)) were dried in a desiccator and hand-picked to obtain resin beads in the 0.8 -0.85 mm size range. One CER and one AER bead were placed in the respective drilled out cavities in the PEEK tube and wetted with water whereupon they expanded and lodged tightly in the cavity. As shown in Figure 2.1, these two bead-bearing tubes were placed opposite each other (fixed in place with 10-32 nuts and ferrules, not shown), with the distance between CER and AER being ~ 0.4 mm. Water inlet and eluent outlet tubes were then similarly connected. At the back side, each bead-bearing tube was cut off essentially flush with the back of the holding nuts and a small segment of Tygon sleeve tubing put over the ends of the 1.6 mm o.d. PEEK tubes. A blunt-ended platinum needle (0.25 mm i.d., 0.45 mm o.d.; 26 ga., 25 mm long, P/N 21126 PT 3, Hamilton Co. Reno, NV) was put in all the way into the PEEK tubing, just touching the bead. The exit of the Pt Needle from the Tygon tube was sealed with hotmelt adhesive. The Pt-needle functioned both as the electrode and the liquid

inlet tube; the liquid outlet was provided by a 0.25 mm. i.d., 0.51 mm o.d. PEEK tube (P/N 1542, Upchurch) breaching the Tygon tube wall, and affixed in place with adhesive. The nominal internal volume of the device, without considering the space that the protrusion of the spherical beads may consume, is ~3.2 µL.

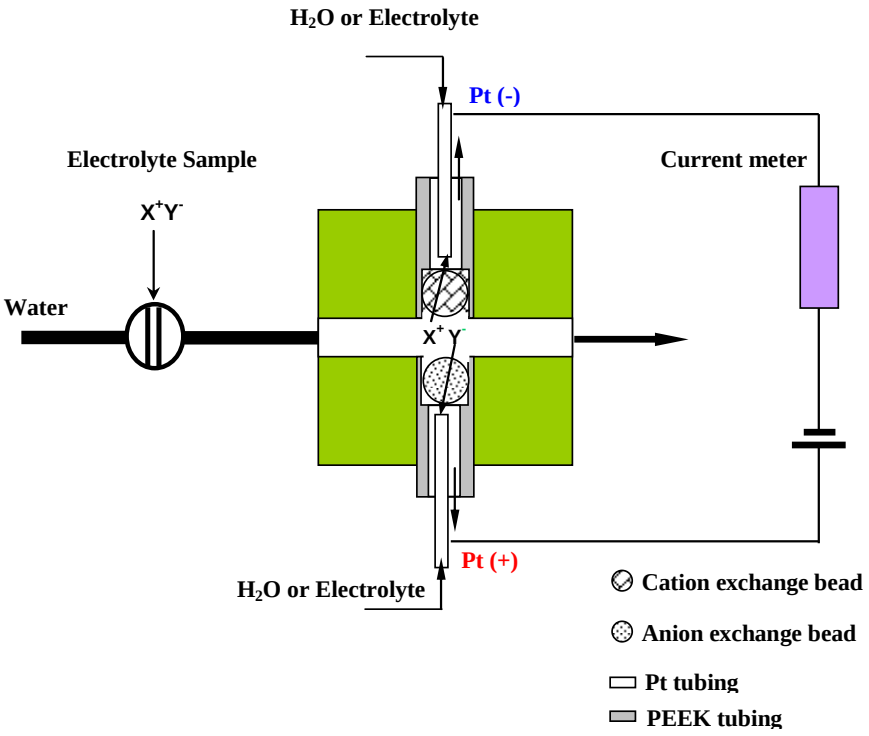

Figure 2.1 Configuration of bead-based charge detector (ChD-B).

2.2.2. Membrane-Based Device

The membrane-based ChD's (ChD-M devices) were fabricated using radiation grafted poly(tetrafluoroethylene) based ion exchange membranes (IEMs). These devices are similar to commercial electrodialytic membrane suppressors (www.Dionex.com) of a three-

compartmented design[51] (See Appendix A for Scheme I and Figure A.1; hardware assembly in Figure A.2).

While an IC suppressor contains two identical IEMs, ChD-M devices use one AEM and one CEM with the adjacent screens correspondingly ion-exchange functionalized, the central screen being neutral. The outer channel flows in a ChD-M device are isolated and independent (as shown in Scheme II in Appendix A).

ChD-M devices were made in two different sub-designs: one involved the electrode being separated from the membrane by the ion exchange screen; heretofore designated as MSSE (membrane with screen separated electrode, Scheme II/Figure A.3 in Appendix A; see Appendix A for screen and electrode material details). Suppressors handle continuous large transmembrane flux of ions; the presence of a screen on the membrane exterior provides for more efficient washout. In contrast, a ChD handles small pulses of analyte ions. The voltage drop in the outer screen regions of a ChD, typically containing high resistivity water, can be avoided if the electrode is directly on the membrane (Appendix A scheme III); most of the data for ChD-M devices in this paper is based on this design, referred to as MAE (membrane with adjacent electrodes); the device is shown in Figure 2.2 (the MSSE design differs only in that the electrodes are in the outermost positions). Both MSSE and MAE devices were built in two different sizes. The membrane device with the larger active membrane area (~14 cm long x 1 cm wide, internal volume ~125 μL) is designated with the suffix-L (e.g.; MSSE-L) while the device with the smaller active membrane area (~14 cm long x 0.26 cm wide, internal volume ~35 μL) is designated with the suffix-S (e.g., MAE-S). In all cases the membranes were separated by a 250 μm thick screen; this defined the central channel.

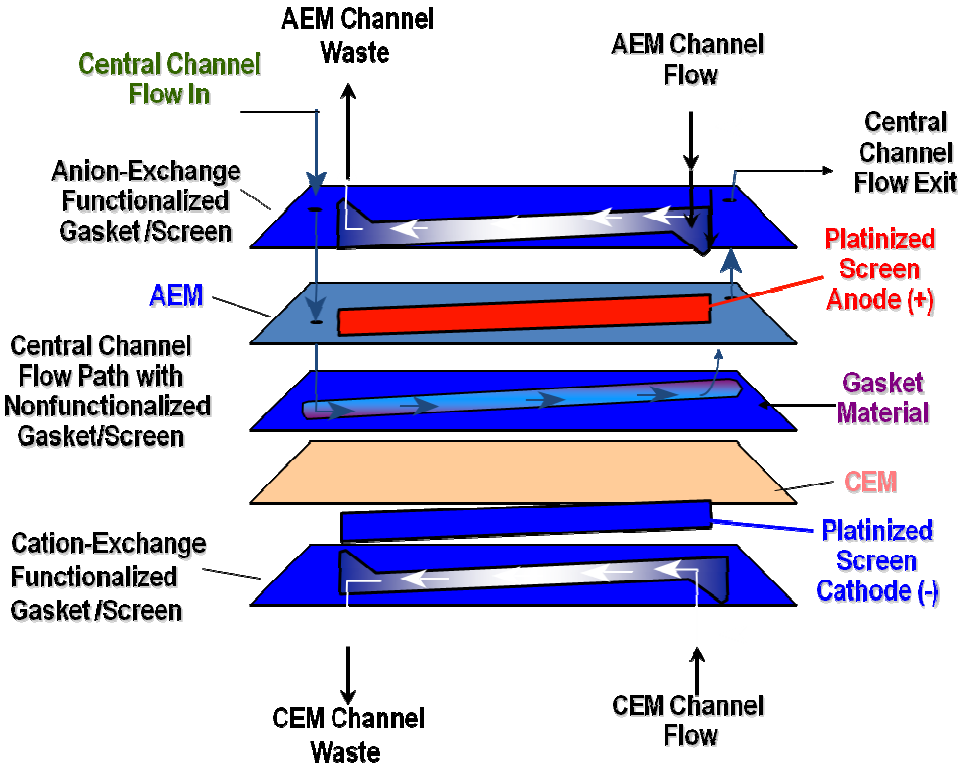

Figure 2.2 Membrane-based charge detector (ChD-M) device with adjacent electrodes (MAE devices).

2.2.3. Experimental Arrangement

A syringe pump (model V6, Kloehn Inc., Reno, NV) equipped with a 1 mL capacity glass syringe established the central channel flow (1-10 μL/min) with ChD-B. Unless otherwise stated, water flowed in the outer compartments behind the beads and was driven either by air-pressure or peristaltically, at 500 μL/min. In-line injections (1.0 μL) were made by an internal loop injector (P/N EDCI4UW1. www.VICI.com). For ChD-M's, a GS-50 pump (Dionex) provided central channel water flow rates (CCFR) of 0.2 and 1 mL/min for -S and -L devices, respectively, with corresponding calibrated analyte injection volumes of 54.0 and 26.4 μL. Pure water or dilute electrolyte solution was pumped by nitrogen pressure through the ChD-M device outer channels at 1.5 mL/min, except as stated.

In this initial exposition, we characterize parametric effects on device behavior; efforts were not made to attain the best possible detection limits. Standard inexpensive power supplies were used for all work and device connections were not shielded. Data acquisition and *i*-V conversion details are given in Appendix A. Conductivity was measured with Dionex ED-50 detectors. All chemicals used were reagent grade; solutions were prepared with 18.2 MΩ·cm Milli-Q deionized water.

2.3 Results and Discussion

2.3.1. Relevance to Bipolar Membrane

Bipolar ion exchange membranes (BIM's) having cationic and anionic functionalities on their opposite faces have been known for 50+ years.[52,53] Models for BIMs assume a thin layer of water at the interface between the two functionalities.[54,55] When the BIM is forward biased (the CEM side positive), current increases steeply especially when V_{app} exceeds the electrolytic breakdown of water; [56,57] electrogenerated H^+ and OH^- moves through the CEM and AEM respectively under the electric field and recombines to water at the junction. Interestingly, when the BIM is reverse biased (AEM side positive), reverse current first begins to flow at a lower V_{app} than when the BIM is forward-biased. Specifically, as V_{app} exceeds the threshold voltage to bring about dissociation of water (ΔG_f° for the process $H_2O \Leftrightarrow H^+ + OH^-$ corresponds to 0.83 V), the reverse current begins.[58] This process has commonly been referred to as *water-splitting* in the BIM literature[55,58] but we avoid this term: in current usage it more commonly suggests the breakdown of water into H_2 and O_2. Rather, we refer to this as enhanced water dissociation. Enhanced dissociation of weak electrolytes at high electric fields was first observed by Wien[59] and subsequent detailed experimental data for weak acids and bases generated by Schiele.[60, 61] A detailed theoretical basis for field-induced increase in dissociation was developed by Onsager.[62] Although a decrease in pK_w of pure water at high field strengths has never been experimentally shown per se, the operation of a reverse-biased BIM is always explained on this basis. The high field across the highly resistive thin layer of water at the CEM-AEM interface is

postulated to result in enhanced water dissociation and the resulting ions, generated without the electrolysis of water, carry the current.[55] In general for IEM's, field-induced water dissociation may also be catalyzed by the ion exchanger surface, particularly an anion exchanger;[63] for a more detailed recent review, see Tanaka.[64] The ChD is much like a BIM except that between the two exchangers there is a real, fluidically accessible, liquid layer. The enhanced water ionization phenomenon observed with BIMs is also important with the present ChD. BIM's are used industrially in the reverse-biased mode; current densities of 0.5-1.5 kA/m^2 are attained at $V_{app} \leq 2.5$ V (equivalent to a resistivity of ~25 Ω/cm^2).[58] The present ChD's show qualitatively similar *i*-V behavior: especially the MAE devices with low outer channel voltage drops show significant currents in both the forward and reverse direction at modest V_{app} values (Figure 2.3). The inset shows the results of discrete measurements (plotted in terms of current density) these steady state currents do not contain capacitive contributions. Although these current densities are less than ~1 A/m^2, this is with pure water while BIM current densities quoted above pertain to ~1 M electrolytes.[58] It will be readily apparent that the *i*-V behavior in the forward and reverse biased modes are not mirror images. In the forward-biased mode, past ca. 2.2 V, the current rises very steeply (electrolysis visibly begins) but significant non-capacitive current begins to flow at much lower voltages in the reversed-biased mode. A comparison of the attained current densities relative to the ionic concentration in solution also suggest that as in BIM's, field induced dissociation of water must play an important role in the present devices to contribute charge carriers in the observed reverse current. With 1 V reverse-bias and pure water flowing throughout the device, the observed current is nearly three times what would be computed for a medium of 18 MΩ.cm resistivity, even ignoring the voltage drop across the membranes. Without the membranes, no asymmetry in the *i*-V behavior is observed.

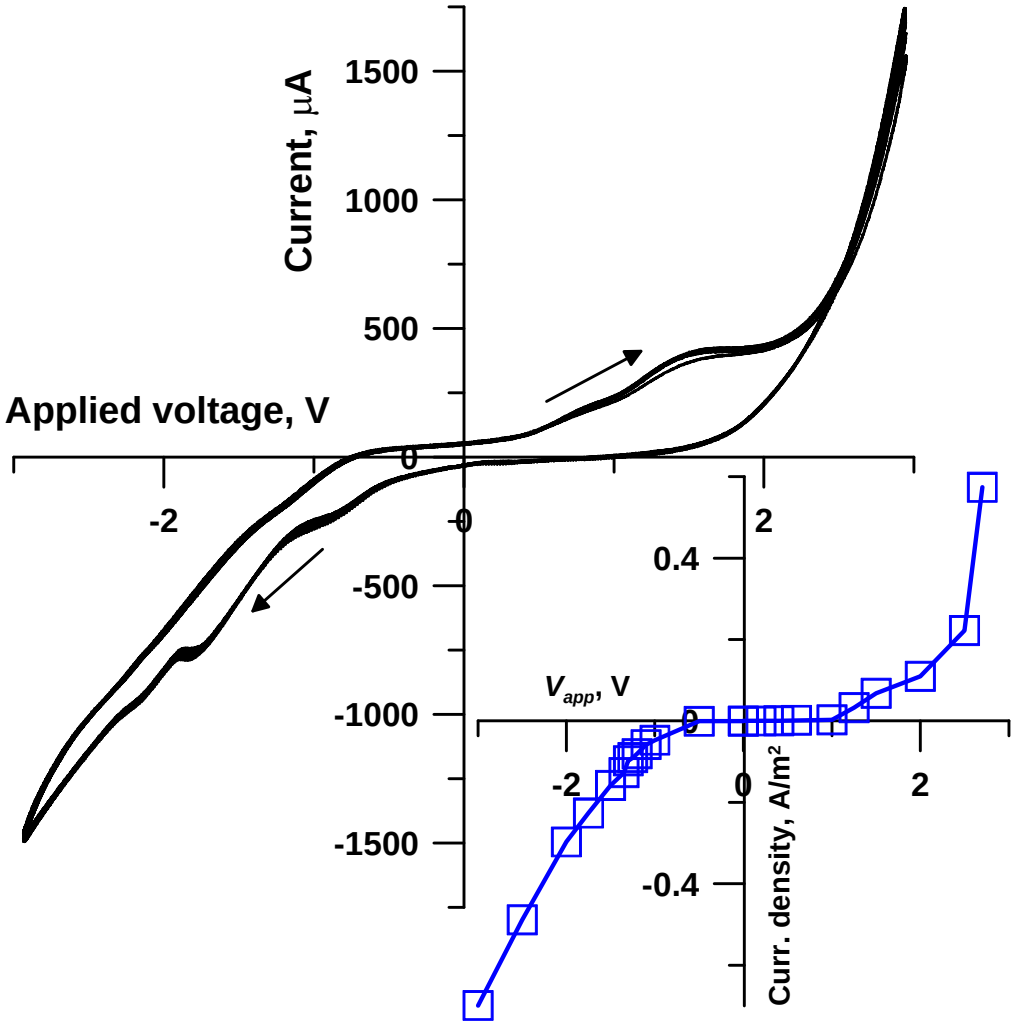

Figure 2.3 Background current as a function of applied voltage for a MAE-L device. The voltage is that of the CEM side relative to the AEM side. Data was obtained @10 Hz using a 2 mHz triangular wave for ~110 min (~13 cycles). Charge detector operation takes place exclusively in the SE quadrant; hereinafter the voltages and currents are shown without the negative sign. Flow in the central channel: water, 1 mL/min; flow in the outer channel: water, 1.5 mL/min. Inset shows a single point by point discrete measurement that avoids capacitive currents, with the ordinate scaling in terms of current density.

2.3.2. The Charge Signal. Equivalent Response to Analytes

A striking aspect of the present ChD's is that they respond with essentially the same signal when equivalent amounts of different strong electrolytes are injected. Figure 2.4 shows the responses to equivalent amounts of $NaNO_3$, KCl, HNO_3, $BaCl_2$, or K_3PO_4 injected into the

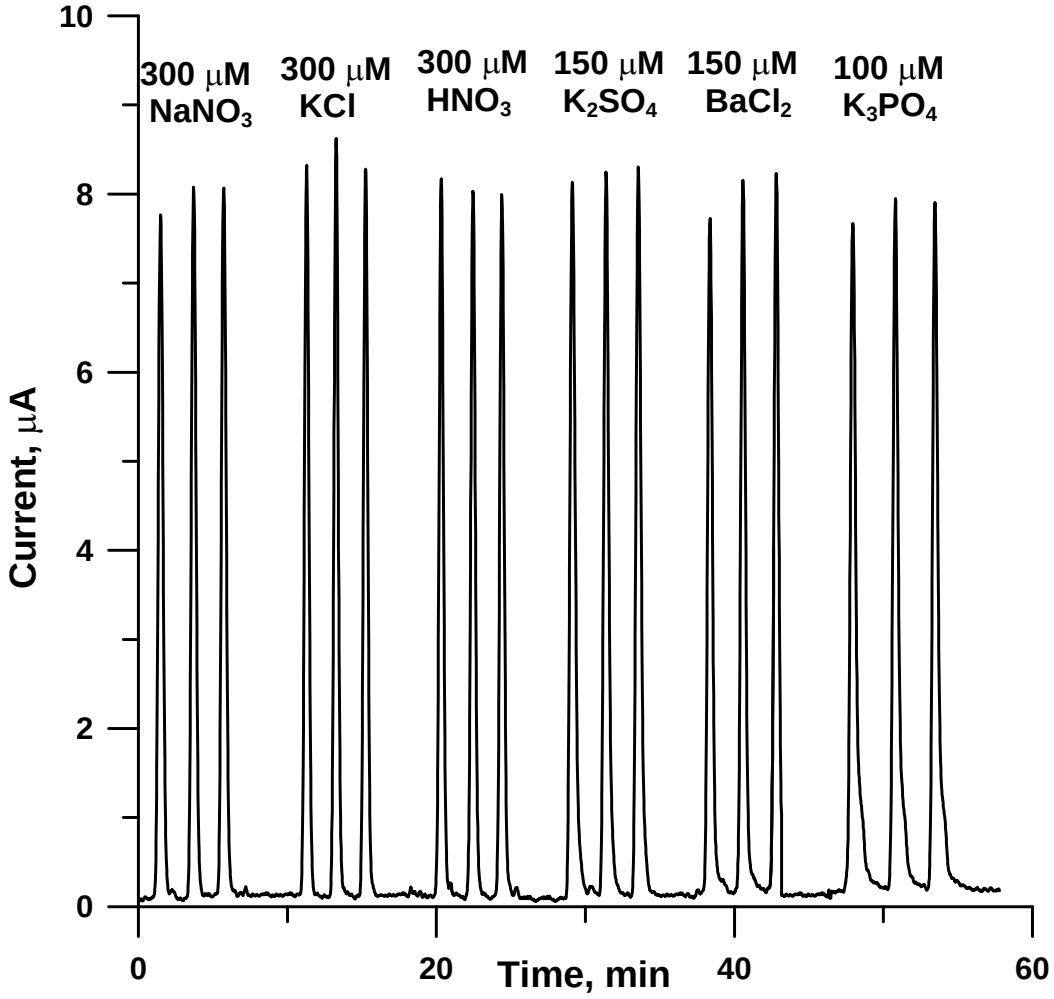

Figure 2.4 Charge detector behavior. Resin bead based type B device. 1 µL of electrolyte of indicated concentration injected into the central stream flowing at 4 µL/min. Applied voltage 14 V, outer channel electrolyte: 20 mM KNO_3.

central channel of a ChD-B device. The peak areas of the individual responses shown are 194 ± 16 µC; the near-uniform response of the different electrolytes are remarkable - in conductance measurement, HNO_3 would have produced a signal 3.5 x that from $NaNO_3$. Protolyzable ions like PO_4^{3-} is present as HPO_4^{2-} at the injected analyte concentration. However, the hydrolysis generates an equivalent amount of OH^-; the total charge equivalents remain the same. It is the peak area and not the peak height that is the coulombic signal, the bulky HPO_4^{2-} moves through the resin bead of substantial thickness perceptibly slower than the monovalent ions leading to

an observably greater base width in the charge signal response. The uniformity of the response behavior is independent of both device and analyte type and also V_{app} (Figure A.4).

2.3.3. Use as a Chromatographic Detector

An MAE-S ChD was put after a conductivity detector in a conventional suppressed IC system. Figure 2.5 (a) shows a low-level chromatogram. Consider that even this smaller ChD-M device has an internal volume of 35 µL, 1.5 orders of magnitude greater than that of the CD. There is increased attendant dispersion and the background signal is directly proportional to the membrane area. A purpose-designed ChD with a smaller membrane area (not just a modified suppressor) should provide much better S/N. However, the present application already shows the potential of the ChD as a sensitive IC detector.

Figures 2.5(b) and (c) respectively shows area based CD and ChD calibrations for chloride, nitrate and acetate. Up to 25 µM, the ChD shows statistically identical response behavior for all three anions; only at 50 µM is the acetate response perceptibly lower. In contrast, there are differences in the conductance response from the very beginning and this difference grows with concentration. For the results in Figure 2.5, V_{app} was 2 V, the ChD response uniformity extends to higher concentrations if V_{app} is increased further (*vide infra*).

2.3.4. Effect of Applied Voltage

The ChD responds in two ways. The primary response is from the ionic analyte constituents injected into the system and their transport into the respective electrode compartments. When KNO_3 is injected, the primary signal is generated from the transport of K^+ and NO_3^- to the negative and positive electrodes, respectively. The secondary response comes from field-induced water ionization that is further enhanced in the presence of a conductive analyte. This is the process responsible for the superfaradaic response behavior. We hypothesize that similar to what is postulated in BIMs, the field across the membrane causes water ionization at the inner surfaces of each membrane: at the AEM inner surface H^+ comes into the central channel and OH^- goes to the + electrode; at the CEM inner surface OH^- comes into the central

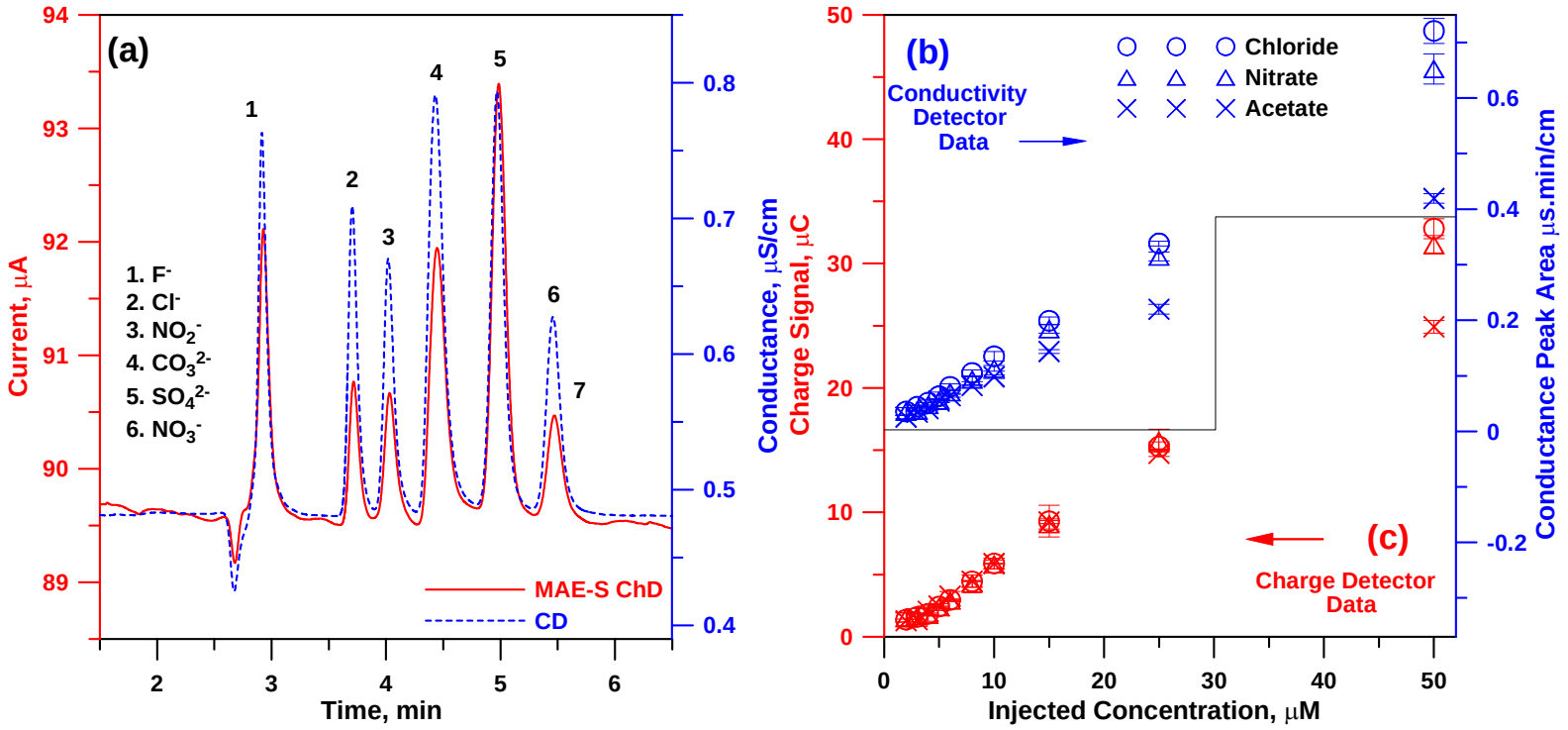

Figure 2.5 Comparison between conductivity and charge detectors (a) Chromatograms by conductivity detector and MAE-S ChD V_{app} = 2 V (outer channels water @ 1.5 mL/min). 24 mM electrogenerated KOH @ 1 mL/min, AG 11-HC (4 x 50 mm)/AS 11-HC (4 x 250 mm) columns, 35 ℃ (LC-30 oven), ASRS Ultra-II suppress or (all from Dionex). Analyte concentrations 1 µM. (b), (c) conductivity and charge detector based calibration plots, respectively. Quadruplicate injections, ±1 standard deviation is shown as an error bar.

channel and H^+ goes to the – electrode. The central channel composition does not change as the H^+ and OH^- recombine to water. Simons[63] proposed that the dominant process takes place at the AEM, our experiments cannot verify this. Note that it is the field across the membrane that is critical. Normally the applied voltage is much greater across the much more resistive and thicker central channel bearing water than across the membranes. But the presence of analyte makes the central channel more conductive and more voltage is now applied across the membranes, water ionization is thus further enhanced, resulting in additional current. Significant growth of the signal begins at voltages less than that needed to cause electrolysis (e.g., 1 V for the MAE devices, while significant growth of noise, which is likely associated with electrolysis, does not begin until >2.5 V (Figures A.5, A.6 in Appendix A).

Diffusive and electromigrative transport are both operative for analyte ion removal to the outer channels. Thus, the residence time in the device and the applied electric field strength are both of importance. The residence time is controlled by the central channel flow rate, discussed in the next section. The electric field governs the electromigrative transport; V_{app} should thus affect Q_m. When the residence time and electric field in combination are sufficient to achieve complete transport of the injected ions (as observed by a CD placed after the ChD), there will be no further increase in the ChD signal. Figure 2.6 shows the Q_m/Q_i ratio for three devices. Q_m reach or approach a plateau (devices ChD-B, MSSE). A maximum value of Q_m/Q_i as a function of V_{app} is reached in a MAE device as shown in Figure 7a; it is not presently understood why Q_m actually decreases with these devices at V_{app} > 3 V. In any case, at V_{app} > 3 V the background current for these devices is very high and the noise is too high for operation in this range to be analytically attractive.

It is also apparent that this maximum Q_m/Q_i is >1. In MSSE devices operated with water in the outer channels (hereinafter operation with pure water in the outer channels is designated w/w) the maximum value just exceeds unity; in contrast for ChD-B (20 mM KNO_3 outer electrolyte) it is >2.5 (Figure 2.6) and for device MAE-L (w/w) it is >4.5 (Figure 2.7a).

The origin of this "superfaradaic" behavior is due to a change in the "background current" generated from H^+ and OH^- produced by enhanced water ionization. Background changes

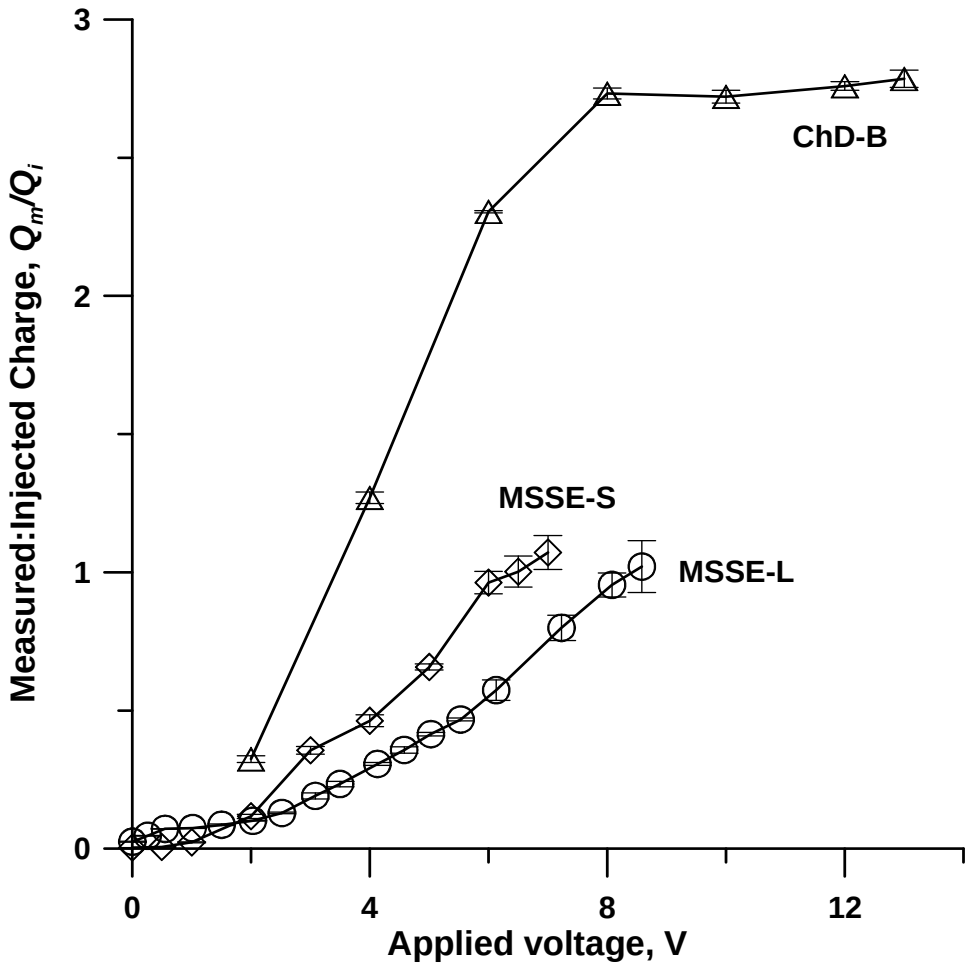

Figure 2.6 Peak area as a function of applied voltage for various devices. ChD-B: 0.8 nmol KCl injected; CCFR: 6 µL/min, outer channel electrolytes 20 mM KNO_3. MSSE-L/MSSE-S: 2.7/1.3 nmol KNO_3 injected, outer channels water. Error bar indicates standard deviation (n = 4).

accompanying analyte elution are not unusual in IC. For example, carbonic acid is formed with carbonate eluents upon suppression. When a strong acid elutes, this suppresses the dissociation of the carbonic acid – the background decreases accompanying analyte elution. This decrease is not apparent to the user except in the nonlinearity of the response – at low analyte concentrations, the slope of the calibration curve is lower than at higher concentrations.[65] There is diminishing returns of increasing the analyte concentration on the carbonic acid dissociation, however; at high analyte concentrations one thus reaches a

constant limiting calibration slope. The situation is analogous here except that the background *increases* with increasing analyte concentration. But there is also a diminishing return – when the analyte bolus becomes sufficiently conductive, the voltage drop across the central channel becomes relatively insignificant to further affect the voltage drop across the membranes and thus further affect field-induced water dissociation.

At low injected amounts the response is superfaradaic (Q_m/Q_i >1) even at low V_{app} values. The response factor generally decreases with increasing concentration at all values of V_{app} (Figure 2.7b; see also Figures A.7-A.14 in Appendix A for more details). For MSSE devices operated w/w, even up to V_{app} =6.5 V, Q_m remains <Q_i (Fig. A.15). But if acid/base is present in the outer channels, the response remains superfaradaic till higher concentrations. The higher the V_{app}, the higher is the concentration till which superfaradaic behavior is maintained: if V_{app} is sufficient (e.g. 3 V for an MAE device), subfaradaic response is not observed for concentration ranges typically encountered in IC. At V_{app} values typically used for bead devices, Q_m remains > Q_i throughout (Figure A.16 in Appendix A).

2.3.5. Central Channel Flow Rate

The ChD response is dependent both on V_{app} and the residence time in the device. The ChD signal for 800 pmol KCl injection in ChD-B at three different flow rates is shown in Figure 2.8. In each case, the signal reaches a plateau, the solid lines shown are first order fits. As may be intuitive, the minimum V_{app} needed to reach the plateau signal decreases with decreasing flow rate. It is also obvious that lower flow rates produce a greater plateau signal; this is because the temporal peak width is larger and the enhanced water dissociation process that contributes to the signal is temporally longer. The general behavior that the V_{app} necessary to reach a plateau signal increases with increasing CCFR is common to all devices (see Figure A.17, A.18 in Appendix A for analogous behavior of ChD-M devices). At any given V_{app}, the observed charge signal exhibits a first order rate process with respect to residence time in the ChD. For a bead-based device, the data for different voltages and flow rates fit a single first order equation with respect to the product of

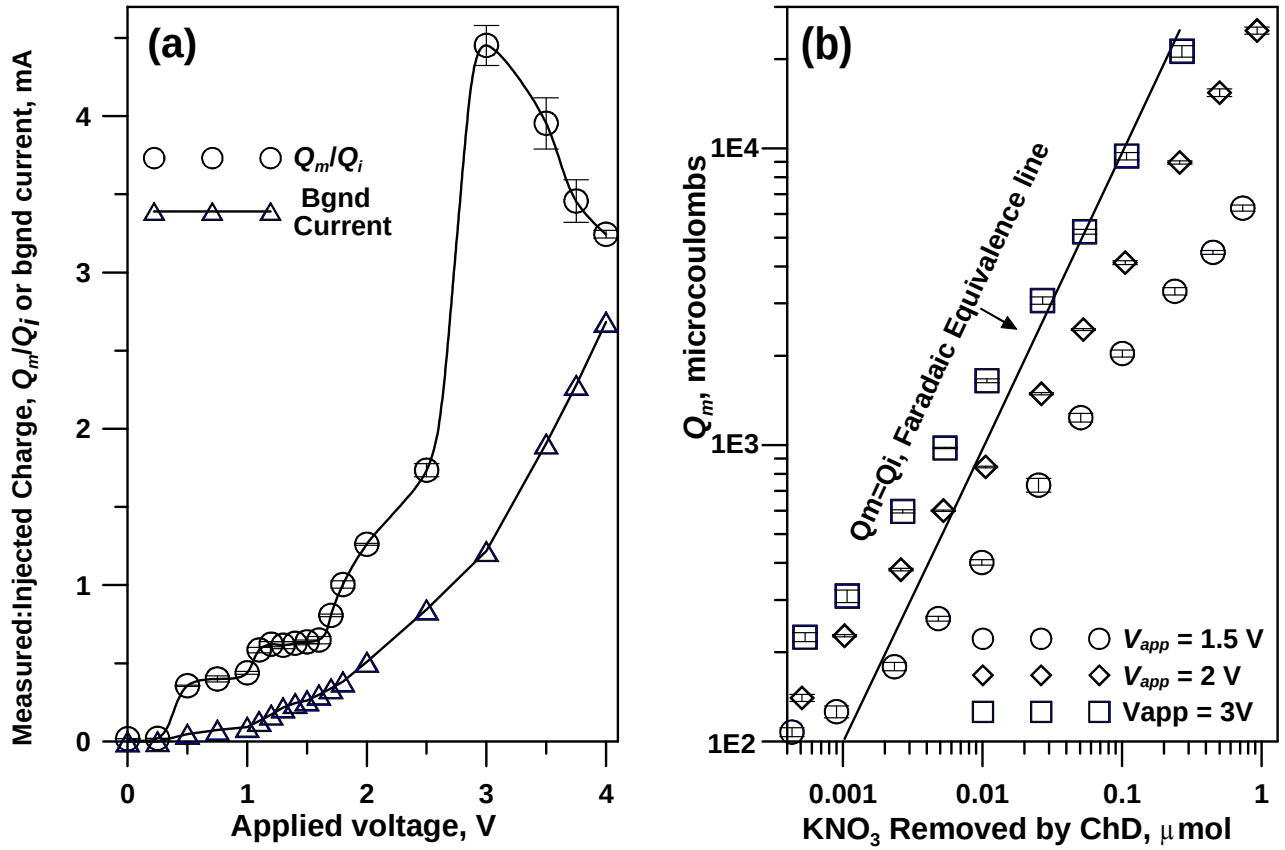

Figure 2.7 Behavior of MAE-L device, operated with water/water/water, central channel 1 mL/min, outer channels 1.5 mL/min, analyte KNO_3, 54 µL injected. (a) triangles show background current, circles Q_m/Q_i for 50 µM KNO_3, (b) calibration curve over a large concentration range of injected KNO_3 for three different V_{app} values; the solid line is the Faradaic response line. The abscissa values are approximately equal to the injected amounts, only at high injected amounts and low V_{app} values there is a significant difference. See Figures A7–A14 and accompanying discussion in Appendix A.

V_{app} and the residence time as shown in Figure 2.8 inset; this allows one to predict response if V_{app} and/or CCFR is varied.

Attaining a plateau signal or complete removal of the injected ions by the device (as indicated by a post-ChD CD), however, does not mean that Q_m at least equals Q_i. This is especially true at low V_{app} and in devices with high outer channel voltage drops. The IEMs have significant capacities: the injected ions can be exchanged by the IEMs that do not move further to the electrode chambers. At low V_{app}, the electrolytic threshold is not crossed and there is no electrogenerated H^+ or OH^- to remove the analyte ions from the membranes. For an MSSE-S device, at V_{app} <6.5 V, Q_m never attains Q_i (Figure A.17 in Appendix A). On the other hand, with V_{app} = 6.5 V, over a significant range of flow rates this MSSE device produces a Q_m essentially equal to Q_i. Here the outer channel voltage drop remains dominant; the voltage across the membrane does not become large enough to significantly enhance water-ionization. An MAE-S device operated w/w and at low V_{app} exhibits similar dependence on residence time and plateau $Q_m/Q_i \sim 1$ (Figure A.18 in Appendix A). As may be anticipated, the CCFR has little or no effect on the background current (Figure A.19 in Appendix A).

2.3.6. Effect of Outer Channel Electrolyte Composition

While we have mostly operated w/w, one potential way of decreasing the outer channel voltage drops, significant in MSSE devices, is to use a more conducting electrolyte. With dilute acid/base behind the CEM/AEM, respectively, minimal electrolyte leakage was observed as measured by a downstream conductivity detector. Accordingly, MSSE devices operated with acid/base exhibited background *i*-V behavior very similar to MAE devices operated w/w (Figure A.20 in Appendix A). The MSSE device response, especially at low V_{app}, is greatly increased by acid/base in the outer channels. With 1 mM H_2SO_4/KOH as outer channel electrolytes, 50 µM $NaNO_3$ produces Q_m/Q_i = 1 at a V_{app} =1.1 V that requires 6.5 V with w/w operation (Figure A.21; the response behavior with different acid/base concentrations is given in Figure A.22 in Appendix A). With acid/base in outer channels, $Q_m<Q_i$ response is not observed except at very

high analyte concentrations (Figure A.7- A.14 in Appendix A). Understandably, the change in response and background of an MAE device is less than that of an MSSE device in going from w/w to acid/base but higher or equivalent S/N is reached at perceptibly lower V_{app} with acid/base operation. (Table A.1 in Appendix A).

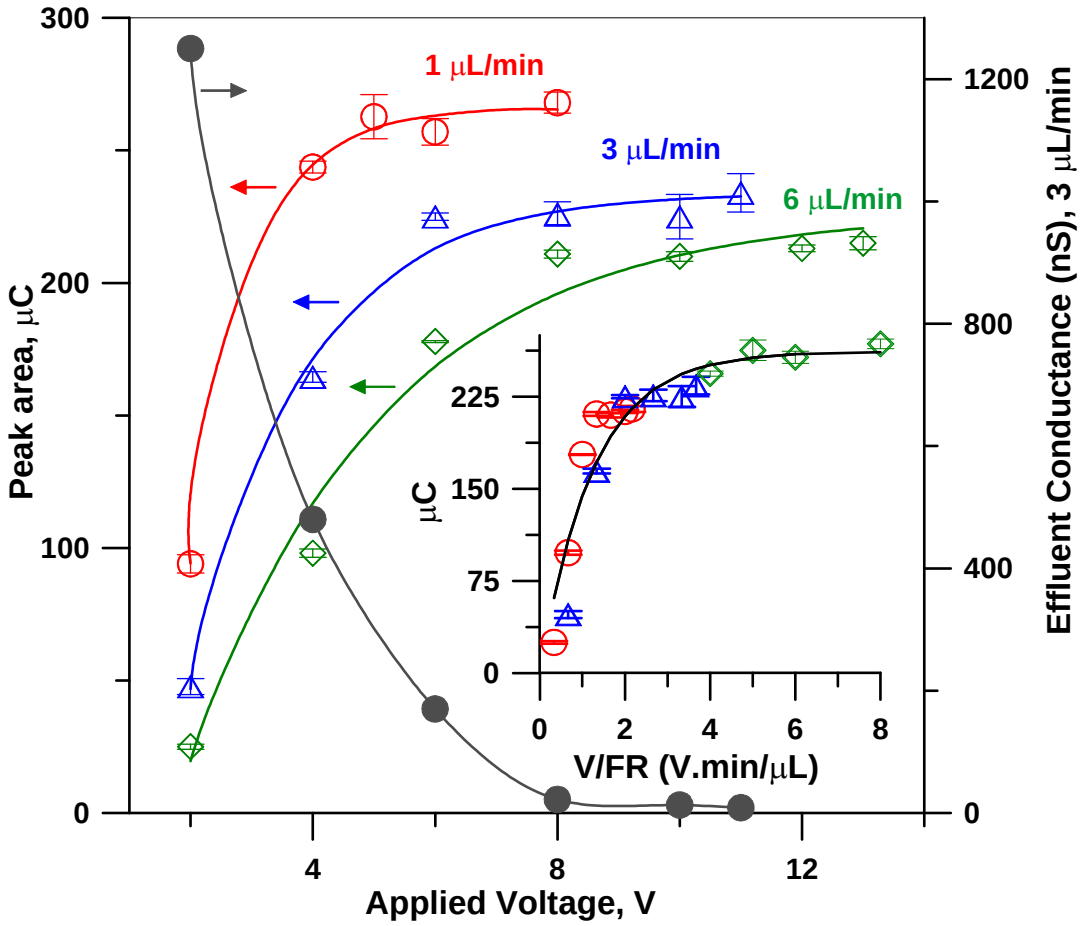

Figure 2.8 Charge detector (Device B) signal as a function of applied voltage at different central channel flow rates. 1 µL 0.8 mM KCl injected. Outer electrolytes 20 mM KNO_3. The effluent conductivity for 3 µL/min flow rate is shown. As the detector signal reaches a plateau, the effluent is deionized. The inset shows a fit of the charge signal (y) to a first order equation $y = y_{max}\ (1\text{-}exp(-0.80x))$ where $x = V_{app}$/flow rate (µL/min).

However, MSSE devices cannot compete with the MAE devices in terms of S/N regardless of w/w or acid/base operation. Figure 2.9 shows the S/N ratio for 50 μM $NaNO_3$ injected into the system as a function of V_{app}; individual signal and noise data in both linear and logarithmic ordinates are presented in Appendix A (Figures A.5-A.6, A.23-A.25). In terms of a practical sensitive detector, the optimum S/N value for an MAE device, which shows little dependence on the nature of solution in the outer channel, is ~100x better than the best MSSE device S/N and for a low concentration analyte, this optimum MAE S/N is attained at a V_{app} of only 1.5 V.

2.3.7. Effect of Flow Rate in Outer Channels

As may be intuitive, there is little or no effect of the outer channel flow rate on the background current (Figure A.26 in Appendix A) except response peak areas for MSSE devices increase at low outer channel flow rates (Figure A.27 in Appendix A). This is because injected analytes lead respectively to bases/acids in the CEM/AEM outer compartments and not efficiently sweeping these off effectively represents operation with small amounts of electrolyte in the outer channels. Predictably, this effect is much smaller for MAE devices.

2.3.8. Response of Strong vs. Weak Electrolyte

A ChD, unlike a CD, is not a nondestructive detector. It splits the anionic and cationic components, ultimately forming an acid and a base. Unlike detecting a weakly dissociated electrolyte by conductivity, a ChD removes the ions that are dissociated; further dissociation must occur to maintain equilibrium thus generating further response. The extent of the total response depends on the residence time of the weak electrolyte in the ChD and its forward dissociation rate. Figure 2.10(a) shows for a MAE-S device the dependence of the response as a function of the central channel flow rate for both a strong and a weak electrolyte, there is a steep increase with residence time in the later case. The analogous case for a bead based device is shown in SI (Figure A.28 in Appendix A). The ChD is better at detecting weak electrolytes than is a CD (Figure A.29 in Appendix A). Higher V_{app} also enhances the response

of a weak electrolyte relative to that of a strong electrolyte although this effect is less than that obtained by increasing residence time; Figure 2.10 (b) shows this for a bead device. The behavior of weak acids will be examined in more detail in a future article.

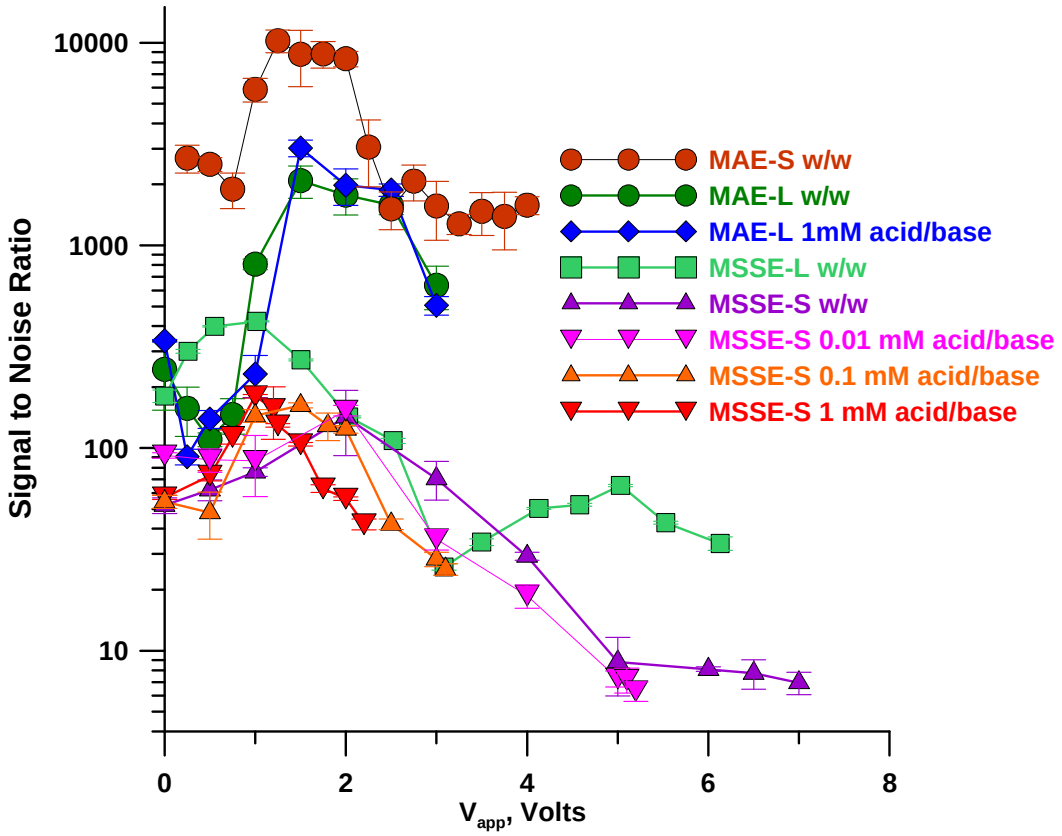

Figure 2.9 Signal to noise ratio shown in logarithmic ordinates for various MAE and MSSE devices operated with CEM/AEM: liquids water/water or acid/base. For acid 0.01, 0.1, or 1.0 mM H_2SO_4 was used, the same molar concentrations of KOH was used as the corresponding base. The central channel was always water. Injection volumes were 54 and 26 µL and CCFR values were 1000 and 200 µL/min, respectively for type -L and –S devices. See Figures S5, S6 andS23-S25 in SI for a version in color and other relevant information.

2.4 Conclusion

We have demonstrated a new principle for detecting and quantitating electrolytes in aqueous solution. This technique responds in an equivalent manner to all ions in aqueous solution based on their charge. There are fundamental differences between the principle and

operations of this approach compared to conductometry and coulometry. The data for many device designs and the effect of varying the various parameters were reported here, at the risk of leading the casual reader to believe that it is difficult to attain optimum operation. In fact, using a MAE-S style device as a detector in a electrogenerated hydroxide eluent 4 mm IC system, using water in the outer channels and applying a modest voltage (1.5 V) is all that is needed to provide an S/N almost the same as that provided by a conductivity detector but with the benefit of universal calibration and enhanced response to very weak acids. Note that the enhanced response to weak acids also implies that the ChD is not as suitable for use with suppressed carbonate eluents unless the CO_2 has been removed prior to detection.[66,67]

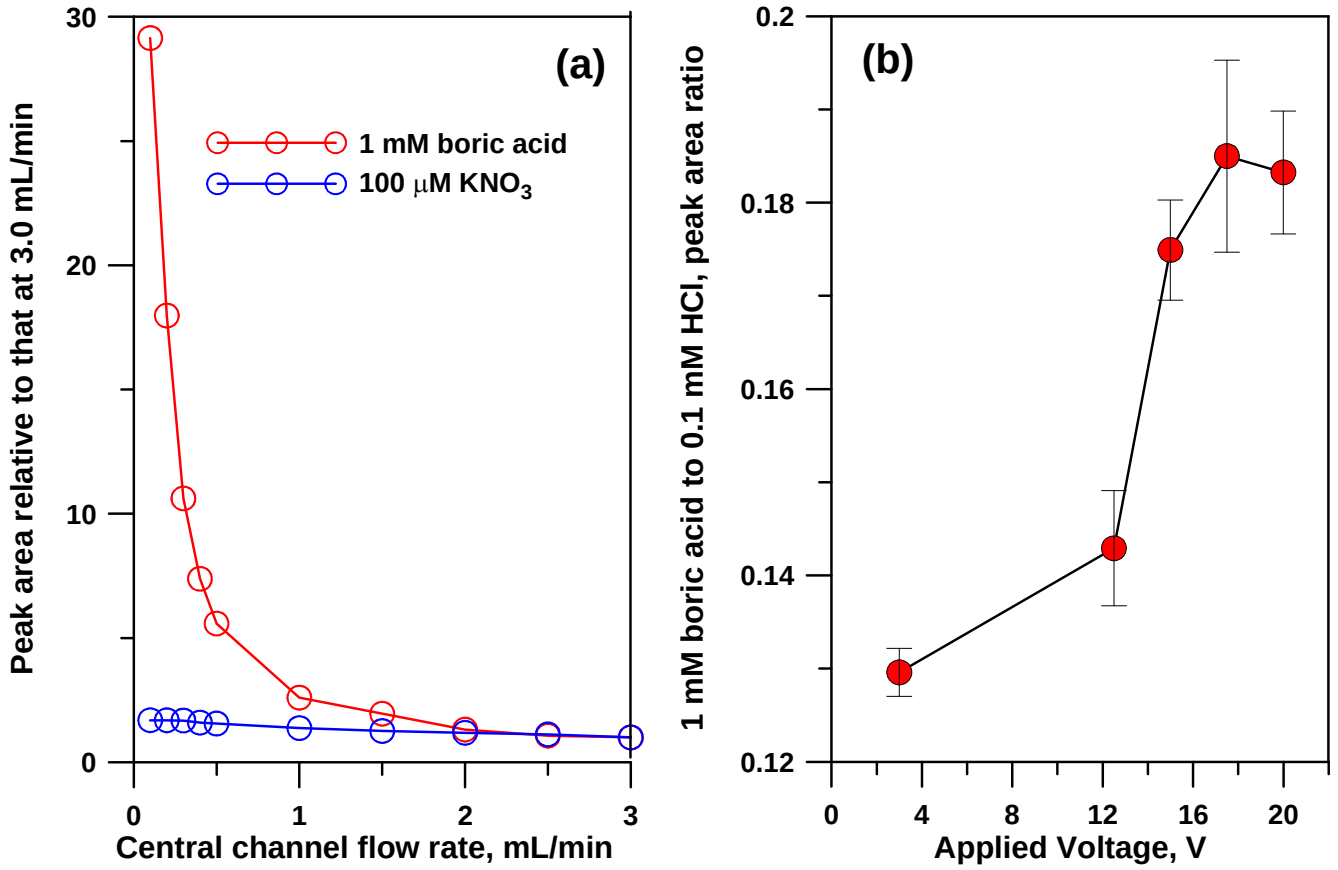

Figure 2.10 Weak vs. strong electrolyte response (a) MAE-S, operated w/w, CCFR 0.1-3 mL/min, outer channels 1.5 mL/min, analyte 100 μM KNO_3 and 1 mM boric acid, 54 μL injected, V_{app} 2 V, (b) Device ChD-B, peak area ratio of 1 mM boric acid relative to that of 100 μM HCl as a function of V_{app}; 2.5 μL injection, CCFR 5 μL/min.

CHAPTER 3

ON-LINE ELECTRODIALYTIC SALT REMOVAL IN ELECTROSPRAY IONIXATION MASS SPECTROMETRY OF PROTEINS

3.1 Introduction

Mass spectrometry (MS) is foremost among present techniques used for the analysis and characterization of biomolecules. Early attempts to transform biological macromolecules into gas-phase ions were hampered by the fragile nature of biomolecules. *Soft* ionization methods introduced during the last 40 years have been shown to produce intact ions from difficult to vaporize molecules of ever-increasing size; electrospray ionization (ESI)[68] and matrix-assisted laser desorption/ionization (MALDI)[69, 70] are the two most popular soft ionization techniques. ESI-MS is easily interfaced to liquid flow systems enabling in particular fast, online analysis of biological samples after chromatographic separation.[71,72]

ESI-MS, however, is incompatible with traditional buffers and nonvolatile salts. Volatile components such as ammonium acetate/formate and acetic/formic acid are typically used instead. However, macromolecular analytes are often extracted from biological samples with significant concentrations of nonvolatile buffers and salts. Alternatively, the latter are used during isolation and may be needed to maintain structural integrity.[73] Sometimes even small amounts of salts can affect electrospray stability, significantly reduce the detected ion signals, cause extensive peak tailing, and result in poor signal-to-noise ratios due to ionization suppression.[74-76] The prevalence of adduct ion formation (e.g., by sodium in positive ionization mode) between analytes and salt species can complicate spectra.[77-80] The presence of adducts is a particular problem with large biomolecules: the probability of forming adducts with non-proton counterions increases with increasing chain length. With many charged salt clusters formed during ESI, the overall ion abundance for a given analyte charge

state is divided among numerous peaks. This results in various charged forms (e.g., $[M + aH + bNa + cK]^{(a+b+c)+}$) instead of exclusive $[M + nH]^{n+}$ ions. The formation of charge-neutral adducts, e.g., by attachment of multiple NaCl moieties to an analyte ion, can further aggravate the situation.[81] Nonvolatile salts especially interfere with the ESI process, resulting in less effective ion desolvation and transmission, as well as build up of salt deposits in the ESI source.[82]

Salt removal has been accomplished by off-line gel filtration (GF). Proteins, originally in a physiologically compatible buffer, are eluted from a GF column by an ESI-compatible buffer; this leaves the original buffer components behind. The biomolecules of interest must remain stable through the sample handling and desalting process; significant analyte loss is common. Alternatively, size exclusion chromatography columns can be similarly used on-line for desalting and buffer exchange prior to ESI-MS. Analysis time can increase markedly;[83,84] small GF cartridges may be more time-efficient.[85] While applicable, GF is often time-consuming, provide limited recovery and increases the chance of sample contamination and degradation.

Solid-phase extraction (SPE) can also be used to desalt and purify proteins and peptides. A C_{18} -SPE sorbent retains peptides and proteins but not ionic salts and detergents.[86-89] Conversely, ion-exchange SPE may be used to selectively remove ionic compounds.[90,91] Combined hydrophilic and lipophilic sorbents reportedly provide high efficiency and high analyte recovery.[92,93] The use of SPE does however result in the use of additional solvents, added steps, or the need to implement column switching when deployed on-line. This adds to methodological complexities.

Microdialysis (MD) has been widely used to desalt proteins and oligonucleotides prior to ESI-MS. The sample is injected into the lumen of a MD fiber. Small molecules/salts dialyze out, while the large molecules remain. A very large counter flow of volatilizable species such as NH_4OAc is typically used when used with ESI-MS.[94-97] On-line MD allows interfacing ESI-MS with capillary isoelectric focusing[98,99] and other liquid phase separations.[71,100] Some dilution is inevitable in MD; small sample volumes can especially suffer. Recently, membraneless laminar

flow devices, similar to the H-filters/T-sensors[101] that rely on the diffusivity difference between the salt and the large protein, have been advocated. Benchmark performance of such a device is, e.g., 90% salt removal with 30% loss of protein.[102] An immiscible extractant that would selectively extract the salt or the protein[103] may perform better but such an extractant will have to be devised. Presently, MD would appear to be the method of choice.

Gregson and Simon[104] showed early that multistage electrodialysis can be used to remove salt from a mixture with various small MW (<600) drugs or amino acids. We recently developed a three-compartmented single stage electrodialysis device where a central channel is sandwiched between a cation-exchange membrane (CEM) and an anion-exchange membrane (AEM), with independent flow through each channel. Each outer compartment has an electrode disposed in it. When the CEM side, bearing an electrolyte A^+B^-, is held positive with respect to the AEM side, bearing an electrolyte X^+Y^-, the device behaves as an electrolyte generator. A^+ and Y^- are brought into the central channel and the electrolyte A^+Y^- is generated with Faradaic efficiency.[39,40] If the electrode polarities are reversed, the central channel is effectively deionized. The cations/anions respectively migrate under the electric field to the CEM/AEM compartments and leave neutral or low mobility species behind.[105] The present device demonstrates this principle. A flow-through on-line salt remover (SR) with a modest internal volume (2.5 µL) was constructed to be placed between a liquid chromatograph and an ESI-MS. The successful on-line performance of the SR placed ahead of an ESI-MS instrument was demonstrated with three benchmark proteins (myoglobin, cytochrome c, and lysozyme) in the presence of up to 154 meq/L NaCl solution and smaller concentrations of citrate and phosphate buffers.

3.2 Experimental Section

3.2.1. Reagents

Bovine heart cytochrome c, equine skeletal muscle myoglobin, and chicken egg white lysozyme were purchased from Sigma-Aldrich and directly used without further purification.

Other chemicals, including potassium nitrate, sodium chloride, methyl isobutyl ketone (MIBK) and methanol (all reagent grades) were from VWR. Solutions were prepared with 18.2 MΩ·cm Milli-Q (Millipore) deionized water.

3.2.2. Fabrication of Salt Remover

The device used in the majority of the experiments was based on ion exchange membrane discs that were readily replaceable. Some initial experiments were done with an ion exchange resin bead based device. The membrane disc-based device is schematically shown in Figure 3.1 and is described briefly below. Construction details of can be found in the Appendix B. The housing is a ¼-28 threaded chromatographic union. Nuts hold 6 mm dia. cation-exchange membrane (CEM) and anion exchange membrane (AEM) discs, separated by a 0.6 mm thick 2.25 mm i.d washer. Silica capillaries (180 μm i.d.) address the central cavity of 2.5 μL volume from opposite sides of the washer perimeter. Provisions were made to flush the outer side of each membrane (with 50 mM KNO_3 at 0.3 or 1 mL/min with a peristaltic pump except as stated) and also to provide each side with a platinum wire electrode (CEM side held at a negative potential). Experiments were carried out both at a constant applied voltage (XP-650 DC supply, www.Elenco.com) and more commonly at a constant current. The constant current source was based on an LM134 (National Semiconductor) integrated circuit, powered by the same above supply at 25V, to provide 100-500 μA to the SR. A current-voltage converter (SR570, Stanford Research Systems) was used to monitor the current. Control experiments were conducted without the SR (peak areas compared) or when accounting for dispersion, without power applied on the SR.

3.2.3. Experimental Arrangement

A syringe pump (P/N 54022, Kloehn) with a 1-mL or 250-μL glass syringe was used to pump water or NaCl solution as carrier via an electrically actuated injector (VICI, 1.94 or 2.5 μL loop) into the SR at stated flow rates. The SR effluent was sent either to (a) an on-capillary (185 μm

i. d., 345 μm o. d.) absorbance detector (CV^4, ISCO) operated at 280 nm followed by a conductivity detector (CD25, Dionex) provided with a homemade capillary cell or (b) the ESI

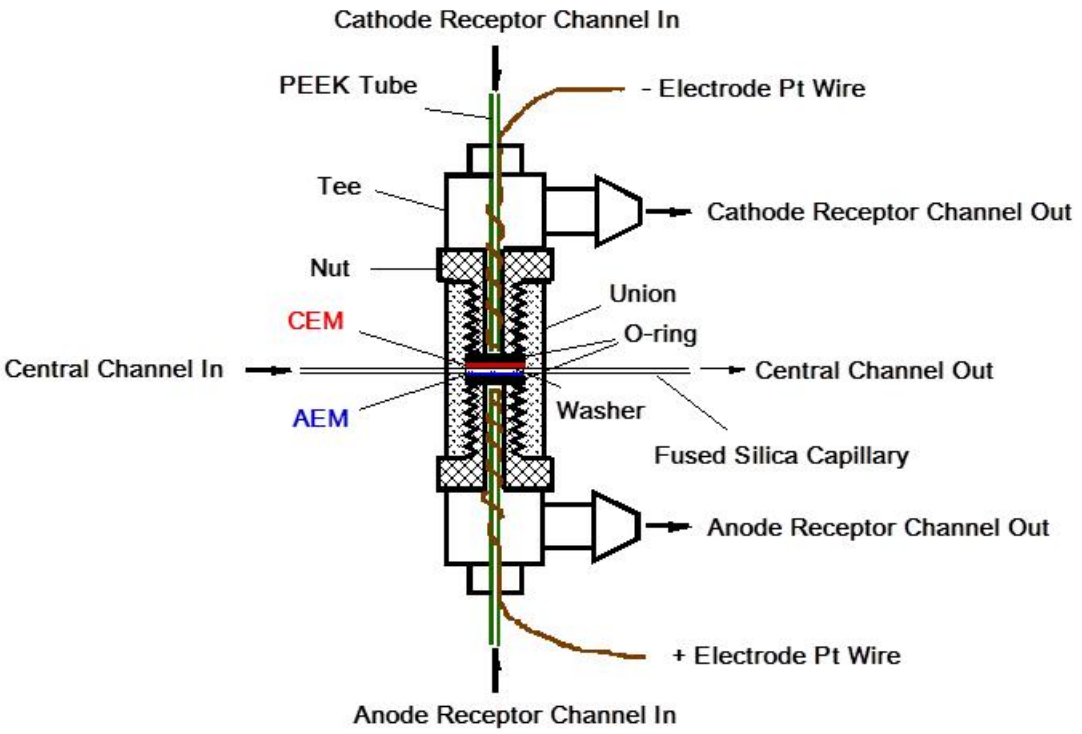

Figure 3.1 Membrane-based salt remover (SR), schematically shown.

inlet of an ESI - quadrupole ion trap – MS (LCQ Deca XP; Thermo-Fisher Scientific). Continuous flow of a saline carrier was used in all MS experiments at a constant flow rate of 1 μL/min. The proteins were prepared in the same saline carrier solution.

3.2.4. Mass Spectrometry

The instrument was operated in the positive ion mode. The electrospray voltage was typically 5.0 kV and data were acquired over 200-4000 Th. The transfer line capillary was maintained at 200 ℃. The mass spectra presented are averages of 40 sequential scans. For performance comparison, we also obtained mass spectra of the same proteins in 5 mM NaCl

injected as a plug into a carrier stream of water without using the SR (larger salt concentrations were not used to avoid having to clean the entire MS inlet system).

3.3 Results and Discussion

3.3.1. Microdialysis or Membraneless Dialysis vs. Electrodialysis

We wish to point out unique differences between electrodialysis (ED) and MD; to make absolute performance comparisons, comparably dimensioned devices have to be built. In principle, ion exchange membranes can sandwich a microfabricated channel as has been used in microdialysis.[106] Such a system will doubtless exhibit improved mass transfer characteristics. Whereas molecules with greater diffusivity are preferentially removed in membraneless dialysis, charged species of greater mobility are preferentially removed in ED. It is not possible to separate small MW uncharged species from ionic solutes in MD; this is readily possible in ED. Perhaps the archetypal example is to show removal of salt from a mixture with sugar. As sugar is optically transparent, we settled for a mixture of NaCl and MIBK (MW 100). NaCl responds exclusively to the conductivity detector while MIBK responds exclusively to the optical absorbance detector. As Figure 3.2 shows, with sufficient applied voltage, the device can completely remove the NaCl with little or no effect on the passage of MIBK. Figure 3.2 also shows the results of an experiment conducted with a similar bead device in which the NaCl was essentially completely removed from its mixture with BSA by 15 V applied, without much effect on the BSA signal. Ability to remove salt without removing low MW neutral analytes will be of value in MS-based pharmacokinetic studies that call for analyzing drugs and their metabolites in physiological matrices. It will be useful in detection schemes that look at aerosol charge or light scattering after evaporation.

Figure 3.2 data also indicate another difference between MD and ED based devices. Transport to the membrane in MD is diffusion-controlled. Other than increasing the diffusivity (e.g., by thermal means), this can only be affected by reducing the diffusion distance. While

minimizing distance to the membrane can benefit ED, there is a second means of control here. Electromigration velocity is directly proportional to the electric field strength.

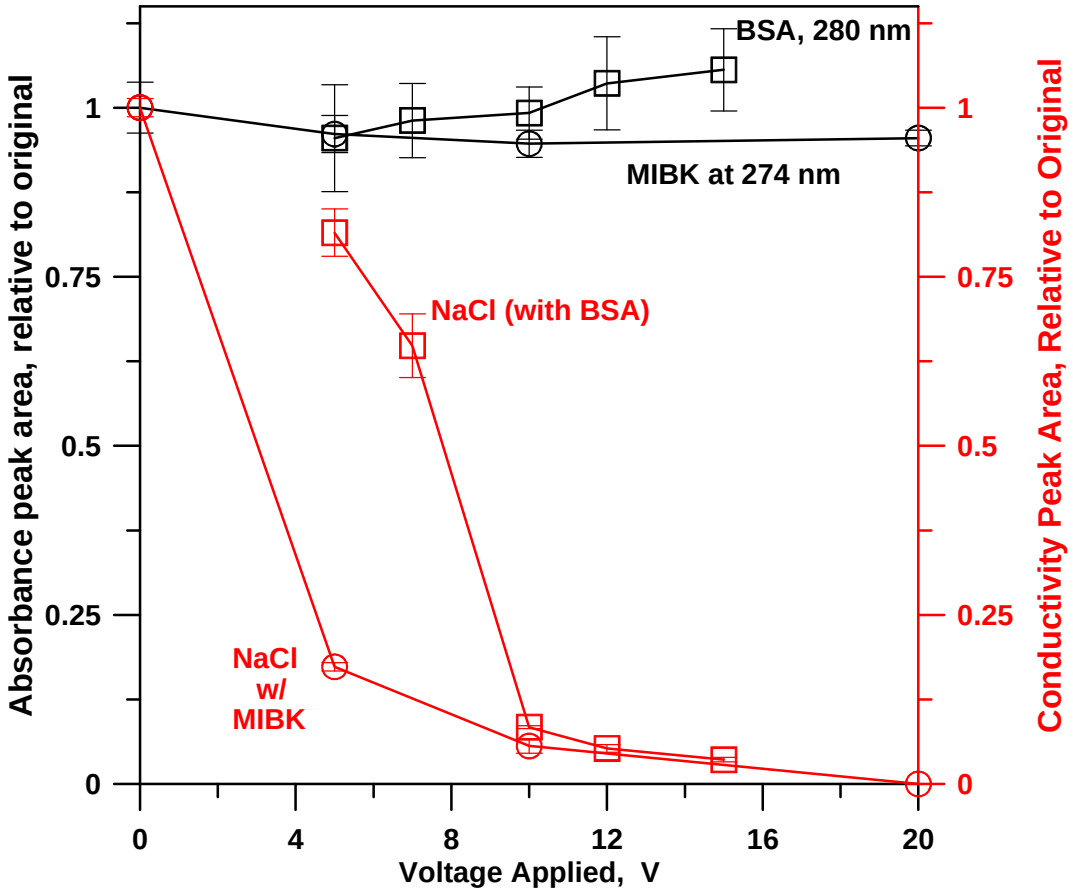

Figure 3.2 Removal of salt with an ion exchange bead based SR. Circles: Mixture of 2 mM NaCl and 10 mM MIBK injected, flow rate 4 μL/min, Squares: Mixture of 5 mM NaCl and 50 μM BSA, flow rate 15 μL/min. Note that BSA has some conductivity response. Injection volume 2.5 μL.

A third aspect is transportation from the exterior of the membrane to the bulk receptor. In MD, the rate of transport and thus the efficiency of removal are dependent on the concentration gradient across the membrane. When concentration polarization develops, the species transported to the exterior of the membrane are not efficiently removed from there. The concentration gradient across the membrane and the transport efficiency will decrease. Flow at

the boundary layer is stagnant by nature. As a result, very high receptor flush flow rates (several mL/min) have to be applied to the exterior of the membrane.[107] ED also requires avoidance of concentration polarization. However, there are two phenomena that mitigate this in ED. The presence of the electric field helps move the transported ions away from the membrane surface. The present device also has very small outer flow chambers. Electrolytically generated gas bubbles that form at the electrodes also create mixing that move material away from the membrane. The purpose of the receptor flow is not only to remove the transported ions but also to remove the gas bubbles to maintain electrical continuity. A modest flow rate of the receptor is sufficient.

3.3.2. Current is the Critical Indicator in ED

A properly-operated ED device operates largely in a domain where the amount being removed is linearly related to the current or more accurately, the charge in Coulombs or Farads passing through the system. However, the current efficiencies tend to be substantially lower than Faradaic; the micro-ED devices require appreciable voltages (up to tens of volts), and across a sub-mm gap, the resulting electric field and electrolytic removal of H^+ and OH^- is sufficient to cause enhanced dissociation of water.[106] When the current is carried by H^+ and OH^-, it does not contribute to salt removal and sub-Faradaic efficiencies result.

3.3.3. Pulse Removal Mode

One operational mode of the SR simulates operation with a mass spectrometer where column effluent flow is diverted to the MS only when the peak(s) of interest elutes. To simulate this, the salt-bearing protein sample is injected into a flowing water carrier stream that goes to a MS or other detector. A constant voltage is applied across the SR. The results in Figure 3.2 were obtained under these conditions. As the injected mixture passes through the SR and the salt ions are dialyzed out, they carry their charge to the electrodes and a current signal is generated at the same time the salt is dialyzed out. A given device operating at a particular voltage generally exhibits a constant efficiency in moles of salt removed per Farad charge

passed. This makes it possible to estimate from the current peak area how much of the salt is being removed without having to measure the conductivity of the SR effluent. At an applied voltage of 15 V, we measured the response from the conductivity detector placed after the SR at flow rates of 10, 15, and 25 μL/min and also measured the integrated peak current peak areas for 12.5 neq (5 mM, 2.5 μL) injected NaCl. Comparing the conductivity peak area of the sample without the SR and those of the effluent, 97.8%, 96.3% and 86.6% of the salt was removed at the three respective flow rates. The corresponding integrated current peak areas were 34.2±1.1, 33.6±1.5, and 30.3±1.6 nF. The computed Faradaic efficiency of the device is 34.2*.978/12.5 = 0.357 eq/F from the first set of data. In comparison with these data, the other two charge signals indicate removal efficiencies of 96.0 and 86.5%, in excellent agreement with the conductivity measurements.

3.3.4. Continuous Removal Mode

The device can also be used to continuously remove salt from a saline carrier, e.g. when it is connected between a chromatographic column and a MS or other detector. The device will typically need to deal with a constant salt flux, making constant current operation desirable. In addition, a thin membrane-based device, with readily replaceable membranes and more able to handle greater mass fluxes, will be more desirable than resin beads. Nevertheless, any given device can naturally remove a greater salt concentration in the briefly pulsed transient operational mode than continuously.

For the membrane-based SR in Figure 3.1, the relationship between current and continuous salt removal is shown in Figure 3.3 for various NaCl concentrations and flow rates. In all cases an initial linear slope is observed where the amount of salt removed per Farad of charge passed is constant. Given equivalent flux, this slope slightly increases with increasing salt concentration. Naturally, if sufficient salt-derived ions are present, H^+ and OH^- derived from water dissociation will not play a major role in carrying the current and will not much affect the observed current efficiency. At higher currents, the response curve attains a plateau because

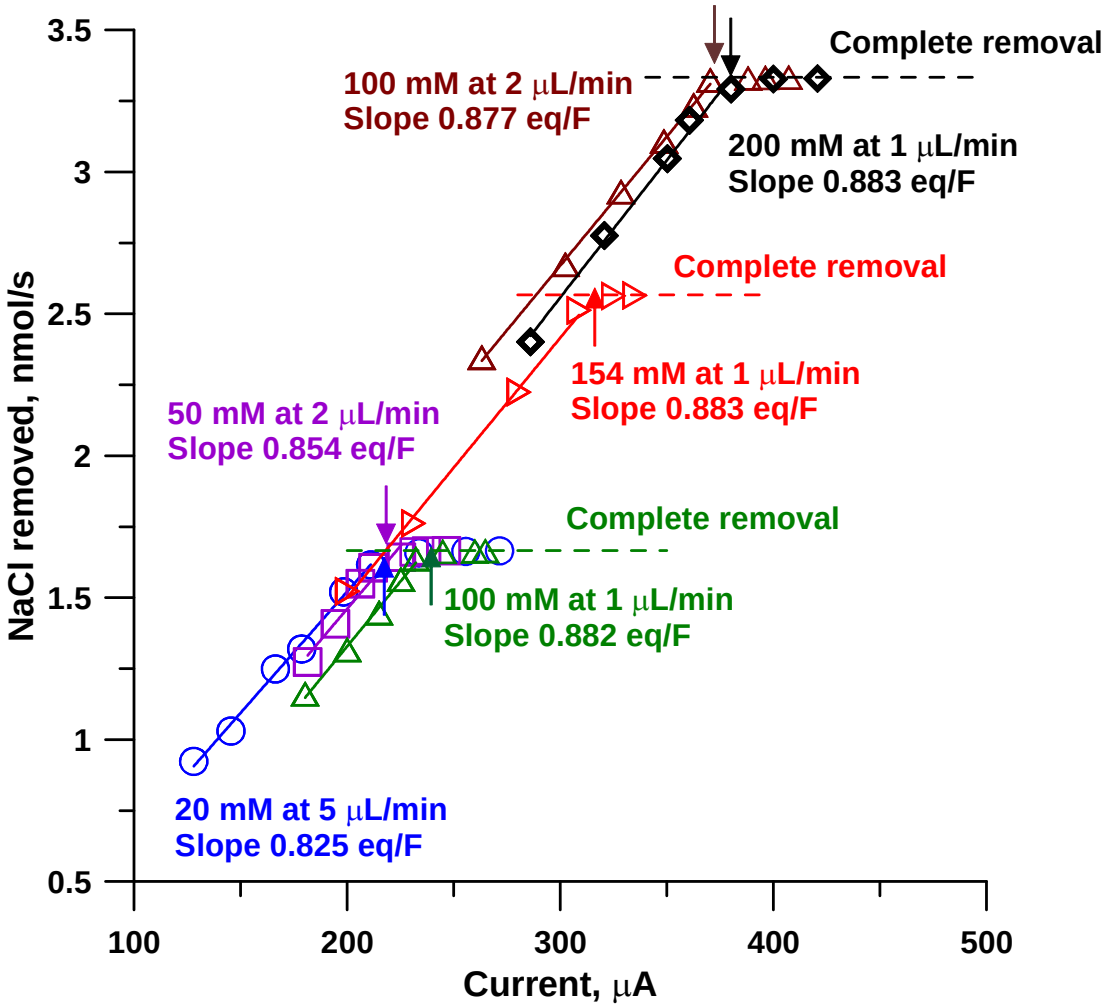

Figure 3.3 Current-Salt Removal relationship for different combinations of NaCl concentration and flow rate for the membrane based SR in Figure 3.1.

very little salt is left to be removed. Operation at the highest possible current (within the limits of heat-induced problems, see "Thermal considerations" in Appendix B) may seem desirable to remove the greatest amount of salt. However, an ED device only *preferentially* removes the salt. Proteins may carry a net charge depending on the pH and if the concentration-mobility product of the protein becomes comparable to that of the residual salt ions, it will travel to the corresponding membrane and be retained. The optimum operating current is located more or less near the intersection (indicated by arrows in Figure 3.3) of the two extrapolated linear

portions. Below this current, an undesirably large amount of salt may remain, and above it, protein removal may become significant and amount of salt further removed per unit current decreases. If operated much above the optimum current, there can be significant protein loss.

3.3.5. Salt Removal and Protein Transmission in Continuous Flow Mode

To examine the loss of protein due to adsorption to the membranes under the influence of electric field, an increasing current was applied until it was clearly above the optimum; currents in the 260-350 μA range was studied, where the current-salt removal curve gradually approaches the plateau and the protein loss starts to occur. At these applied current levels, sufficient salt is not present to carry the current; the proteins have to be the charge carriers. The three chosen proteins all carry some amount of charge under the operational conditions. As shown in Figure 3.4, the response of myoglobin starts to decrease when the applied current exceeds 300 μA while for lysozyme and cytochrome c, a similar onset of decrease is observed when the current reaches 290 and 288 μA, respectively. This is reasonable; based on their pI values, the latter two proteins will carry more charge at a neutral pH than myoglobin. However, loss as a function of current is not that different between myoglobin and the other two proteins. It is not only the charge that governs the migration of the proteins but also their mobilities. The current was simultaneously measured and was observed to remain constant throughout the process when the plug of the sample, prepared in the same saline solution as the carrier, passes through the SR (see Figure B.1 in Appendix B).

Fouling the membranes with proteins can have deleterious effects over time. The proteins can bind to the ion exchange sites and render them unavailable for salt transport. We found that one way to regenerate the membranes is to apply a reverse electric field (< 5 V, < 20 μA) to the electrodes while washing the SR with water at higher flow rates. After such regeneration, the SR typically works as well as with new membranes; in any case, ion exchange membranes are not especially expensive and are easily replaced.

For continuous removal of salt en route to an ESI-MS, with the SR operating at the optimum current, the salt input into the ESI is low enough to minimize the deleterious effect on spectra and loss of protein; a stable spray is also maintained. Based on experimental observations, a current of around 315 µA was chosen to be the optimized current for 154 mM NaCl at 1 µL/min, where loss of any of the proteins studied was less than 20 %.

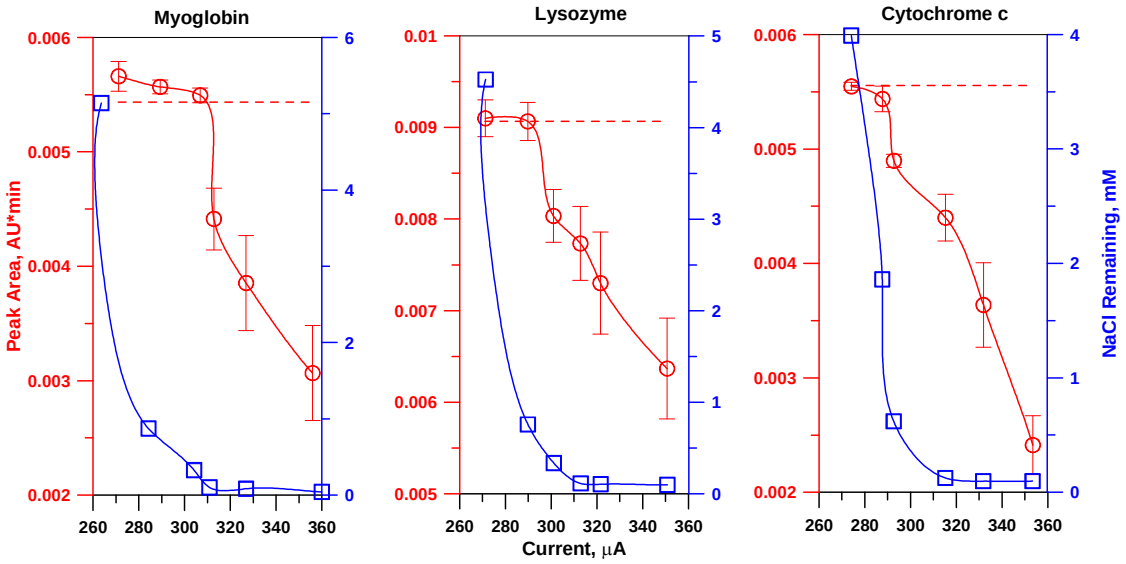

Figure 3.4 Absorbance peak area (in red) and amount of NaCl remaining in mM (in blue) as a function of applied current. Carrier: 154 mM NaCl, 1 µL/min; injection: 1.94 µL of 20 µM protein in 154 mM NaCl. Identity of protein is labeled on top of each figure. The red dashed line (-------) is the peak area obtained when the same concentration of protein in water was injected into the water carrier through the SR and the absorbance detector. The error bar indicates standard deviation (n = 3).

3.3.6. In-Line Desalting on ESI-MS in Continuous Flow Mode

The ability of the SR to continuously handle 154 mM NaCl (isotonic saline) at 1 µL/min was studied. The applied current was held constant at 315 µA. These conditions showed a background specific conductance of < 35 µS/cm, or <0.28 mM NaCl passing through, indicating 99.8+% removal. Note that in the ~5.5 min that it takes for the injected sample to traverse the 5.5 µL residence time between the injector and the spray needle tip, <0.55 nmol salt can

accumulate in the needle tip and thus affect the spectra. The spectra obtained with cytochrome c in 154 mM NaCl with the SR and 5 mM NaCl without the SR are shown in Figures 3.5(a) and (b), respectively. The major charge states are easily distinguished in 3.5(a) and it is an excellent match with the spectra shown in Figure 3.6(a), obtained without any salt. The spectra in Figure 3.5(b) in contrast exhibits increased baseline noise, extensive peak tailing and suppression of the analyte signal. The charge state can also shift towards higher m/z (see Figure 3.5(a) vs 3.5(b); B.4(a) vs. B.4(b) in Appendix B). Figure B.2 and B.3 in Appendix B present similar data for lysozyme and myoglobin. In Figure 3.6 we show that low concentrations of citrate and phosphate buffers (2.5 meq/L and 5 meq/L, respectively) are also equally well removed.

3.4 Conclusion

In summary, an in-line protein desalting method was demonstrated. It allows the charge-carrying salt ions to be removed from the central channel through ion-exchange membranes under the influence of electric field, allowing proteins to proceed on. The amount of salts removed is shown to be proportional to the current applied; this allows estimation of the amount of salt that is removed from the current peak generated, without having to measure the conductivity of the SR effluent. Protein loss becomes significant only at high currents, after most of the salt has been removed. Satisfactory salt removal performance was observed by obtaining ESI-MS spectra of myoglobin, lysozyme and cytochrome c in isotonic saline (154 mM NaCl) under continuous flow conditions after they passed through the SR under optimum applied current.

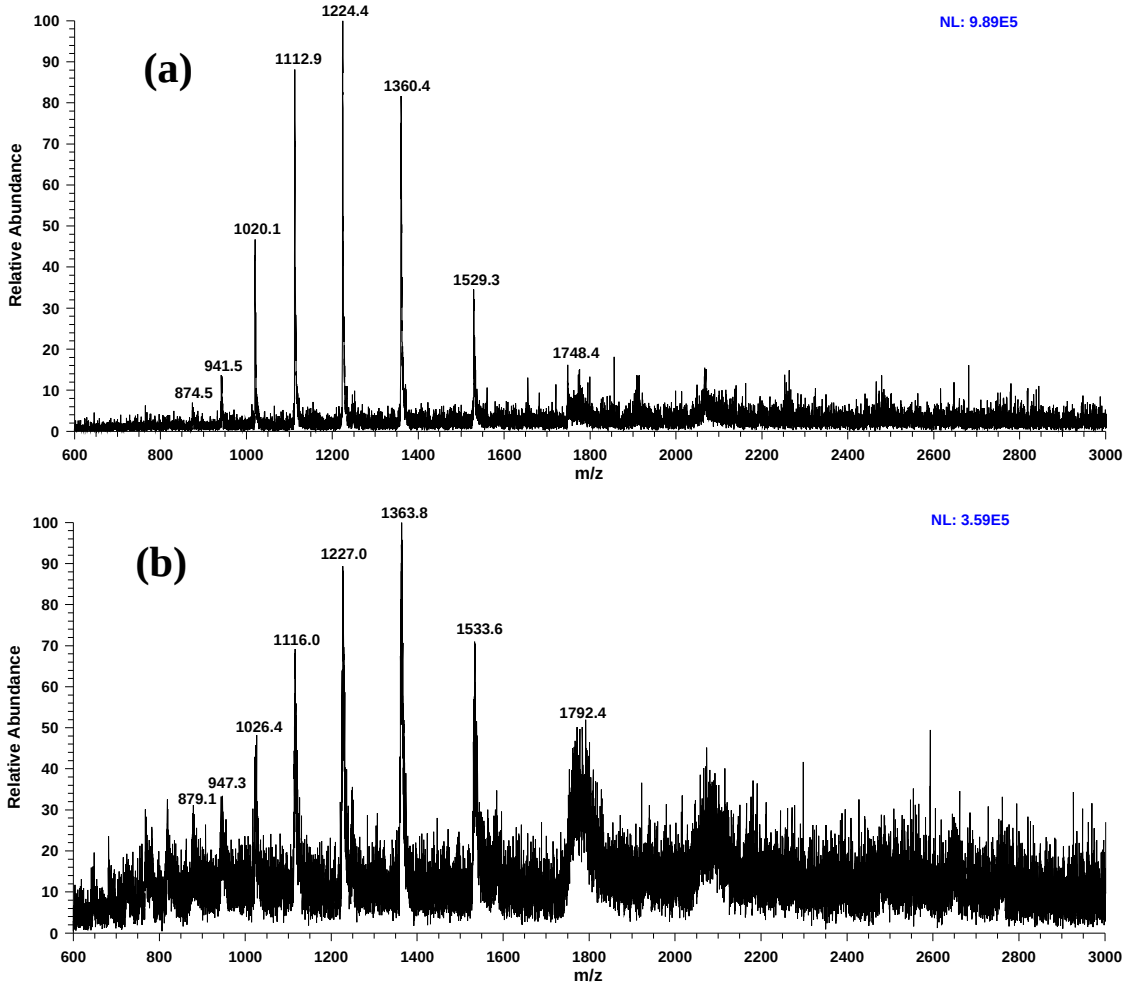

Figure 3.5 Positive ion ESI mass spectra of (a) 10 μM cytochrome c in 10% (v/v) methanol aqueous solutions containing 154 mM NaCl, with SR operated at 315 μA; (b) 10 μM cytochrome c in 10% (v/v) methanol aqueous solutions containing 5 mM NaCl without SR respectively. Flow rate: 1 μL/min; Injection volume: 1.94 μL.

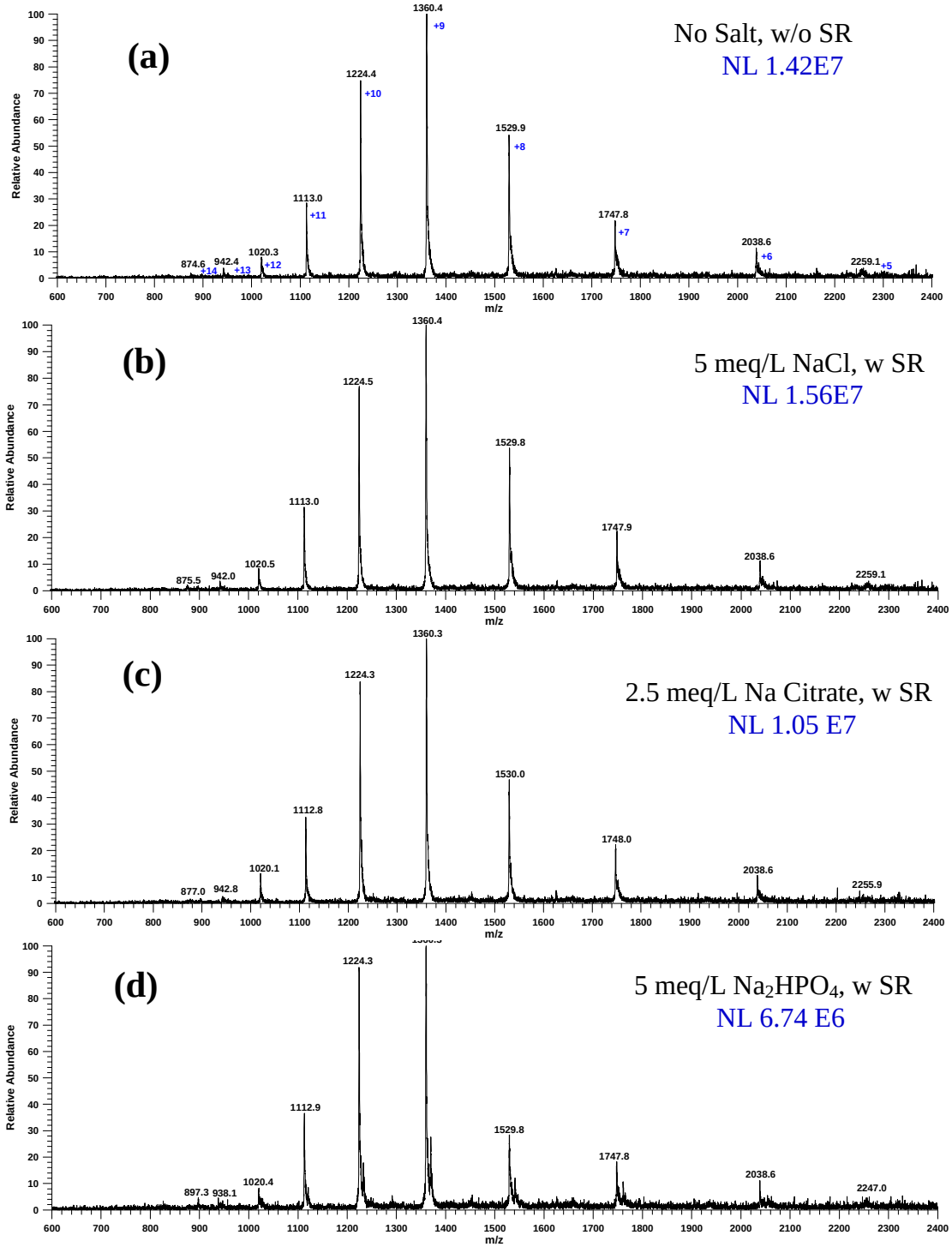

Figure 3.6 ESI-MS spectra of 10 μM cytochrome c in 10%methanol (a) as such, (b)-(d) also respectively containing 5 meq/L NaCl, 2.5 meq/L Na_3 Citrate and 5 meq/L Na_2HPO_4, all passed through the

CHAPTER 4

ELECTRODIALYTIC MEMBRANE SUPPRESSORS FOR ION CHROMATOGRAPHY MAKE PROGRAMMABLE BUFFER GENERATORS

4.1 Introduction

Buffers are of paramount importance in chemistry and biology. Buffers resist the change in activity/concentration of a specific ion when agents that would otherwise affect its concentration are added (or removed e.g., by precipitation or volatilization). While the term usually refers to pH buffers, metal ion buffers are also in common use. In most living systems, buffering mechanisms exist to control pH within tight limits: Arterial blood pH for a healthy human ranges from 7.35-7.45[108] and almost within the same range for all terrestrial mammals. For a living organism, pH of each (sub)cellular compartment must be precisely controlled so that each reaction proceeds at the proper rate.[109,110] Similar pH control is needed in myriad other processes, e.g. in organic synthesis, where a pH electrode is used for pH measurement and constitutes part of a feedback system to add acid or base to maintain the pH at a preset level.[111] The use of such pH-stats is so common in biochemistry that 50+ year old reviews exist.[112] It has also long been realized that a constant pH can be maintained by electrochemically generating H^+ or OH^- *in-situ*, rather than physically adding acid or base. For feedback, the pH can be measured directly by a pH electrode[113] (or better, after appropriate electrical isolation[114]) or photometrically via an indicator.[115] Historically, the intent was often to follow the amount of acid or base generated by an enzymatic reaction at constant pH, the amount of base or acid needed and electrochemically generated to neutralize this was then coulometrically available. Some 50 years after the initial work,[114] Gratzl, with his admirable penchant for working with tiny drops, have demonstrated the ability to achieve the same ends in a single 20 μL hemispherical drop.[116]

In biology/biochemistry, buffers based on phosphate, tris(hydroxymethyl) aminomethane (Tris) and citrate are among the most common. From capillary electrophoresis[117] to microbial fuel cells, [118] where H^+ and OH^- are electrolytically generated at the electrodes, consistent performance cannot be obtained without buffers.

A particularly important use of buffers is as eluent components in liquid chromatography (LC), especially for ionizable compounds, this includes virtually all bioanalytes.[119,120] Degree of ionization control the retention of ionizable compounds. Even small changes in eluent pH and ionic strength (in addition to organic solvent content) can dramatically affect retention and efficiency, thus affecting the selectivity, peak shape, resolution and reproducibility. [121] Measuring pH in mixed hydroorganic solvents is problematic. Theoretical computations are not straightforward and are typically of limited value. [122 , 123] The merit of pH-gradient liquid chromatography, with[124,125] or without[126,127] a concurrent solvent gradient has recently been highlighted in a series of remarkable papers by Kaliszan et al: A theoretical framework has been constructed;[128] it has been shown that pK_a values of analytes can be obtained by such a technique.[129]

Ion-exchange chromatography of proteins has also long relied on buffers and pH gradients. A linear pH gradient for the mobile phase in conjunction with a weak anion-exchanger stationary phase was termed *chromatofocusing;*[130] proteins elute in the order of their pI. This has also been demonstrated in the capillary scale.[131] Concave and convex pH gradients may also have merit.[132] pH gradient separations with low MW buffers has been pursued[133] and attractive separations of monoclonal antibodies demonstrated. [134] Both pH and buffer concentrations have a profound effect.[135] pH gradients during chromatography are generated by blending two or more different solutions. It is generally not straightforward to independently control both pH and buffer concentration.

Manipulations of pH by electrolysis as carried out in the electrochemical pH-stats result in electrolytic gas evolution. Depending on the specific experimental system this may or may

not be detrimental. In electrodialytically induced ion exchange or acid/base introduction, gas evolution can be isolated from the fluid of principal interest. The best known embodiment of this is the dual membrane suppressor used IC.[136,137] In a typical application, an eluent MX flows in a central channel bounded by two cation exchange membranes (CEMs) and water flows on the exterior of each CEM. With an electrode each placed in each outer channel, the M^+ ion (typically K^+ or Na^+) is removed to the negative electrode chamber while H^+ generated in the positive electrode chamber comes into the central channel to make HX (X^- typically being OH^-, HCO_3^-, $^1/_2CO_3^{2-}$, $B(OH)_4^-$, etc.). The suppressor explicitly accomplishes *quantitative* exchange of MX to HX. Indeed, it is critical that it does so because the detection limits are directly related to the stoichiometric completion of the exchange process.[138] The evolution of suppressors, from packed columns to chemically regenerated membrane devices through the early current-inefficient electrodialytic units reflect a history in which the only extent of exchange that could be precisely reproduced was quantitative exchange. The present generation of suppressors has very little or no ion exchange capacity in the central channel and operate in a near-Faradaic manner.[50] But the need to achieve stoichiometric exchange has not changed; overdriving such suppressors do not lead to lower background conductance but greater noise and can cause loss of certain amphoteric analytes in the suppressor.[139]

For strong acids and bases used most commonly as eluents in present-day IC, subquantitative exchange would not lead to a buffer. But for eluents like $NaHCO_3/Na_2CO_3$ or $Na_2B_4O_7$, adjustable subquantitative exchange would have adjusted the pH of the respective buffer systems, albeit the accessible pH values would have only been in the alkaline range. These eluents are typically used in low mM concentrations, substantially lower than what would be used for a typical buffer. They gradually become nonconductive as exchange occurs. This makes accurate control of exchange difficult while maintaining current efficiency when much of the cation has been exchanged. It would otherwise be obvious that if HX is a weak acid and a solution of MX is pumped through a CEM-based suppressor, substoichiometric cation exchange

will be able to produce adjustable pH buffers under electrical control. Whether because of the above reasons or our collective myopic focus solely on quantitative suppression, this has never been attempted.

Herein we discuss the operation of electrodialytic membrane suppressors used in IC as electrodialytic buffer generators (EBG's) and their nature and characteristics when so operated.

4.2 Principles

Consider the schematic in Figure 4.1a. A solution of the fully neutralized Na salt of a *n*-protic acid, Na_nX, is influent into a CEM-based suppressor and the Na^+ is at least partially electrodialytically removed by current *I* and replaced. For simplicity we assume a NaX-HX buffer system but the general scheme is applicable to corresponding multiprotic acid-base systems. *C M* NaX flows through the central channel at *Q* mL/min while a current *i* mA is made to flow through the system. Under conditions when significant concentration of non-H^+/non-OH^- ions remain to be transported, the efficiency of present suppressors can be taken to be Faradaic. At steady state, 0.06 *i*/*F* moles/min of Na^+ is removed to the negative electrode compartment from the center and an equal amount of H^+ from the anode compartment is introduced. This amounts to HX formation in the center channel equal to 60 *i*/*FQ M*, while NaX concentration drops to *C* **-** 60 *i*/*FQ M*. Neglecting activity corrections for the moment, the pH is then simply computed from the familiar Henderson-Hasselbalch equation as:

$$pH = pK_a + \log (CFQ - 60\, i)/60\, i \quad \ldots(4.1)$$

This is usable in the range when an appreciable amount (e.g. >5%) of HX has formed but also an appreciable amount of NaX remains (and $[Na^+]$ still remains >>$[H^+]$). At low pH if $[H^+]$ in the central channel becomes comparable to $[Na^+]$, we can no longer assume that Na^+ transport is the sole Faradaic process. Also, at high HX values, HX can be lost through the ion exchange membranes as there are no barriers towards the transport of neutrals. However, there is no influence of the electric field on the electrical transport of a neutral species and the loss through the membrane, driven by the concentration difference, in most cases is not large. Such losses

can also be avoided by using a buffer system based on a multiprotic acid/base. For example if *C M* Na_3PO_4 or Na_3Citrate is introduced into the system, current controlled H^+-Na^+ exchange can create an adjustable pH buffer system. There will be no loss of the neutral acid until significant amounts of the free acid forms at the high end of the exchange. For the general case of the introduction of the *C M* solution a fully neutralized salt (M_nX) of an *n*-protic acid (H_nX) being introduced into the system, the charge balance equation is:

$$\left(nC - \frac{60i}{FQ}\right) + [H^+] - \frac{K_W}{[H^+]} - pC\sum_{p=1}^{n}\alpha_p = 0 \quad \ldots(4.2)$$

Where the first term indicates the remaining M^+ concentration and α_p indicates the fraction of the total anion that exists with a charge of *p*-. The general procedure for solution, including activity corrections, is given in the Appendix C.

An EBG based on a weak base and its salt proceeds very much the same way. The general case is that of a base which can take up upto *n* protons and a solution of the fully neutralized salt BH_nY_n is influent into an AEM-based suppressor. Some (or all) of the Y^- is removed to through the AEM to the anode compartment while an equal amount of OH- enters from the cathode compartment to neutralize H^+ (Figure 4.1b). For the simple case of a monoacidic base B and its salt BHY, eq 4.1 still applies with K_a being the acid dissociation constant of BH^+ and the sign of the log-term reversed:

$$pH = pK_a - \log (CFQ - 60\,i)/60\,i \quad \ldots(4.3)$$

The use of a multiprotic base will avoid loss of the free base and the applicable equation will be similar to eq 4.2.

A suppressor based EBG has the advantage that the device is commercially available and many commercial ICs allow current programming of the suppressor. In principle, no gas is evolved in the fluid channel of interest. The buffer concentration is fixed; a constant buffer ion concentration is maintained while pH is adjusted by applying controlled removal of the counterion. The approach can thus be thought of as subtractive. While the counterion is subtracted, H^+ or OH^- (as appropriate) takes its place to maintain charge balance. It is

interesting to note that the system is not operationally symmetric: It is possible to introduce Na_2HPO_4 and render it into NaH_2PO_4 quite effectively and efficiently by removing Na^+, but it is not possible to predictably and efficiently convert NaH_2PO_4 into Na_2HPO_4 by current controlled Na^+ introduction from the anode compartment; this will result in an equal amount of sodium being lost to the cathode compartment. This does not mean, however, that a temporally increasing pH gradient will not be possible with a CEM- suppressor based EBG with a phosphate buffer. Such a system will use a temporally negative current gradient.

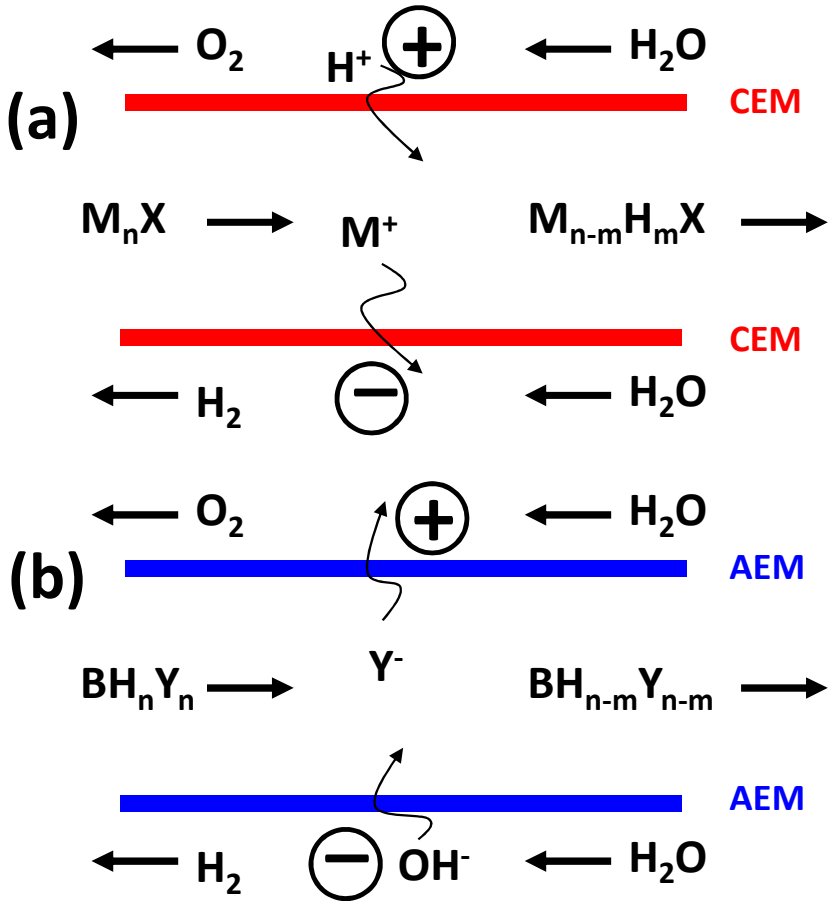

Figure 4.1 EBG scheme with (a) an anion suppressor (a dual CEM device) with the strong base salt of a multiprotic acid as the feed solution and (b) a cation suppressor (a dual AEM device) with the strong acid salt of a multiprotic base as the feed solution. The drive current controls how much of the strong base cations in a and the strong acid anions in b are respectively removed of the system thus attaining the desired pH.

4.3 Experimental Section

4.3.1 Reagents

All chemicals were commonly available reagent grade and distilled deionized water was used throughout. See Appendix C.

4.3.2 Electrolytic Buffer Generators

ASRS Ultra II and CSRS Ultra (both 4-mm, www.dionex.com) were used as EBG's. Electrolyte solutions were delivered by an ICS2000 IC pump through the eluent channel; water was peristaltically pumped (Gilson Minipuls 2) through the regenerant channels. The suppressor current was software programmed (Chromeleon V.6.60). The conductivity of the generated buffer solutions are much higher than the typical solutions measured by our conductivity detectors. To keep the conductance in the measurable range, we prepared high cell constant (6400 cm^{-1}) flow-through detection cells (two tubular electrodes separated by a spacer tube) coupled to a Dionex CD25 conductivity detector. The pH was measured after two point calibration with standard buffers. Because of concern that applied voltage in the EBG or the preceding conductivity detector may affect in-line pH-measurement, much of the initial pH measurements were made by applying constant current steps and collecting the device effluent in discrete aliquots. Since monitoring results of a programmed current profile was not practical this way, a narrow long tube was connected between the conductivity cell and the home-built pH flow cell. Experiments established that the measured pH is the same in collected aliquots and in an in-line arrangement; pH was measured in-line henceforth. However, the volume of the tubing between the conductivity flow cell and the pH electrode flow cell, the significant volume of the latter, the slower response of the pH electrode all combine to produce a slower pH response compared to the conductivity change.

4.3.3 Removal of Micro Bubbles

Although no gas is formed in principle in the central channel, much gas is formed in the outer channels, especially at high operating currents. The central channel liquid thus becomes

saturated with the electrolytic gas (which readily permeates the membranes). In the absence of significant backpressure, micro bubbles are formed in the detectors, the frequency of such bubbles predictably increasing with applied electrodialytic current. An example is shown in Figure C.1 in the Appendix C. We chose therefore to remove the gas from the central channel. Gas collection with a tubular porous membrane was first described 25 years ago[140] and removal of gases by the reverse process shortly thereafter.[141] We presently used a commercially available carbon dioxide removal device (CRD 200-4mm, Dionex) immediately after the EBG, with both of the external jacket (regenerant) inlet/outlets of the CRD tied in common by a tee and connected to house vacuum (~180 Torr). While the CRD[142,143] is designed for dissolved CO_2 removal, with vacuum applied, it can remove dissolved as well as physically present gas bubbles.

4.4 Results and Discussion

4.4.1 Behavior of a Phosphate EBG

Figure 4.2 shows the measured effluent pH (filled circles, left ordinate) for a CEM-suppressor system with 68 mM Na_3PO_4 as feed. The current vs. effluent pH profile exactly reflects the plot for a coulometric titration, which it really is. Rather than a fixed solution volume, there is a constant flow rate; hence the appropriate control variable is current, rather than charge.

We also theoretically estimated the pH. Details are given in the Appendix C. Briefly, the following sequence was used: (a) estimate the ionic strength (I) of the solution, (b) compute individual ion activity coefficients from the Davies equation,[144] (c) for each applicable constant, compute the applicable equilibrium constants in terms of concentrations, (d) express individual ionic concentrations based on these constants and H^+, (e) solve the relevant charge balance equation that contains all ions in solution for H^+ using Microsoft Excel Solver™, (f) compute all ion concentrations (g) cycle through a-f until convergence, (h) calculate the activity coefficient of H^+, a_{H+}, and activity-based pH. The theoretically calculated pH is represented as a

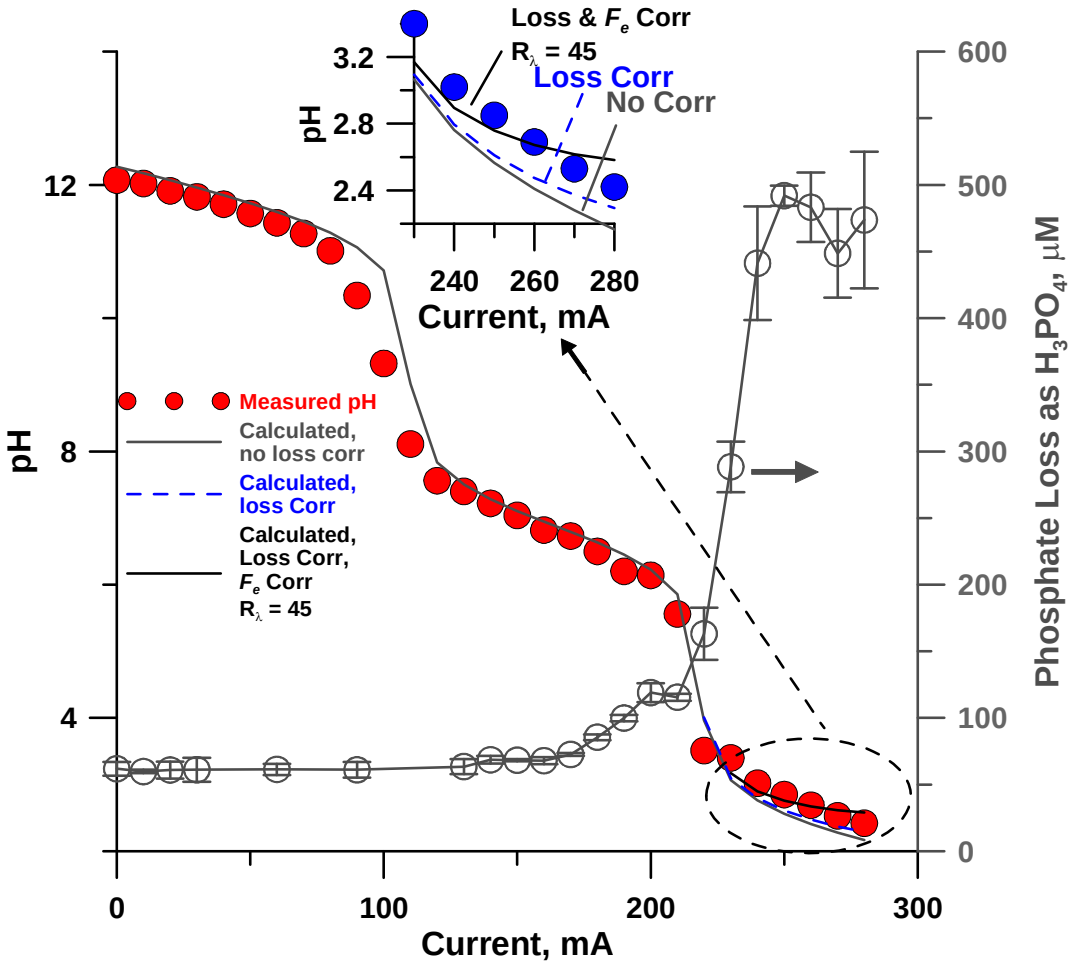

Figure 4.2 pH as a function of applied current for 68 mM Na_3PO_4, CEM Suppressor (ASRS Ultra II (4-mm) 1 mL/min. The hollow circles (right ordinate) represent the concentration of the total phosphate lost through the membranes determined by IC analysis of outer channel effluent. The bottom right is shown in magnified form in the inset. The lines in the pH traces indicate computed values. See text for an explanation for the different computations.

solid gray line – it is slightly higher throughout the alkaline pH range compared to the measured pH values. This difference is ascribed to discrete collection and measurement in room air and consequent exposure to CO_2. On the other hand, at the low pH end, the theoretically computed pH values fall below the experimental values. While the negatively charged membranes effectively inhibit the loss of negative ions, there is no barrier towards the transport of a neutral molecule. There is a small but perceptible loss of PO_4^{3-} as H_3PO_4 throughout the entire

operating range. The amount lost was measured by IC and is shown in terms of the central channel concentration as hollow circles with error bars in Figure 4.2 (right ordinate). Note that the highest loss (lowest pH) amounts to 0.7% of the total phosphate, not a significant amount. Also this occurs at the extreme end where it is not likely to be used as a buffer. In a suppressor, the two outer electrode channels are fluidically tied together; it is not possible to experimentally determine via which membrane the loss primarily occurs. However, logically it must be primarily through the anodic membrane, as PO_4^{3-} is directed electrically to this membrane and the H^+ generated keeps the membrane in H^+-form. Therefore H_3PO_4 must be present as a thin layer at the internal surface of the membrane. The pattern of the loss is consistent with this view: the loss is low and essentially constant over a large current range and then starts increasing as $H_2PO_4^-$ begins to be titrated to H_3PO_4 in the final step and H_3PO_4 begins to be formed in significant concentration in the bulk solution. Incorporating this loss of H_3PO_4 into our computations (blue dashed line) make a difference only at the lowest pH end and brings the theoretical values closer to the measured values but still remain lower than the measured values.

Another factor to be considered at low pH is that the Faradaic efficiency (F_e) for Na^+ transport may not remain unity. In a CEM-based suppressor, current is carried by all cations, both Na^+ and H^+. When $[H^+]$ is no longer negligible relative to $[Na^+]$, the fraction of the current carried by Na^+ or F_e will be given by:

$$F_e = \frac{\lambda_{Na+}[Na^+]}{(\lambda_{Na+}[Na^+])+(\lambda_{H+}[H^+])} = \frac{1}{(1+ R_c R_\lambda)} \quad \ldots(4.4)$$

where λ_i is the equivalent conductance (proportional to ionic mobility) of ion *i* and R_c and R_λ are, respectively, the concentration ratio and the mobility ratios of H^+ and Na^+. The infinite dilution R_λ value in solution, 6.98, is readily computed from known values for λ_{Na+} and λ_{H+}. This provides at least a first approximation value to use in the computation; the exact F_e value is also dependent on the selectivity coefficient (that governs membrane uptake) and relative transport speeds in the membrane. Available evidence[145] suggests that in the membrane itself (which

may be the limiting element), the mobility ratio of H^+ to Na^+ may be much greater than in free solution. In either case, the applicable form of eq 4.2 is:

$$\left(nC - F_e \frac{60i}{FQ}\right) + [H^+] - \frac{K_W}{[H^+]} - pC \sum_{p=1}^{n} \alpha_p = 0 \quad \ldots(4.5)$$

Using nonunity F_e that results from a R_λ value of 7 we calculate values at the low pH end that are numerically higher than the values where only H_3PO_4 loss is accounted for. But the difference is too small to be discerned in the scale of Figure 4.2, even in the magnified inset view of the low pH end and hence was not plotted. However, if we keep increasing R_λ values, agreement at the low end pH keeps getting better (note that this correction has no effect on pH$\geq$4.) but by the time R_λ is made 45 (plotted as solid black line, see Figure 4.2 inset), one is perceptibly overcorrecting relative to the lowest measured pH. We conclude that nonunity F_e plays a role that is only of significance at the near-quantitative exchange end; this is of limited interest in buffer generation applications.

4.4.2 Reproducibility and Response Time

Figure 4.3 shows both conductivity and pH traces for a programmed current ascending and descending step gradient for the same phosphate system over four cycles. The system does exhibit some hysteresis. The membranes have significant ion exchange capacity and their ionic status depends on previous history and current flux. This creates a difference between the same current steps on ascending vs. descending profiles. Details are given in Tables C.1 and C.2 in Appendix C. However, absolute conductance values at either ascending or descending current steps are repeatable (0.30-0.43% rsd, average 0.36% rsd), the conductance values being slightly (0.14-0.38%) but perceptibly higher than descending current steps. Similar results are observed for pH: pH values for ascending steps being slightly (0.05-0.10 units) higher and the reproducibility within each type of step being within 0.005 to 0.05 pH unit. Response times to step changes in current were calculated from the conductivity detector response (as the pH electrode response is slower) and appears to depend on the status of the membrane. In ascending current steps, conductivity decreases and the 90-10% fall times for 0-40, 40-80, 80-

120 and 120-160 mA steps were 2.54 ± 0.27, 2.07 ± 0.09, 1.60 ± 0.07 and 0.95 ± 0.03 min, while the 10-90% rise times for 160-120, 120-80, 80-40 and 40-0 mA steps were 0.68 ± 0.06, 0.92 ± 0.15, 2.12 ± 0.05 and 3.43 ± 0.10 min, respectively. The response is clearly faster at high currents when much of the membrane is in the more labile H^+-form and faster during descending current steps, which calls for less transport through the membrane. This suggests that the primary process that limits the response time is transport through the membrane. The response time may thus be faster where smaller current changes demand a small transport change, as in generating a pH gradient over a period of time. Detailed results are given in Figure C.2, Tables C.3 and C.4 in the Appendix C for a current step of 2 mA (104 ⇔102 mA) for the same system. In this case, the respective 90-10% fall and 10-90% rise times for the conductance signals were lower and were more comparable to each other. They ranged from 0.61-1.41 and 0.72 ± 1.85 min, respectively.

4.4.3 Other Buffers

Figure 4.4a shows results for 50 mM trisodium citrate as the influent solution with the same CEM-based suppressor system. Since citric acid has three closely spaced pK_a values (3.13, 4.75 and 6.40), individual titration steps are not observed; rather, a nearly linear gradient in pH (from 6.5 to 3) is seen. Citric acid is a substantially larger molecule than H_3PO_4. We have previously observed that under otherwise identical conditions, transport of citrate through an AEM is slower than phosphate.[146] Since the loss of phosphate through the membrane was small and hardly affected the calculated pH, we did not measure citric acid loss and calculated pH without any loss assumption. It can be observed that the measured pH begins to significantly deviate from the computed values only below a pH of ~3.5.

Also in Figure 4a is the behavior of a Tris-based buffer system with an AEM-based suppressor system. With a pKa of 8.1, it provides useful buffering in biologically important buffering range of 7-9. Loss of Tris as a free base was not measured. The computed pH of the

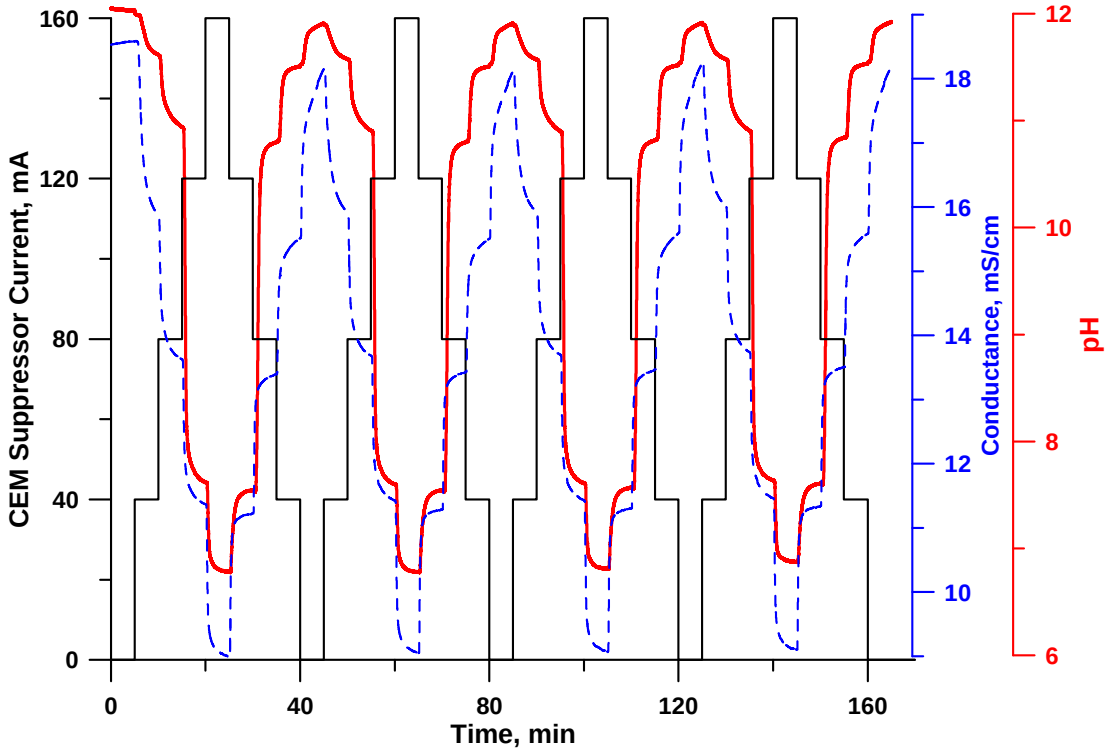

Figure 4.3 Step gradient response. Four cycles are shown for a Na_3PO_4 feed CEM suppressor system with an inflent dflow of 1 mL/min. Current steps are 0→40→80→120→160→120→80→40→0 mA (solid black), pH response is in the thicker line (solid red) and conductivity response is the dashed line (blue).

initial solution is lower than the observed value, the commercial product that we assumed to be the pure hydrochloride likely contains a small amount of the free base. Thereafter the computed and observed values of pH agreed well up to pH ~9 (current ~200 mA). The point at which the theoretical and observed values begin to differ is where the last of the HCl is removed: the observed values show a much more gradual transition than the sharp change seen in theory. The calculation does not take into account any intrusion of dissolved CO_2 from the outer compartments to the center or during collection and measurement.

The two respective pKa values of the ethylenediammonium ion are 6.85 and 9.93. Both titration steps are observed, and the computed pH again agree with the observed pH over much

of the useful buffering range. This establishes that the principle is equally applicable to multiprotic cationic (basic) buffer systems.

4.4.4 Electrodialytic Generation of a Large Range Linear pH Gradient

Leithe[147] was the first to devise "linear buffers"[148,149] for "single point titrations". The idea was to determine the concentration of a strong acid or strong base by simply adding an aliquot of it to a fixed volume of such a specially prepared buffer mixture and measuring the pH change. The buffer composition will be such that the pH change will be linearly related to the amount of the acid or the base added. Polyprotic acid-base buffering systems and mixtures thereof have been both theoretically and experimentally studied for the purpose;[150] and at least two "polybuffers" based on polyampholytes that accomplish this over a limited pH range are commercially available[151] (these are expensive: present cost is >$1/mL). Efforts to develop buffer compositions with multiple low MW species are given in a number of the papers cited in the introductory discussion on *chromatofocusing*. Instead of chromatography, the area of interest may be high-throughput pK_a measurement.[152] However, a common desired goal is a linear pH gradient. In reality what has been demonstrated is rather limited either in terms of an extended pH range or linearity. In flow applications, including chromatography, a further desired requirement must be to maintain a constant flow rate for a binary component mixture; otherwise a ternary or more complex gradient including a diluent will be needed. Box et al. describe mixing of two solutions, each consisting of six components, to achieve a linear gradient. Although data were not shown for the (linear) composition change vs. actual pH, between pH 3 and 11.6 the linear r^2 value between the computed and measured pH was stated to be 0.99.[153]

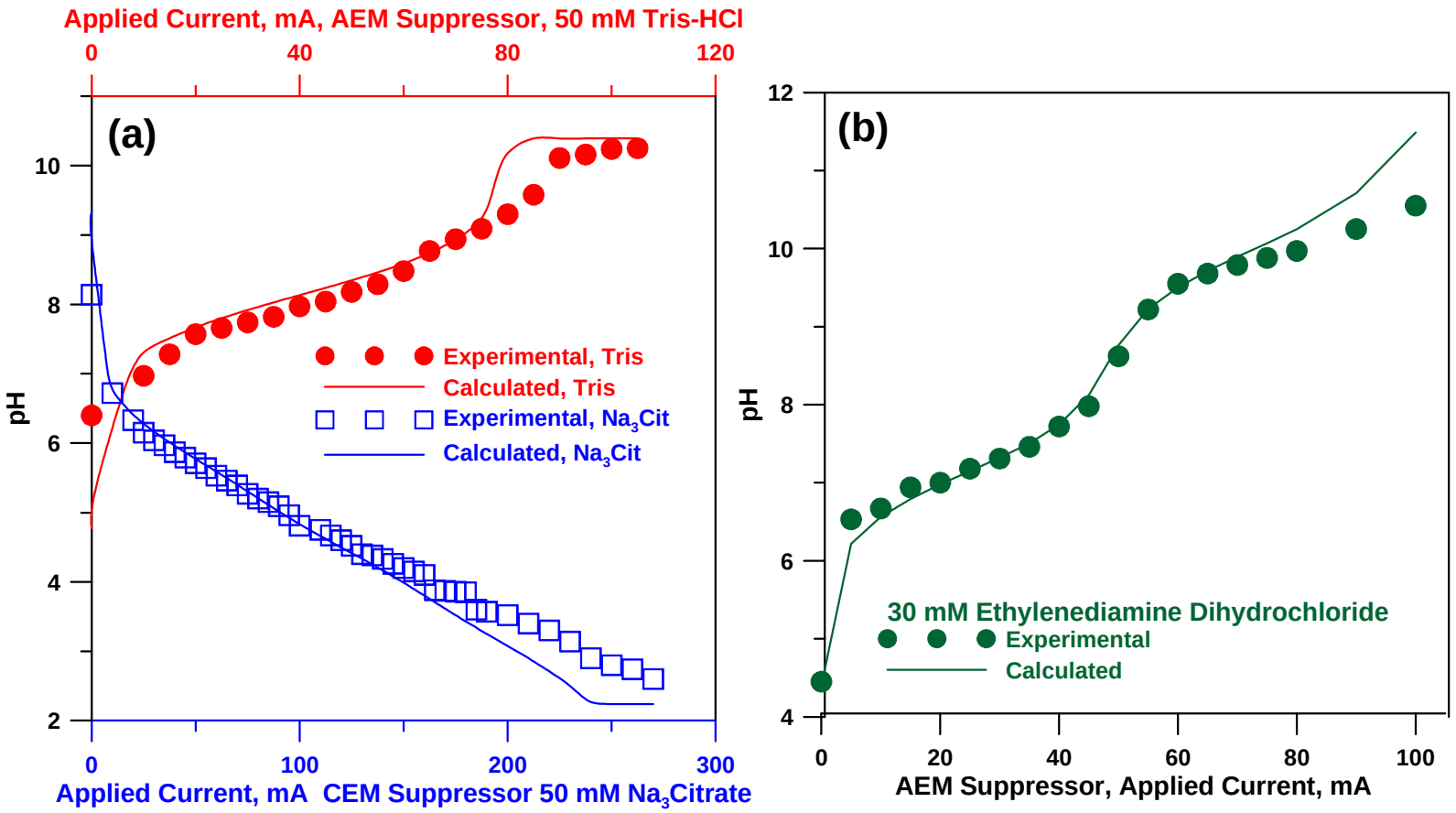

Figure 4.4 pH as a function of drive current for (a) 50 mM Na_3Citrate as the feed solution (ASRS Ultra II, 4-mm) and 50 mM Tris-HCl (CSRS Ultra, 4-mm), and (b) 30 mM ethylenediamine dihydrochloride (CSRS Ultra, 4-mm), all at 1.00 mL/min. The solid lines represent computed pH values, see text.

Any buffer system generated by an EBG that generates a pH gradient with one or more buffering species is unlikely to produce a linear pH gradient that is driven by a linear current gradient, unless previous "linear buffer" compositions are adopted. Otherwise one ends up revisiting the same computation-composition experimentation-pH measurement-optimization steps common to previous efforts. A constant buffer capacity that accompanies a linear pH gradient is a great attribute but is not really needed for chromatography. What is needed is a buffer capacity sufficient to withstand a change in pH (within specified tolerance limits) when the analyte is added at any point in the gradient. For analytical scale chromatography this does not necessarily imply a large buffer capacity and is not a major limitation.

To achieve a linear pH gradient, let us pick several common buffering agents with pK_a values spread across the range of interest. Phosphoric, citric and boric acids together provide pKa values of 2.10, 3.13, 4.75, 6.40, 7.20, 9.24 and 12.38. This potentially covers a large pH range of 2-12 with more of a gap between 9.24 and 12.38. This shortcoming can perhaps be partially addressed by increasing the borate concentration. The change in pH upon incremental removal of K^+ from a mixture containing 15 mM K_3PO_4, 15 mM K_3Citrate, 11.25 mM $K_2B_4O_7$ and sufficient KOH to adjust the pH to 12 (the last two components, equivalent to ~45 mM $KB(OH)_4$, provides 3x the buffer capacity of the final neutralization step of 15 mM Na_3PO_4) was computed (see Appendix C). The same system was also experimentally studied with a staircase current gradient (t = 0-120 min, i = 0-300 mA; Δt = 2 min, Δi = 5 mA). From applying a current step to seeing the onset of the pH response was observed to be ~0.45 min. After accounting for this time lag, the pH data was averaged over 2 min increments and are plotted in Figure 4.5a as the solid line. The computed data that (a) ignores the onset of nonunity F_e and (b) incorporates nonunity F_e with an R_λ value of 15 (the dilute solution R_λ value for K^+ and H^+ is ~4.76) are shown as dashed lines and differ only at the complete exchange end. Even for a relatively complex system, the relatively simple computation provides pH values close to measured values, useful at least for guidance. Knowing the behavior of the current vs. pH makes it simple

to generate a substantially more linear pH gradient against time and also eliminate the wasted time near the end of the run where pH only decreases slowly. A single iteration of the original uniform current steps (red) to that suggested by the current-pH behavior produces the results in blue (Figure 4.5b). Since the time steps are still obviously too long, reducing time steps to 0.5 min and taking this opportunity to do a further iteration of the current program to improve linearity produces the results in Figure 4.6 which actually contains three overlaid traces of the generated pH profile indicating excellent reproducibility (among the triplicate set of 7500 time vs. pH points the maximum variance was 0.70%, average $0.20 \pm 0.14\%$ RSD). The algorithm used for this iteration is discussed in the Appendix C. While there are minor deviations that can still be improved on, our present hardware/software combination did not allow better than 1 mA resolution in current. This can be readily solved. Non-uniform time steps were possible but were eschewed for complexity. The linearity of the gradient generated with time exhibits an r^2 value of 0.9996, 0.9996 and 0.9997 from a pH range of 11.9 to 3. To manipulate the experimental pH to whatever desired form (linear, convex, concave), it must be obvious that it is much easier experimentally to reprogram a current profile than to alter solution compositions or mixing ratios between one or more components. In principle software that iteratively achieves any desired profile is relatively easily set up.

4.4.5 Maintaining a Relatively Constant Ionic Strength

Figure 4.5a also shows the computed ionic strength profile that decreases continuously as the pH decreases; this may not be desirable. As long as the ionic strength provided by the buffering species concentration is significantly less than ionic strength provided by an indifferent salt, an approximately constant ionic strength can be maintained by the addition of a large amount of indifferent salt, e.g., NaCl. Aside from maintaining a near constant ionic strength, this has the added advantages that (a) F_e will never have a nonunity value and (b) the buffer can have both cationic and anionic buffering components, e.g.; *n*-butylamine[153] pK_a 10.61, can be added to our previous phosphate-citrate-borate mixture to better fill the pK gap in this region. In

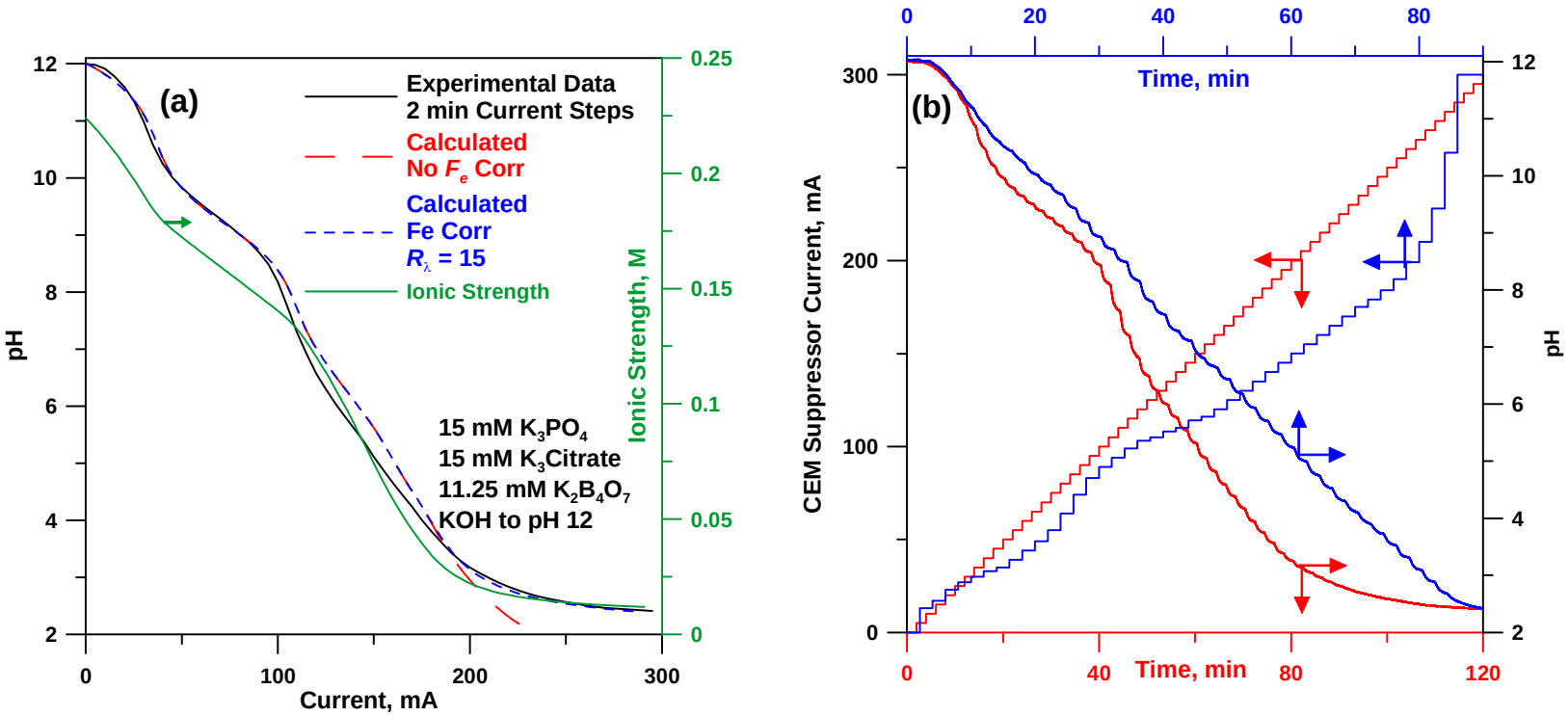

Figure 4.5 CEM Suppressor (ASRS 4 mm), 1 mL/min; feed composition is in the inset. (a) Solid line depicts experimental data obtained with 2 min current steps, the corresponding (time-lag corrected) 2 min averages for pH are plotted. The computed values are shown as dashed lines, the shorter dashed line (blue) takes nonunity Faradaic efficiency (F_e) due to current conduction by H^+ into account. See text. The green line shows the ionic strength (right ordinate). (b) red traces, bottom abscissa: 2 min uniform 5 mA current steps generate the pH profile which appears in 2 min averaged version in a; based on the observed profile a substantially linear gradient is generated using nonuniform current steps dictated by the observed current vs. pH values.

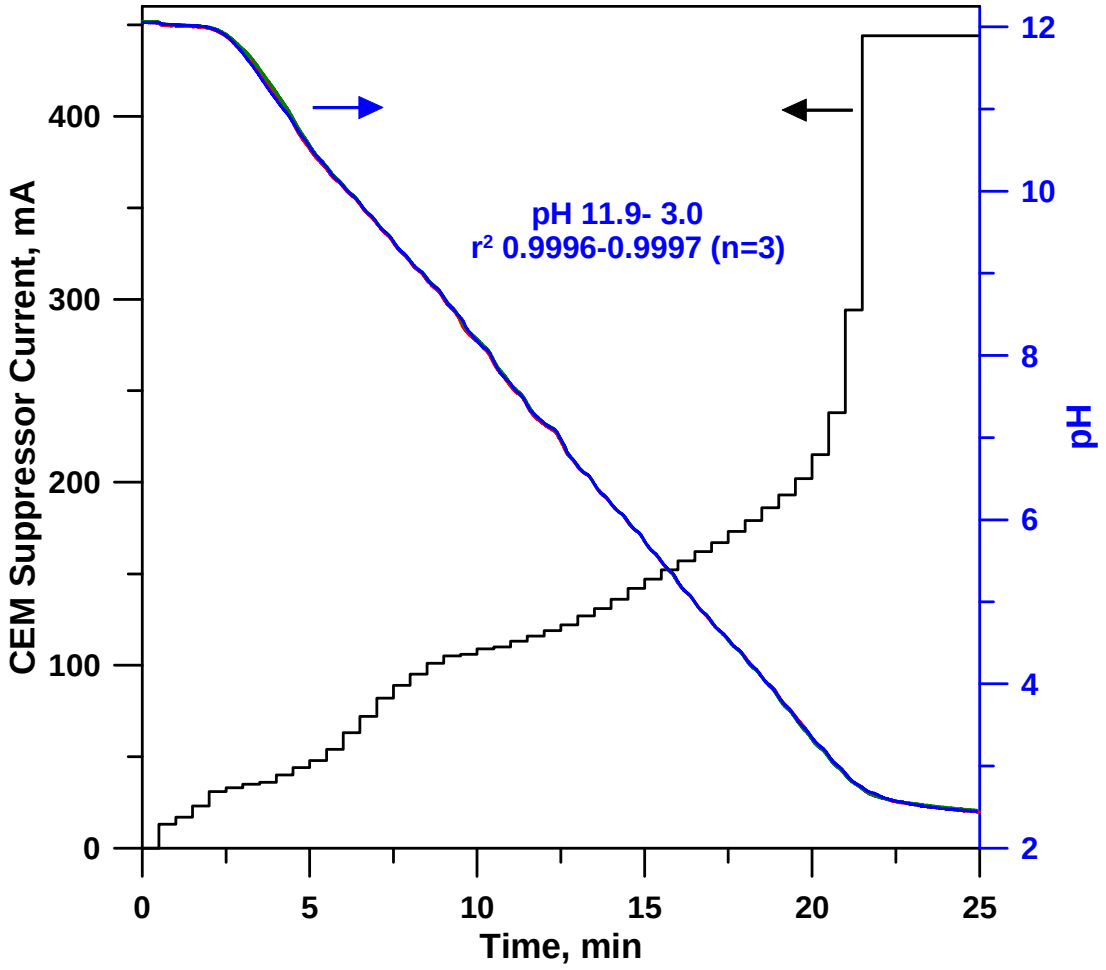

Figure 4.6 Three repeated 25 min linear pH gradient runs overlaid (right ordinate); the current program uses the left ordinate.

the absence of large concentrations of NaCl, we would have lost the butylammonium ($BuNH_3^+$) ion from the system as a cationic charge carrier. But in the presence of a large excess of Na^+, the loss of the much less mobile (especially through the membrane) $BuNH_3^+$ will be expected to be insignificant.

Thus, we dissolved 15 mmol/L each of K_3PO_4, K_3Citrate, and $BuNH_2$ and 3.75 mmol/L of $K_2B_4O_7$ per liter of water and added 0.500 mol NaCl to this solution. Computations were

made using the known mean ionic activity coefficient of NaCl for a 0.5 *m* solution (0.680)[153] and single ion activity coefficients were calculated therefrom noting charge and size dependence. Both computed and experimental results are shown in Figure 4.7. Note that since F_e remains unity throughout, the buffer capacity at any point is essentially the reciprocal of the pH vs the drive current plot. Herein we have used a descending current gradient to demonstrate the capability of a CEM-based suppressor to generate a temporally increasing pH profile which has a relatively minor accompanying change in ionic strength.

4.5 Conclusion

In summary, we have demonstrated the principles and practice of generating pH buffers electrodialytically with commonly available suppressors for IC. While present suppressors will not support pressures high enough to conveniently locate the device on the high pressure side of a pump, ion exchange bead based devices that tolerate much higher pressures have already been described.[39,40,105,146,148] Such devices can be readily constructed in an array format. With a ternary gradient system, an organic solvent gradient can be incorporated without a change in buffer ion concentration. To generate an additional gradient in ionic strength/salt beyond that resulting from pH change, a further pumping channel will be needed to add more or less salt.

It is also clear that suppressors can be used as flow-through coulometric ion removal devices. This property can be readily exploited as a process titrator, especially in conjunction with rapid triangular wave current sweeps as previously reported.[154,155] For sample streams that can flow through the suppressor, an AEM-based suppressor can be used to remove anions, introduce OH^- and titrate an acidic stream while a CEM based suppressor can be used to remove cations, introduce H^+ and titrate a base. For streams that are not compatible to directly flow through the suppressor, salt solutions flowing through a CEM/AEM suppressor can generate the titrant acid/base, respectively, in current-controlled mode to be added to the sample stream.

Even in a purely aqueous system, it is not possible to independently control both pH and ionic strength with a suppressor based EBG, especially when the ionic strength is controlled by the buffering species. This is possible with a different, additive electrodialytic membrane device that will be described in a future article.

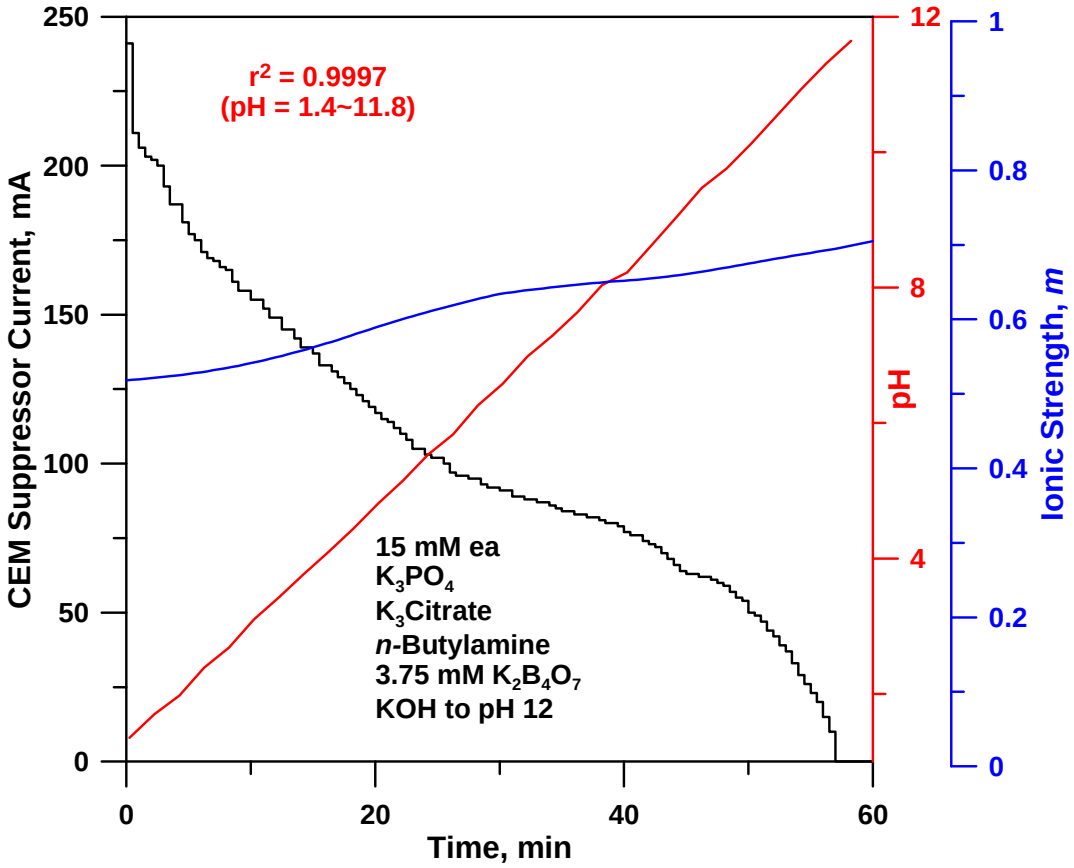

Figure 4.7 A four-component buffering mixture with an increasing linear pH gradient in the presence of a large amounts of NaCl. Without the presence of the salt, the ionic strength will change by more than an order of magnitude (see Figure 4.5a).

CHAPTER 5

pH AND CONCENTRATION PROGRAMMABLE ELECTRODIALYTIC BUFFER GENERATOR

5.1 Introduction

Buffer solutions are one of the most important types of chemical reagents used in chemical research, biological research and industry. pH control is crucial in successfully completing a large number of chemical reactions, especially biological reactions. Buffers are also used to maximize the stability of pharmaceutical formulations by maintaining the drug in either ionized or unionized form.[156] Reverse-phase high performance liquid chromatography (RP-HPLC) requires pH buffers as eluent component in separation of ionic or ionizable compounds. The degree of ionization depends on eluent pH and directly affects the retention of the compounds. Without a proper selection of pH buffer, peak shape, efficiency, resolution and reproducibility will all suffer.[157,158] Although organic solvent gradient elution is more commonly used for routine chemical and biomedical assay,[159,160] pH gradients have also been found to provide unique predictable selectivities,[161] and are useful in analysis of complex samples performed in a multidimensional mode.[162] Subsequent efforts focused on wide-ranging pH gradients[125] and theoretical development.[127-129] Combined pH/organic solvent gradient enhanced resolution in RP-HPLC.[126, 163]

Ion-exchange chromatography (IEC) is a versatile separation technique for profiling the charge heterogeneity of proteins as complex as monoclonal antibodies. Although salt gradients are typically used to separate components of widely divergent chromatographic affinity,[164-166] pH gradients can provide improved separations,[167, 168] and predicting elution profiles with isoelectric points (pI) and *vice-versa*.[169] The buffering capacity of an IEC column can itself be exploited to generate an outlet pH-gradient (*chromatofocusing*[131]) or by introducing a pH-

gradient at the column inlet (*gradient chromatofocusing*);[134] the latter uses inexpensive buffers, displays better pH control and permits higher buffer concentrations.[170]

High-throughput measurement of pK_a values, especially of candidate pharmaceuticals, via multiwavelength UV absorbance measurement in a linear pH gradient produced by mixing two solutions has proven to be very powerful.[153] Both pK_a and lipophilicity can be determined in multicomponent mixtures through pH gradient RP-HPLC retention data.[130,171]

Electrodialysis, charge-selective transport through an ion exchange membrane, and electrolysis have played a paramount role in ion chromatography.[172] Electrodialytic suppressors induce and facilitate ion exchange without additional reagents; the dual membrane configuration ensures that gas evolution can be isolated from the fluid of principal interest.[18, 173] In a companion paper we have shown that such electrodialytic suppressors can be utilized to generate buffers and even existing current programmability in present-day IC system can be directly programmed to generate reproducible pH gradients, in principle, in any desired profile.[174] Electrodialytic eluent generation (EEG) followed[175,176] electrodialytic suppression. IC is unique in that the mobile phase is generated on-demand in-line and at the desired concentration. Indeed, without the purity afforded by EEG, intrusion of CO_2 and the consequent change in eluent behavior would have made hydroxide eluent IC impractical. Throughout however, EEG devices have used a one or stacked membranes as a single barrier; the generated gas was removed through a gas-permeable membrane. Only recently suppressor-like devices that utilize, however, both a cation exchange membrane (CEM) and an anion exchange membrane (AEM), were introduced. Acids, bases, salts, even chromogenic dyes can be generated in the central channel without gas evolution with appropriate external feeds in the CEM and AEM compartments that are respectively provided with positive and negative electrodes.[39,40,177] Conversely, with opposite electrode polarities, ionic species already present in the central channel can be removed with such a device.[105,146] However, it is not possible to independently control cation and anion introduction of into the central channel (and thereby

control the pH) because obviously the same current serially flows through both membranes. We remove this limitation in this paper via a third electrode in the central channel. In the configuration generally discussed here this electrode constitutes the ground in a dual power supply where the CEM electrode is held positive and the AEM electrode is held negative. Individual amperostatic control can then independently vary the current through each membrane. We denote the cation (base) introduction current through the CEM as i_{cat}^{in} and the anion (acid) introduction current through the AEM as i_{an}^{in}. (For cases where cations and anions are removed through the CEM and AEM, respectively by reversing electrode polarities these currents will be analogously described as i_{cat}^{out} and i_{an}^{out}.) For $i_{cat}^{in} > i_{an}^{in}$ and $i_{cat}^{in} < i_{an}^{in}$, charge balance is respectively brought about by OH^- and H^+ generated in the center channel. The absolute magnitudes of i_{cat}^{in} and i_{an}^{in} govern the buffer concentration and the ratio between them governs the pH.

Herein we discuss buffer generation and the nature and the characteristics of the 3-electrode CEM-AEM type electrodialytic buffer generators (Three-Electrode EBGs), and demonstrate its performance on producing a variety of pH/concentration gradients.

5.2 Principles

Unlike the suppressor based EBG's, that work strictly on a subtractive principle, where the influent cation or anion is taken out and replaced by H^+ or OH^- respectively in a current-controlled manner to achieve a change in pH. The present generators can operated on both a subtractive or an additive manner depending on the directions of the independent electric fields through the two membranes; we focus in this paper primarily on the additive mode where the cation and the anion are independently added to the central channel and the pH of the central channel effluent (flow rate *Q* mL/min) is thus determined. Consider for example that Tris-HNO_3 solution (easily redox convertible ions, notably halides, needs to be avoided) is fed into both the cathode and anode compartments. *F* being the Faraday constant, the molar concentrations of

the Tris cation (TrH^+) and NO_3^- brought into the central channel are respectively given by 60 i_{cat}^{in}/FQ and 60 i_{an}^{in}/FQ, respectively; charge balance gives

$$\left(\frac{60 i_{cat}^{in}\,\alpha_0}{FQ}\right) + [H^+] - \frac{K_W}{[H^+]} - \frac{60 i_{an}^{in}}{FQ} = 0 \quad \ldots(5.1)$$

where α_0 is the fraction of Tris present as TrH^+. An analogous equation can be readily constructed for a weak acid based buffer. Current-dependent pH computations for substantially more complex systems are also readily implemented by iterative methods as with Microsoft Excel Solver.™

However, for most practical use of buffers, the relationship between pH and the electrolytic currents can be readily established by Henderson-Hasselbalch equation.[178, 179] Taking a NaOAc-HOAc buffer system for example, for any buffering to occur, $[OAc]_T > [Na^+]$ and therefore, $i_{cat}^{in} < i_{an}^{in}$. While i_{cat}^{in} controls [NaOAc], i_{an}^{in} controls $[OAc]_T$, so [HOAc] is related to (i_{an}^{in} - i_{cat}^{in}). This then takes the simple form (see the Appendix D for a more detailed derivation)

$$pH = pK_a + log\frac{R}{1-R} \quad \ldots(5.2)$$

Where *R* is the current ratio i_{cat}^{in}/i_{an}^{in}. Eqn (5.2) indicates that pH increases as a result of increase in *R* under the condition that *R*<1. At constant *R*, pH is constant. Obviously, an analogous equation can be constructed for any weak base based buffer system.

The 3-electrode EBG is capable of independently handling both types of buffering ions (cationic, anionic) through the respective individual membranes and thus deliver buffer mixtures consisting of more than one type of buffering ions (although any one system may be important at a given pH), beneficial in generating pH gradient with reasonably large range. Consider a relatively simple multiple-buffer system, a mixture of NH_3 and HOAc, with NH_4^+ and OAc^- feeds respectively on the CEM and the AEM sides. The $[NH_4^+]$ and $[OAc^-]$ in the central channel are thus 60 i_{cat}^{in}/FQ and 60 i_{an}^{in}/FQ, respectively. There are two useful buffer ranges, one each

around the pK_a's of HOAc and NH_4^+. Around the pK_a of HOAc, the weak base identity of NH_3 plays no role, it is entirely present as NH_4^+; conversely, around the pK_a of NH_4^+ the weak acid nature of HOAc plays no role. Thus around the pK_a of HOAc, eqn (5.2) above is still the relevant equation except K_a pertains to $K_{aHOAC.}$ Near the pK_a of NH_4^+ the relevant equation is (where *R*>1)

$$pH = pK_{aNH_4^+} + log(R-1) \qquad \ldots(5.3)$$

When *R* = 1, equivalent amounts of NH_4^+ and OAc^- are driven into the central channel, as is well known (see Appendix D), at reasonable concentrations the pH will be equal to ½ (pK_{aHOAc} +pK_{aNH4+}).

In general, while the basic considerations still apply to multiprotic buffering cations or anion feeds, the exact species that is introduced is not certain. Consider that if we use $Na_2HCitrate$ as AEM feed, significant concentrations of Cit^{3-}, $HCit^{2-}$ and H_2Cit^- are all present. The current that will transfer a given amount of Cit^{3-} will transfer 1.5x as many moles of $HCit^{2-}$ and 3x as much H_2Cit^-. This has consequences on both the concentration and pH. Even when the feed is almost the pure form of a potentially multiprotic ion, the feed pH may be high or low enough to result in significant transport of OH^- (as happens with Na_3PO_4 feeds on an AEM) or H^+ rather than the buffer ion. In a future paper we will address this competition for transport between protolytically related species as well as independent species when present together (e.g., chloride vs. bromide or phosphate vs. citrate in a mixed feed). However, for the present purpose, the total amounts of the charged species transported through the membrane are directly related to the current passing through that membrane. Experimental calibration data of how much of a buffering ion is transported as a function of current for a given feed system does still allow us to predict the concentration and pH of the buffer produced and other relevant parameters, e.g., buffer capacity (β) and ionic strength.

5.3 Experimental Section

5.3.1 Fabrication of Three-Electrode EBG

The three-electrode EBG (Figure 5.1) was constructed with two Plexiglas blocks (120 x 42.4 x 10 mm (LxWxH)) with a polypropylene spacer of 0.25 mm thickness, with flow I/O and electrode access as shown. A 60 x 2.0 x 0.25 mm (LxWxH) groove is machined into the inside surface of each Plexiglas block and form the outer flow channels. The central channel in the spacer has an aligned but somewhat longer cutout (80 mm) as the outer channels allowing the entry/exit of the central channel flow from one of the Plexiglas blocks without crosstalk from the outer channel(s). Platinum electrodes (0.25 mm) enter through sealed apertures in each channel. Gaskets were made from ETFE monofilament screens (0.29 mm thick, 0.25 mm mesh opening, www.micromold.com) with pressed on Parafilm sheets containing cutouts that were somewhat wider than the flow channels to reduce the flow resistance and facilitate gas escape at high applied currents. One gasket-screen was placed on each side of each membrane to prevent direct electrode contact of the membranes:

Electrode(+)|Gasket-Screen|CEM|Gasket-Screen|Electrode(GND)|Gasket-Screen|AEM|Gasket-Screen|Electrode(-)

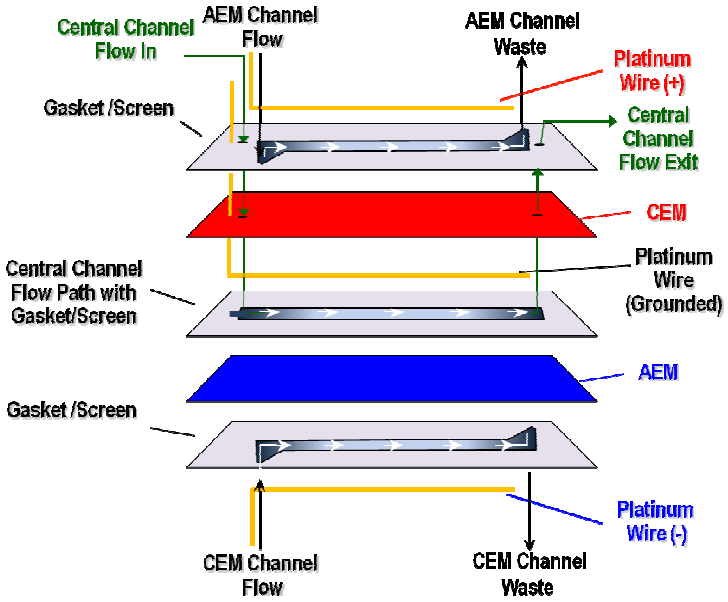

Figure 5.1 Schematic of the 3-electrode EBG

5.3.2 Experimental Arrangement

Water was delivered to the central channel at 0.25-0.5 mL/min by a ICS 2000 pump (www.Dionex.com). Individual outer electrolytes were fed pneumatically at flow rates of 1.5-3 mL/min. The flow rate was not controlled and the feed solutions generally recycled. The device was deliberately oriented vertically with all three streams flowing upward to facilitate gas escape. An independent voltage-controlled bipolar constant current source (See Figure D.1 in Appendix D) was used for each membrane. To generate pH/concentration gradients, the current sources were driven by a LabView program that controlled the outputs of a 14-bit card (USB-1408FS, www.mccdaq.com). The current data was acquired via serially connected precision 10 Ω sense resistors. All data were acquired through the same data acquisition card.

5.3.3 Other Measurements

Buffering ion concentrations (e.g., ethylenediamine (*en*), phosphate, citrate, etc.) were determined by effluent collection after reaching equilibrium under constant current conditions and ion chromatographic analysis after dilution, using appropriate calibration curves.

5.3.4 Gas Removal from Generated Buffer

Except when i_{cat} and i_{an} are equal, gas is generated in the central channel. In the absence of significant backpressure that we were reluctant to use with experimental membrane devices, detectors see bubble-induced noise, the frequency predictably increasing with current. A carbon dioxide removal device (CRD 200-4mm, Dionex), which is designed for dissolved CO_2 removal in IC,[142-143] was placed immediately after the EBG, with both of the external jacket (regenerant) inlet/outlets of the CRD tied in common by a tee and connected to house vacuum (~180 Torr) to facilitate gas removal. All chemicals were commonly available reagent grade and distilled deionized water was used throughout.

5.4 Results and Discussion

5.4.1 pH Control and Gas Generation in a 3-Electrode EBG

With suppressor-based EBGs,[174] the maximum buffer concentration is determined by the suppressor feed and this must be made beforehand to be pumped into the suppressor. Then, pH is changed under electrodialytic control either by taking out cations and replacement by H^+ or by taking out anions and replacing them with OH^-, depending on the suppressor type. This can be done in a 3-Electrode EBG as well, and either charge types can be removed as desired, allowing for greater flexibility. However, unlike the suppressor, the 3-electrode EBG can operate in the additive mode, by bringing in any desired amount of cations through the CEM and anions through the AEM. Premade fixed feed concentrations are not needed and device effluent concentrations can be <=>feed concentrations, assuming the input is not mass limited. Under any conditions when the cation (anion) equivalents brought into the central channel exceeds the anion(cation) equivalents, charge balance is made up by central channel generation of OH^-/H_2 (H^+/O_2). This is unlike suppressor-based EBGs, where gas generation only takes place in the outer channels, presently gas is expected to be produced for all conditions other than when i_{cat}^{in}=i_{an}^{in}. With a number of different experimental values for i_{cat}^{in} and i_{an}^{in}, we did indeed find that the evolved gas volume in the central channel is minimized when $i_{cat}^{in} = i_{an}^{in}$ (Figure D.2 in Appendix D). This functioning of a 3-electrode EBG is thus depicted in Figure 5.2, illustrated with a phosphate buffer. Hereinafter, all references to an EBG in this paper connotes a 3-electrode EBG, unless a suppressor EBG is explicitly noted.

5.4.2 Behavior of a Phosphate EBG

Phosphate is one of the most common buffering systems in use, with a good buffering range in pH 6-8, $H_2PO_4^-/HPO_4^{2-}$ being the dominant buffering species. At the same molar concentration, Na_2HPO_4 is more conductive and we chose 0.5 M Na_2PO_4 as the feed on both sides. With i_{an}^{in} held constant at 22 mA, as i_{cat}^{in} is increased, the pH increases monotonically with the lowest dpH/di_{cat}^{in}. slope being in the buffering range of 6-8. Note that i_{an}^{in} and i_{cat}^{in}

respectively control phosphate and Na^+ introduction and as i_{an}^{in} is held constant, so is phosphate concentration (Figure 5.3 (a)). On the other hand, when i_{cat}^{in} is held constant and i_{an}^{in} is varied, we observe the reverse titration curve (titrating NaOH with H_3PO_4. Now the total phosphate concentration increases linearly with i_{an}^{in}. Device behavior with higher applied currents with pH limited to the buffer range of pH 6-8 are shown as 3-D plots of the drive currents with total phosphate concentration (Fig. 5.4a) and pH (Fig. 5.4b) as the dependent ordinate variables. The device can deliver phosphate buffers of concentration up to and exceeding 140 mM.

5.4.3 An Ethylenediamine/Citrate EBG

The present system allows the simultaneous/ sequential introduction/removal of both weak acid and weak base buffering ions, allowing in principle a pH gradient over a large range. We chose ethylenediammonium sulfate and tripotassium citrate as CEM and AEM feeds respectively, the relevant pK_as span a range of 3-10 (it would have also been possible to feed ethylenediammonium citrate as a common feed). The transport of ethylenediammonium as a function of i_{cat}^{in} and that of citrate as a function of i_{an}^{in} were experimentally determined; the data are in Figure D.3 in the Appendix D. The absolute current efficiencies for transport of *en* and citrate are respectively, 0.977 and 0.836. A zero-intercept linear dependence of transport on current paradigm was used for fitting the data. Because the observed behavior closely follow theoretical simulations, it is simpler to first examine the theoretical expectations. From concentrations predicted from i_{cat}^{in} and i_{an}^{in}, charge-balance based computation[31] allows the estimate of pH, β and ionic strength (*I*). Figure 5.5(a)-(d) show these i_{cat}^{in} and i_{an}^{in}. The sum of *en* and citrate species concentrations remains constant as the sum of i_{cat}^{in} and i_{an}^{in} remains constant (Figure 5.5a). A constant current ratio will produce a constant pH *isoline* (Figure 5.5b). The buffer capacity increases with increasing i_{cat}^{in} and i_{an}^{in} and is maximum when both are high (Figure 5.5c). Bearing the relevant pK_a values in mind (see Figure 5.5 legend), a superposition of Figures 5.5a and 5.5b essentially leads to the results in 5.5c: β is high at higher concentrations as long as the pH corresponds to one or more of the pK_a values. One item of

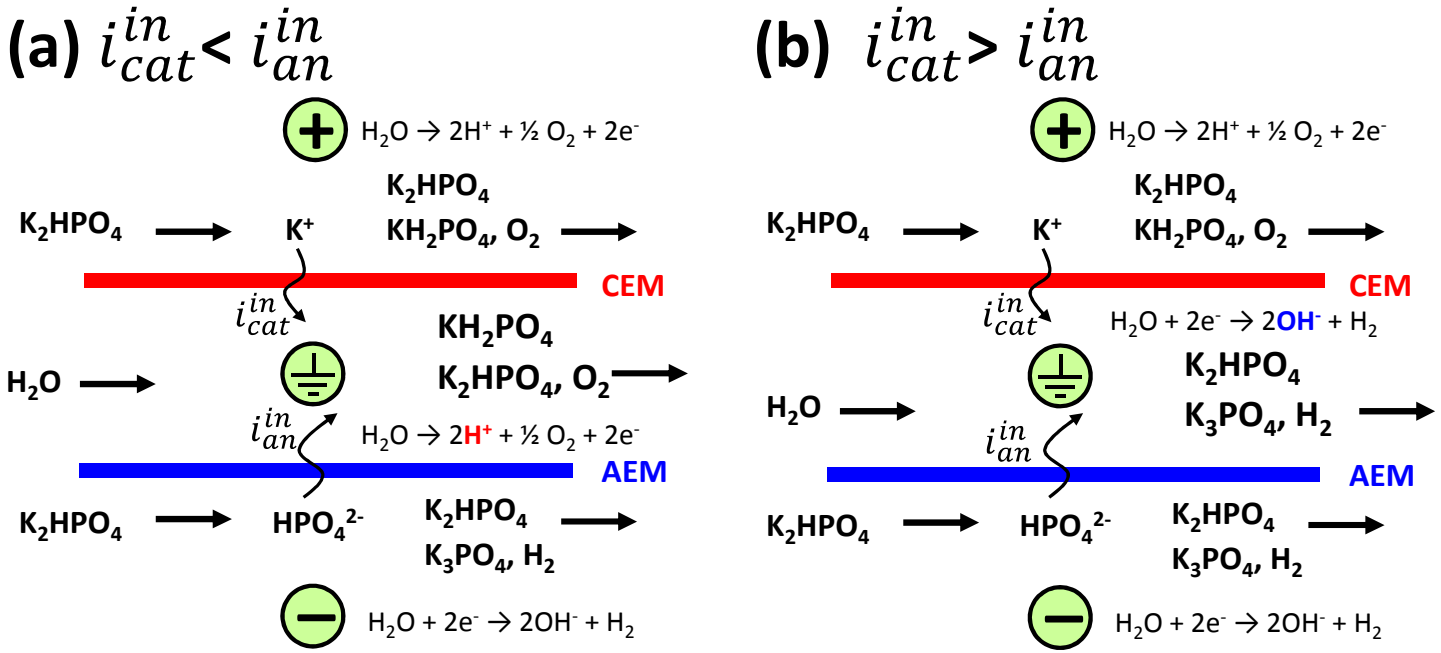

Figure 5.2 A 3-electrode electrical buffer generator schematic, using phosphate buffer as the example. (a) $i_{cat}^{in} < i_{an}^{in}$, (b) $i_{cat}^{in} > i_{an}^{in}$.

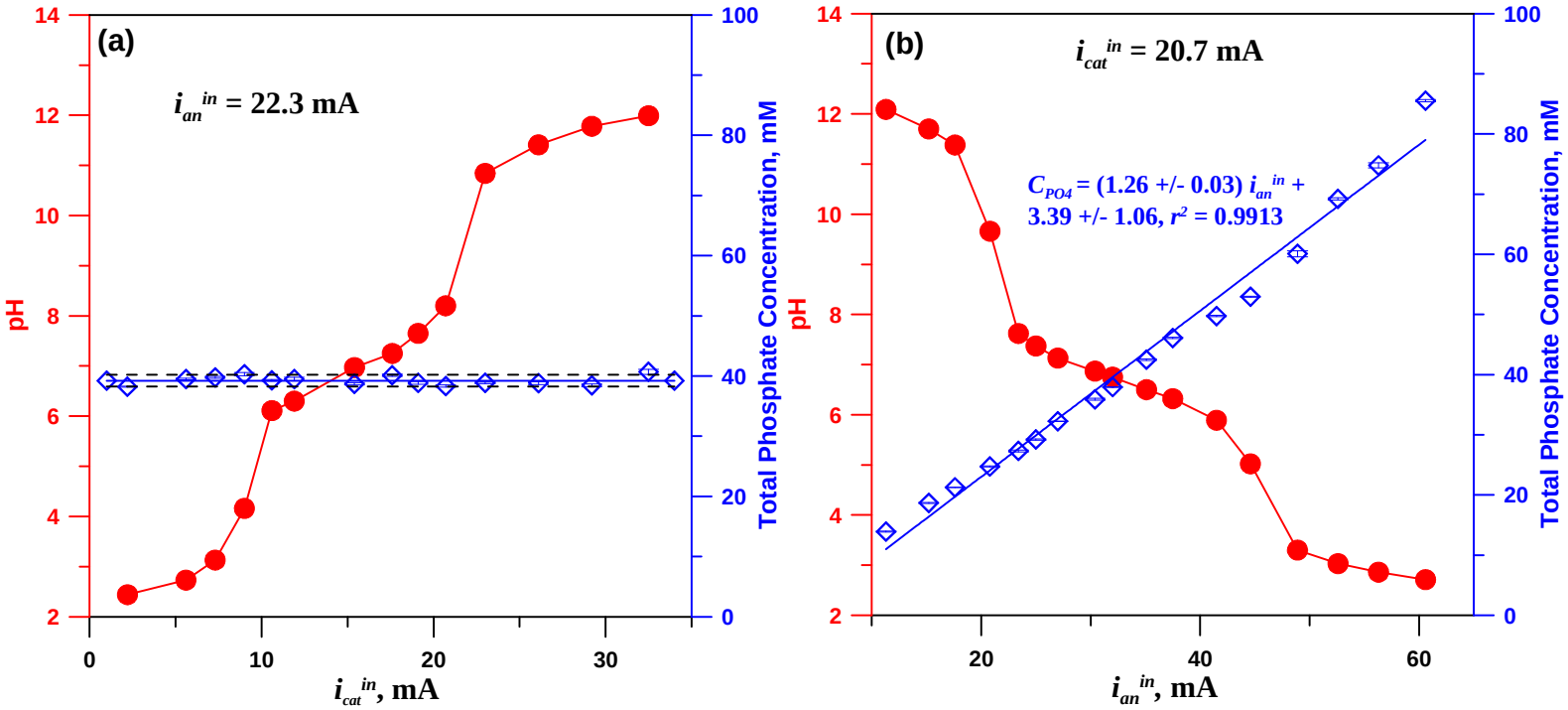

Figure 5.3 Concentration and pH as a function of (a) $i_{cat}^{in}$when i_{an}^{in} is held constant, the horizontal dashed lines show 95% uncertainty limits of the best fit (invariant) phosphate concentration; (b) $i_{cat}^{in}$when i_{an}^{in} is held constant. The generated buffers were collected and buffering ion concentration was determined by IC. Central channel: water, 0.25 mL/min; CEM side outer channel: 0.5 M K_2HPO_4, 1.5 mL/min; AEM side outer channel: 0.5 M K_2HPO_4, 3.0 mL/min.

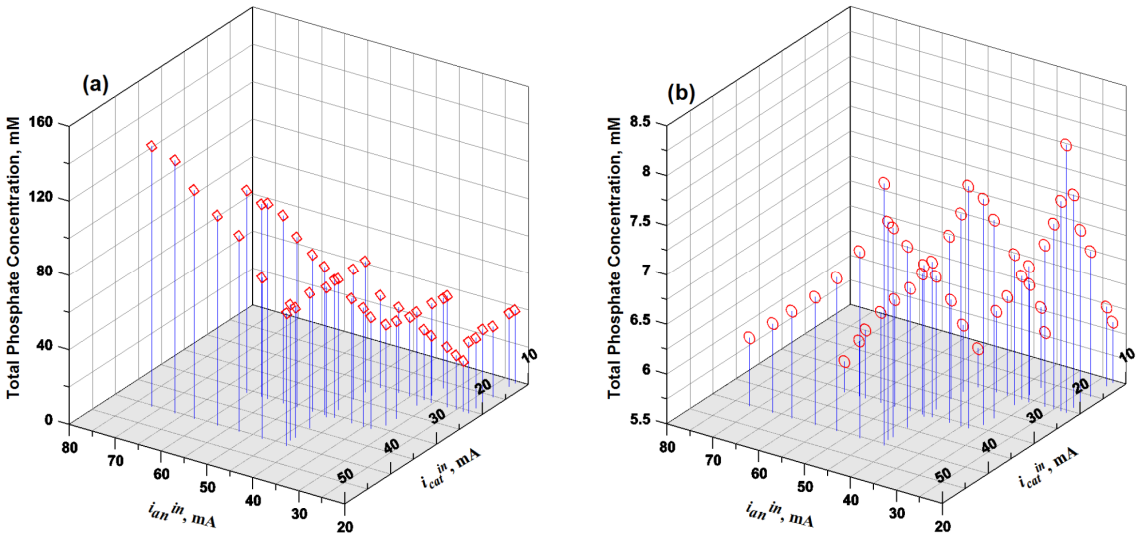

Figure 5.4 3-D plots of (a) Concentration of the total phosphate generated and (b) pH as a function of applied currents. The generated buffers were collected. Concentration was determined by ion chromatography; pH was measured off-line. Central channel: water, 0.25 mL/min; CEM side outer channel: 0.5 M K_2HPO_4, 1.5 mL/min; AEM side outer channel: 0.5 M K_2HPO_4, 3.0 mL/min.

note in Figure D.3 (Appendix D) is that the transport of *en* is significantly more current-efficient than that of citrate; hence in the highest buffer capacity regions, $i_{cat}^{in} < i_{an}^{in}$, they are not equal. Figure 5d depicts *I isolines*. Because only charged species contribute to *I*, when $i_{cat}^{in} \simeq i_{an}^{in}$ (within limits of the different transport efficiencies), *I* increases linearly with the currents. The corresponding 3-D surface plots provide a different perspective of the system (See Figure D.4-D.7 in Appendix D).

In a chromatographic context, the experimental performance in temporally variable buffer pH and concentration (and reproducibility thereof) is the most important**.** In suppressor-based EBGs,[31] total buffer concentration remains unchanged and cannot be programmed. The present device permits both pH and concentration programming. Some of the major modes of operation may be as follows. (a) Hold i_{cat}^{in} constant with a linear increase in i_{an}^{in} over time whence the pH executes a descending and approximately linear gradient between pH 10→6 and then executes a less steep and approximately linear pH change as the citrate buffer range

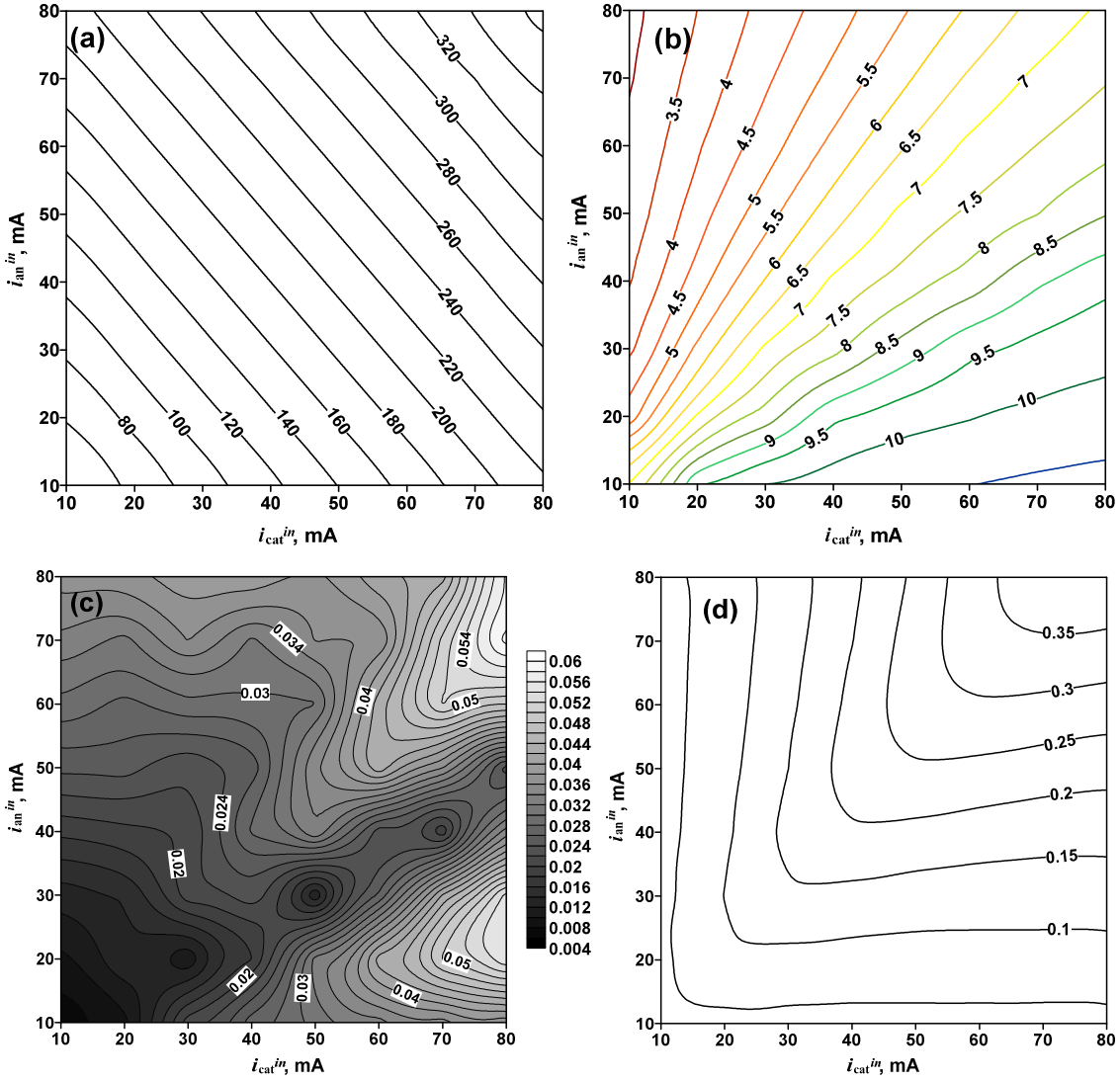

Figure 5.5 Contour maps of (a) total concentration (meq/L) as a function of currents; (b) pH as function of two currents; (c) buffer capacity β (M/pH Unit) as a function of currents; (d) ionic strength (M) as a function of currents. pK_a values for citric acid and ethylene diammonium are respectively 3.1, 4.8, 6.4, 6.8, 9.9. Feed in CEM side outer channel: 0.3 M ethylenediamine sulfate; feed in AEM side outer channel: 0.2 M tripotassium citrate; central channel feed: water, 0.25 mL/min.

is reached (Figure 5.6a). If it is desired that the same *d*pH/*d*t slope extends below pH 6, obviously di_{an}^{in}/dt must be increased in this region. (b) If i_{an}^{in} is held constant and i_{cat}^{in} linearly increased, we observe an increasing pH gradient with two approximately linear regions, pH 4→7 and then a less steep slope at higher pH (Figure 5.6b). (c) Rather than holding either

current constant, if we start one at a high value and decrease linearly in time and start the other at a low value and increase linearly at the same rate in time (or better, have the *di/dt* slopes reflect the difference in ion transport efficiency), we will observe a linear gradient in pH. The pH can be either increasing with time (at *t* = 0, i_{cat}^{in} low and i_{an}^{in} high) or decreasing with time (at *t* = 0, i_{an}^{in} low and i_{cat}^{in} high, See Figure 5.6c). In such an operation a reasonably linear 10→3 pH gradient is attained; β also varies less during the run than in the previous two cases (detailed results on the same cases that includes β and *I* data are in Figures D.8-D.11 in the Appendix D). A final mode of interest involves an increasing buffer concentration gradient with or without a change in pH; the latter is easily accomplished by simultaneously increasing both i_{cat}^{in} and i_{an}^{in} while maintaining a constant ratio (Figure 5.6d). Obviously, innumerable permutation/combination of these basic modes are possible.

5.4.4 Complex Feed Systems: Ethylenediamine-Citrate-Phosphate EBG

Multiprotic polyampholytes[180] had been classically attractive in generating pH gradients because approximately evenly spaced pKa values can provide a smooth gradient in pH with reasonably constant β. An alternative way to achieve this is to provide multiple buffering agents that are widely (and evenly) spaced in their pK_a values. The EBGs permit the introduction of not just buffering ions of different charge types but also more than one buffering ion of the same charge type, e.g., both phosphate and citrate can be present in the AEM feed. Competition for transport in such systems extend from protolytically related (e.g., $H_2PO_4^-$ vs. HPO_4^{2-}) species to altogether unrelated species (e.g., PO_4^{3-} vs. Cit^{3-}). At the present time, there is no theoretical framework on competitive transmembrane transport in these systems as a function of the electric field, especially when charge magnitudes between competing ions differ. We will report on these aspects in the future. Presently we wanted to characterize the experimental behavior of such a more complex buffering system and chose a mixture of *en*, phosphate and citrate because of the wide pKa range and the wide use of citrate and phosphate as both biological

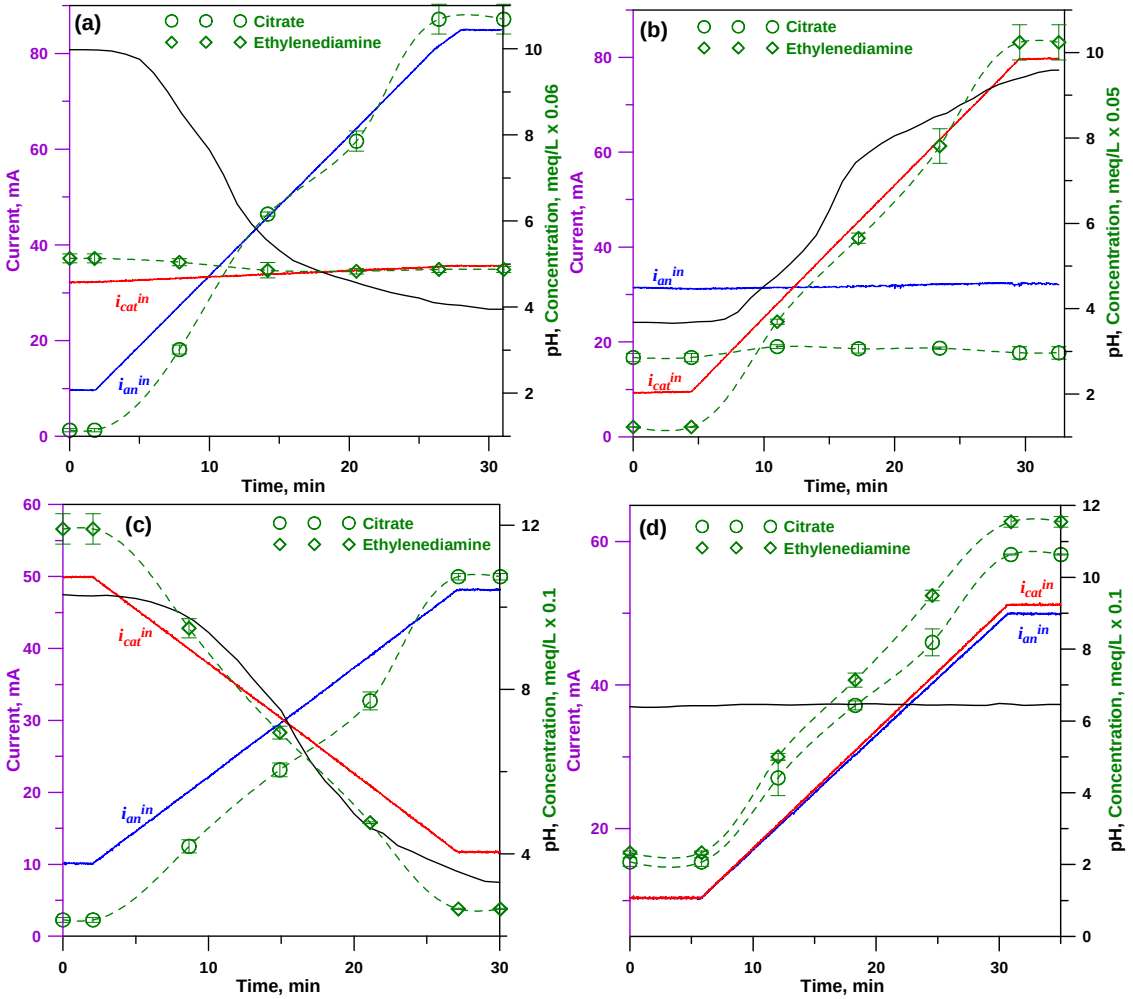

Figure 5.6 Various concentration and pH gradients (a) Citrate concentration gradient and pH descending gradient by varying i_{an}^{in} and keeping i_{cat}^{in} constant; (b) ethylenediamine concentration gradient and pH ascending gradient by varying i_{cat}^{in} and keeping i_{an}^{in} constant; (c) linear pH gradient and relatively constant concentration when i_{an}^{in} is increased and i_{cat}^{in} is decreased; (d) constant pH and concentration gradient when $i_{an}^{in}$and $i_{cat}^{in}$are equal and increased at the same rate. Feed in CEM side outer channel: 0.3 M ethylenediamine sulfate; feed in AEM side outer channel: 0.2 M tripotassium citrate; central channel feed: water, 0.25 mL/min.

and chromatographic buffer systems. To achieve comparable buffer capacities near each pK_a, comparable concentrations must be introduced. With the specific membranes we used, citrate was preferentially transported over phosphate and phosphate feed concentration had to be maintained 4.7x that of citrate to introduce the same concentration. The behavior of the

en/citrate-phosphate EBG is demonstrated with an ascending pH gradient (Figure 5.7a) and a concentration gradient at constant pH (Figure 5.7b) where the i_{an}^{in}/i_{cat}^{in} ratio is held constant at 3.

5.4.5 Subtractive and Additive-Subtractive Operation

Although the present device differs from suppressor-EBG's with its ability to operate in an additive mode, it would be obvious that they can also operate in a subtractive mode. Moreover, unlike suppressor-EBG's, either charge type ion can be removed. In Figure D.9-D.11 (Appendix D)we show how *en* and/or citrate can both be removed from an initial *en*-citrate buffer for pH and/or buffer concentration control. The ability to add one type of ion through one membrane and remove another type through another is a particularly powerful combination. We show an example where *en*-phosphate is flowed in through the central channel with citrate and butylammonium as the AEM and CEM feeds. Such a system can start e.g., at a low pH end where citrate is brought in through the AEM and *en*H_2^{2+} is simultaneously removed through the CEM to a high pH end citrate is actively removed through the AEM and butylammonium is put in through the CEM (Figure 5.8). Obviously, there are many possible permutations with a high degree of flexibility that such a system can provide.

5.5 Conclusion

In summary, a dual membrane three-electrode current programmable EBG provides a unique and convenient way to generate buffers from multiple species where both buffer concentration and pH can be altered under current control. The flexibility is much greater compared to a suppressor-based EBG; gas may be present, however, in the product; this can be removed on-line.

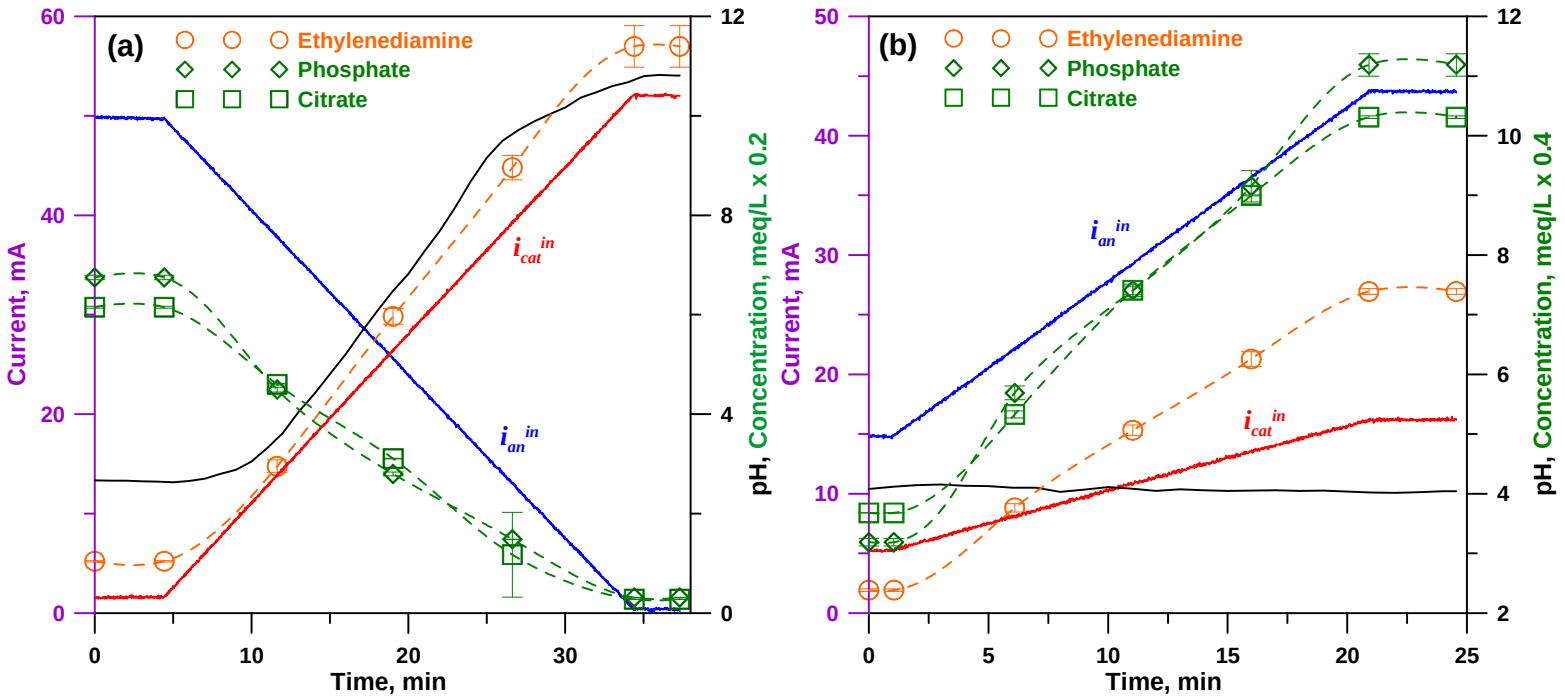

Figure 5.7 Concentration and pH gradients (a) pH ascending gradient and relatively constant concentration when i_{an}^{in} is decreased and i_{cat}^{in} is increased; (d) constant pH and concentration gradient when i_{an}^{in}/i_{cat}^{in} is kept at 3. CEM feed 0.3 M ethylenediamine sulfate; AEM feed: 0.165 M K_3PO_4/0.035 M K_3Citrate; central channel feed: water, 0.5 mL/min.

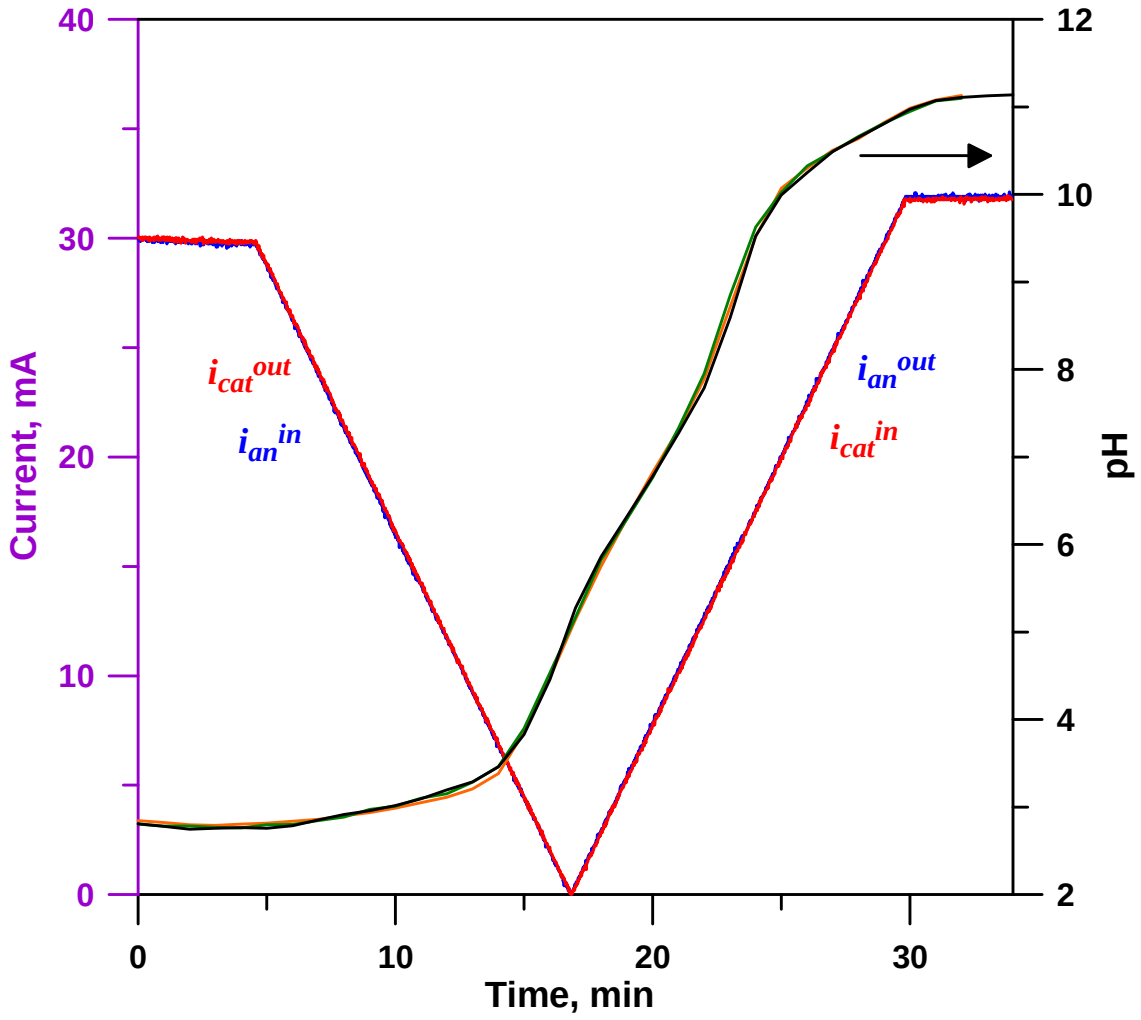

Figure 5.8 Three repeated ascending pH gradient runs overlaid (right ordinate) when i_{cat}^{out} and i_{an}^{in} is decreased followed by increased i_{an}^{out} and i_{cat}^{in}. CEM feed: 0.2 M butylamine (pH adjusted to 4.46 with concentrated H_2SO_4); AEM feed: 0.2 M K_3Citrate; central channel feed: 15 mM ethylenediamine (pH adjusted to 5.91 with concentrated H_3PO_4), 0.5 mL/min.

CHAPTER 6

SUMMARY AND CONCLUSION

Ion exchange has been firmly established as a unit operation and ion exchangers have been extensively used in industries such as in wastewater treatment, semiconductor processing, power generation plants etc. and in laboratories, both in analytical and preparative chemistry. A wide selection of ion exchange media is available in various particle sizes, ionic forms, and purity ranges. One particularly important use of ion exchangers is as a stationary phase, as well as in the form of secondary components in modern IC. A great variety of ion exchange stationary phase for different selectivities and applications have been developed. The suppressors, one of the key components in IC, have evolved from ion exchange resin bead-based column[4] which requires frequent offline regeneration to self-regenerating flat membrane device,[17] which contributes to the excellent detection sensitivity. The invention of electrodialytic eluent generator[28-30, 33] is a milestone in the development of modern IC. It obviates the need to prepare the eluent and precludes the inconvenience associated with manual preparation of alkali hydroxide and the contamination from intrusion of CO_2. The electrodialytically generated eluent, whether isocratic and gradient, is controlled by the current applied to the eluent generator and is generated with high-purity. With the above-mentioned technological innovation, modern state-of-the-art IC systems require just water to operate.

The research described in this dissertation is, to some extent, inspired by some of the innovation of electrolytic devices in IC.

The charge detector (ChD) was developed based on the CEM/AEM-based eluent generator.[35] In a configuration where a CEM and an AEM separating three independent channels, and there is one electrode disposed in each of the outer channels, when the electrod

electrode on CEM side is positive with respect to the electrode on AEM side (forward-biased), the device behaves as an electrolyte generator, producing any electrolyte, depending on the feed electrolyte solutions in the outer channels. When the polarity is reversed (reverse-biased), the device behaves as a “deionizer”. When water carries the injected ions through the central channel, cations and anions are driven by the electric field through CEM and AEM to the outer channels respectively. With the current through the device monitored, there is an increase corresponding to the passing of the analytes. The integrated area (charge) is directly related to the charge carried by the analyte ions. Therefore the device can function as a “charge detector”, which responses to charge of the analytes, regardless of their electrochemical properties. Besides offering the potential of having universal calibration for strong electrolytes, a ChD has a relatively higher response to weak electrolytes compared to a conductivity detector.

Since the charge detector is a “deionizer” that removes ions from the central channel into the outer channels, the approach allows the removal of all charged species without affecting a neutral uncharged species and allows this to be performed down to sub-microliter volume scales. Salts and buffers, commonly used in isolation and stabilization of biological analytes, have a deleterious effect on ESI-MS. Since proteins have poorer electrophoretic mobility relative to the buffer components, the present approach permits removal of the salt, leaving the salt-free proteins proceed to the ESI source. A capillary scale salt remover (SR) was fabricated and operated with constant current. It was found that the amount of salts removed is linearly related to the current applied, allowing the salts to be removed in a predictable fashion. Satisfactory salt removal performance was demonstrated with ESI-MS spectra of myoglobin, lysozyme, and cytochrome c in isotonic saline (154 mM NaCl) under continuous flow conditions after they passed through the SR under optimum applied current.

The use of buffer solutions is immensely important in a great variety of areas. Two types of electrodialytic buffer generators (EBG), developed based on the concept of electrolytic

suppressor in IC and ChD respectively, can produce pH buffers of variable compositions continuously in a controllable fashion.

In an ASRS suppressor, by feeding the salt of the weak acid into the central channel and varying the applied current, a buffer based on a weak acid-salt combination can be generated by introducing increasing amounts of H^+ by increasing current. In a CSRS suppressor, a buffer based on a weak base/salt is generated by feeding salt of weak base into the central channel, with increasing amount of OH^- brought in by increasing current to increase the pH of the buffer. In the suppressor-based EBGs, the total concentration of the generated buffer is constant; the pH can be adjusted with the applied current. pH gradients with excellent linearity and reproducibility were demonstrated with a mixture of salts/buffering agents used as the feed in the central channel.

Compared to the suppressor-based EBGs, the second type of EBG offers greater versatility in generating buffers. The configuration is similar to that of ChD, consisting of a CEM and an AEM separating three channels, except that there is one electrode in each of the flowing channels. When the electrode in the CEM side outer channel is held positive, the electrode in the AEM side outer channels is held negative and the central electrode the grounded, the three-electrode EBG functions in "additive mode", bringing in buffer components from the outer channel feeds with amount of cations controlled by i_{cat}^{in} and amount of anions controlled by i_{an}^{in}; in the central channel, OH^- is generated when $i_{cat}^{in} > i_{an}^{in}$ and H^+ is generated when $i_{cat}^{in} < i_{an}^{in}$, therefore the pH is adjustable. With the polarity of the electrodes reversed, the device can be operated in "subtractive mode", like a "deionizer" but with cations removed by i_{cat}^{out} and anions removed by i_{an}^{out}. pH is varied by the H^+ or OH^- generated depending on the difference between i_{cat}^{out} and i_{an}^{out}. pH gradients generated in "additive mode" and "subtractive mode" as well as "additive-subtractive mode" are demonstrated.

APPENDIX A

SUPPORTING INFORMATION FOR CHAPTER 2

Construction of Bead-based Charge Detector (ChD-B)

The through-channels of both arms of a 10-32 4-way cross fitting (P-730, Upchurch) were bored out for 1.6 mm o.d. PEEK tubing to just pass through. For each of two segments of 0.5 mm i.d., 1.6 mm o.d. PEEK tubing, the terminal bore at one end was widened to 0.9 mm to a depth of ~1 mm. Ion exchange resin beads (Rexyn 101 H^+-type for the cation exchange resin (CER) and Dowex AG -2X8 Cl^-form for the anion exchange resin (AER)) were dried in a desiccator and hand-picked to obtain resin beads in the 0.8 -0.85 mm size range. One CER and one AER bead were placed in the respective drilled out cavities in the PEEK tube and wetted with water whereupon they expanded and lodged tightly in the cavity. As shown in Figure 2.1, these two bead-bearing tubes were placed opposite each other (fixed in place with 10-32 nuts and ferrules, not shown), with the distance between CER and AER being ~ 0.4 mm. Water inlet and eluent outlet tubes were then similarly connected. At the back side, each bead-bearing tube was cut off essentially flush with the back of the holding nuts and a small segment of Tygon sleeve tubing put over the ends of the 1.6 mm o.d. PEEK tubes. A blunt-ended platinum needle (0.25 mm i.d., 0.45 mm o.d.; 26 ga., 25 mm long, P/N 21126 PT 3, Hamilton Co. Reno, NV) was put in all the way into the PEEK tubing, just touching the bead. The exit of the Pt Needle from the Tygon tube was sealed with hot-melt adhesive. The Pt-needle functioned both as the electrode and the liquid inlet tube; the liquid outlet was provided by a 0.25 mm. i.d., 0.51 mm o.d. PEEK tube (P/N 1542, Upchurch) breaching the Tygon tube wall, and affixed in place with adhesive. The nominal internal volume of the device, without considering the space that the protrusion of the spherical beads may consume, is ~3.2 μL.

Dionex Suppresor Design

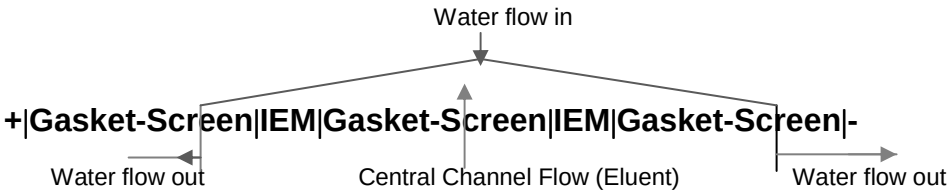

Scheme I

The screens referred to above break up flow laminarity to enhance mass transport to the membranes.

The basic suppressor design of the above scheme and shown in Figure A.1 is described below. Each outer compartment contains a platinum electrode in contact with a flow channel which consists of a gasketed screen with an ion exchange membrane (IEM) on the other side of the screen. The central compartment contains an IEM on both sides. The screens have an integral proprietary soft polymeric gasket material, the portion of the screens not covered by the gasket define the fluidic pathway. The purpose of the screen structure in each flow path is to break up flow laminarity and improve mass transfer to the membrane. The screens in the outer channels are also ion exchange functionalized similar to the membranes they are adjacent to, thus effectively increasing the ion exchange capacities of the membranes. Water or a regenerant solution comes in and splits into two parts, flowing through each of the two outer channels to waste while the central channel flow proceeds independently. Detailed physical design of these devices is complex. The unfamiliar reader is referred to the original papers describing such designs,[16, 181] the patents,[17, 182] and a more recent review.[183] The hardware used to hold the assembly together is shown in Figure A.2.

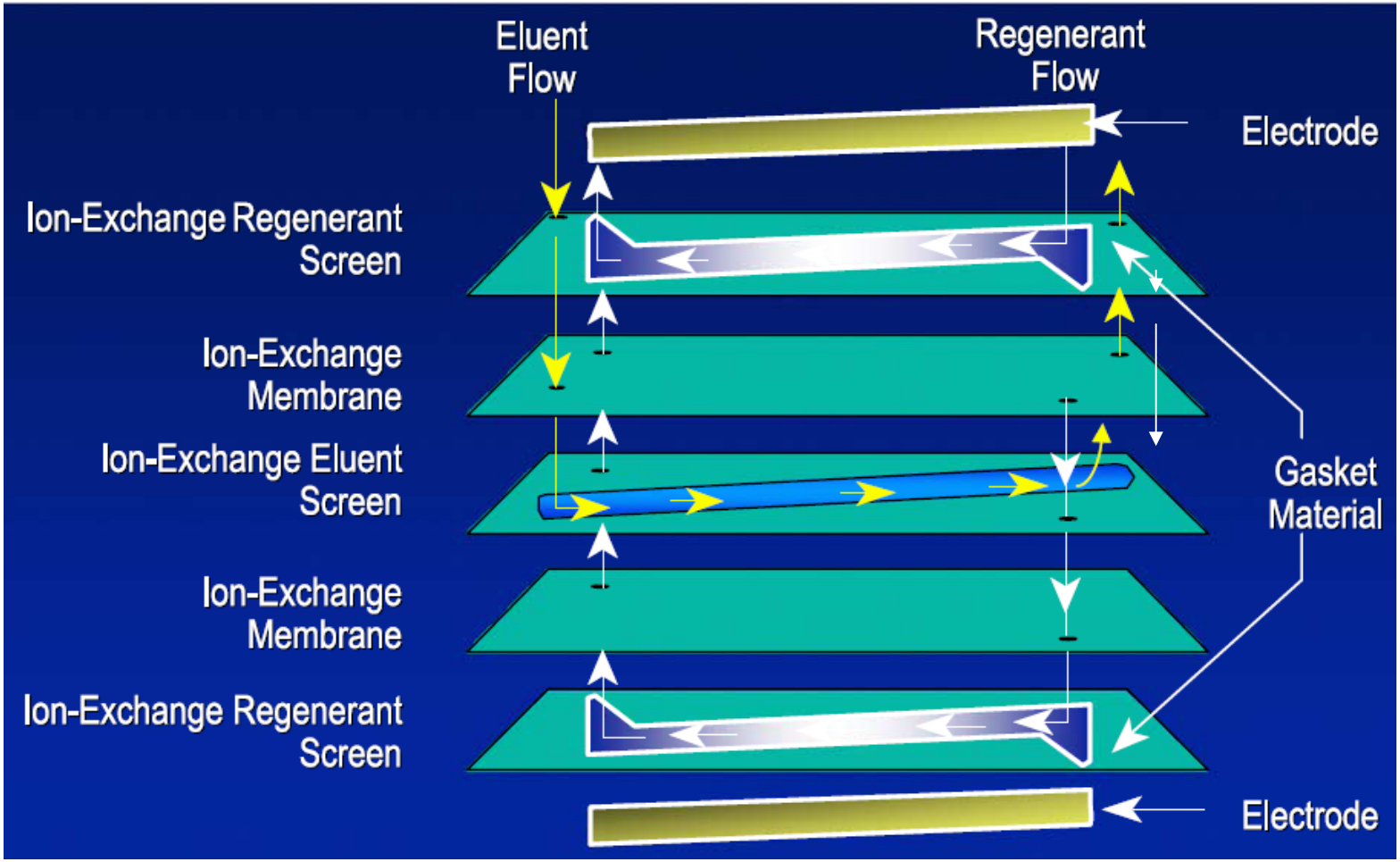

Figure A.1 Dionex electrical suppressor configuration.[51]

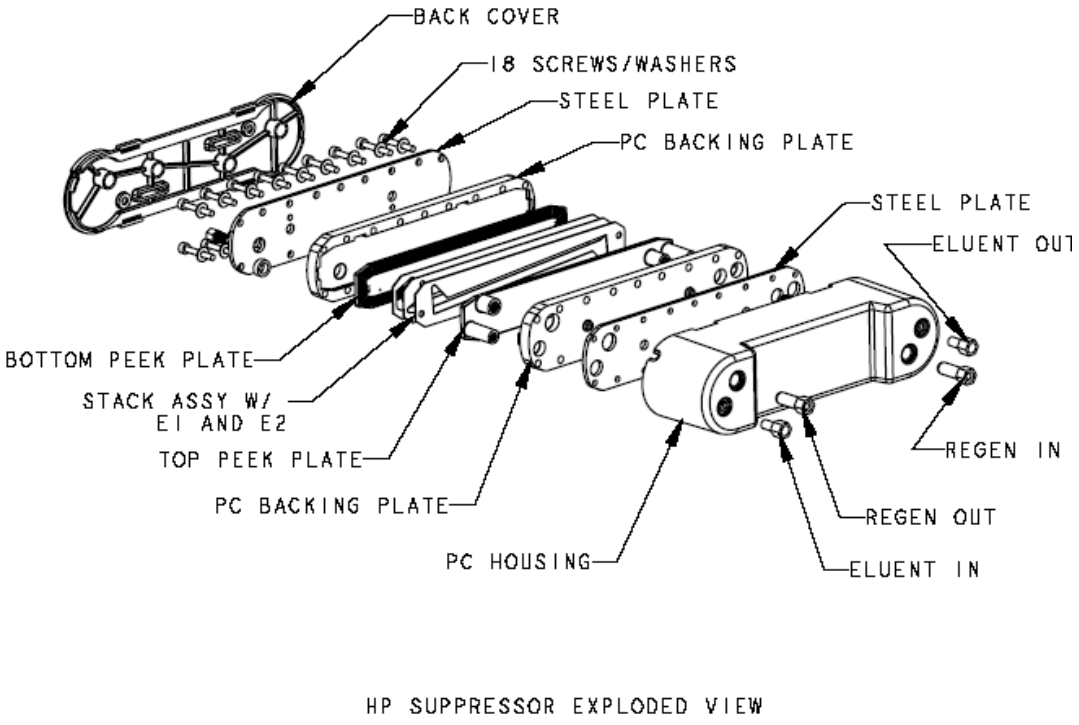

Figure A.2 Electrical Suppressor Assembly Hardware.

Electrode(+)|Gasket-Screen|AEM|Gasket-Screen|CEM|Gasket-Screen|Electrode(-)

Outer channel flow Central Channel Flow Outer channel flow

Scheme II

To construct a ChD, conventional suppressor hardware must be modified to accomplish this independent flow scheme as shown above in Scheme II.

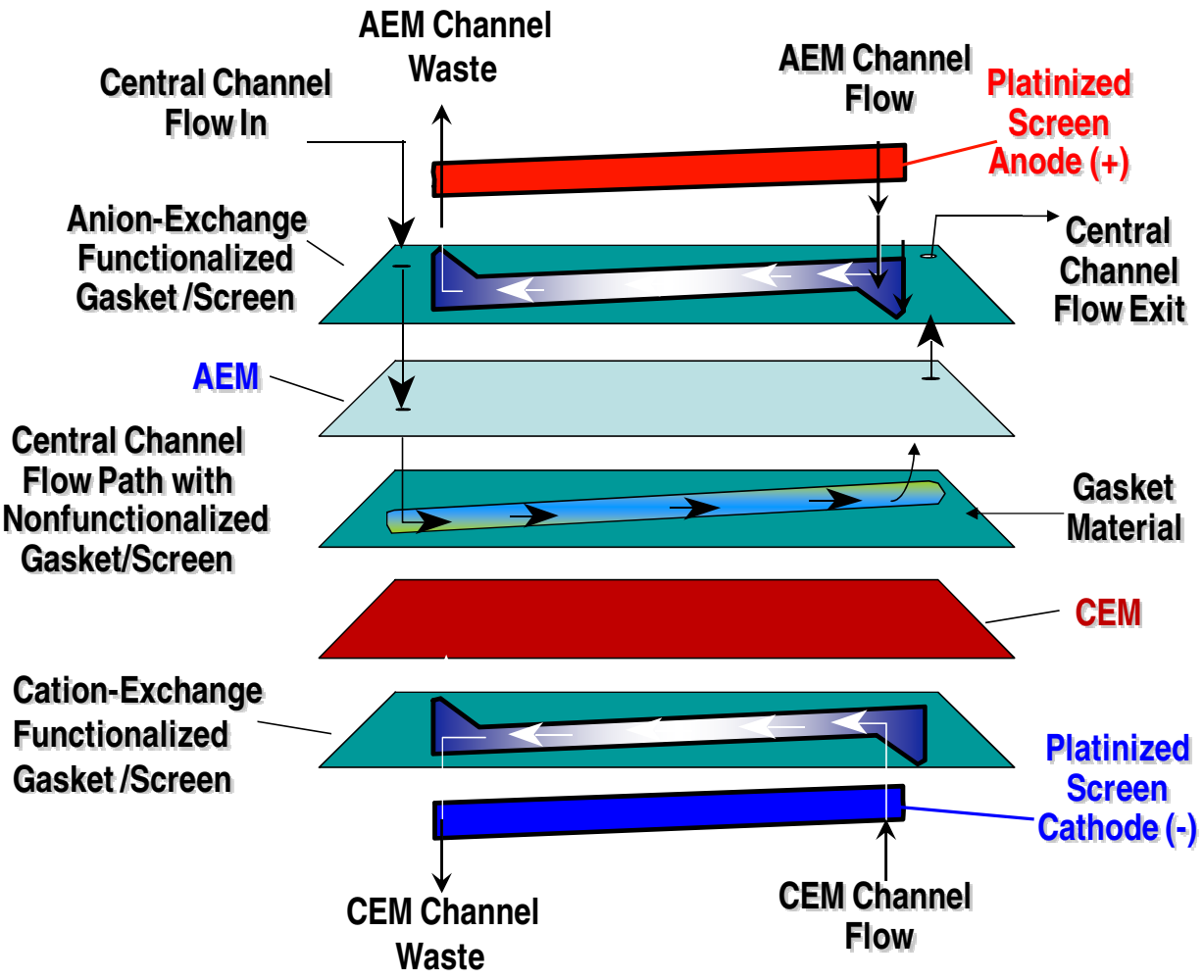

Figure A.3 Membrane based charge detector with screen separated electrodes (MSSE devices)

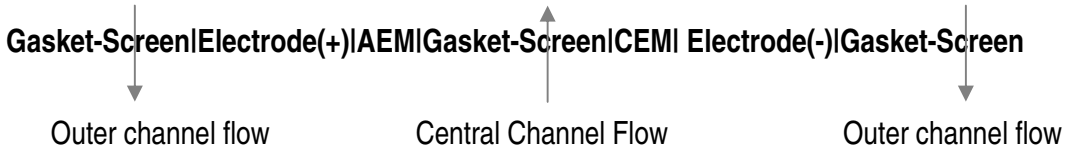

Scheme III

Details of screens and electrodes for membrane devices.

We use polyethylene (PE) monofilament screens (410 mesh, approximately 500 μm thick) that are radiation grafted and then appropriately ion exchange functionalized in the outer channels. The central channel contains a 250 μm thick 140 mesh unmodified PE screen. The IEMs are 75 or 125 μm thick poly(tetrafluoroethylene) films that are radiation grafted and then ion exchange functionalized;[184] the ion exchange capacities are ~1.2-2 meq/g. The entire assembly is placed between two PEEK plates that have appropriate fittings to facilitate fluidic inlet and outlet for the three independent channels. The platinized screen electrodes are connected to platinum wires that are routed via orifices in the PEEK plate to the exterior of the device.

Current to Voltage Conversion and Data Acquisition.

Current-to-Voltage conversion was carried out with either (a) model 427A current amplifier (www.keithley.com), (b) National Instruments NI USB 4065 $6^1/_2$-digit multimeter (www.ni.com) (c) a homebuilt converter based on a FET input operational amplifier (TL082, www.ti.com), (d) a homebuilt converter based on an electrometer grade operational amplifier (OPA128, www.ti.com) or (e) Stanford Research System-low-noise current preamplifier (Model SR570). The best performance was observed with d and e, which generally provided 1.5-2x better S/N than b. The data were recorded after current to voltage conversion (see below) with either a 12–bit A/D card (PC-CARD-DAS16/12AO, www.measurementcomputing.com) at 1 Hz or, when

using the membrane based devices, with the Chromeleon™ data system (www.dionex.com) at 5 Hz.

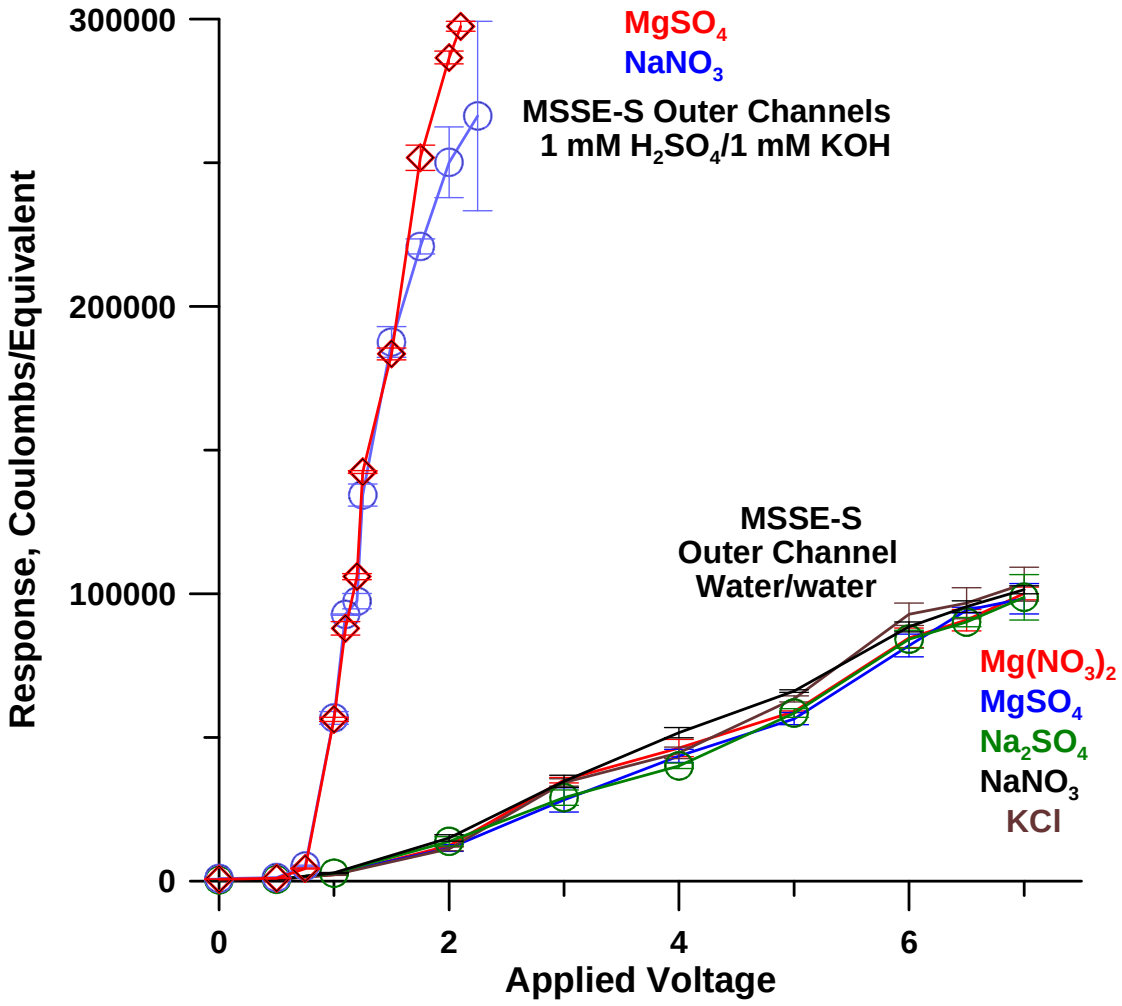

Figure A.4 Response on an equivalent basis is virtually identical for a variety of strong electrolytes (1.32 neq) injected in this example in a MSSE-S device, across a range of applied voltages and whether water/water or dilute acid/base are used as CEM/AEM electrolytes. The latter dramatically increases the response but it affects the different analytes in the same manner. Error bars in this and all subsequent figures indicate ±1 standard deviation for three to five measurements (typically four) at each point. In some cases error bars are smaller than the dimensions of the symbols plotted and cannot be seen.

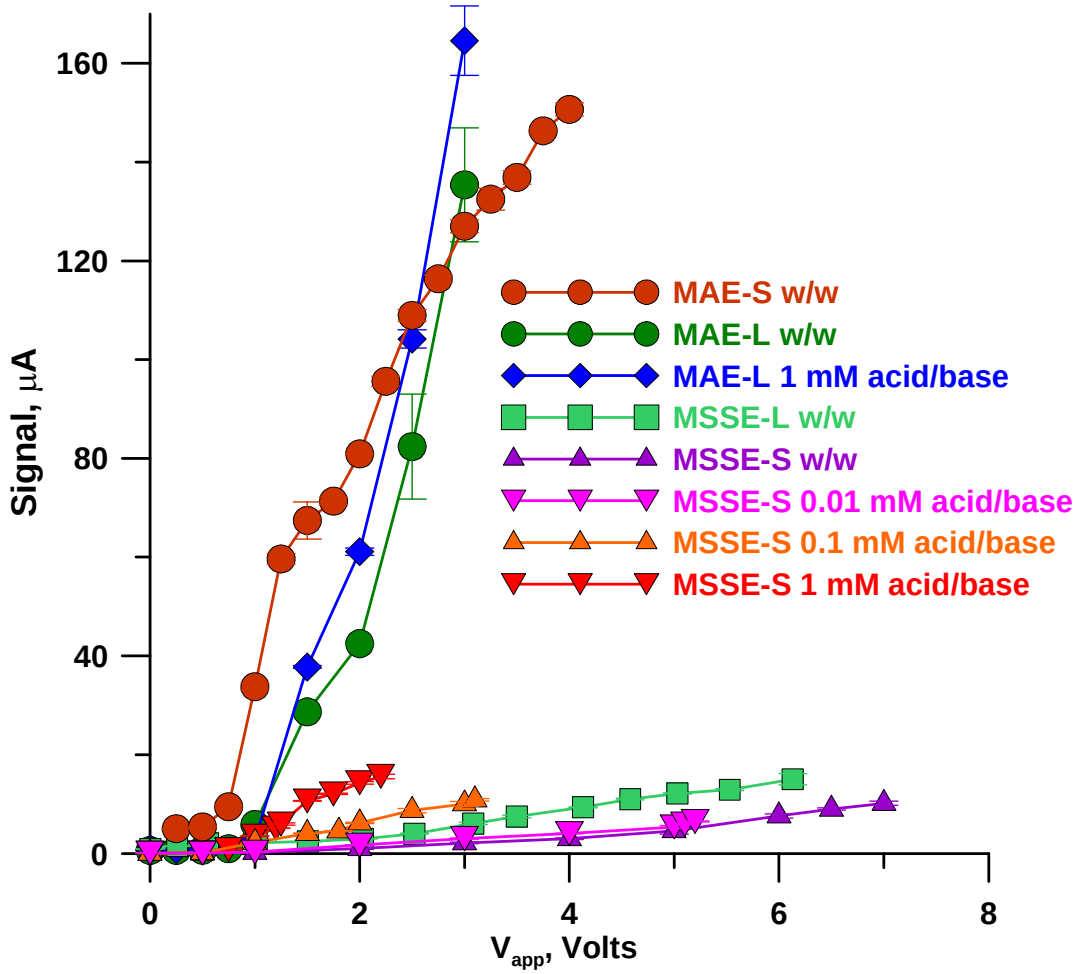

Figure A.5 Signal height in µA shown for various membrane based ChD devices operated with CEM/AEM channels water/water or acid/base. For acid 0.01, 0.1, or 1.0 mM H_2SO_4 was used, the same molar concentrations of KOH were used as the corresponding base. Injection volumes of 50 µM $NaNO_3$ were 54 and 26 µL and the central channel flow rate 1000 and 200 µL/min, respectively for type -L and –S devices.

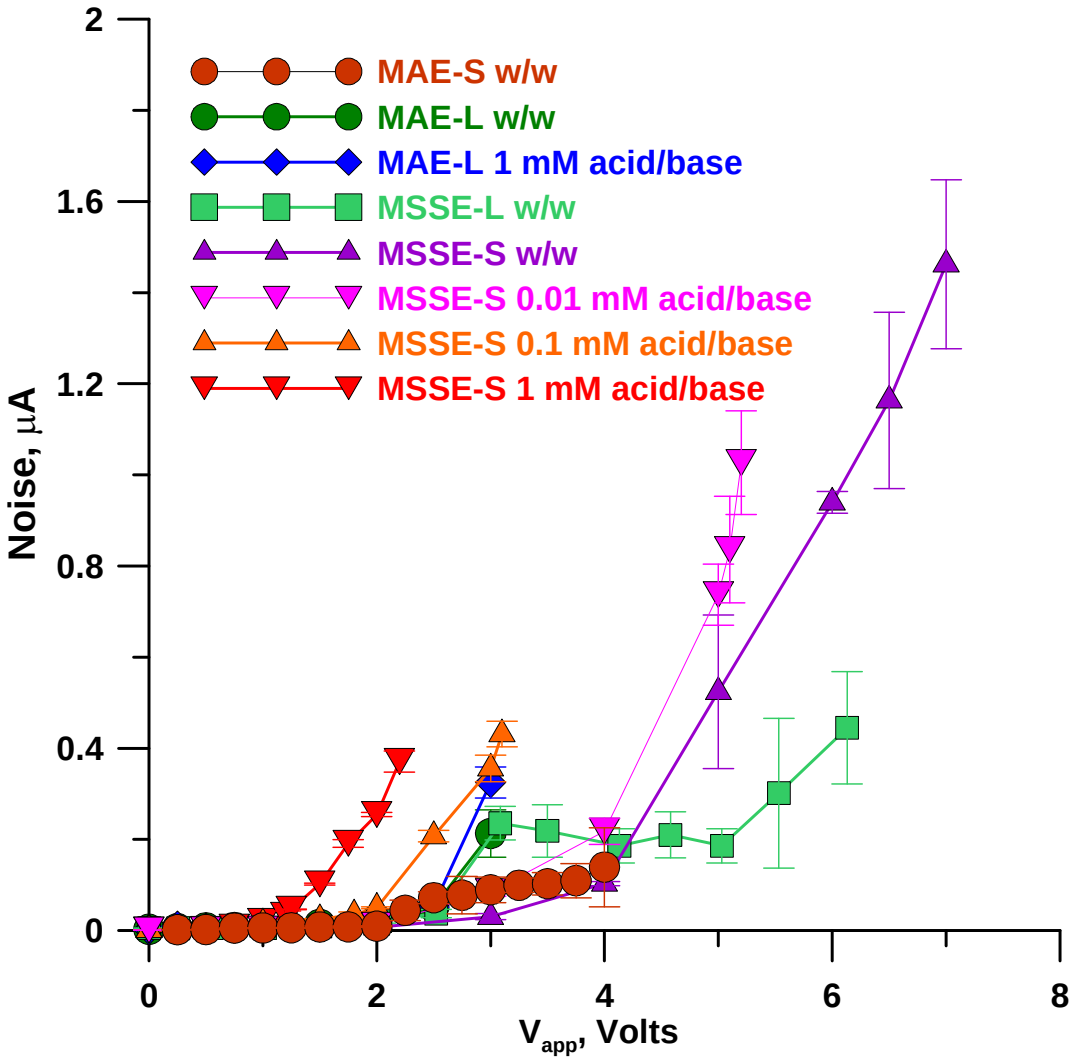

Figure A.6 Background noise for the experiments in the previous figure (Figure A.5).

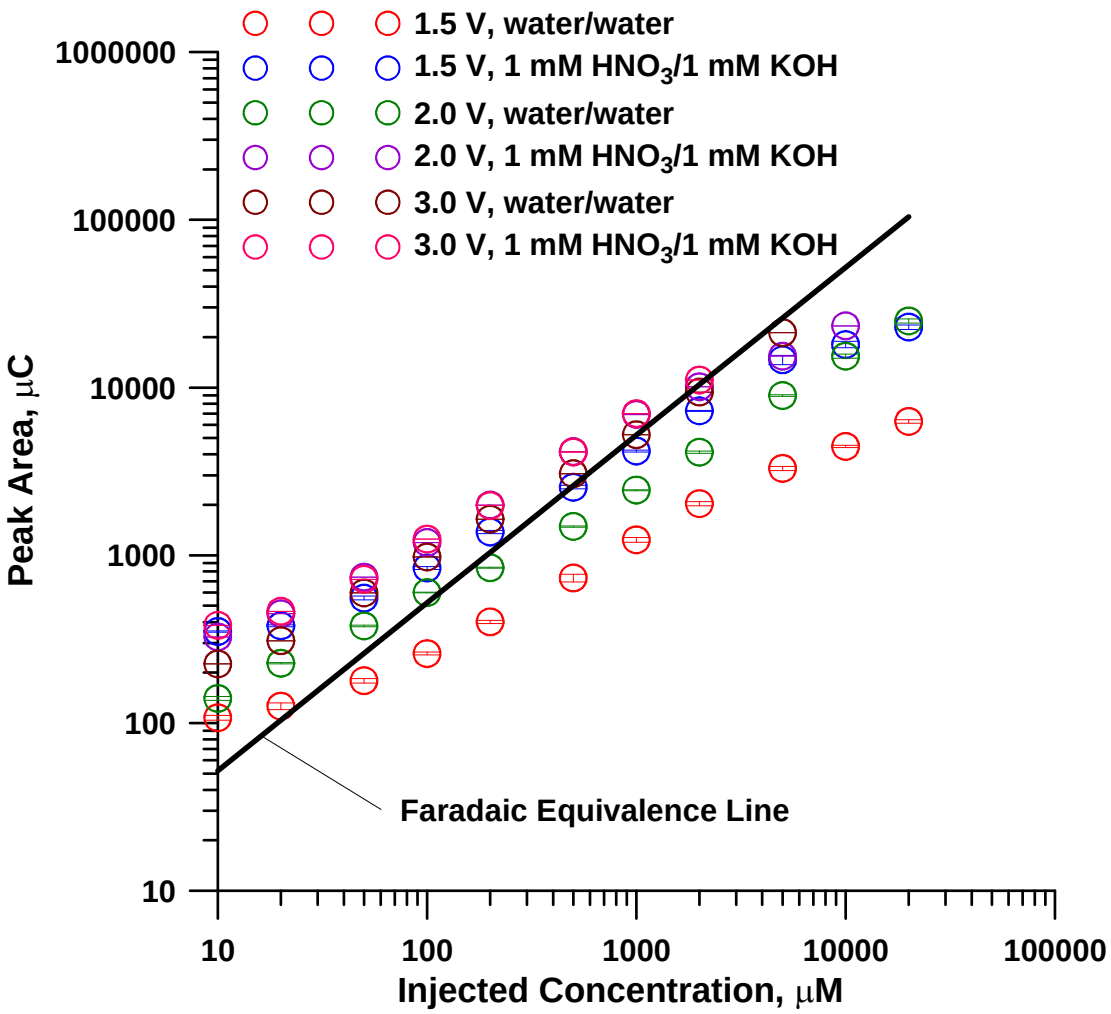

Figure A.7 Enlarged color version of Figure 2.7(b). Calibration behavior for different injected concentrations of KNO_3 over a large concentration range. Device MAE-L operated with different fluid compositions in the CEM/AEM outer channels.

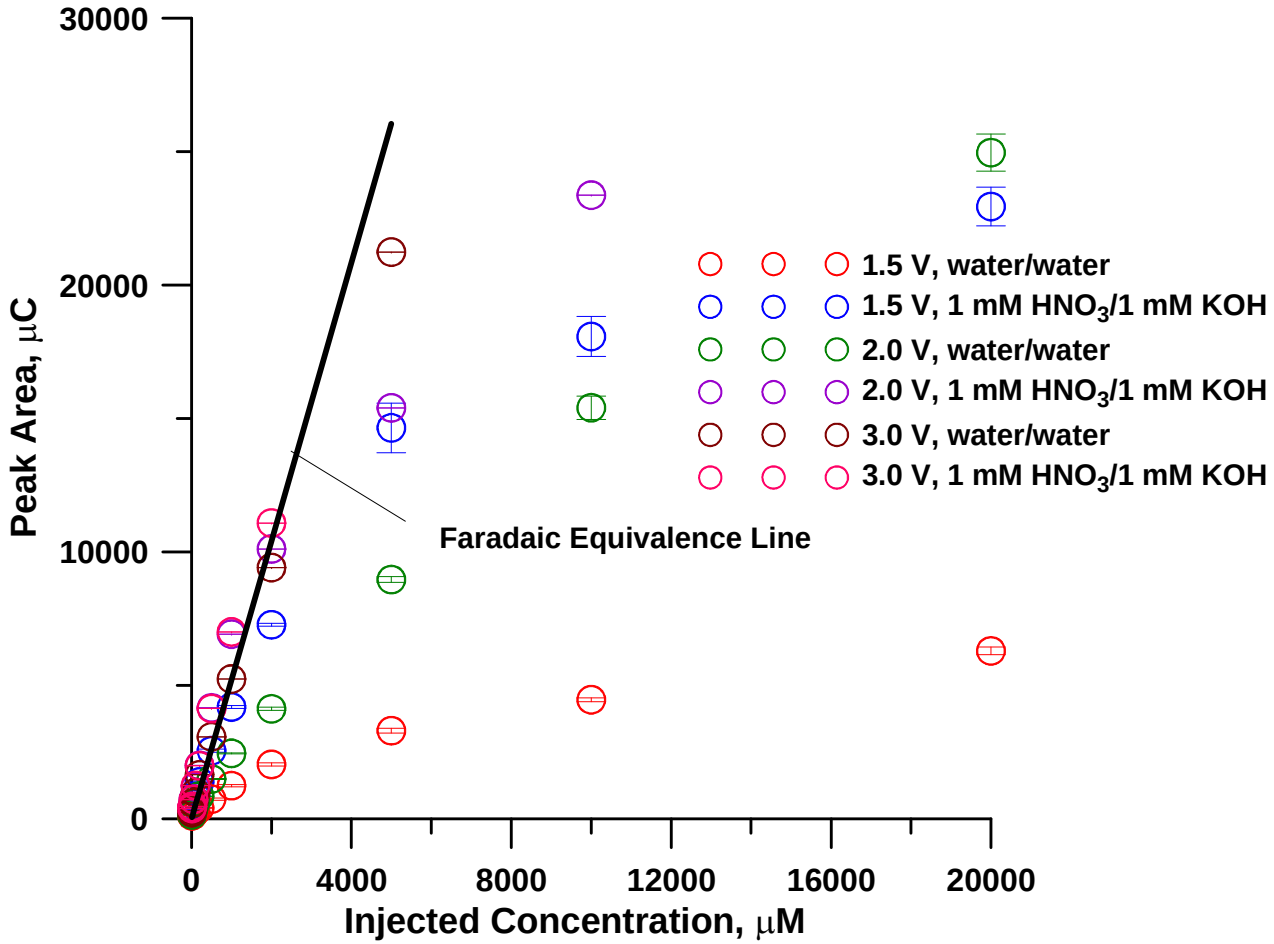

Figure A.8 Linear abscissa ordinate version of the previous figure (Figure A.7). The response is obviously nonlinear at V_{app} = 1.5V and 2V. However, Figures A.9-A.11 (that follow) show that over isolated decadal concentration spans, linear behavior can be assumed without significant error.

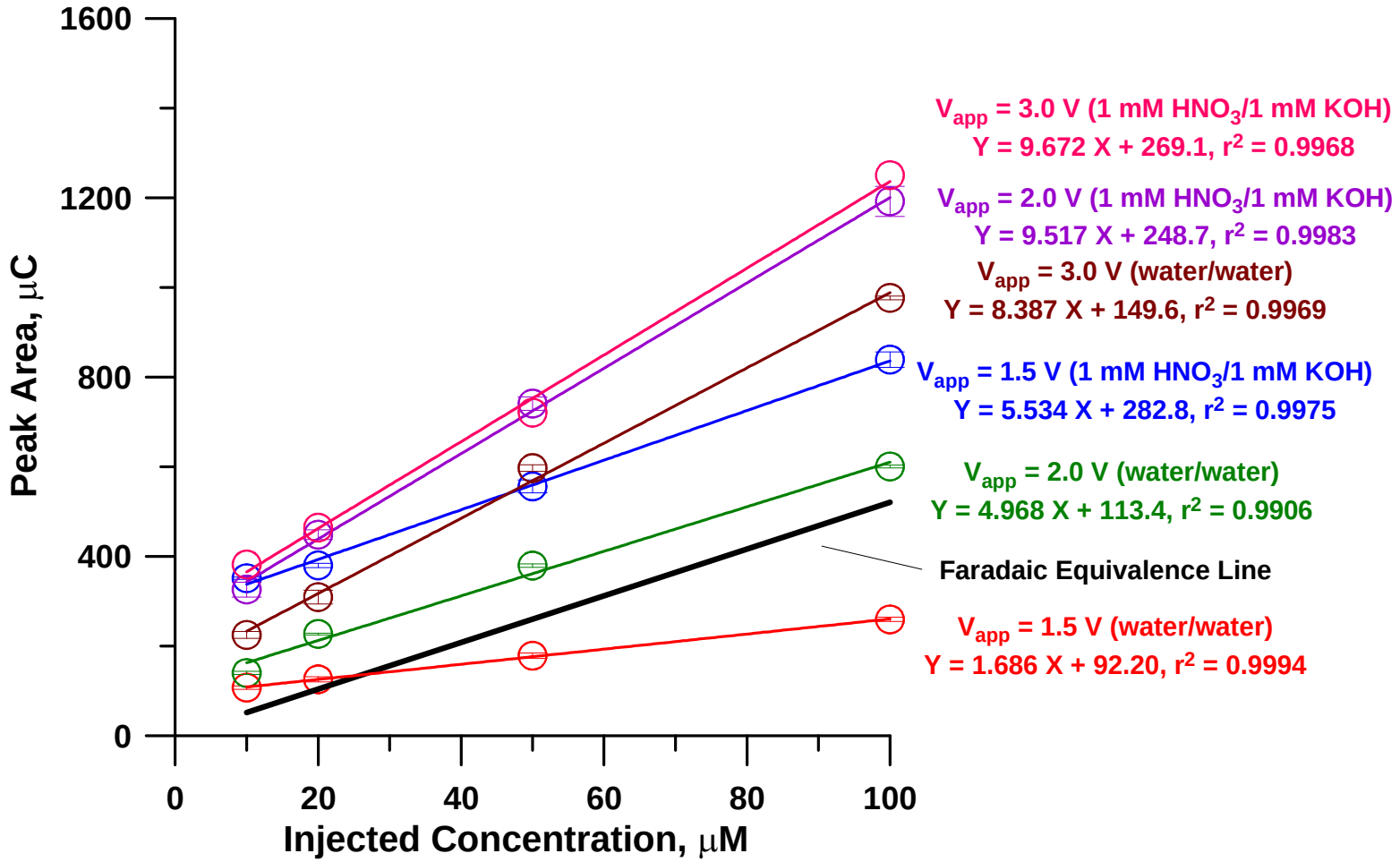

Figure A.9 Linear behavior in the 10-100 μM concentration range.

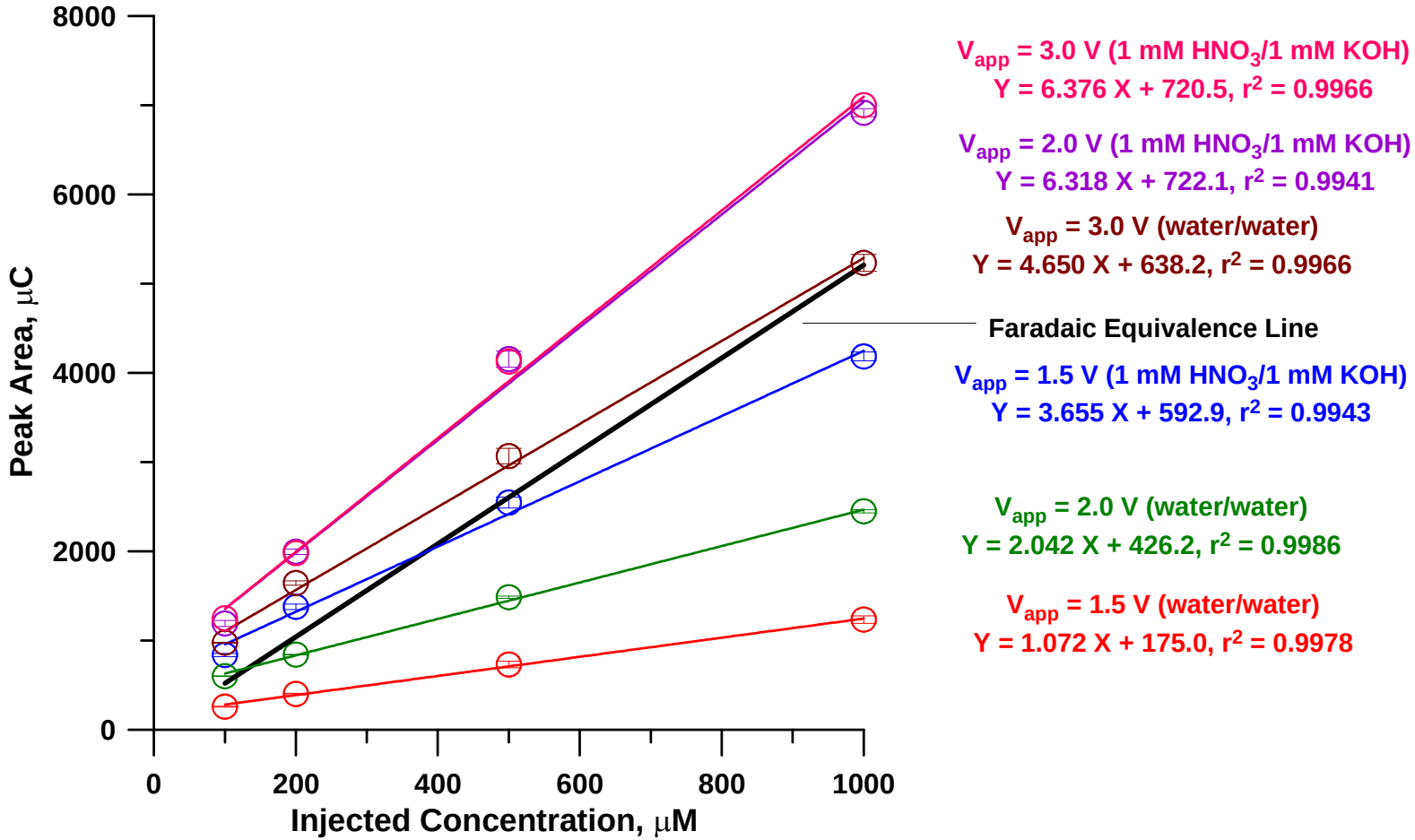

Figure A.10 Linear behavior in the 100-1000 μM concentration range. Note the decrease in slope from the previous figure.

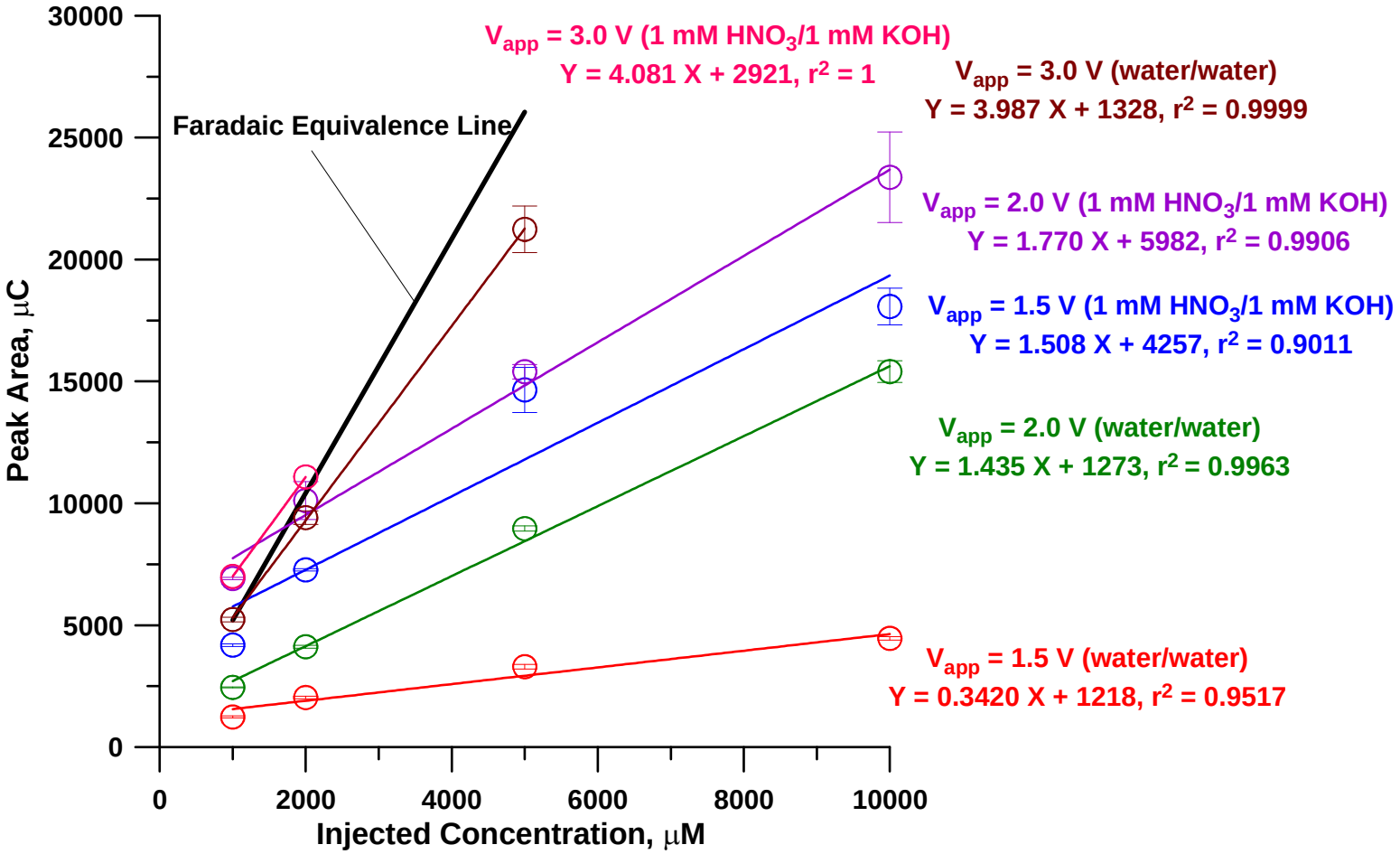

Figure A.11 Linear behavior in the 1-10 mM concentration range. Note the decrease in slope from the previous two figures.

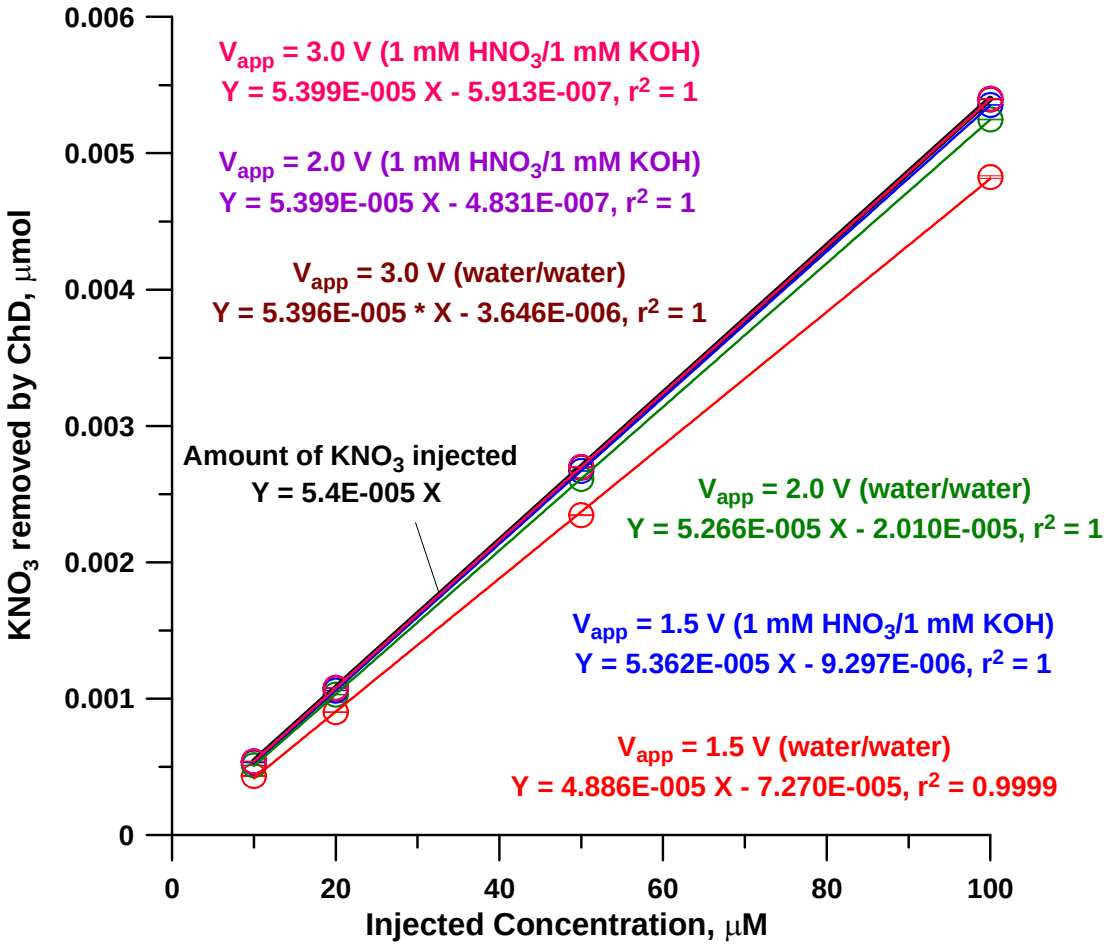

Figure A.12 This is the same data as in Figure A.9. The ordinate is not the peak area but the amount removed by the ChD as measured by the ratio of the response of two calibrated conductivity detectors (measured in terms of peak area) one placed before and the other after the ChD. The amount removed generally decreases with increasing concentration and decreasing V_{app}. At V_{app} =1.5 V (w/w), 87-94% of the injected amount is removed (except at 10 and 20 mM analyte concentrations, when 83 and 69% are respectively removed); at V_{app} =2.0 V (w/w), 95-98% is removed (except 92.4 and 86% are respectively removed at 10 and 20 mM analyte concentrations), at V_{app} = 3.0V (w/w), 99.4-99.9% is removed across the entire concentration range. Note that instead of water, when acid/base is present in the outer channels, the fraction removed is greatly increased at a given V_{app}. V_{app} = 2.0 V (1 mM HNO_3/1 mM KOH) and V_{app} = 3.0 V (1 mM HNO_3/1 mM KOH), more than 99.9% were removed at the whole concentration range up to 20 mM; except for V_{app} = 1.5 V (1 mM HNO_3/1 mM KOH), 98.0-99.5 % were removed, which is still much higher than V_{app} =2.0 V (w/w).

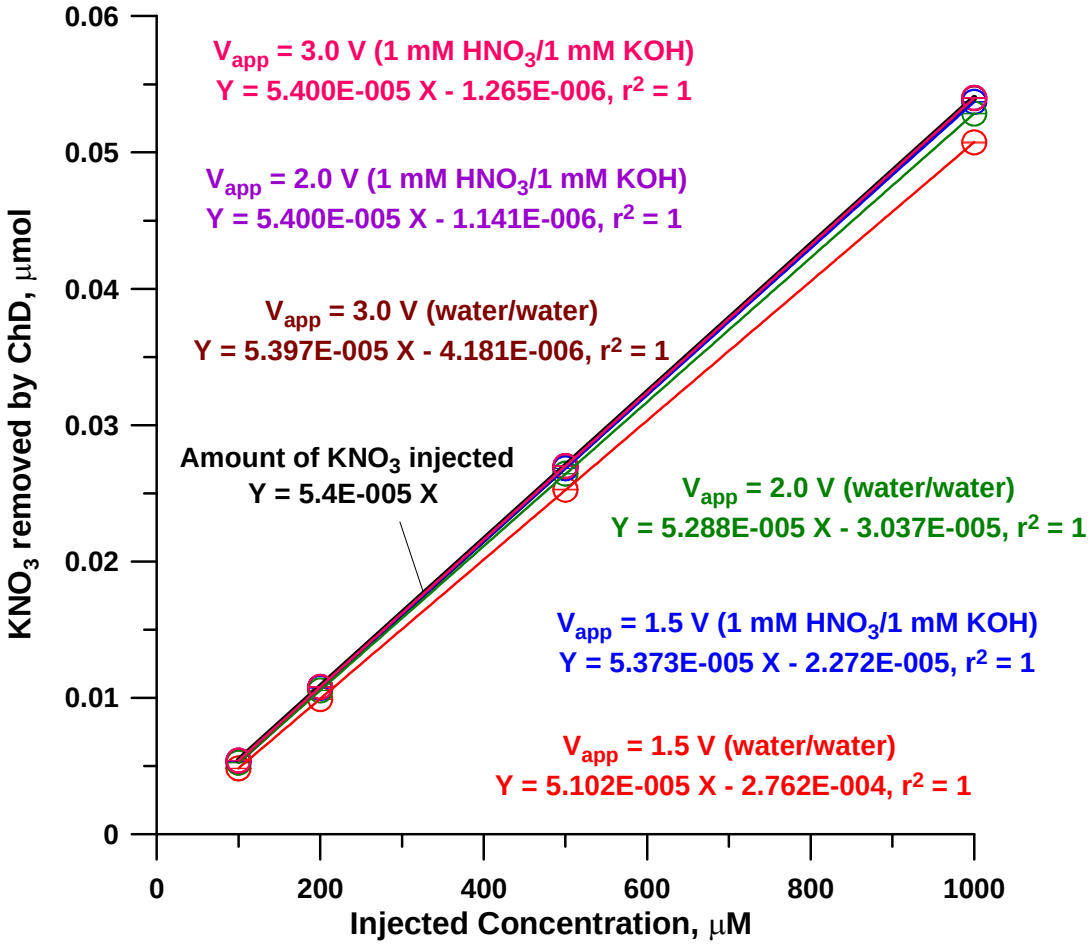

Figure A.13 As in Figure A.12, 100-1000 μM concentration range.

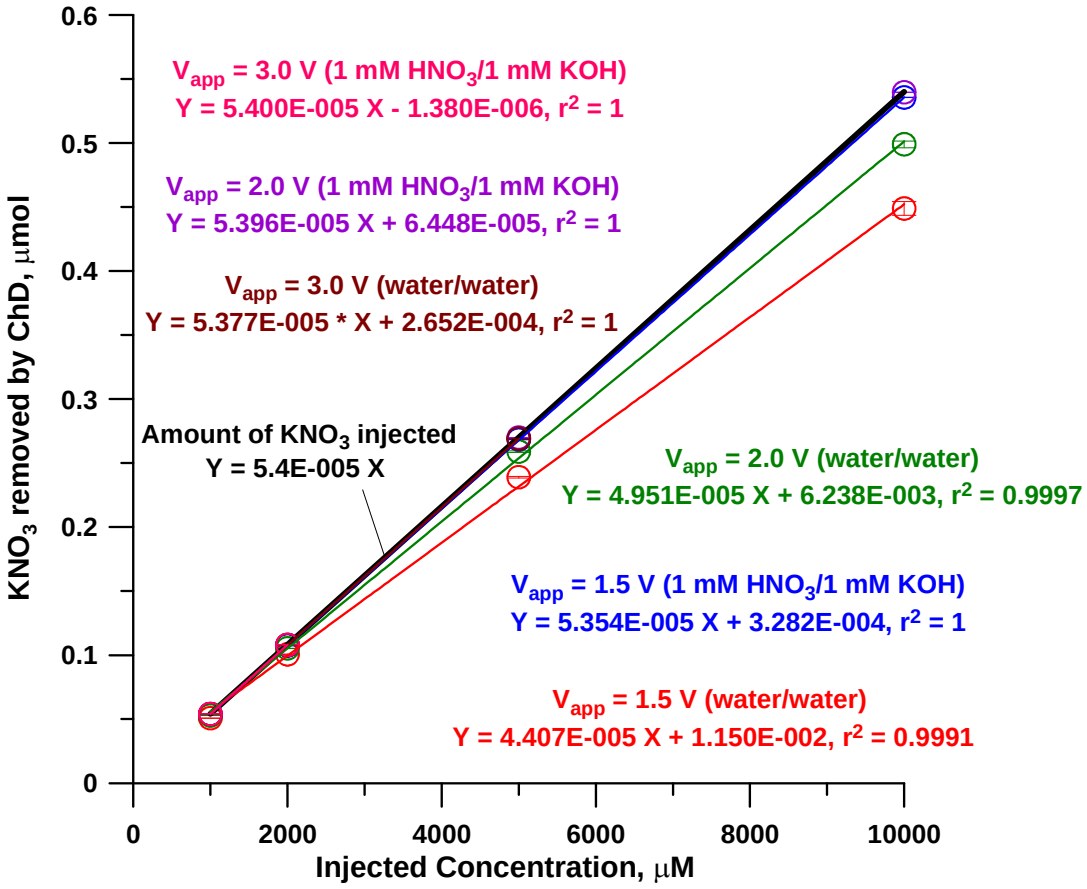

Figure A.14 As in Figure A.12 and A.13, 1-10 mM concentration range.

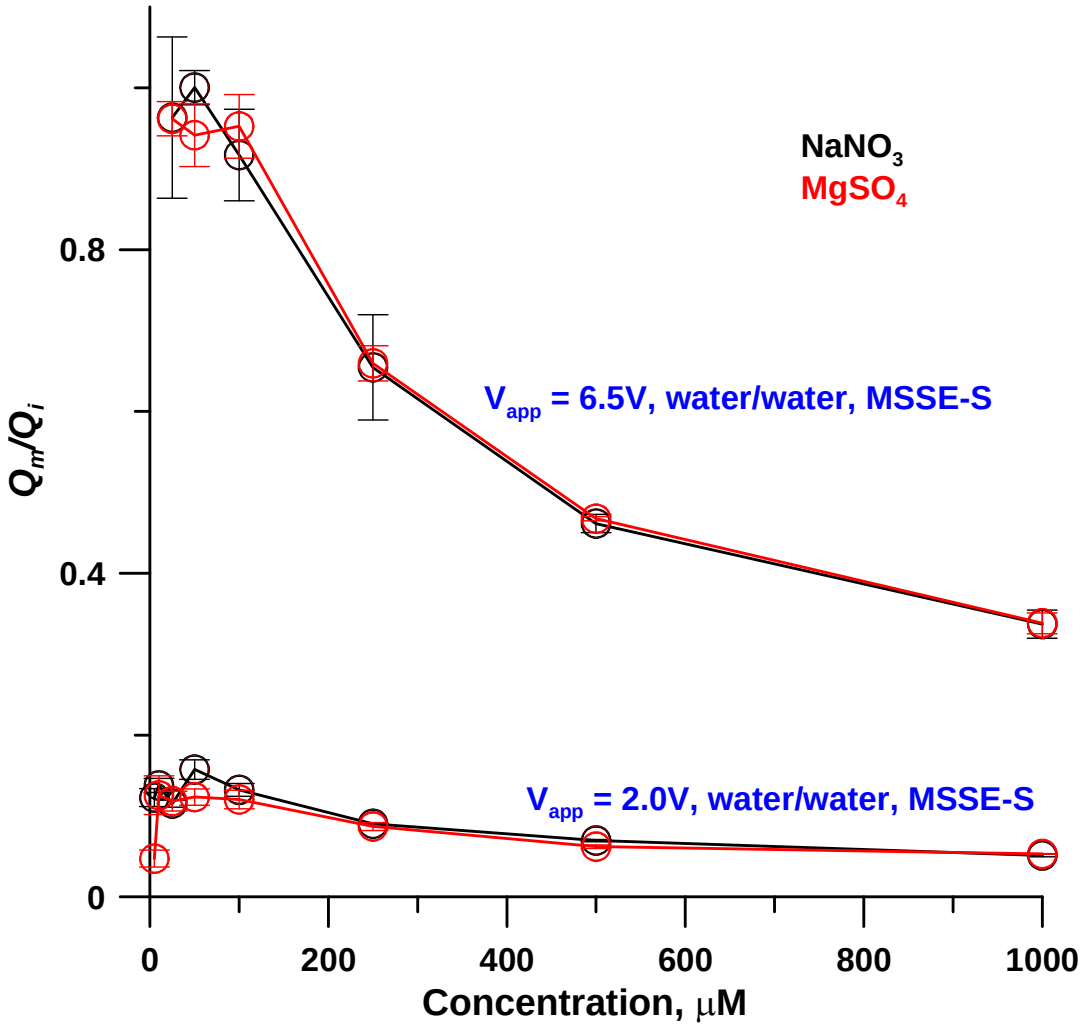

Figure A.15 In MSSE devices operated with water in the outer channels, the response decreases with increasing concentration even at low concentrations.

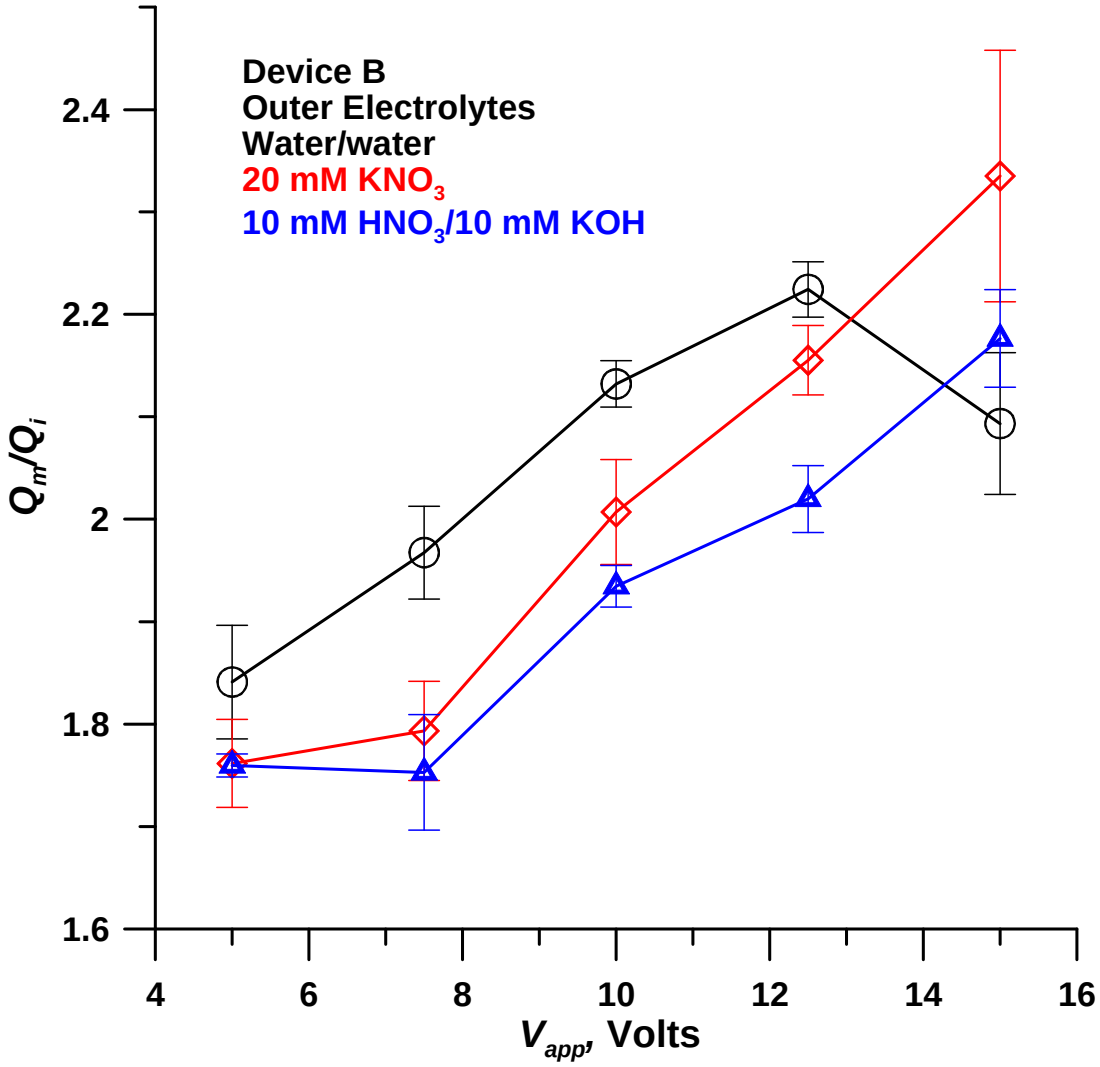

Figure A.16 Device ChD-B. Q_m/Q_i shows a maximum value with V_{app} when operated with water/water in the outer channels but not when electrolytes are present. Analyte 2.5 µL 100 µM HCl, CCFR 20 µL/min.

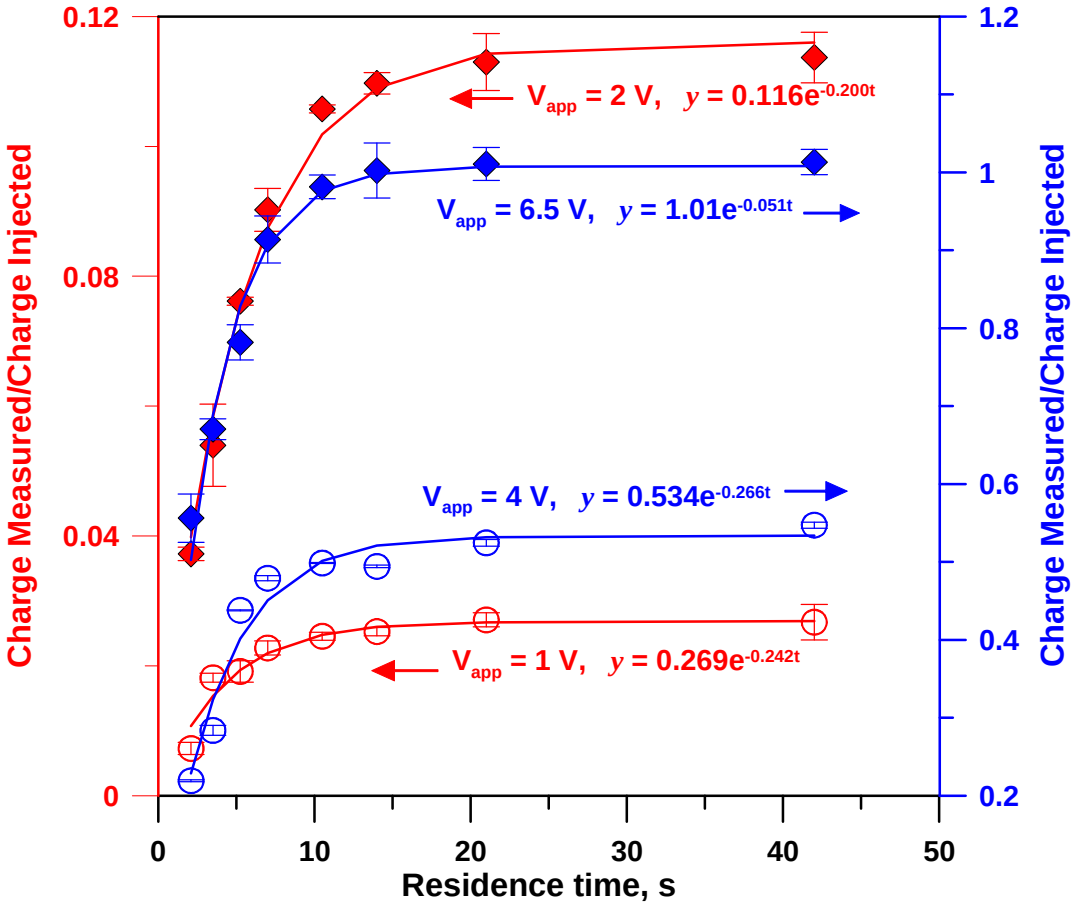

Figure A.17 Charge signal injected charge ratio (26.4 µL of 50 µM KNO_3) at 4 different applied voltages as a function of residence time in the device. Device MSSE-S, internal volume 35 µL, central channel flow rates from 50 -1000 µL/min. Both outer channel electrolytes: water, 1.5 mL/min. All solid lines are first order fits in time, the best fit equations are indicated.

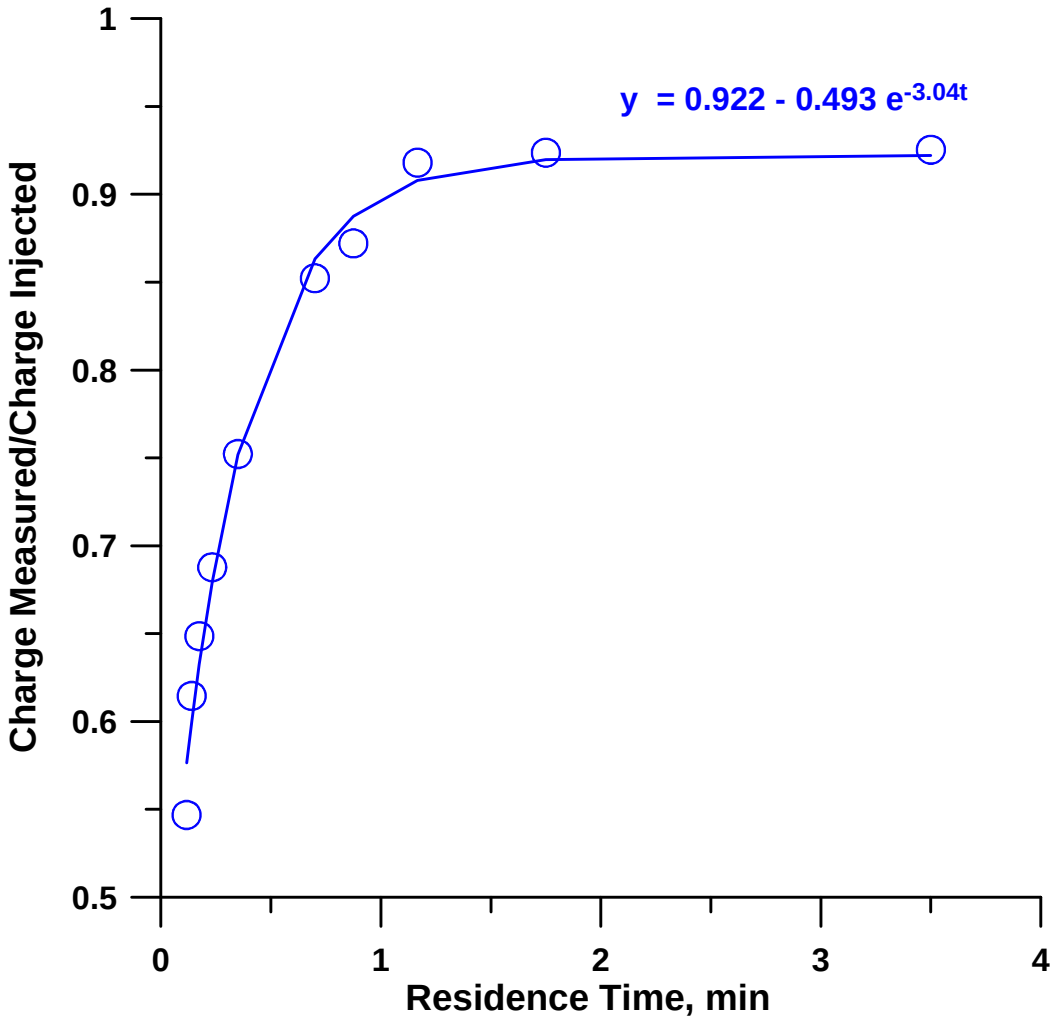

Figure A.18 Ratio of the measured charge signal to the injected charge (54.0 µL of 100 µM KNO_3) at 2 V as a function of residence time in the device. Device MAE-S, internal volume 35 µL, central channel flow rates from 100-3000 µL/min. Outer channel electrolytes: water, 1.5 mL/min. The solid line is first order fit in residence time, the best fit equation is indicated.

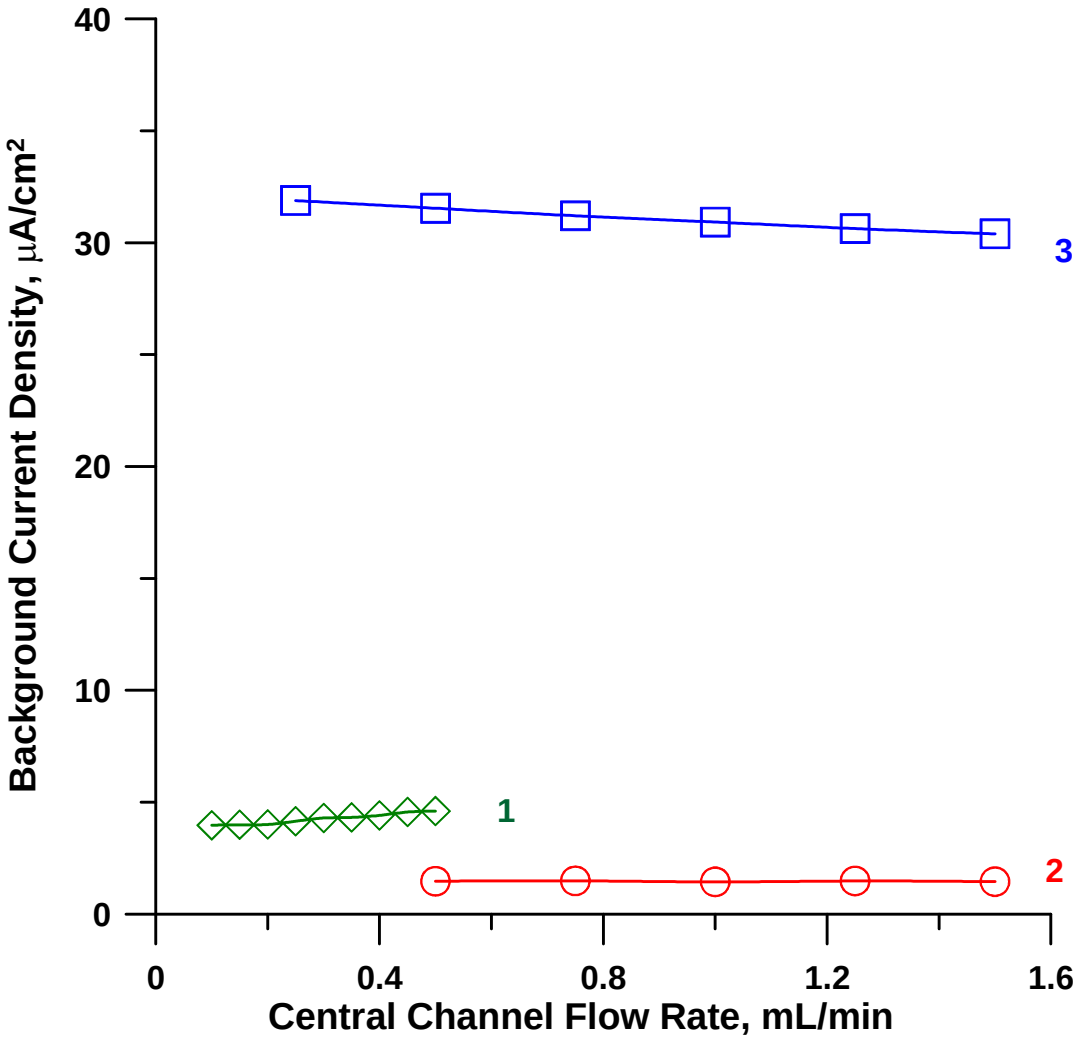

Figure A.19 Background current density as a function of water flow rate in the central channel. (1) MSSE-S, water/water; (2) MSSE-L, water/water; (3) MAE-L, water/water. Applied voltage: 2 V; flow rate in the outer channel: 1.5 mL/min for MSSE–S device, 2.0 mL/min for –L devices.

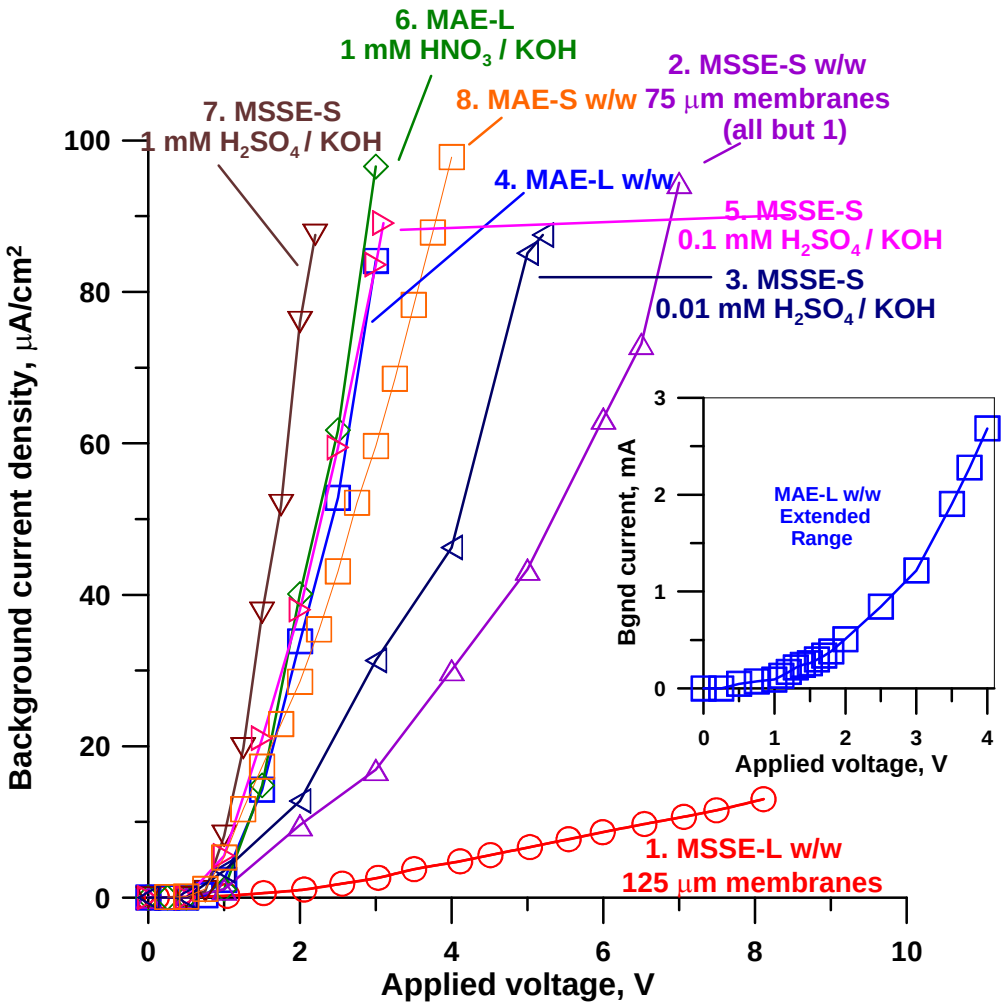

Figure A.20 Background current density as a function of applied voltage (reversed bias charge detector operation mode). Devices as indicated. Device 1 used 125 µm thick membranes, all others used 75 µm thick membranes. Water is indicated by w. Central channel: water at 1.00 and 0.20 mL/min for –L and -S devices, respectively; outer channel flow rates ~1.5 mL/min for all devices.

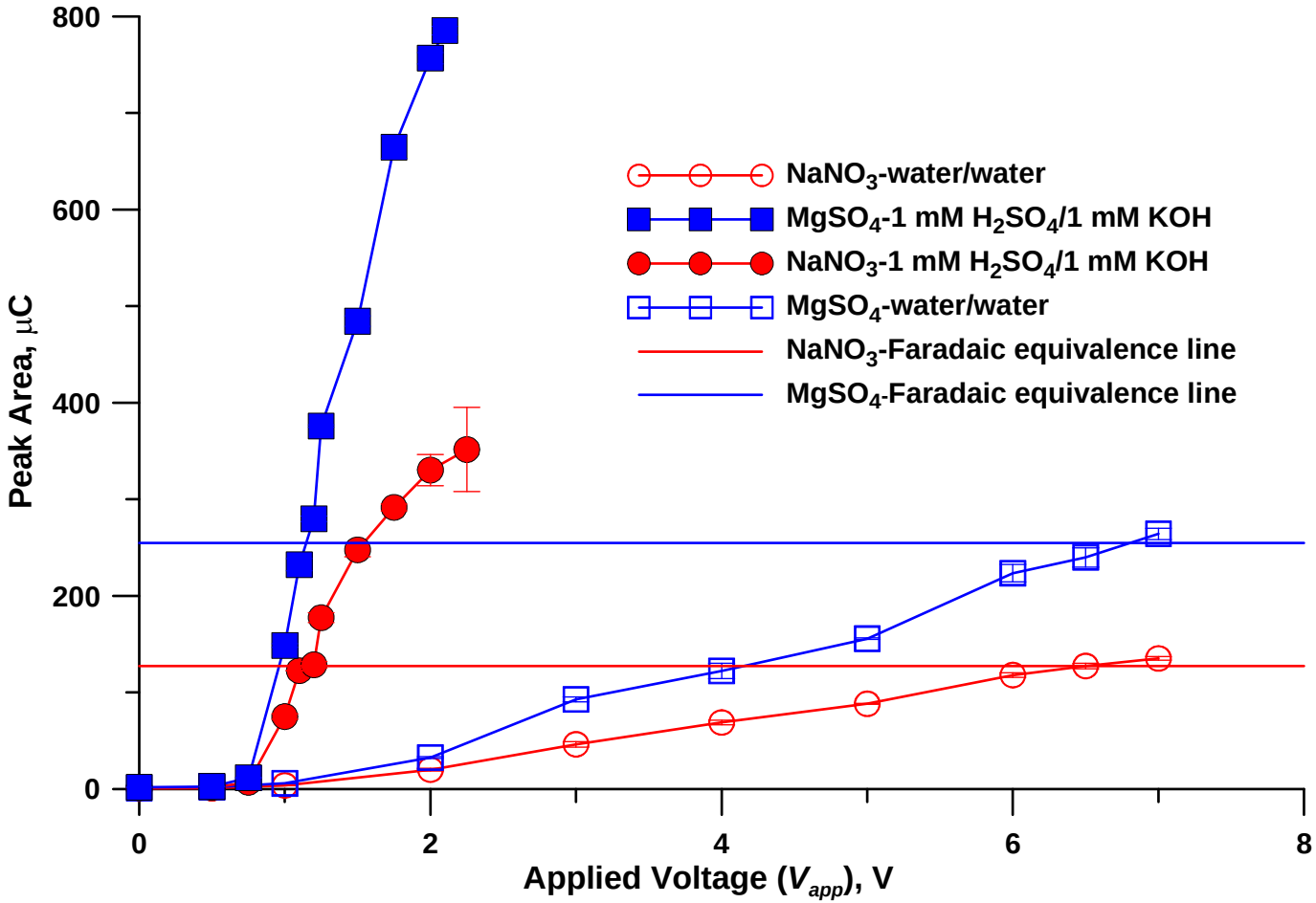

Figure A.21 Effect of strong electrolytes (acid and base) in the outer compartments on peak area as a function of applied voltage of a MSSE-S device. Flow in the central channel: water, 0.20 mL/min; flow in the outer channel: water or 1 mM H_2SO_4 on the CEM side and 1 mM KOH on the AEM side, 1.5 mL/min; injected sample: 50 μM $NaNO_3$ and 50 μM $MgSO_4$; injection volume: 26.4 μL. The Faradaic equivalence value is the charge carried by the electrolyte injected. Error bar indicates standard deviation (n = 4).

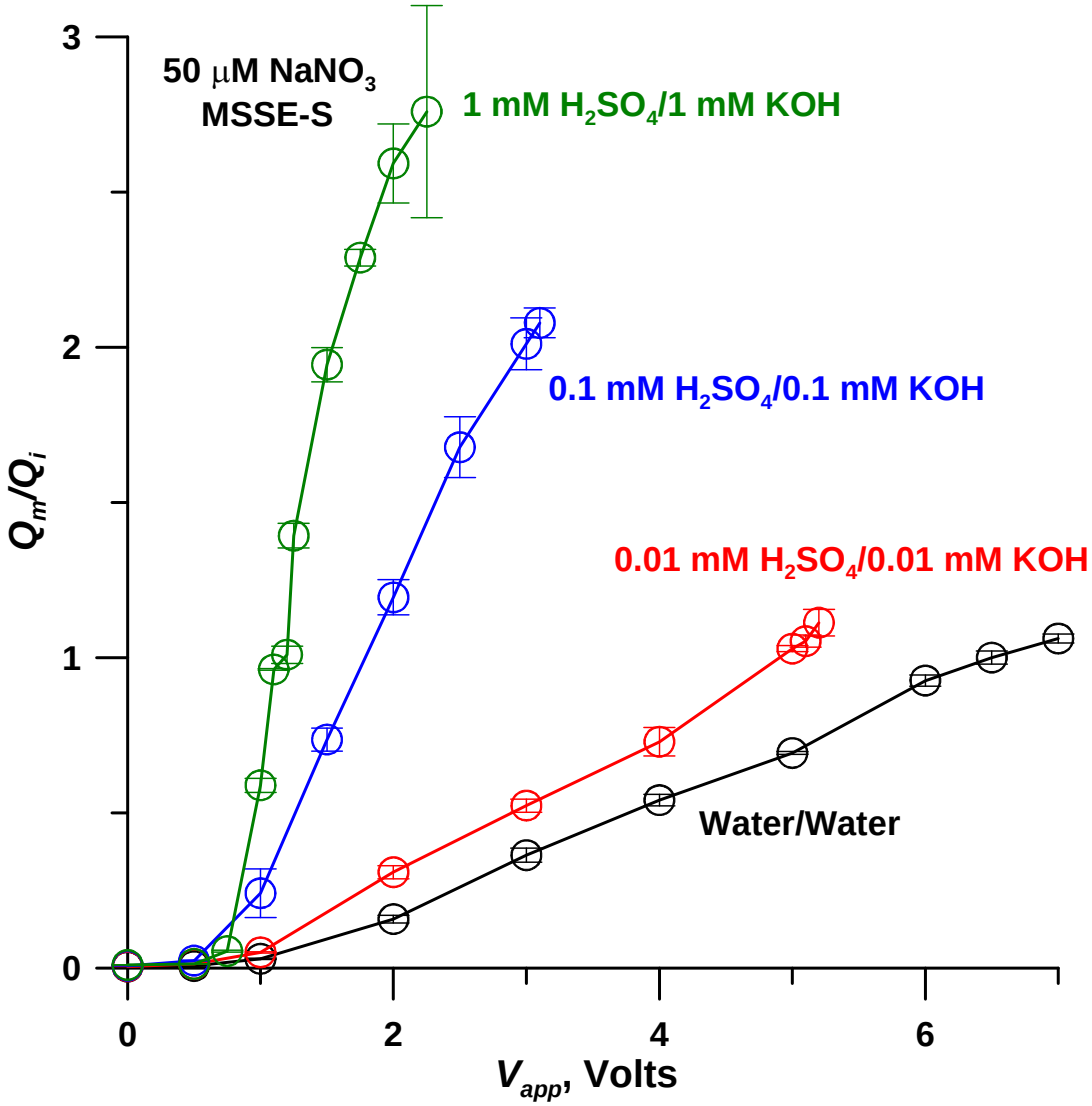

Figure A.22 Behavior of a MSSE-S device with different electrolytes in the outer channel and 26.4 μL 50 μM $NaNO_3$ injected. Flow in the central channel: water, 0.20 mL/min; flow in the outer channels: 1.5 mL/min.

Table A.1 Signal to noise ratio of a MAE-L device operated with water/water or 1 mM HNO_3/1 mM KOH in the outer channels at three different voltages.

Applied voltage (CEM/AEM)	Signal, μA	Noise, μA	S/N
1.5 V (water/water)	33.0	0.0225	1470
2.0 V (water/water)	66.5	0.0283	2350
3.0 V (water/water)	139	0.232	600
1.5 V (HNO_3/KOH)	107	0.049	2180
2.0 V (HNO_3/KOH)	148	0.0592	2500
3.0 V (HNO_3/KOH)	178	0.296	600

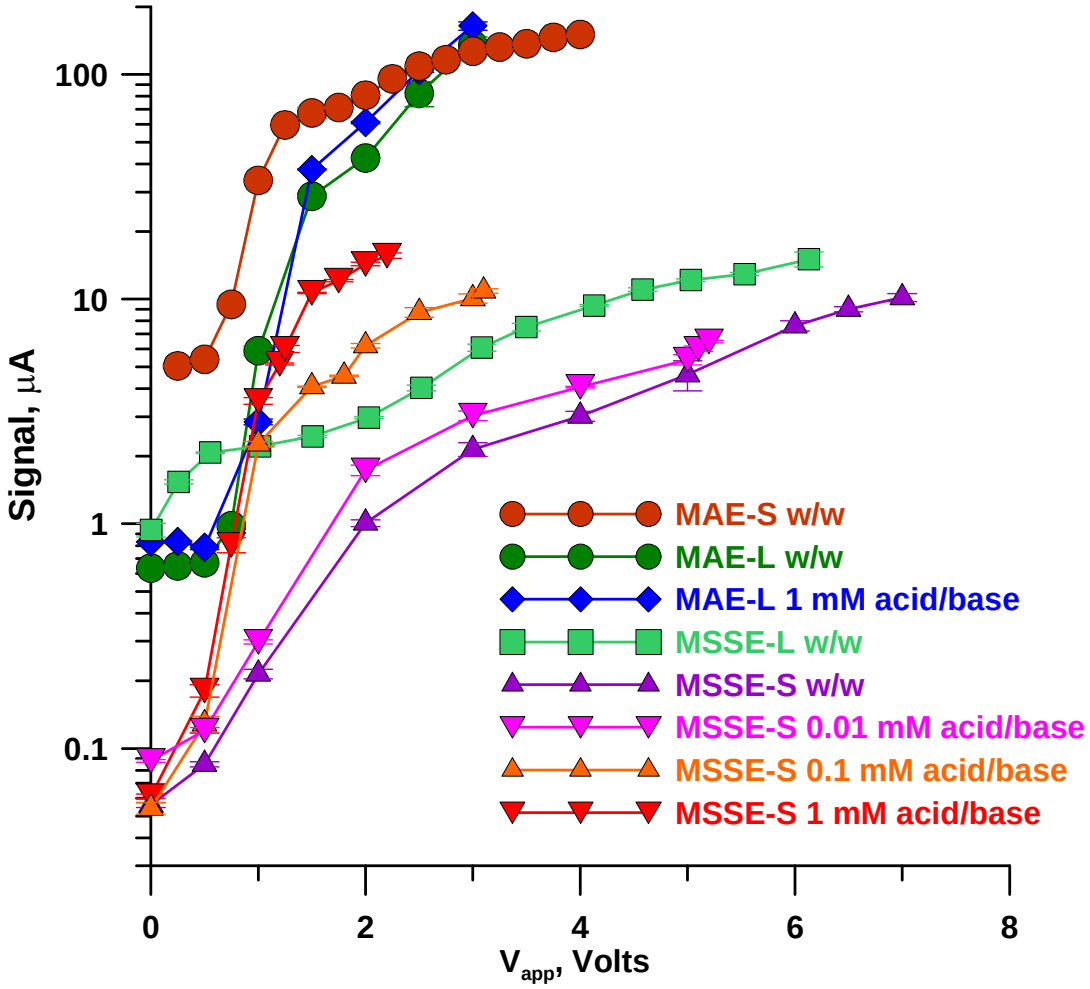

Figure A.23 Signal height in µA shown in logarithmic ordinates for various MAE and MSSE devices operated with CEM/AEM channels water/water or acid/ base. For acid 0.01, 0.1, or 1.0 mM H_2SO_4 was used, the same molar concentrations of KOH was used as the corresponding base. Injection volumes of 50 µM $NaNO_3$ were 54 and 26 µL, respectively, for type -L and –S devices. Central channel flow rates were 1000 and 200 µL/min, respectively for type -L and –S devices. See Figure A.5 for depiction of these data in a linear ordinate scale.

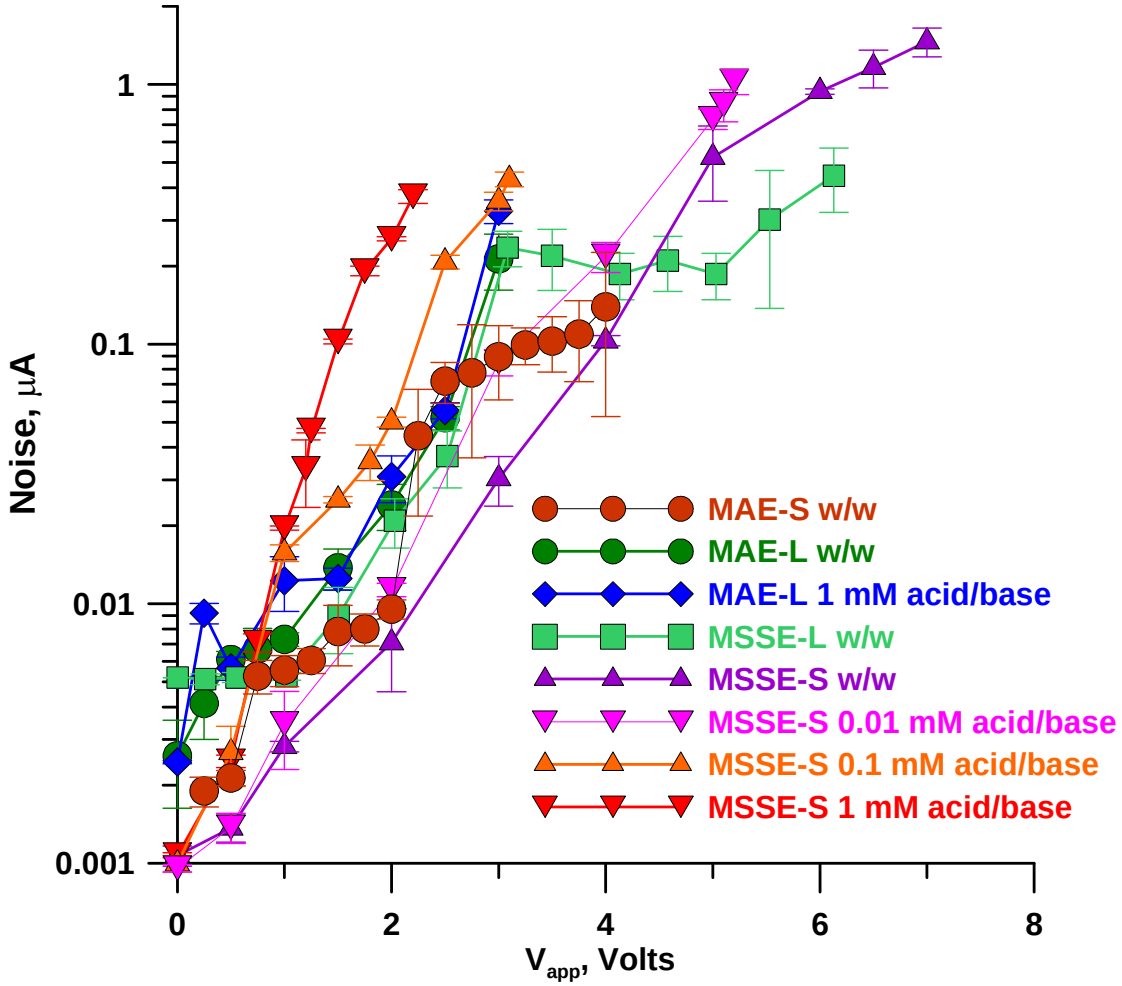

Figure A.24 Background noise in experiments described in Figure A.23; logarithmic ordinate. For a linear ordinate see Figure A.6.

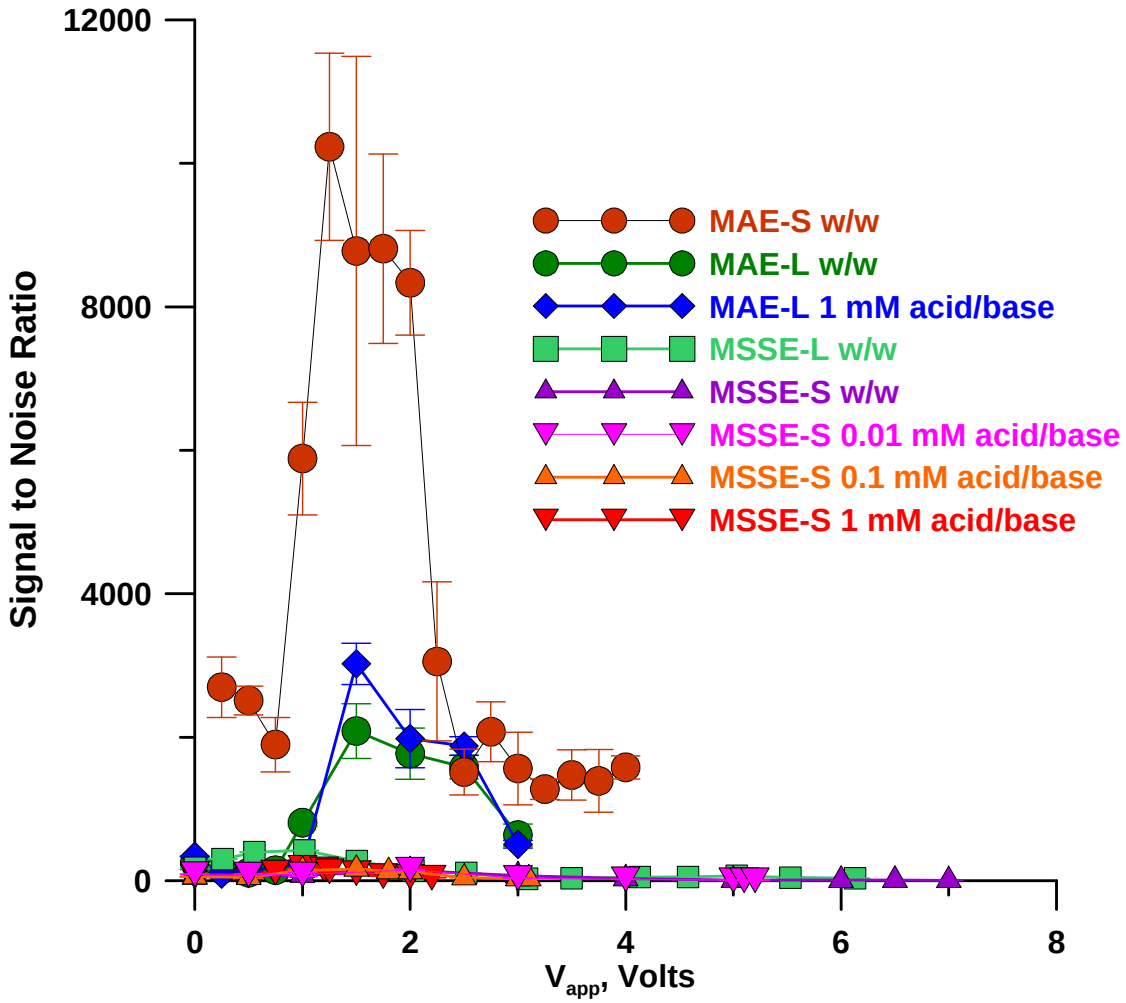

Figure A.25 The data in Figure 2.9 plotted with a linear ordinate.

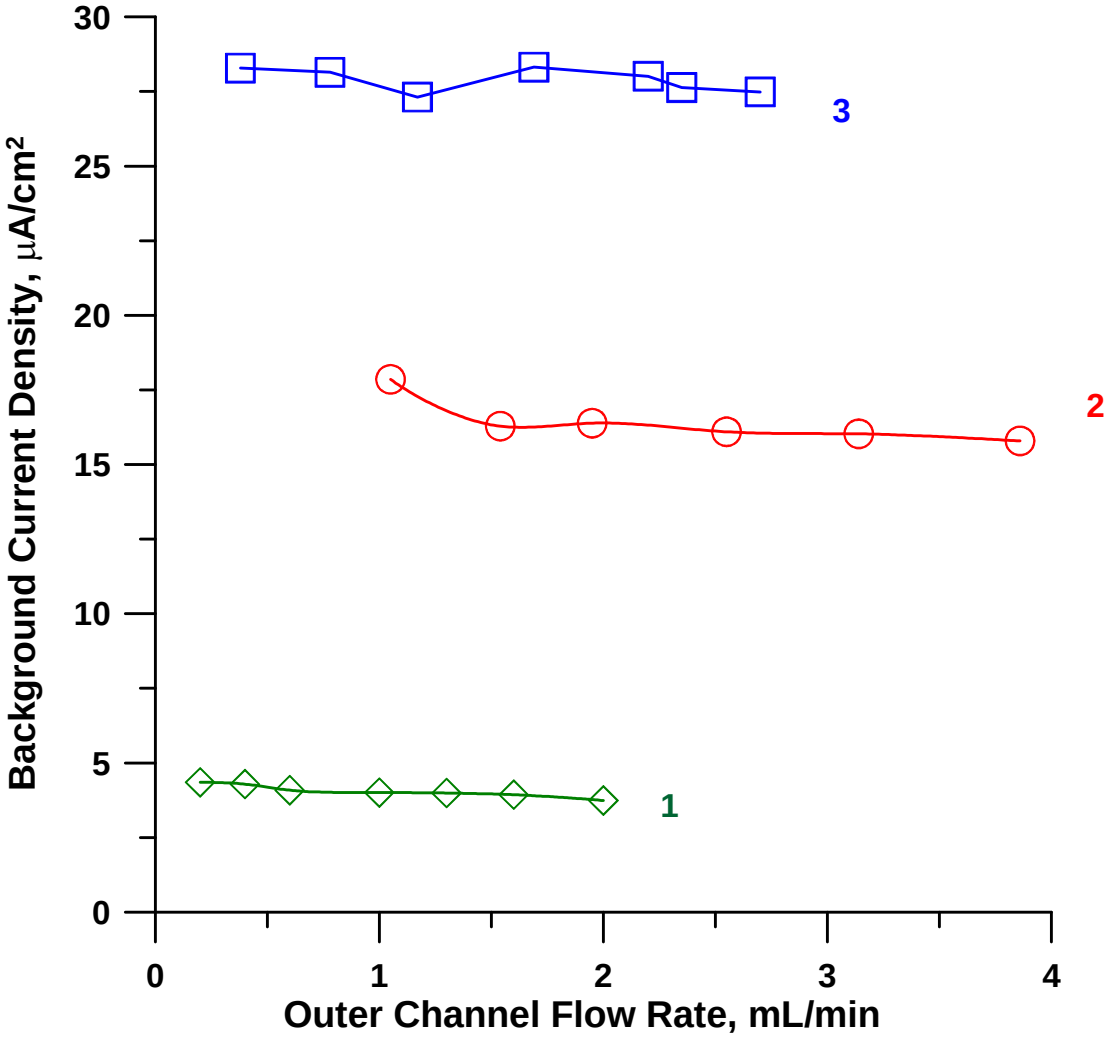

Figure A.26 Background current density as a function of flow rate in the outer channel**.** (1) MSSE-S, water/water; (2) MSSE-L, water/water; (3) MAE-L, water/water. Applied voltage: 2 V; flow rate in the central channel: 0.20 mL/min for the –S devices, 1.00 mL/min for both -L devices. What little change is observed relates to purity of the water actually entering the outer channel of the devices. It is difficult to prevent CO_2 intrusion to the water flowing in the connecting tubing between the water sources and the device inlet. At slower flow rates, the residence time of the water in the interconnecting tubing is higher and effectively the CO_2 content of the water reaching the outer channels of the device is higher. In MSSE devices this reduces the voltage drop in the outer channels. Some of the CO_2 can also permeate through the membranes into the central channel, ionize and then be removed by the normal operation of the device, contributing to background current.

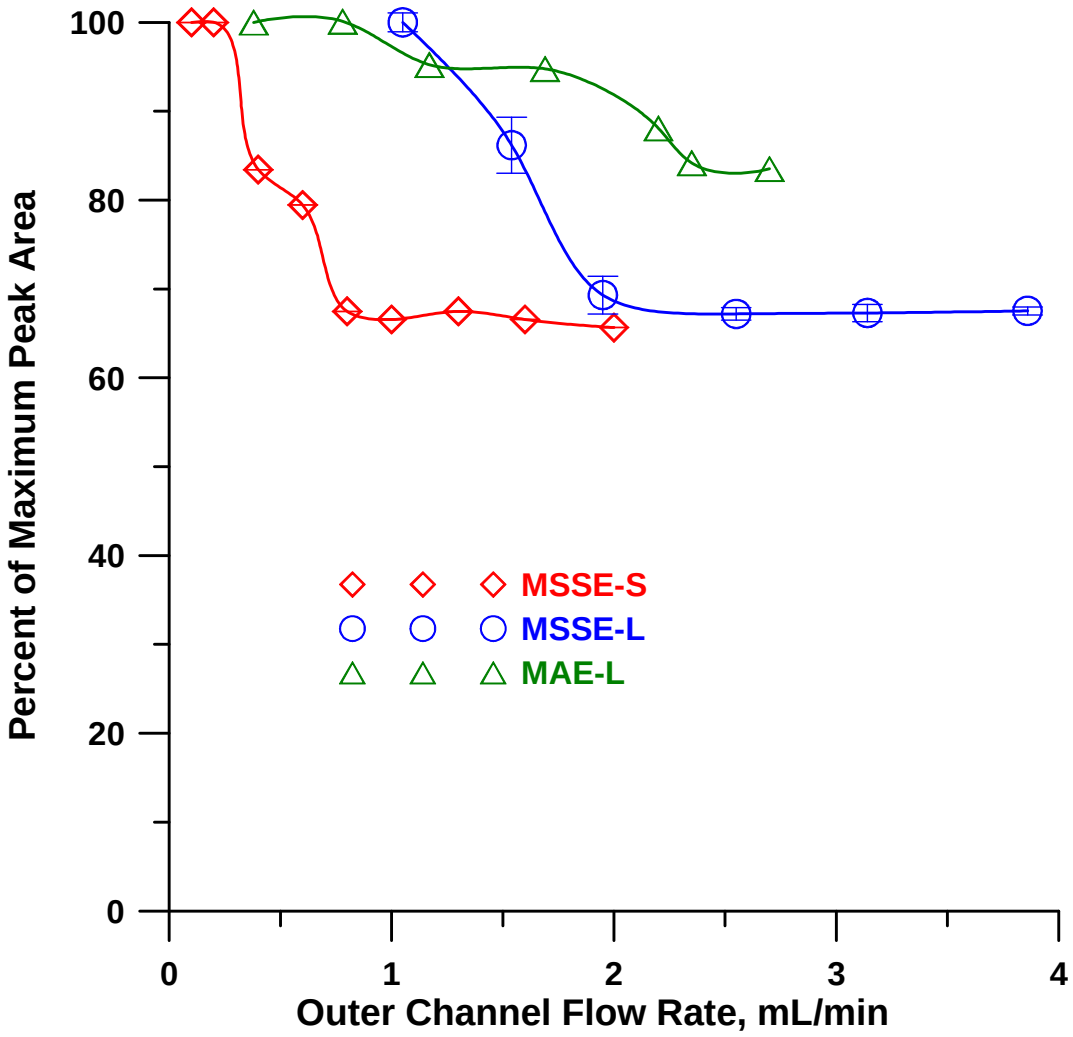

Figure A.27 The dependence of the observed charge signal (Q_m) on the outer channel flow rates. All devices operated water/water and both outer channels had the same flow rate. Central channel flow rates were 0.20 and 1.00 mL/min, respectively for -S and -L devices. Analyte: 50 µM KNO_3, 26 and 54 µL, respectively, for -S and -L devices.

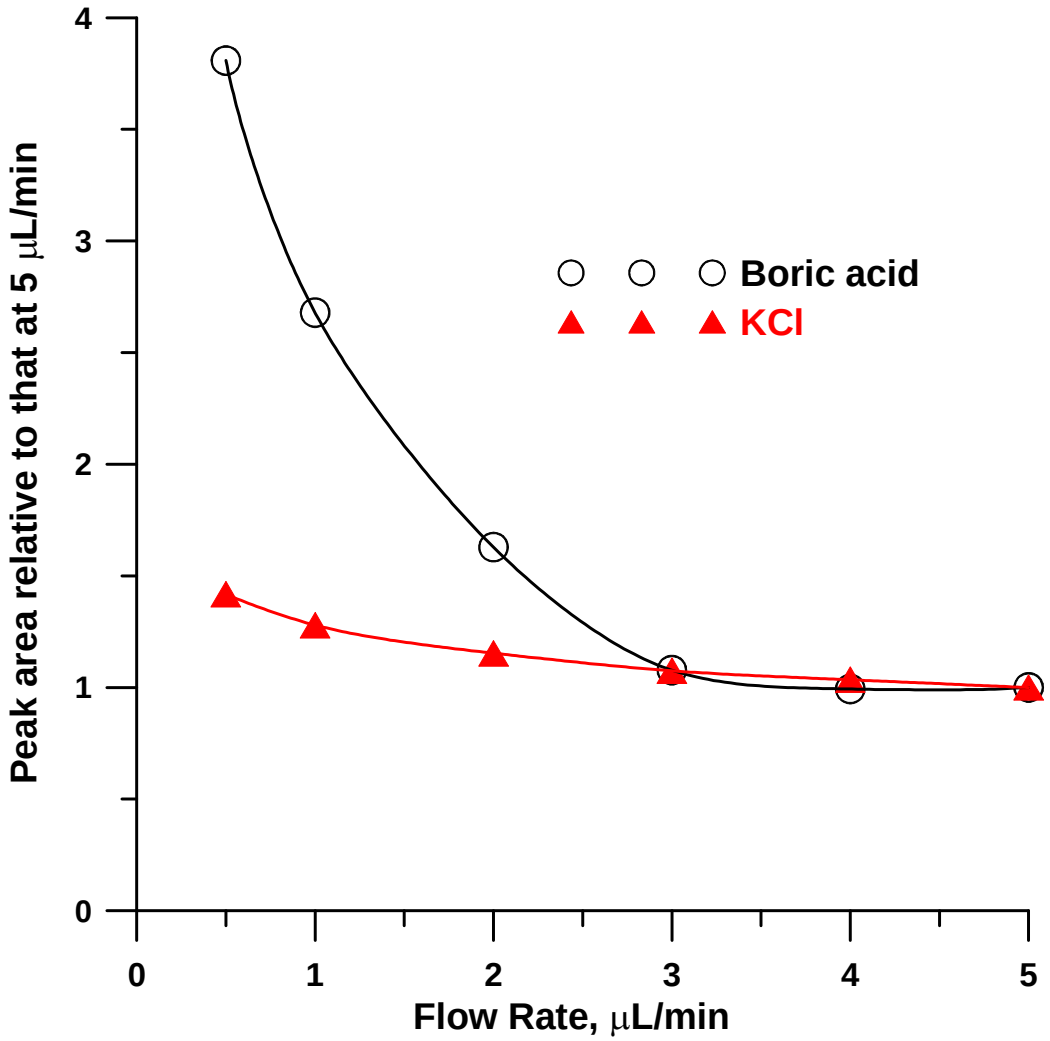

Figure A.28 Charge detector (Device ChD-B) signal as a function of flow rate. Applied voltage 14 V, 2.5 nmol each of KCl and boric acid are injected.

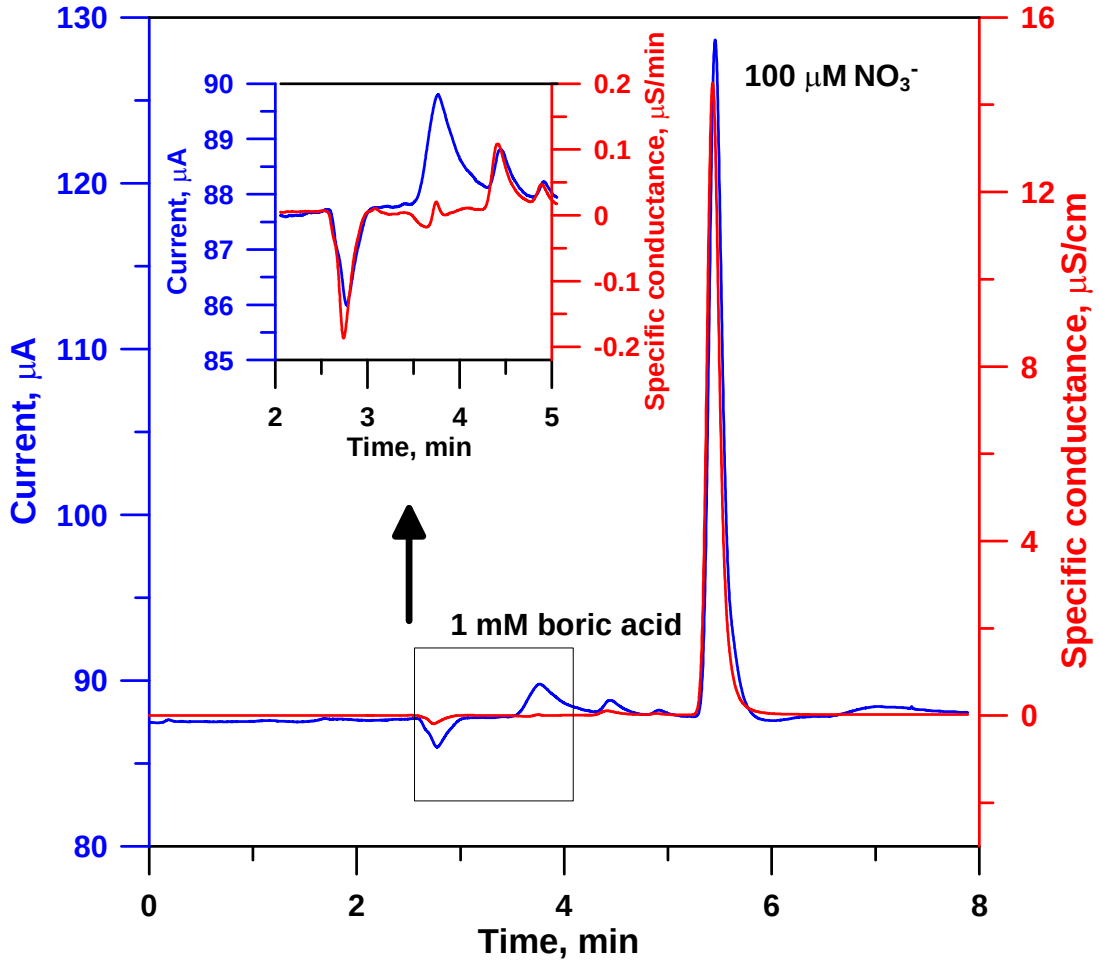

Figure A.29 Chromatograms by serial conductivity detector (CD 25) followed by MAE-S ChD V_{app} = 2 V (outer channels water @ 1.5 mL/min). GS-50 .pump pumping 25 mM electrogenerated KOH @ 1 mL/min, AG11-HC (4 x 50 mm)/AS 11-HC (4 x 250 mm) columns, 35 ℃ (LC-30 oven), ASRS Ultra-II suppressor (all f rom Dionex). Analyte concentrations 100 μM KNO_3 and 1 mM boric acid. The inset shows a much higher signal for boric acid obtained with ChD than CD.

GLOSSARY

AEM: Anion Exchange Membrane

BIM: Bipolar Ion Exchange Membrane

CCFR: Central Channel Flow Rate

CD: Conductivity Detector

CEM: Cation Exchange Membrane

ChD: Charge Detector, as described in this paper

ChD-B: Ion exchange resin bead based charge detector

ChD-M: Ion exchange membrane based charge detector

IC: Ion Chromatography

IEM: Ion Exchange Membrane

MAE: A ChD-M devices with adjacent electrodes, electrodes are in contact with the membrane, the larger and smaller scale devices (MAE-L, MAE-S) have active membrane areas of 14 and 3.6 cm^2), respectively

MSSE: A ChD-M device with the electrodes separated from the membranes by a screen. Also built with large (-L) and small (-S) membrane areas, as above

Q_m: Measured charge response, peak area in coulombs

Q_i: Total charge in coulombs injected into the system, based on the amount of the strong electrolyte injected in moles

V_{app}: Total voltage applied across a device

w/w: Refers to the two outer channels being operated with water and water

APPENDIX B

SUPPORTING INFORMATION FOR CHAPTER 3

Fabrication of membrane-based salt remover.

A thin segment was sliced from a 2.25 mm i.d. tygon tube to form a 0.635 mm thick washer. Two 0.015 in. dia holes were drilled from opposite sides of the disc perimeter. Two $^{1}/_{32}$ in. dia. holes were also drilled into opposite sides of a $^{1}/_{4}$-28 threaded polypropylene union (all fittings and tubing from Idex) about the middle of union. A $^{1}/_{4}$-28 male nut is threaded into the union until its tip is just below the holes made into the sides of the union. The washer is inserted from the top until it rests on the nut, rotated as needed have the holes in the washer aligned with those in the union, the vertical position of the nut is also adjusted as needed. One silica capillary each (180 µm i. d.; 365 µm o. d., Polymicro) were inserted through the holes in the union and into the washer all the way to the central cavity and then affixed in place with epoxy adhesive. The ¼-28 nut was now removed. Discs, 6 mm dia., were punched out from 125 µm thick ion exchange membranes (poly(tetrafluoroethylene) films radiation grafted and ion exchange funtionalized,[103] ion exchange capacities 1.2-2 meq/g). A CEM was placed on the top of the washer, with an O-ring on top of it. A ¼-28 short male nut was next threaded into the union to reach the O-ring but not tightened. The union was flipped, the AEM disk and another O-ring put in, followed by a ¼-28 nut. The nuts are now modestly tightened to seal the membranes in place; the inner cavity has a volume of 2.5 µL. The horizontal arm on both sides of a $^{1}/_{16}$" barbed nylon tee were cut and one tee was affixed at the head of each ¼-28 nut by epoxy adhesive. A length of 0.25 mm dia. platinum wire was wound around a 3-cm length of PEEK tubing (0.015"/0.025" i. d./o. d.). One of these was each inserted through the top of each tee all the way to each membrane, and affixed with epoxy at the entrance point; the protruding Pt-wires provided electrical connections to the power supply. CEM/AEM compartment liquids enered through the PEEK tubes and left through the tee arms while the central channel was addressed by the silica capillaries.

Thermal Considerations. Calculations show that thermal management is not a big issue with these devices. Consider that for a device with 200 mM NaCl being pumped at 1 µL/min, for a

membrane device used nearly every day for various experiments over a three month period[a] displays a current of just under 1 mA with 70 V applied. A power dissipation of 70 mJ/sec basically corresponds to 16.7 mcal/s, that is taken up by the 33 mg/s total "coolant" flow on the receiver side (each side has 1 mL/ min of receiver electrolyte flowing). The net temperature rise should be only ~0.5 ℃.

[a] The age and usage history of the membrane is important in that adsorption of proteins or other strongly adsorbed ions essentially block the sites and increase the electrical resistance of the membrane. Methanol wash can, to a degree, restore the membrane. For the same current, the voltage drop across a membrane increases with time it has been in use, other factors being held constant.

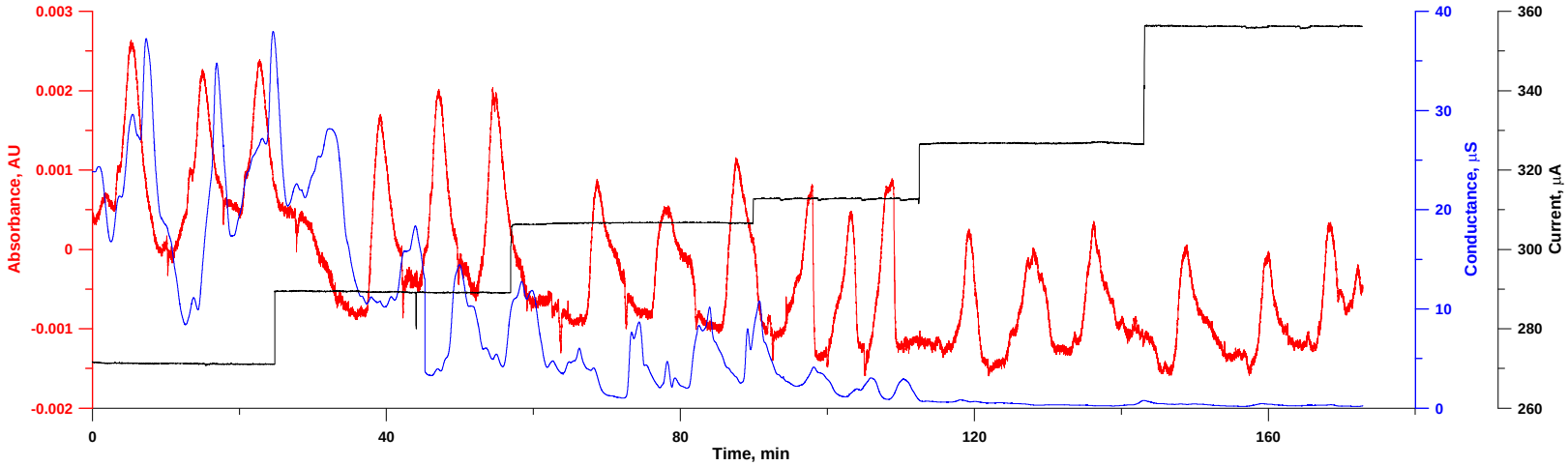

Figure B.1 Peak profile of absorbance, conductance and current when 20 µM myoglobin in 154 mM NaCl was injected into the 154 mM NaCl carrier. Flow rate: 1 µL/min. Note that even with ~270 µA applied, the maximum conductance observed is ~35 µS; under the same conditions the conductance of 154 mM NaCl is >71,000 µS; i.e., removal is 99.95% even under these circumstances.

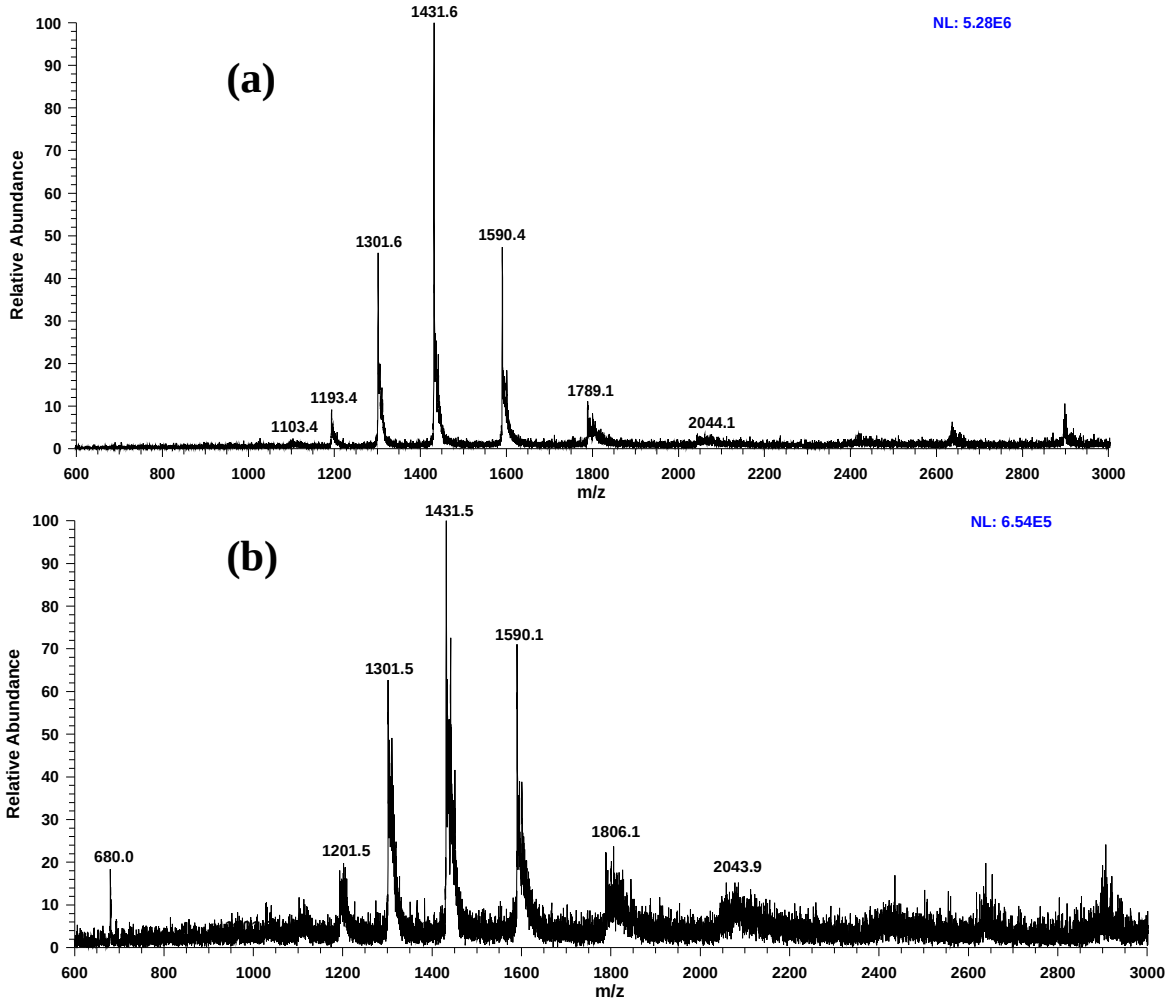

Figure B.2 Positive ion ESI mass spectra of (a) 10 μM lysozyme in 10% (v/v) methanol and 154 mM NaCl passed through an SR operated at 315 μA, (b) 10 μM lysozyme in 10% (v/v) methanol aqueous solutions containing 5 mM NaCl without SR. Flow rate: 1 μL/min; Injection volume: 1.94 μL.

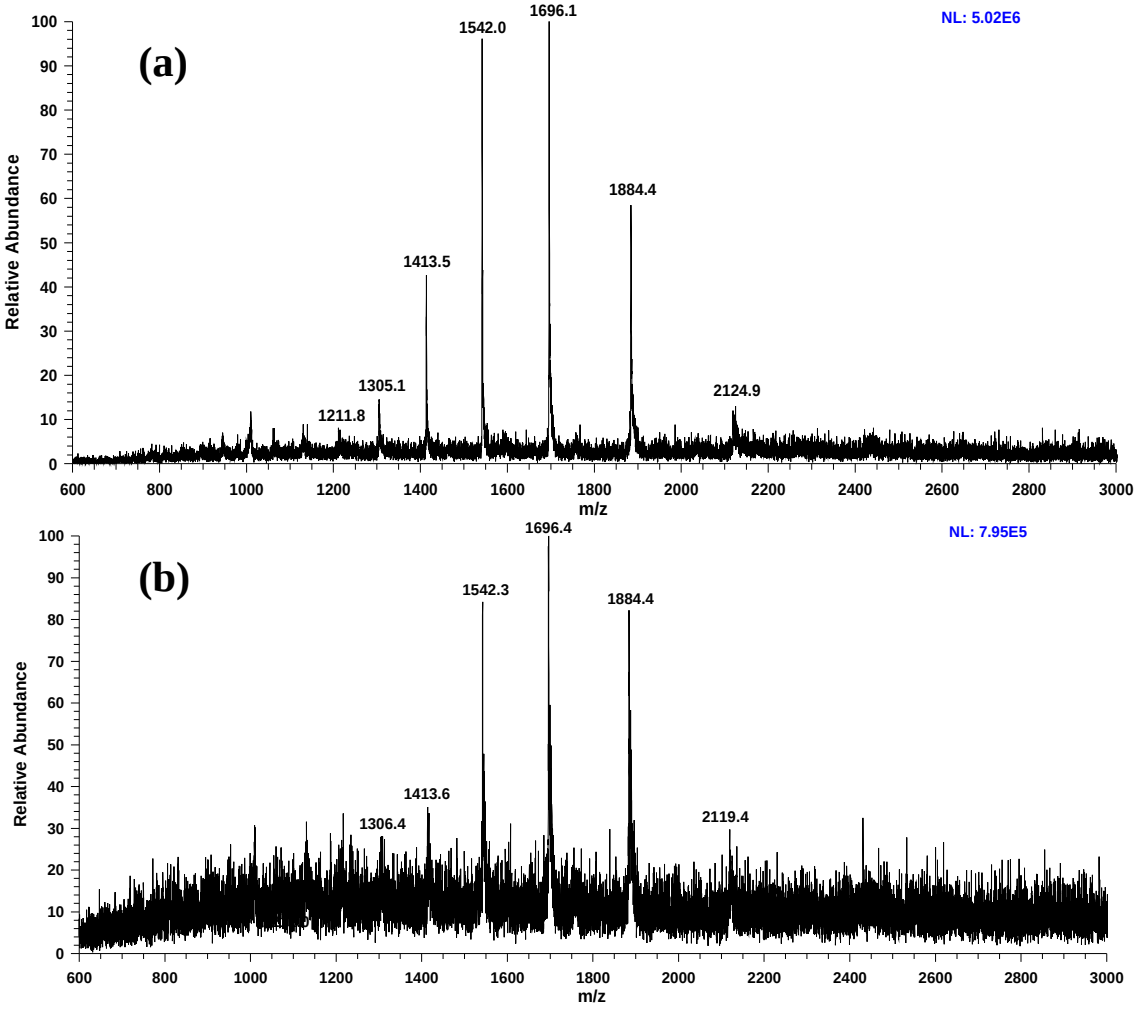

Figure B.3 Positive ion ESI mass spectra of (a) 10 μM myoglobin in 10% (v/v) methanol and 154 mM NaCl passed through an SR operated at 315 μA, (b) 10 μM myoglobin in 10% (v/v) methanol aqueous solutions containing 5 mM NaCl without SR. Flow rate: 1 μL/min; Injection volume: 1.94 μL.

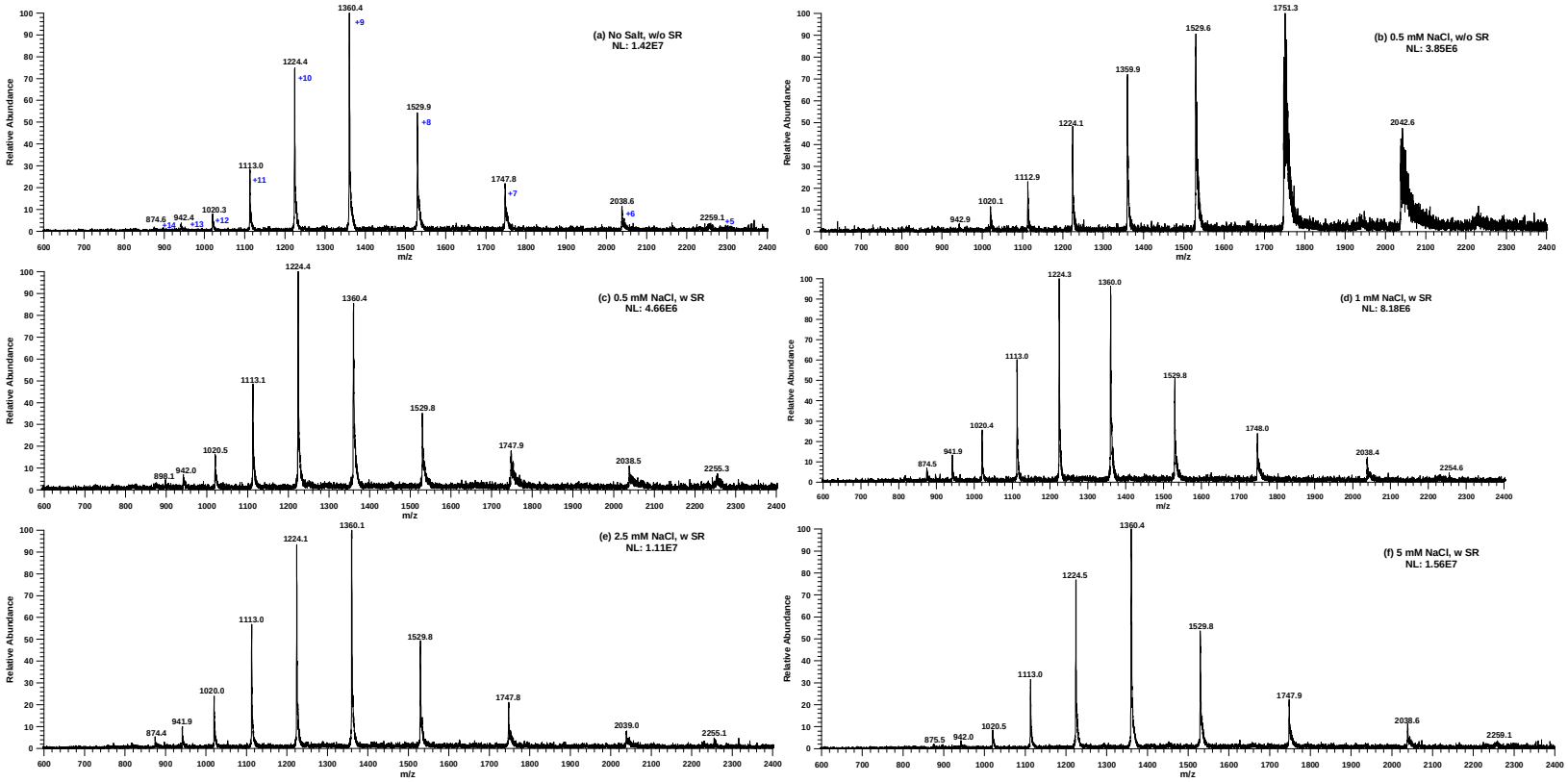

Figure B.4 Positive ESI mass spectra of 10 μM cytochrome c in 10% (v/v) methanol aqueous solutions, which contain no or various amounts of salts, (a) contains no salt, direct infusion without passing through SR; (b) contains 0.5 mM NaCl, direct infusion without passing through SR; all others through SR: (c)-(f) contain 0.5, 1.0. 2.5, 5 mM NaCl respectively, direct infusion passing through SR.

APPENDIX C

SUPPORTING INFORMATION FOR CHAPTER 4

Reagents

Disodium hydrogen phosphate heptahydrate and sodium citrate dihydrate was purchased from Mallinckrodt. Ethylenediamine dihydrochloride was purchased from Acros Organics. Tris(hydroxymethyl)aminomethane hydrochloride and dipotassium hydrogen phosphate was purchased from J. T. Baker. All the chemicals are reagent grade and solutions were prepared with 18.2 MΩ·cm Milli-Q (Millipore) deionized water.

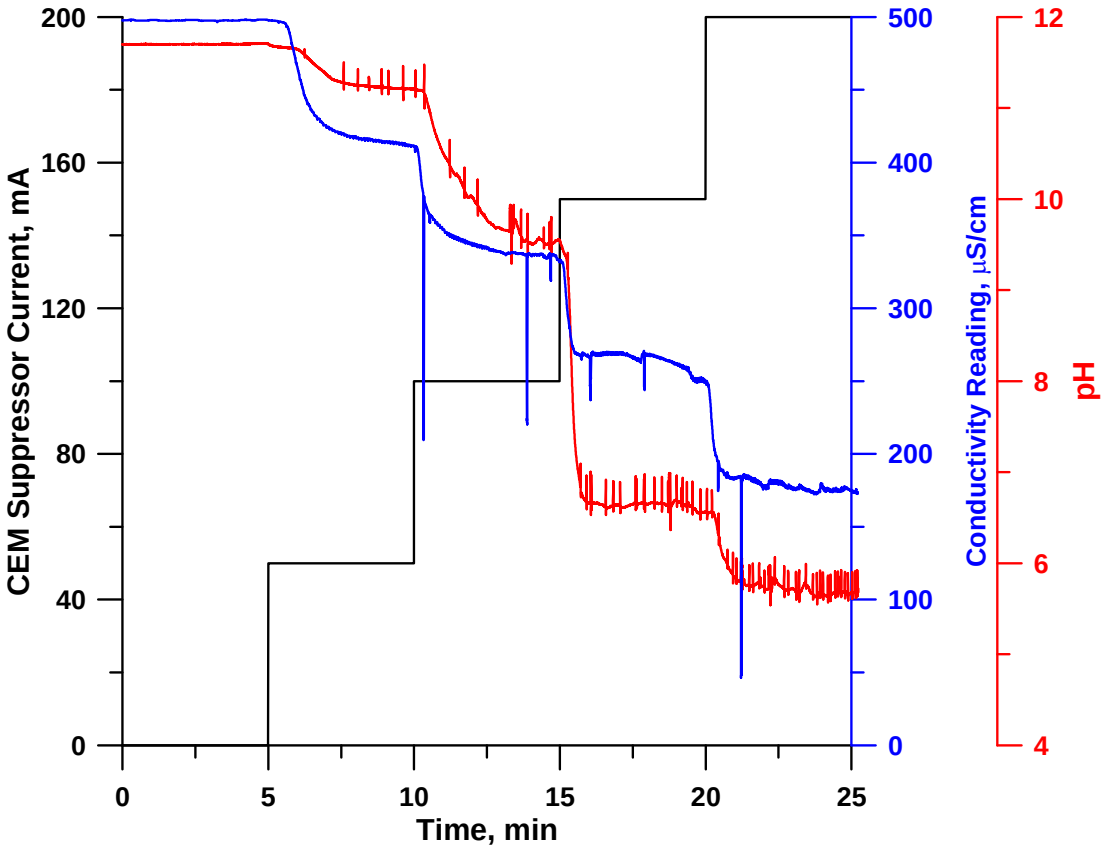

Figure C.1 Noise observed in absence of the CRD gas removing device. The pH electrode flow cell has essentially no back pressure and the pH trace (red) shows increasing noise spikes with increasing current. Noise is also observed on the conductivity trace (blue) with greater frequency at increased current levels (aside from spikes, look at the thicker trace that is the result of noise from micro bubbles). The current program is shown the black trace (left ordinate).

Theoretical Estimation of pH

This Excel™ based calculation is demonstrated using the system of Figure 5a; this is also attached as separate file as Mater pH.xlsx. In the top part of the spreadsheet, the respective acid dissociation constants (K for boric acid, K_1, K_2, K_3 for phosphoric acid and citric acid) are respectively written down and given the names KB, KPA, KPB, KPC, KCA, KCB and KCC. The total borate, phosphate and citrate concentrations (0.045, 0.015 and 0.015 M) are respectively given the names CB, CP and CC. In column X titled I_{used}, we put down some ionic strength (I) of the solution (to start with, we used 0.3). Using this trial value of this ionic strength, in columns Y:AG (respectively headed GH, GOH, GBor, GP1, GP2, GP3, GC1, GC2, and GC3) we compute the activity coefficients of H^+, OH^-, $B(OH)_4^-$, $H_2PO_4^-$, HPO_4^{2-}, PO_4^{3-}, $H_2Citrate^-$, $HCitrate^-$ and $Citrate^{3-}$, respectively, from the Davies equation:

$$-\log \gamma_i = 0.51 Z_i^2 \left(\frac{\sqrt{I}}{1+0.33 d_i \sqrt{I}} - 0.3I\right) \quad \ldots(C.1)$$

Where Z_i is the charge magnitude of ion *i* (respectively 1, 2, 3) and d_i is the ion size parameter. After Kielland[185] we assumed the ion size parameters of H^+, OH^-, $H_2PO_4^-$, HPO_4^{2-}, PO_4^{3-}, $H_2Citrate^-$, $HCitrate^-$ and $Citrate^{3-}$ to be 9, 3.5, 4.25, 4, 4, 3.5, 4.5 and 5; we estimated $d_{B(OH)4-}$ to be 6. Based on the these activity coefficients we computed equilibrium constants KW, KB, KPA, KPB, KPC, KCA, KCB and KCC in concentration terms in columns AI:AP titled respectively CKW, CKB, CKPA, CKPB, CKPC, CKCA, CKCB and CKCC from the following relationships:

$$CKW = KW/(\gamma_{H+} * \gamma_{OH-}) \quad \ldots(C.2)$$

$$CKB = KB/(\gamma_{H+} * \gamma_{Bor-}) \quad \ldots(C.3)$$

$$CKPA = KPA/(\gamma_{H+} * \gamma_{H2PO4-}) \quad \ldots(C.4)$$

$$CKPB = KPB * \gamma_{H2PO4-}/(\gamma_{H+} * \gamma_{HPO42-}) \quad \ldots(C.5)$$

$$CKPC = KPC * \gamma_{HPO42-}/(\gamma_{H+} * \gamma_{PO43-}) \quad \ldots(C.6)$$

$$CKCA = KCA/(\gamma_{H+} * \gamma_{H2Cit-}) \quad \ldots(C.7)$$

$$CKCB = KCB^{*}\gamma_{H2Cit^-}/(\gamma_{H^+}{}^{*}\gamma_{HCit2^-}) \quad \ldots(C.8)$$

$$CKCC = KPC^{*}\gamma_{H2PO4^-}/(\gamma_{H^+}{}^{*}\gamma_{Cit3^-}) \quad \ldots(C.9)$$

The potassium concentration was not explicitly measured but sufficient KOH was added to adjust the pH to 12.00; since iterative calculations (*vide infra*) indicated that this pH was attained (to the nearest mM) with 143 mM K^+ (this suggests ~30.5 mM KOH was added to the concoction), we used 0.143 M K^+ in our calculations. This is the starting value of $[K^+]$ in the column titled CK and begins in cell E9. In E9:E152 the $[K^+]$ values are decremented by 0.001 M at each step to 0 in E152. In cell F9 a trial value of pH (any value between 0 and 14) is initially entered. In cell G9 $[H^+]$ is computed as 10^-pH (the entry in G9 is =10^-F9). The α-values (fraction present in a specific ionic form) are defined as (K_0 =1):

$$\alpha_i = \frac{K_0 \ldots K_i [H^+]^{n-i}}{\sum_{i=0}^{i=n} K_0 \ldots K_i [H^+]^{n-i}} \quad \ldots(C.10)$$

We designate the denominator as Q, and the values for the borate, citrate and phosphate systems are computed in the columns QB, QC and QP as:

$$QB = [H^+] + KB \quad \ldots(C.11)$$

$$QC = [H^+]^3 + KCA[H^+]^2 + KCA{*}KCB{*}[H^+] + KCA{*}KCB{*}KCC \quad \ldots(C.12)$$

$$QP = [H^+]^3 + KPA[H^+]^2 + KPA{*}KPB{*}[H^+] + KPA{*}KPB{*}KPC \quad \ldots(C.13)$$

The individual ionic concentrations are now computed in columns K:R headed B, C1, C2, C3, P1, P2, P3 and OH (respectively $Borate^-$, $H_2Citrate^-$, $HCitrate^-$, $Citrate^{3-}$, $H_2PO_4^-$, HPO_4^{2-}, PO_4^{3-} and OH^-) based on

$$[Bor^-] = CB{*}\alpha_{B^-} \quad \ldots(C.14)$$

$$[H_2Citrate^-] = CC{**}\alpha_{H2Cit^-} \quad \ldots(C.15)$$

$$[HCitrate^{2-}] = CC{**}\alpha_{HCit2^-} \quad \ldots(C.16)$$

$$[Citrate^{3-}] = CC{**}\alpha_{Cit3^-} \quad \ldots(C.17)$$

$$[H_2PO_4^-] = CC{**}\alpha_{H2PO4^-} \quad \ldots(C.18)$$

$$[HPO4^{2-}] = CC{**}\alpha_{HPO42^-} \quad \ldots(C.19)$$

$$[PO_4^{3-}] = CC^{**}\alpha_{PO43-} \quad \ldots(C.20)$$

$$[OH^-] = CKW/[H^+] \quad \ldots(C.21)$$

Now for the charge balance equation:

$$[H^+] + [K^+] - ([Bor^-] + [H_2Citrate^-] + [H_2PO_4^-] + [OH^-] + 2([HCitrate^{2-}] + [HPO4^{2-}]) + 3([Citrate^{3-}] + [PO_4^{3-}])) = 0 \quad \ldots(C.22)$$

is simply written as an expression in column S titled Poly (for Polynomial value). We square the whole expression to make it sign-independent and multiply by a large number (in this case 10^{10}). The latter is done to satisfy one of Solver's quirks, that it stops optimization when it decides it his close enough. The multiplier simply accentuates the difference to keep the computations ongoing.

In Column W we calculate the ionic strength value (I_{calc}) based on the definition of ionic strength:

$$I_{calc} = [H^+] + [K^+] + [Bor^-] + [OH^-] + [H_2Citrate^-] + [H_2PO_4^-] + 4([HCitrate^{2-}] + [HPO4^{2-}]) + 9([Citrate^{3-}] + [PO_4^{3-}])) \quad \ldots(C.23)$$

The entire 143 rows are now filled in by copying and pasting row 9, only the values already filled in Column E for CK remain unique. On the bottom of column S154, we sum up all the values in column S. We invoke Solver and ask it to minimize S154 by varying the entire pH column (F9:F152). Solver is repeated until S154 value no longer changes. Now all the computed values for I_{calc} (column W) are pasted (not formulas but values: [Alt-E]-S-V) into the I_{used} column (W). The difference between the two (Delta I) is also kept a tab of (column V), when this approaches 10^{-4}, further iteration is not meaningful. Solver is asked to recompute the values (minimize S154 etc.) and the process is repeated (rarely more than 3 cycles) before I and pH values converge. The activity of the hydrogen ion AH (equal to $GH^*[H^+]$) and the activity corrected pH (PAH) are computed in columns T and U, respectively.

A flow rate of 1 mL/min is equal to 16.667 μL/s. removing 1 mM K^+ is 16.667 neq/s. Multiplying by the Faraday (96485 coulombs/eq) gives us the current necessary, 1.608 mA. Column D gives sequentially cumulative mM K^+ removed. Column C, the current needed in mA (labeled

cum curr) will just be 1.608 multiplied by the value in Column D if the Faradaic efficiency F_e was unity throughout.

Correction for Nonunity F_e. If we use F_e as defined by eq 4 in the main text and use herein a value of 15 for R_λ (the free solution value is ~5 and is expected to be much higher in a membrane, we can calculate the value of F_e; this is done in column A; the value of this efficiency factor will always lie between 1 and 0, tending to the latter when $[H^+]$ is large relative to the ion to be removed. We assume that F_e computed for the terminal results obtained in row 9 applies to the current needed for row 10 and so on. The actual current needed in the step is thus the 1.608 mA divided by F_e; this is thus computed in Column B. The cumulative current in Column C is thus the immediately preceding value in the cell above plus the new increment in the cell to the immediate left.

Table C.1 Conductance Values for Current Steps in Figure 4.3

0 mA, A*	Cond	40 mA, A	Cond	40 mA, D*	Cond	80 mA , A	Cond	80 mA, D	Cond	120 mA, D	Cond	120 mA, D	Cond	160 mA, D	Cond
t, min	**mS/cm**	**t, min**	**mS/cm**	**t, min**	**mS/cm**	**t, min**	**mS/cm**	**t, min**	**mS/cm**	**t, min**	**mS/cm**	**t, min**	**mS/cm**	**t, min**	**mS/cm**
45.00	18.15	10.00	15.87	40.00	15.51	15.00	13.63	35.00	13.39	20.00	11.37	30.00	11.22	25.00	8.99
85.00	18.12	50.00	15.93	80.00	15.51	55.00	13.68	75.00	13.43	60.00	11.43	70.00	11.28	65.00	9.05
125.00	18.25	90.00	15.93	120.00	15.59	95.00	13.70	115.00	13.47	100.00	11.43	110.00	11.30	105.00	9.07
165.00	18.19	130.00	16.00	160.00	15.58	135.00	13.74	155.00	13.51	140.00	11.47	150.00	11.34	145.00	9.11
mean	18.18		15.93		15.55		13.69		13.45		11.42		11.29		11.29
sd	0.06		0.06		0.05		0.05		0.05		0.04		0.05		0.05
%Rsd	0.31		0.35		0.29		0.33		0.36		0.36		0.43		0.43
						Diff				**Diff**				**diff**	
						0.38				0.24				0.14	
					%diff	1.22			**%diff**	0.88			**%diff**	0.61	

* A indicates ascending step, D indicates descending step.

Table C.2 pH Values for Current Steps in Figure 4.3

0 mA, A*	pH	40 mA, A	pH	40 mA, D*	pH	80 mA , A	pH	80 mA, D	pH	120 mA, D	pH	120 mA, D	pH	160 mA, D	pH
t, min		**t, min**		**t, min**		**t, min**		**t, min**		**t, min**		**t, min**		**t, min**	**mS/cm**
45.00	11.91	10.00	11.62	40.00	11.51	15.00	10.94	35.00	10.80	20.00	7.62	30.00	7.54	25.00	6.78
85.00	11.91	50.00	11.58	80.00	11.51	55.00	10.91	75.00	10.80	60.00	7.60	70.00	7.54	65.00	6.78
125.00	11.91	90.00	11.57	120.00	11.52	95.00	10.90	115.00	10.82	100.00	7.61	110.00	7.57	105.00	6.81
165.00	11.92	130.00	11.58	160.00	11.54	135.00	10.91	155.00	10.84	140.00	7.64	150.00	7.61	145.00	6.87
mean	11.91		11.59		11.52		10.91		10.81		7.62		7.57		6.81
sd	0.01		0.02		0.01		0.02		0.02		0.02		0.03		0.05
%Rsd	0.04		0.19		0.12		0.16		0.17		0.21		0.40		0.67
				difference				**difference**				**difference**			
				0.07				0.10				0.05			

* A indicates ascending step, D indicates descending step.

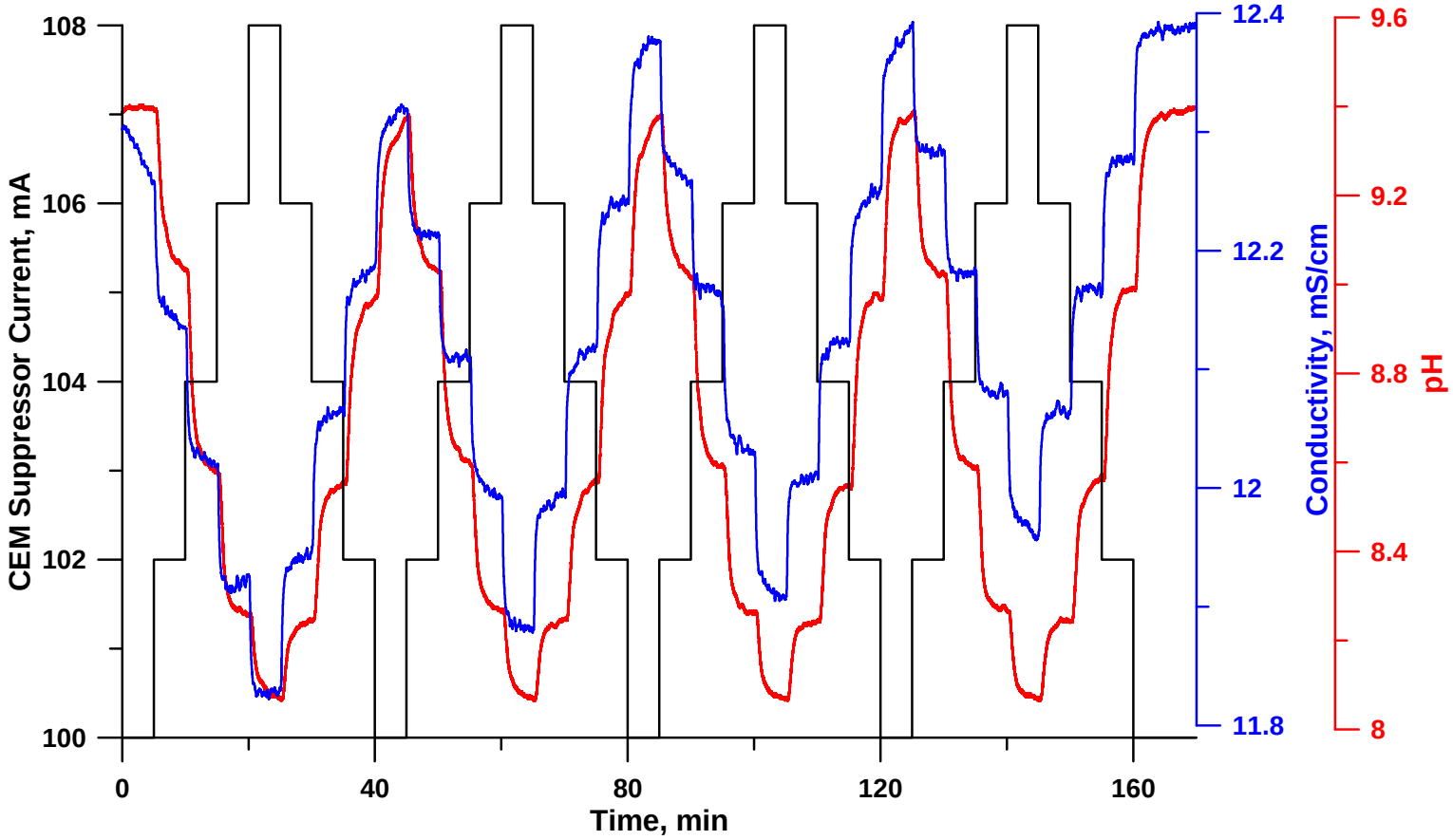

Figure C.2 Repeatability and reproducibility of small current steps. Detailed numerical data are presented in Tables C.3 and C.4.

Table C.3 Conductance Values for Small Current Steps, Figure C.2

100 mA, A	Cond	102 mA, A	Cond	102 mA, D	Cond	104 mA, A	Cond	104 mA, D	Cond	106 mA, A	Cond	106 mA, D	Cond	108 mA, D	Cond
t, min	**mS/cm**	**t, min**	**mS/cm**	**t, min**	**mS/cm**	**t, min**	**mS/cm**	**t, min**	**mS/cm**	**t, min**	**mS/cm**	**t, min**	**mS/cm**	**t, min**	**mS/cm**
45.00	12.32	10.00	12.13	40.00	12.19	15.00	12.02	35.00	12.07	20.00	11.93	30.00	11.95	25.00	11.83
85.00	12.38	50.00	12.22	80.00	12.24	55.00	12.11	75.00	12.12	60.00	11.99	70.00	12.00	65.00	11.88
125.00	12.39	90.00	12.25	120.00	12.25	95.00	12.15	115.00	12.12	100.00	12.03	110.00	12.01	105.00	11.91
165.00	12.39	130.00	12.28	160.00	12.28	135.00	12.18	155.00	12.16	140.00	12.08	150.00	12.06	145.00	11.96
mean	12.37		12.22		12.24		12.12		12.12		12.01		12.00		11.89
sd	0.03		0.06		0.04		0.07		0.04		0.06		0.05		0.05
%Rsd	0.27		0.53		0.30		0.60		0.33		0.54		0.41		0.46
			Differences in ascending and descending steps within measurement uncertainty												

* A indicates ascending step, D indicates descending step.

Table C.4 pH Values for Small Current Steps, Figure C.2

100 mA, A	pH	102 mA, A	pH	102 mA, D	pH	104 mA, A	pH	104 mA, D	pH	106 mA, A	pH	106 mA, D	pH	108 mA, D	pH
t, min		**t, min**		**t, min**		**t, min**		**t, min**		**t, min**		**t, min**		**t, min**	
45.00	9.37	10.00	9.03	40.00	8.97	15.00	8.58	35.00	8.55	20.00	8.25	30.00	8.24	25.00	8.07
85.00	9.38	50.00	9.03	80.00	8.98	55.00	8.60	75.00	8.56	60.00	8.27	70.00	8.25	65.00	8.07
125.00	9.38	90.00	9.02	120.00	8.97	95.00	8.59	115.00	8.55	100.00	8.26	110.00	8.24	105.00	8.07
165.00	9.37	130.00	9.03	160.00	8.99	135.00	8.59	155.00	8.57	140.00	8.27	150.00	8.24	145.00	8.07
Mean	9.38		9.03		8.98		8.59		8.56		8.26		8.24		8.07
Sd	0.00		0.01		0.01		0.01		0.01		0.01		0.00		0.00
%Rsd	0.04		0.07		0.14		0.09		0.12		0.10		0.04		0.02

Given pH electrode response times, the difference between ascending and descending steps are likely not significant.

* A indicates ascending step, D indicates descending step.

Algorithm for Iterative Correction of a Current Program to Produce a Desired pH Profile.

The basic logic is straightforward: Create an initial current vs. time profile. Record the resulting time-current-pH data. Using the observed results as a template, construct a linear (or concave/convex) pH gradient using as many of these points (or being as close to these points as possible. If this can be given in the form of an equation, the desired pH at any given time point is readily available. For a linear gradient, a straight line may well be a linear least squares fit in the desired range whose equation is readily available and this best fit line can be taken as the eventually desired profile. In order to get to this profile, at any given time point, the desired pH is looked up and the observed data is searched for what current produces this pH and this current is then used at this time point.

As an example, in iterative correction.xlsx, the first three columns list time, current and pH. Note that the lag time between a current step and the onset of the pH change was observed to be ~0.45 min and the pH data was accordingly shifted in time. The desired pH corresponding to the best linear fit in the desired range is listed in column D and the difference (observed - desired) is listed in column E as Delta pH. In the present instance, most of these values are negative, i.e., the observed pH is less than the desired pH, suggesting less potassium removal and hence less current is needed. The local slope $\Delta pH/\Delta i$ is computed. The desired difference ΔpH is then divided by the slope to obtain the needed current change; this is then added to the extant current program.

APPENDIX D

SUPPORTING INFORMATION FOR CHAPTER 5

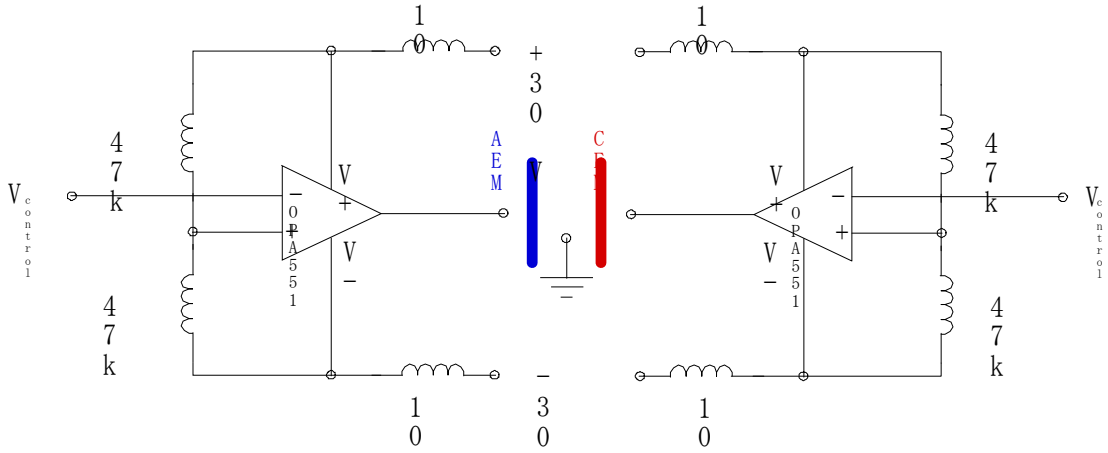

Figure D.1 Two independent home-built voltage-controlled bipolar current sources and their arrangement with the EBG.

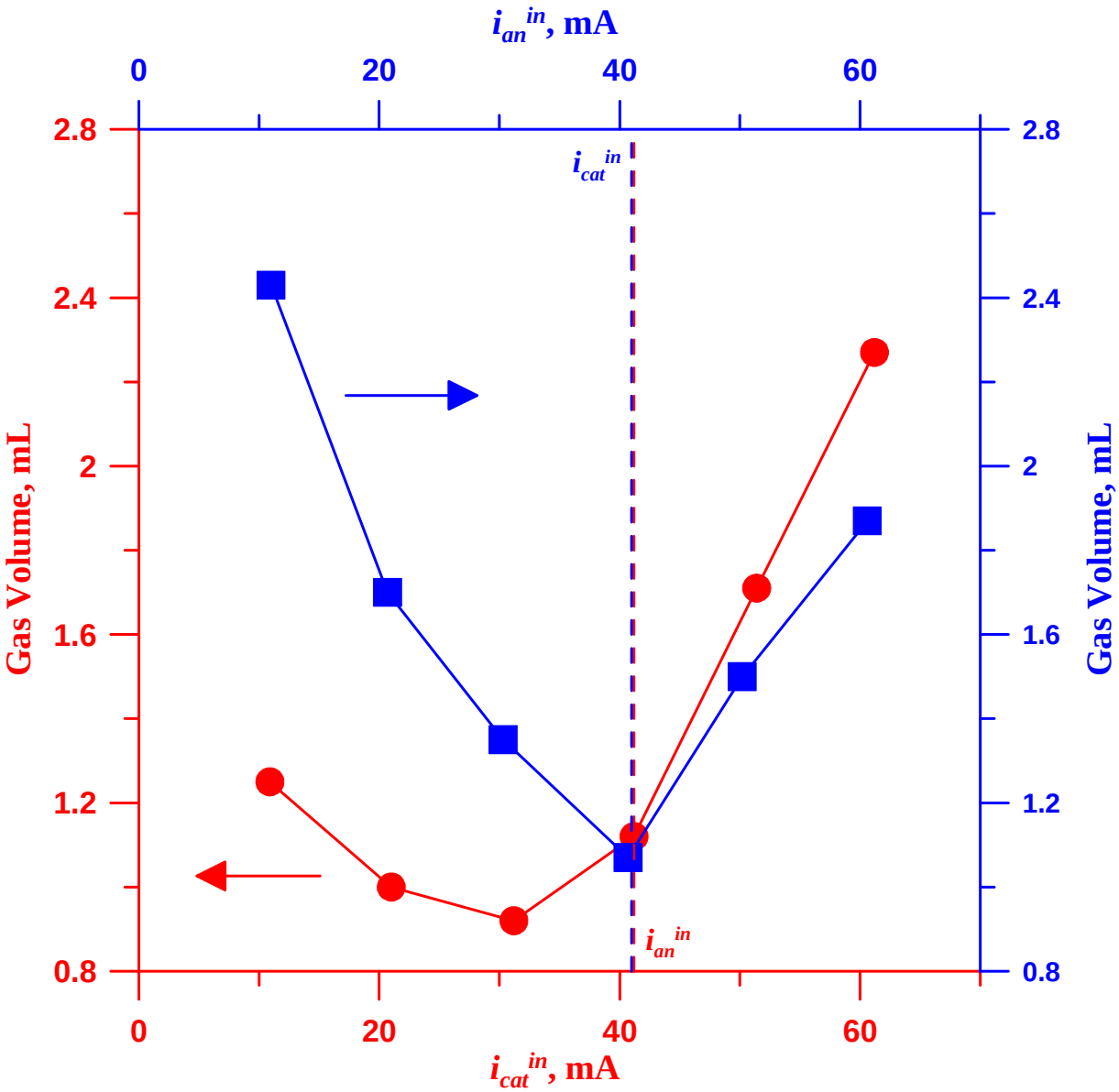

Figure D.2 Volume of gas generated as a function of applied current. Central channel: water, 0.25 mL/min; CEM/AEM outer channels 0.5 M K_2HPO_4, CEM flow 1.5 mL/min; AEM flow 3.0 mL/min. Gas collection time: 10 min. The gas was simply collected in an inverted water filled 10-ml graduated cylinder.

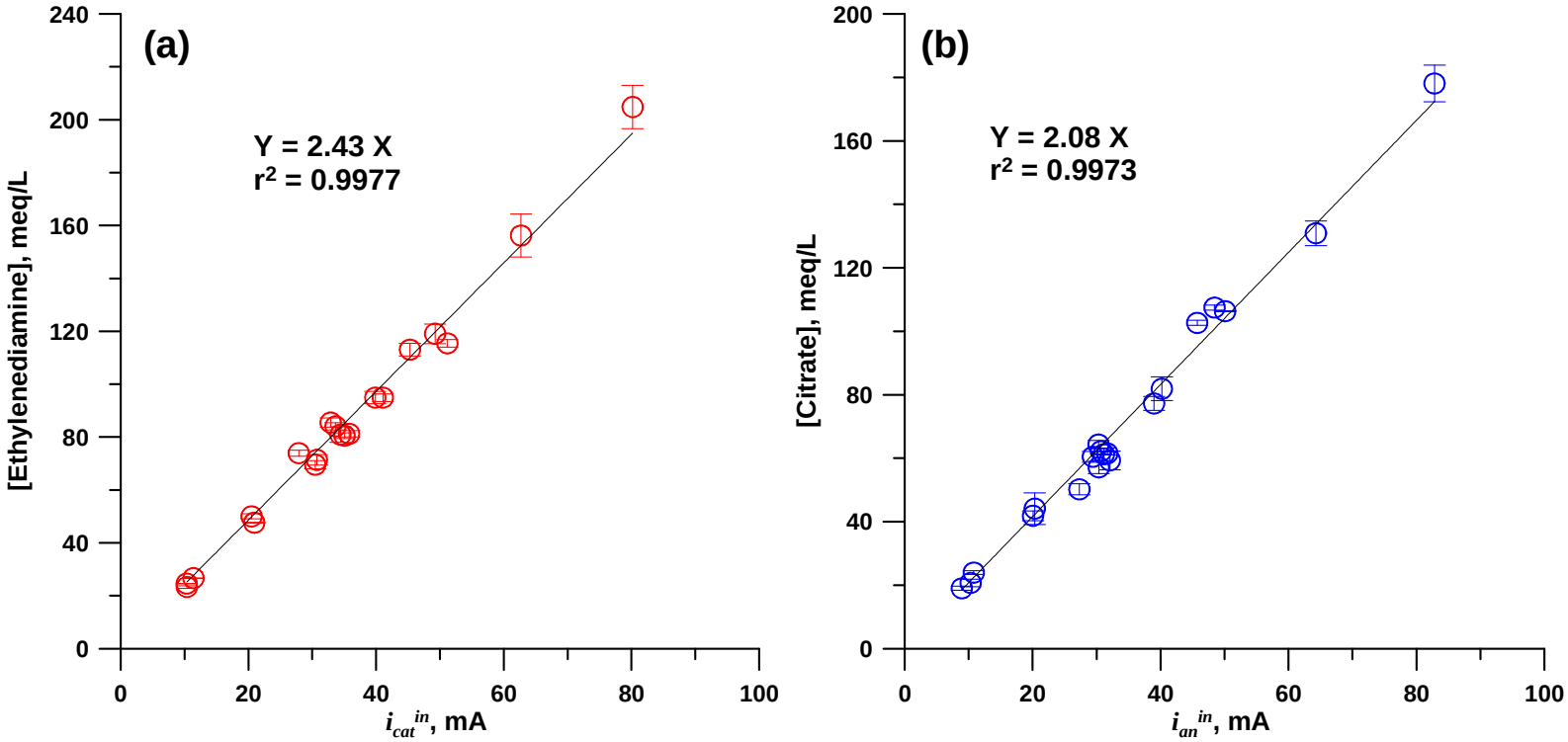

Figure D.3 (a) Central channel total concentration of ethylenediamine as a function of i_{cat}^{in}; (b) Central channel total concentration of citrate as a function of i_{an}^{in}.

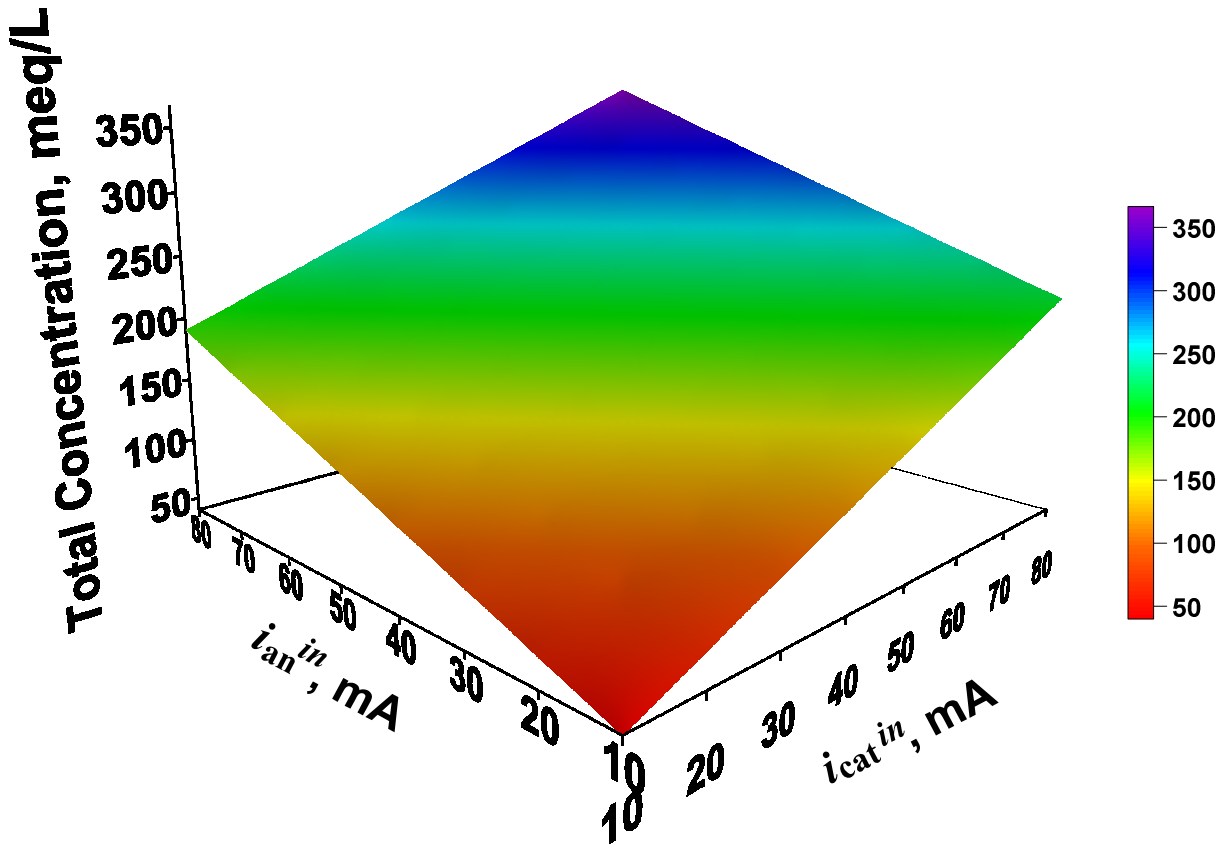

Figure D.4 3-D surface maps of total concentration (meq/L) as a function of currents.

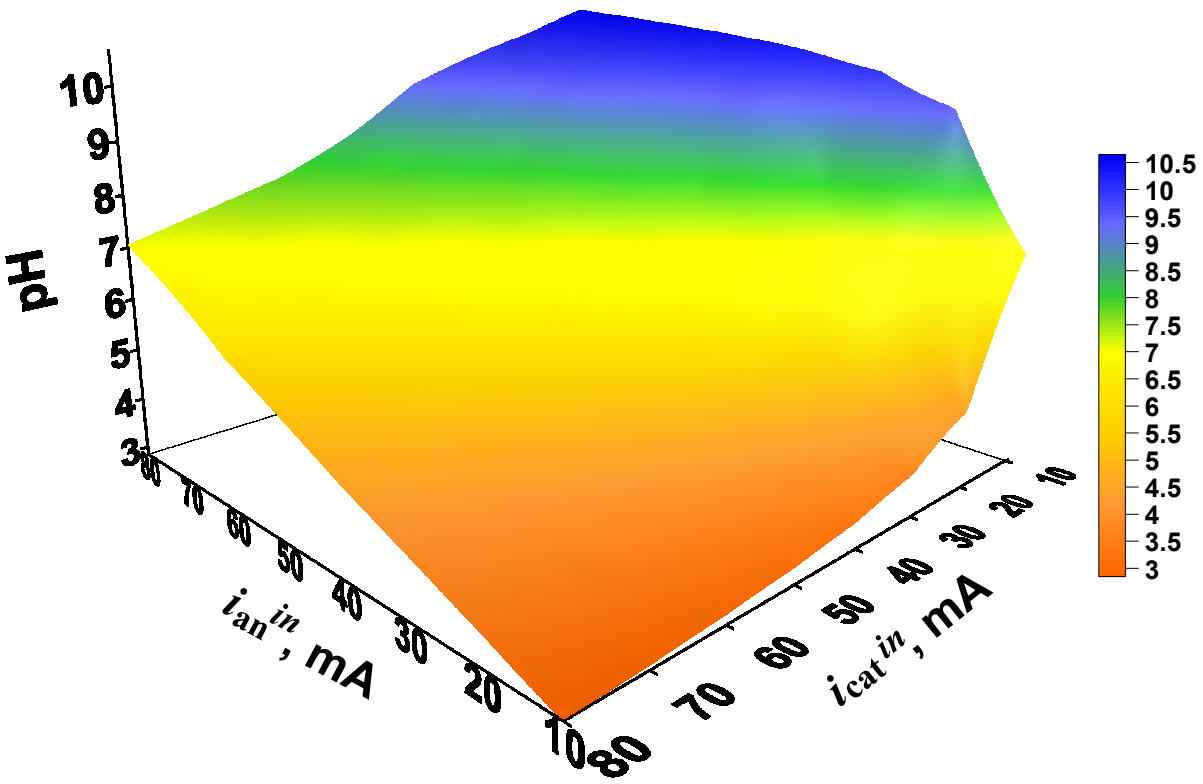

Figure D.5 3-D surface maps of pH as function of two currents.

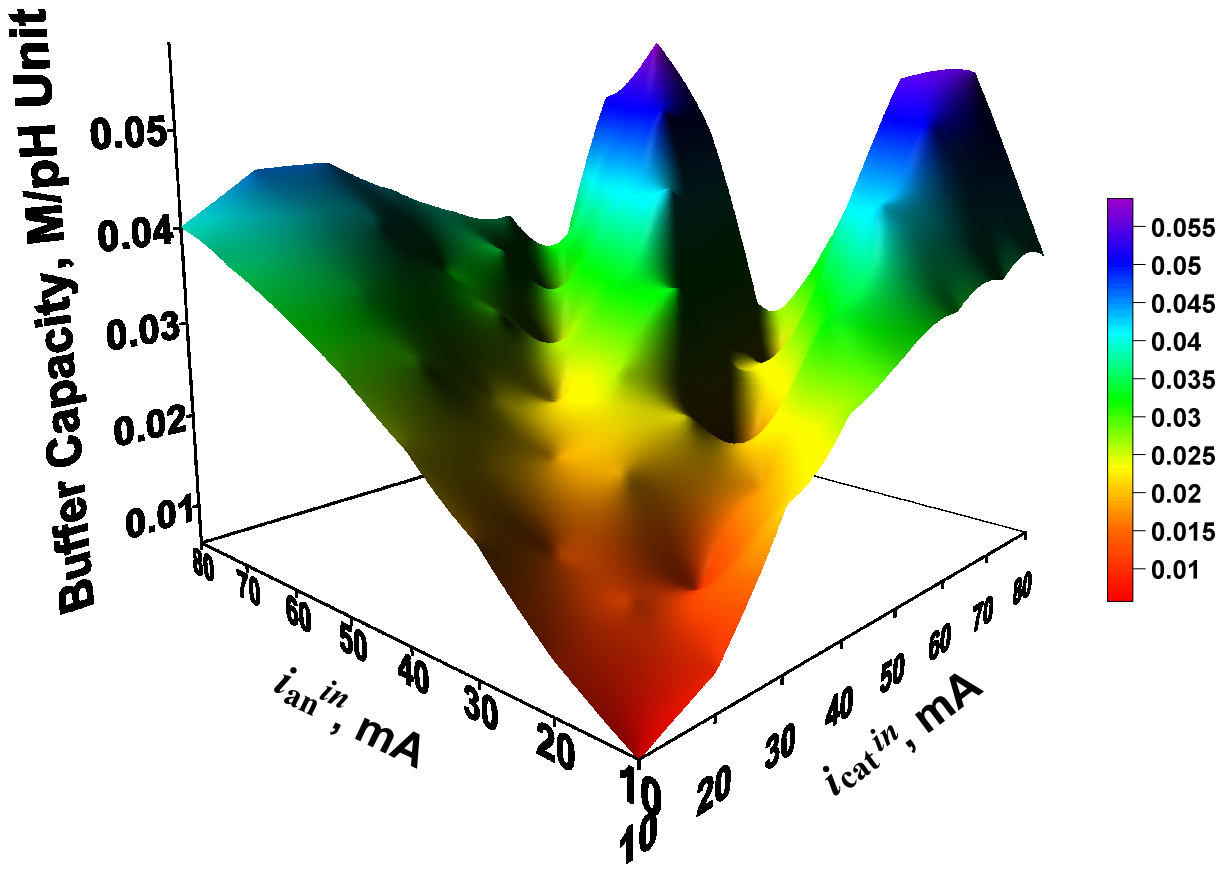

Figure D.6 3-D surface maps of buffer capacity (M/pH Unit) as a function of currents.

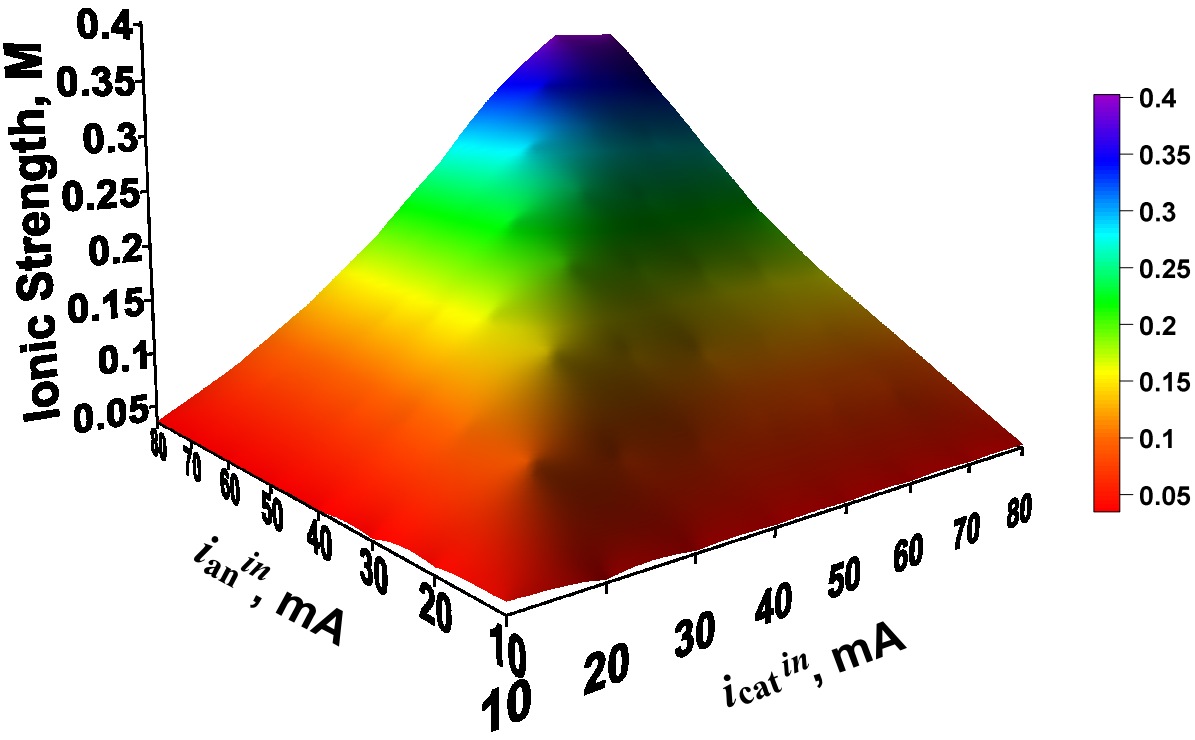

Figure D.7 3-D surface maps of ionic strength (M) as a function of currents.

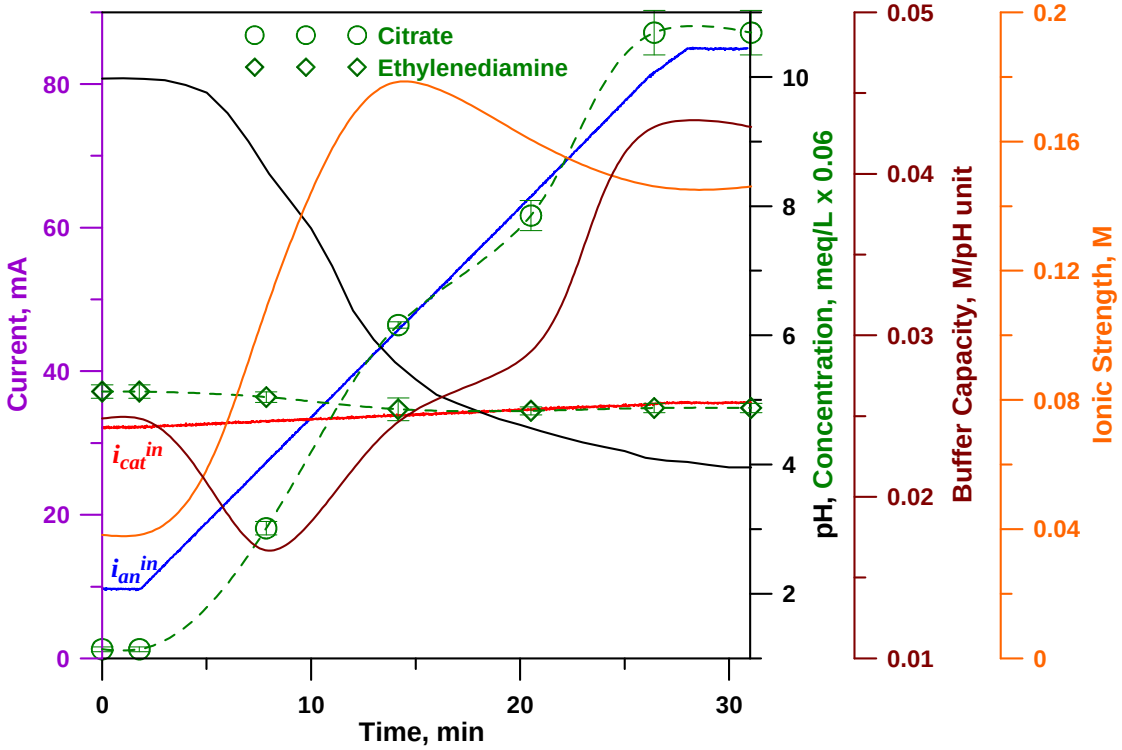

Figure D.8 Citrate concentration ascending gradient at constant [*en*] with resulting descending pH gradient by increasing i_{an}^{in} at constant i_{cat}^{in}. Orange and brown traces show Ionic strength and buffer capacity, respectively, in addition to the other traces depicted in Figure 5.6a.

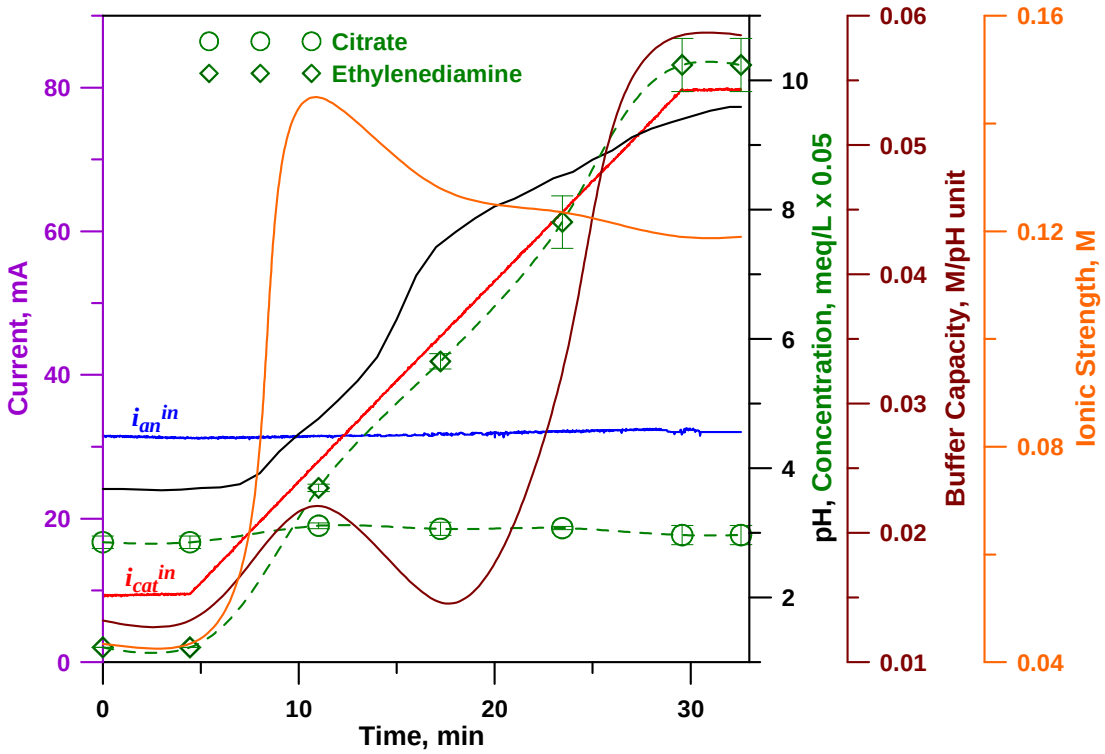

Figure D.9 Ethylenediamine concentration ascending gradient at constant [Citrate] with resulting ascending pH gradient by increasing i_{cat}^{in} at constant i_{an}^{in}. Orange and brown traces show Ionic strength and buffer capacity, respectively, in addition to the other traces depicted in Figure 5.6b.

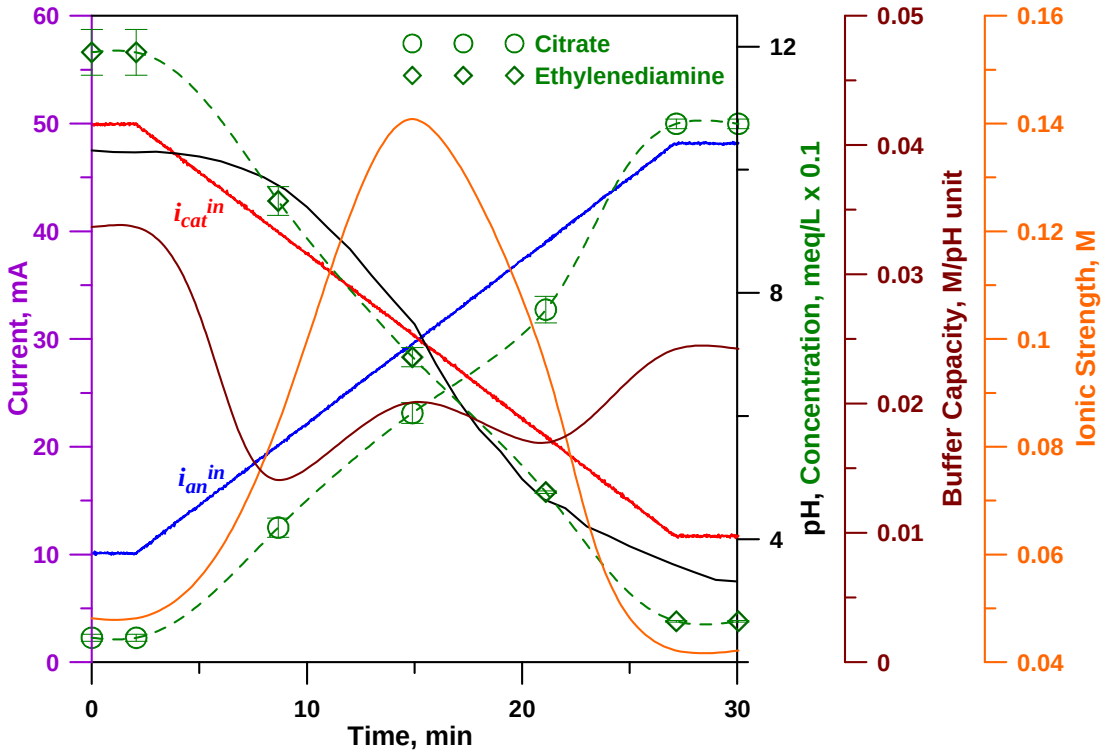

Figure D.10 Linear pH gradient and relatively constant total buffer concentration / buffer capacity by opposing changes in i_{cat}^{in} and constant i_{an}^{in}.

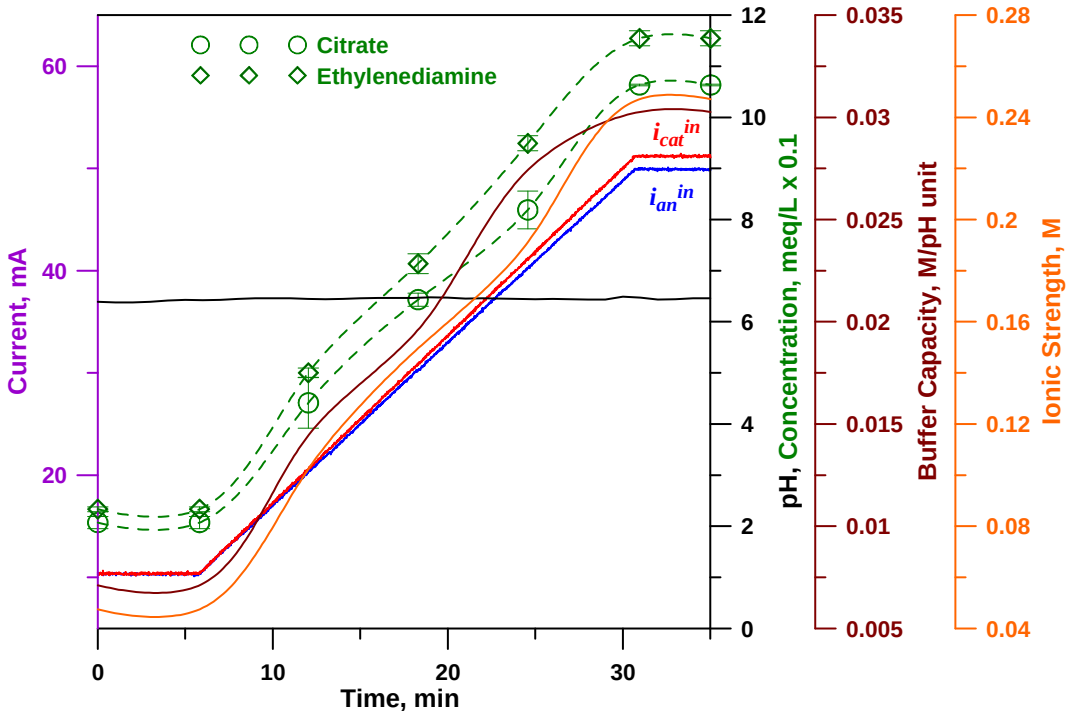

Figure D.11 Increasing buffer strength at constant pH by simultaneous increase of i_{cat}^{in} and i_{an}^{in}. Both β and *I* follow the current increase.

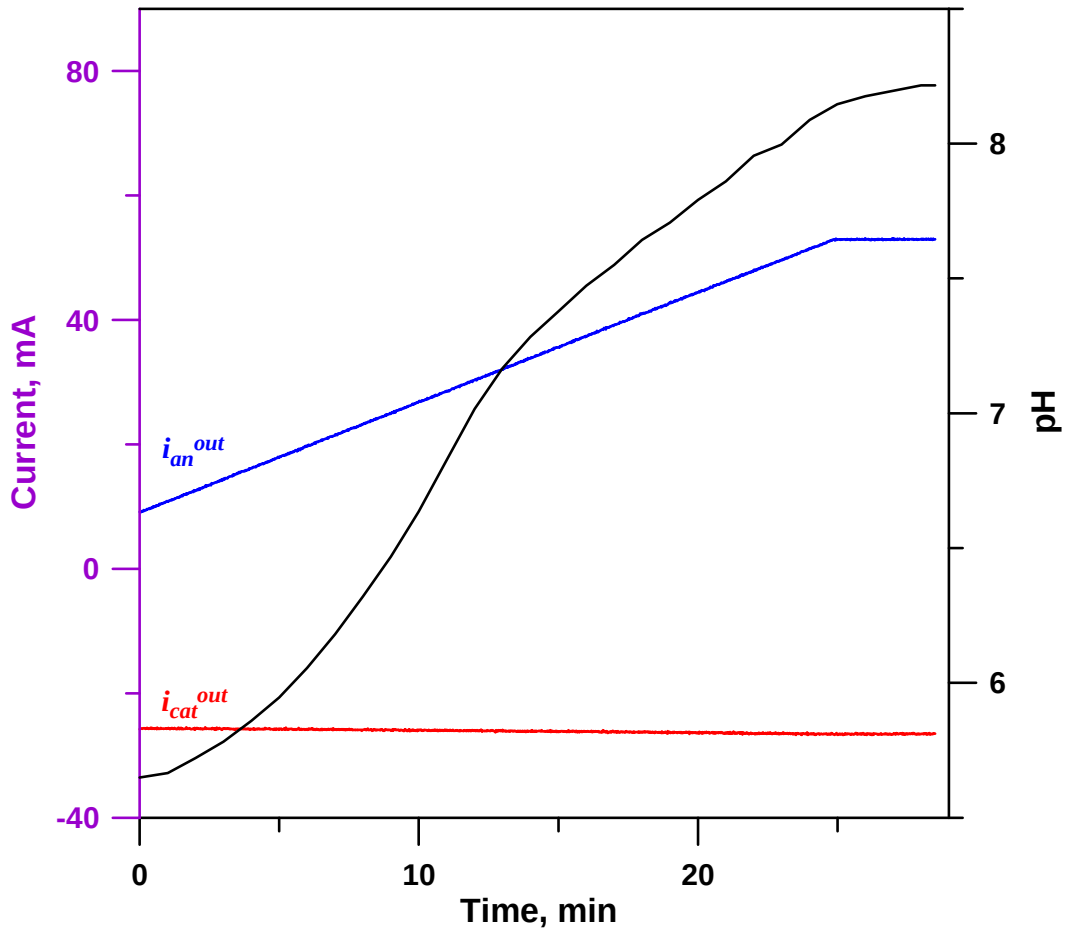

Figure D.12 EBG operated at subtractive mode. Ascending pH gradient by increasing i_{an}^{out} at constant i_{cat}^{out}. Central feed: 50 mM ethylenediamine sulfate and 50 mM tripotassium citrate at 0.5 mL/min; CEM and AEM feed: 0.2 M KNO_3 at 2.5 mL/min.

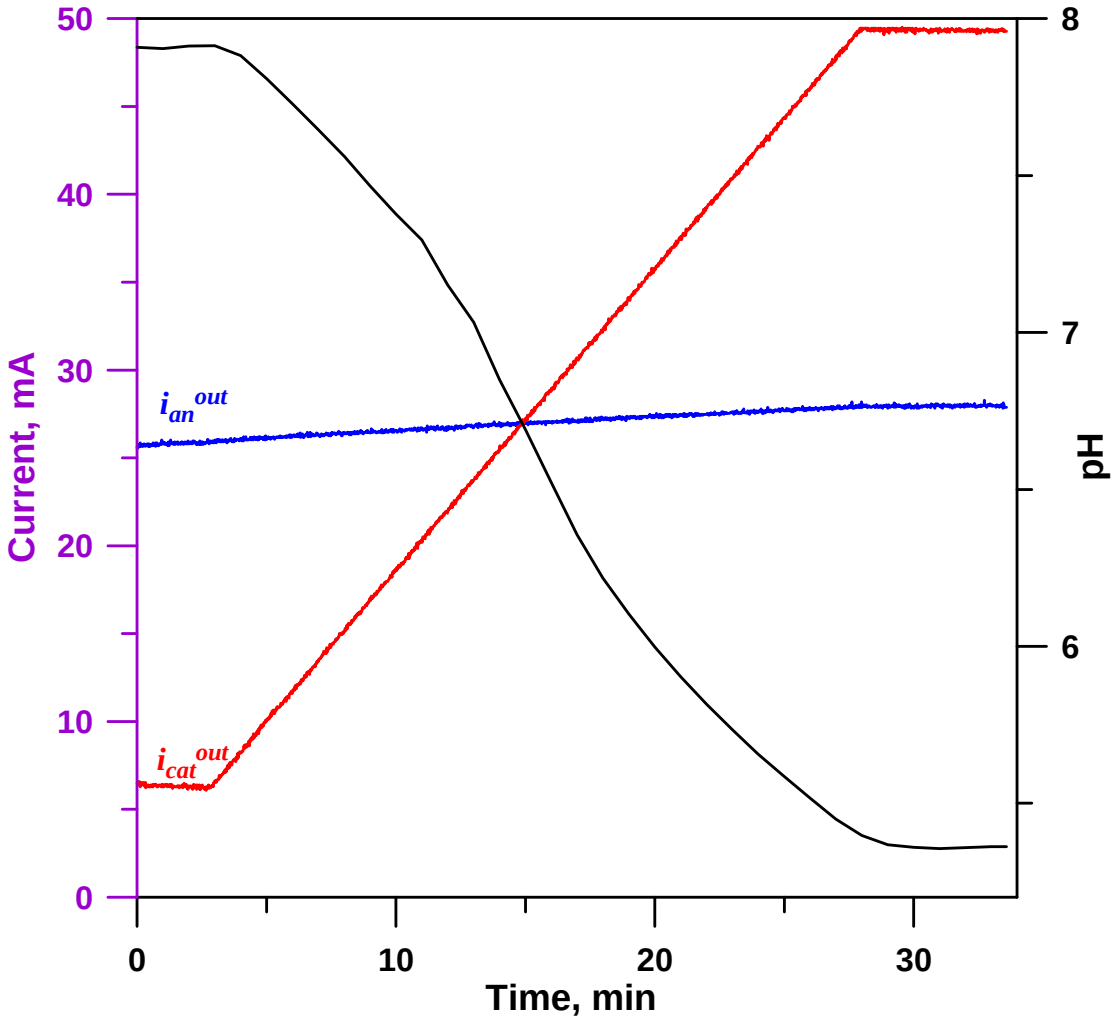

Figure D.13 EBG operated at subtractive mode. Descending pH gradient by increasing i_{cat}^{out} at constant i_{an}^{out}. Central feed: 50 mM ethylenediamine sulfate and 50 mM tripotassium citrate at 0.5 mL/min; CEM and AEM feed: 0.2 M KNO_3 at 2.5 mL/min.

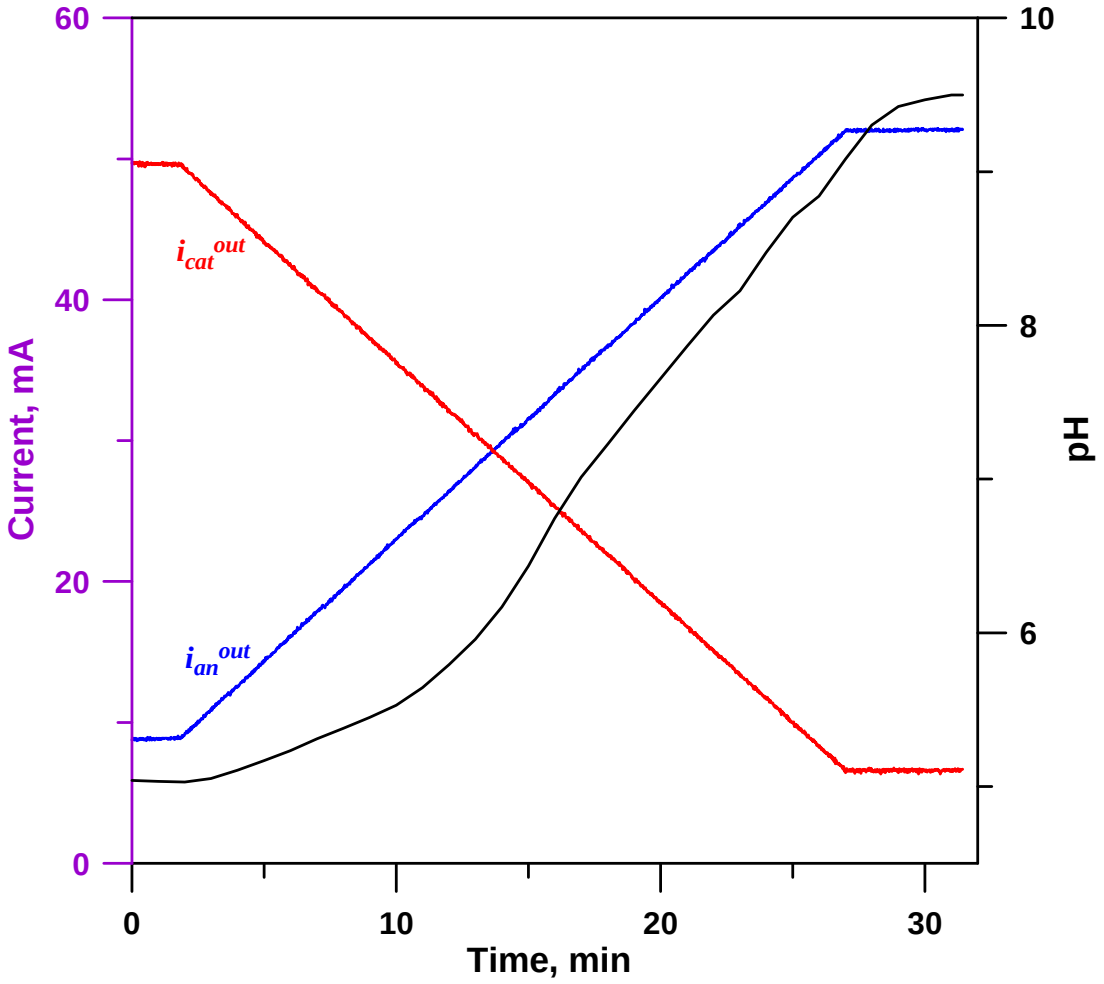

Figure D.14 EBG operated at subtractive mode. Ascending pH gradient when i_{an}^{out} is increased and i_{cat}^{out} is decreased. Central feed: 50 mM ethylenediamine sulfate and 50 mM tripotassium citrate at 0.5 mL/min; CEM and AEM feed: 0.2 M KNO_3 at 2.5 mL/min.

REFERENCES

[1] Tanaka, Y. *Ind. Eng Chem. Res.* **2011**, *50*, 7494-7503.

[2] Elisseeva, T. V.; Shaposhnik, V. A.; Luschik, I. G. *Desalination*, **2002**, *149*, 405-409.

[3] Haddad, P. R.; Jackson, P, E. *Ion Chromatography: Principles and Applications*, Elsevier, Amsterdam, 1990

[4] Small, H.; Stevens, T. S.; Bauman, W. C. *Anal. Chem.* **1975**, *47*, 1801-1809.

[5] Spedding, F. H.; Voight, F. H.; Gladrow, E. M.; Sleight, N. R. *J. Am. Chem. Soc.***1981**, *69*, 2777-2781.

[6] Stillian, J. R.; Pohl, C. A. *J. Chromatogr.* **1990***, 499,* 249-266.

[7] Pohl, C. *LC GC Eur.* **2003**, *16*, 51-54.

[8] Lucy, C. A. *J. Chromatogr. A* **2003**, *1000*, 711-724.

[9] Michalske, R. *Encycl. Chromatogr. (3rd Ed.)* **2010**, *2*, 1241-1246.

[10] Pohl, C. A.; Johnson, E. L. *J. Chromatogr. Sci.* **1980**, *18*, 442-452.

[11] Stevens, T. S.; Davis, J. C; Small, H. *Anal. Chem.,* **1981**, *53*, 1488-1492.

[12] Stevens, T. S.; Jewett, G. L.; Bredeweg, R. A. *Anal. Chem.* **1982**, *54*, 1206-1208.

[13] Dasgupta, P. K. *Anal. Chem.* **1984**, *56,* 103-105.

[14] Dasgupta, P. K. *Anal. Chem.* **1984**, *56*, 769-772.

[15] Dasgupta, P. K.; Bligh, R. Q.; Mercurio, M. A. *Anal. Chem.***1985**, *57*, 484-489.

[16] Stillian, J. *LC Mag,* 1985, *3*, 802-812.

[17] Pohl, C.; Slingsby, R. W.; Stillian, J.; Gajek, R. *Modified Membrane Suppressor and Method For Use,* US Patent 4,999,098; 1991

[18] Strong, D. L.; Dasgupta, P. K. *Anal. Chem.* **1989**, *61*, 939-945.

[19] Waiz. S.; Cedillo, B. M.; Jambunathan, S.; Hohnholt, S. G.; Dasgupta, P. K.; Wolcott, D. K. *Anal. Chim. Acta.* 2001, *428,* 163-171.[20] Srinivasan, K. Pohl, C. A. *Method and Apparatus for Gas-Assisted Suppressed Chromatography*, US Patent 6,425, 284; 2002.

[21] Srinivasan, K.; Saini, S.; Avdalovic, N. Paper 136, Pittcon 2001; 2001.

[22] Small, H.; Riviello, J. *Anal. Chem.* **1998**, *70*, 2205-2212.

[23] Small, H.; Liu, Y.; Riviello, J.; Avdalovic, N.; Srinivasan, K. *Continuous Electrolytically Regenerated Packed Bed Suppressor for Ion Chromatograph*, US Patent 6,325,976; 2001.

[24] Rocklin, R. D.; Pohl, C. A.; Schibler, J. A. *J. Chromatogr.* **1987**, *411*, 107-119.

[25] Shintani, H.; Dasgupta, P. K. *Anal. Chem.* **1987**, *59*, 802-808.

[26] Shintani, H.; Dasgupta, P. K. *Anal. Chem.* **1987**, *59*, 1963-1969.

[27] Technical Note 19, Gradient Elution in Ion Chromatography: Anion Exchange with Conductivity Detection. Dionex Corporation, Sunnyvale, CA, January, 1987.

[28] Product Information Bulletin, HPIC-5A-5µ, Dionex Corporation, Sunnyvale, CA, December, 1986.

[29] Doury-Berthod, M.; Giampaoli, P.; Pitsch, H.; Sella, C.; Poitrenaud, C. *Anal. Chem.* **1985**, *57*, 2257-2263.

[30] Martin, M. W.; Giacofei, R. A. In *Advances in Ion Chromatography*; Jandik, P.; Cassidy, R. M. Eds.; Century International: Franklin, MA, 1989; Vol. I, pp119-137.

[31] Berglund, I.; Dasgupta, P. K. *Anal. Chem.* **1991**, *63,* 2175-2183.

[32] Strong D. L.; Dasgupta, P. K.; Friedman, L.; Stillian J. R. *Anal. Chem.* **1991**, *63*, 480-486.

[33] Strong, D. L.; Young, C. U.; Dasgupta, P. K.; Friedman, L. *J. Chromatogr.* **1991**, *546*, 159-173.

[34] Strong, D. L.; Dasgupta, P. K. *J. Membr. Sci.* **1991**, *57*, 321-336.

[35] Sjögren, A.; Boring, C. B.; Dasgupta, P. K. *Anal. Chem.* **1997**, *69*, 1385-1391.

[36] Sjögren, A.; Dasgupta, P. K. *Anal. Chim. Acta* **1999**, *384*, 135-141.

[37] Liu, Y.; Avdalovic, N.; Pohl, C.; Matt, R.; Dhillon, H.; Kiser, R. *Am. Lab* **1998**, *November Issue,* 48C-58C.

[38] Liu, Y.; Small, H. Avdalovic, N. Large Capacity Acid Or Base Generation Apparatus and Method Of Use. US Patent No. 6225129, 2001.

[39] Yang, B.; Takeuchi, M.; Dasgupta, P. K. *Anal. Chem.* **2008**, *80*, 40-47.

[40] Yang, B.; Zhang, F.; Liang, X.; Dasgupta, P. K. *J. Chromatogr. A* **2009**, *1216*, 2412-2416.

[41] Stock, J. T. *Anal. Chem.* **1984**, *56,* 561A- 570A.

[42] Maxwell, J. C.; Larmor, J. Eds. *The Scientific Papers of the Honourable Henry Cavendish, F.R.S.* University Press, Cambridge, 1921. Volume 1. p. 23, 311.

[43] Kohlrausch, F.; Holborn, L. Eds. *Das Leitvërmogen der Elektrolyte.* Teubner, Leipzig, Germany, 1898. p5.

[44] Hu, W.; Haddad, P. R. *Trends Anal. Chem.* **1998,** *17*, 73-79.

[45] Hu, W.; Haddad, P. R.; Hasebe, K.; Tanaka, K. *Anal. Commun.* **1999,** *36*, 97–100.

[46] Masuda W.; Kozaki, D.; Nakatani, N.; Goto, R.; Mori, M.; Fugetsu, B.; Tanaka, K. *Buns Kag.* **2009,** *58*, 311-315.

[47] Bud, R.; Warner, D. J. Eds. *Instruments of Science: An Historical Encyclopedia*. Garland, New York, 1998, p 650-651.

[48] Richards, T. W; Stull, W. N. *Z. Phys. Chem.* **1903,** *42*, 621-625.

[49] Grower, G. G. *Am. Soc. Testing Materials Proc*. **1917**, *17,* 129-155.

[50] Szebelledy, L.; Somogyi, Z. I. *Z. Analyt. Chem.* **1938**, *112,* 313-323.

[51] Liu, Y.; Srinivasan, K.; Pohl, C.; Avdalovic, N. *J. Biochem. Biophys. Methods* **2004,** *60,* 205–232.

[52] Frilette, V. J. *J. Phys. Chem.* **1956**, *60***,** 435-439.

[53] Glueckauf, E.; Kitt, G. P. *J. Appl. Chem.* **1956**, *6***,** 511-516.

[54] Ohki, S. *J. Phys. Soc. Jpn.* **1965**, *20***,** 1674-1685.

[55] Bassignana, I. C.; Reiss, H. *J. Memb. Sci.* **1983***, 15***,** 27-41.

[56] Lovreček, B.; Despić, A.; Bockris, J. O'M. *J. Phys. Chem.* **1959**, *63,* 750-751.

[57] Senŏ, M.; Yamabe, T. *Bull. Chem. Soc. Jpn,* **1964**, *37*, 668-671.

[58] Mani, K. N. *J. Memb. Sci.* **1991**, *58***,** 117-138.

[59] Wien, M. *Phys. Zeit.* **1931,** *32,* 545.

[60] Schiele, J. *Ann. Physik.* **1932,** *5,* 811-830.

[61] Schiele, J. *Phys. Zeit.* **1933,** *34*, 60-61.

[62] Onsager, L. *J. Chem. Phys.* **1934,** *2*, 599-615.

[63] Simons, R. *Nature* **1979**, *280*, 824-826.

[64] Tanaka, Y. *J. Memb. Sci.* **2007**, *303*, 234–243.

[65] Doury-Berthod, M.; Giampoli, P.; Pitsch, H.; Sella, C.; Poitrenaud, C. *Anal. Chem.* **1985,** *57*, 2257-2263.

[66] Ullah, SM. R.; Adams, R. L.; Srinivasan, K.; Dasgupta, P. K. *Anal. Chem.* **2004,** *76*, 7084-7093.

[67] Dasgupta, P. K.; Ullah, SM. R.; Srinivasan, K. U.S. Patent 7,306,720. December 11, 2007

[68] Fenn, J. B.; Mann, M.; Meng, C. K.; Wong, S. F.; Whitehouse, C. M. *Science* **1989**, 246, 64-71.

[69] Karas, M.; Hillenkamp, F. *Anal. Chem*. **1988**, *60*, 2299-2301.

[70] Tanaka, K.; Waki, H.; Ido, Y.; Akita, S.; Yoshida, Y.; Yoshida, T. *Rapid Commun. Mass Spectrom.* **1988**, *2*, 151-153.

[71] Liu, C. L.; Verma, S. S. *J. Chromatogr. A.* **1999**, *835*, 93-104.

[72] Cech, N. B.; Enke, C. G. *Mass Spectrom. Rev.* **2001**, *20*, 362-387.

[73] Tolic, P. L.; Bruce, J. E.; Lei, Q. P.; Anderson, G. A.; Smith, R. D. *Anal. Chem.* **1998**, *70*, 405-408

[74] Beaudry, F.; Vachon, P. *Biomed. Chromatogr.* **2006**, *20*, 200-205.

[75] Mallet, C. R.; Lu, Z. L. Mazzeo, J. R. Rapid C*ommun. Mass Spectrom.* **2004**, *18*, 49-58.

[76] Lavarone, A. T.; Udekwu, O. A.; Williams, E. R. *Anal. Chem.* **2004**, *76*, 3944-3950.

[77] Stults, J. T.; Marsters, J. C. *Rapid Commun. Mass Spectrom.* **1991**, *5*, 359-363.

[78] Nordhoff, E.; Ingendoh, A.; Cramer, R.; Overberg, A.; Stahl, B.; Karas, M.; Hillenkamp, F.; Crain, P. F. *Rapid Commun. Mass Spectrom.* **1992**, *6*, 771-776.

[79] Schug, K.; McNair, H. M. *J. Sep. Sci.* **2002**, *25*, 760-766.

[80] Schug, K.; McNair, H. M. *J. Chromatogr. A* **2003**, *985*, 531-539.

[81] Verkerk, U. H.; Kebarle, P. *J. Am. Soc. Mass Spectrom.* **2005**, *16*, 1325-1341.

[82] Constantopoulos, T. L.; Jackson, G. S.; Enke, C. G. *J. Am. Soc. Mass Spectrom.* **1999**, *10*, 625-634.

[83] Shen, M. L.; Benson, L. M.; Johnson, K. L.; Lipsky, J. J.; Naylor, S. *J. Am. Soc. Mass Spectrom.* **2001**, *12*, 97-104.

[84] Cavanagh, J.; Thompson, R.; Bobay, B.; Benson, L. M.; Naylor, S. *Biochemistry* **2002**, *41*, 7859-7865.

[85] Cavanagh, J.; Benson, L. M.; Thompson, R.; Naylor, S. *Anal. Chem.* **2003**, *75*, 3281-3286.

[86] Saber, A. L. *Talanta*, **2009**, *78*, 295-299.

[87] Fernandez, M. M. R.; Wille, S. M. R.; Samyn, N.; Wood, M.; Lopez-Rivadulla, M.; Boeck, G. D. *J. Chromatogr., B: Anal. Technol. Biomed. Life Sci.* **2009**, *877*, 2153-2157.

[88] Fosefsson, M.; Sabanovic, A. *J. Chromatogr., A*, **2006**, *1120*, 1-12.

[89] Fountain, K. J.; Gilar, M.; Gebler, J. C. *Rapid Commun. Mass Spectrom.* **2004**, *18*, 1295-1302.

[90] Aznar, M.; Canellas, E.; Nerin, C. *J. Chromatogr., A*, **2009**, *1216*, 5176-5181.

[91] Zhou, W.; Ding, L.; Xu, G.; Wang, Y.; Sun, L.; He, J.; Huang, Y.; Hu, L.; Chen, X. *J. Pharm. Biomed. Anal.* **2009**, *50*, 35-40.

[92] Zheng, J. J.; Lynch, E. D.; Unger, S. E.; *J. Pharm. Biomed. Anal.* **2002**, *28*, 279-285.

[93] Cai, M-Q.; Chen, X-H.; Yan, Y-Q.; Jin, M-C. *Chromatographia*, **2009**, *69*, 33-38.

[94] Wu, Q.; Liu, C.; Simith, R. D. *Rapid Commun. Mass Spectrom.* **1996**, *10*, 835-838.

[95] Liu, C.; Wu, Q.; Harms, A. C.; Smith, R. D. *Anal. Chem.* **1996**, 68, 3295-3299.

[96] Liu, C.; Muddiman, D. C.; Tang, K.; Smith, R. D. *J. Mass Spectrom.* **1997**, *32*, 425-431.

[97] Jakubowski, J. A.; Hatcher, N. G.; Sweedler, J. V. *J. Mass Spectrom.* **2005**, *40*, 924-931.

[98] Lamoree, M. H.; Tjaden, U.R.; vander Greef, J. *J. Chromatogr., A*, **1997**, *777*, 31-39.

[99] Lamoree, M. H.; Vander Hoeven, R. A. M.; Tjaden, U. R.; vander Greef, J. *J. Mass Spectrom.* **1998**, *33*, 453-460.

[100] Canarelli, S.; Fisch, I.; Freitag, R. *J. Chromatogr., A*, **2002**, *948*, 139-149.

[101] Kamholz, A. E.; Schilling, E. A.; Yager, P. *Biophys. J.* **2001,** *80*, 1967-1972.

[102] Wilson, D. H.; Konermann, R. *Anal. Chem.* **2005**, *77*, 6887-6894.

[103] Kuban, P.; Berg, J. Dasgupta, P. K. *Anal. Chem.* **2003,** *75*, 3549-3556.

[104] Gregson, R.; Simons, R. *Aust. J. Pharm. Sci.* **1981,** *10,* 78-79.

[105] Yang, B.; Chen, Y.; Mori, M.; Ohira, S-I.; Azad, A. K.; Dasgupta, P. K.; Srinivasan, K. *Anal. Chem*. **2010**, *82*, 951–958.

[106] Xu, N.; Lin, Y.; Hofstadler, S. L.; Matson, D.; Call, C. J.; Smith, R. D. *Anal. Chem*. **1998**, *70*, 3553-3556.

[107] Sun, L. L.; Duan, J.; Tao, D.; Liang, Z.; Zhang, W. *Rapid Commun. Mass Spectrom.* **2008,** *22,* 2391–2397.

[108] McKenzie, S. B. *Textbook of Hematology*, Lippincott, Williams &Wilkins, Ann Arbor, MI. 2nd Ed., 1996.

[109] Li, Y.-C.; Wiklund, L.; Tarkkila, P.; Bjerneroth, G. *Resuscitation*, **1996**, *32*, 33-44.

[110] Kang, J.; Ramu, S.; Lee, S.; Aguilar, B.; Ganesan, S. K.; Yoo, J.; Kalra, V. K.; Koh, C. J.; Hong Y.-K. *Anal. Biochem.* **2009**, *386*, 251-255

[111] Fringuelli, F.; Pizzo, F.; Vaccaro, L. *J. Org. Chem.*, **2001**, *66*, 4719–4722.

[112] Jacobsen, C. F.; Leonis, J.; Linderstrom-Lang, K.; Ottesen, M. *Methods Biochem Anal.* **1957**, *4,* 171-210.

[113] Einsel, D. W., Jr.; Trurnit, H. J.; Silver, S. D.; Steiner, E. C. *Anal. Chem.* **1956**, *28*, 408–410.

[114] Adams, R. E.; Betso, S. R.; Carr, P. W. *Anal. Chem.* **1976**, *48*, 1989–1996.

[115] Karcher, R. E.; Pardue, H. L. *Clin. Chem.* **1971**, *17*, 214–221.

[116] Kao, L. T. H.; Hsu, H.-Y.; Gratzl, M. *Anal. Chem.* **2008,** *80,* 4065–4069.

[117] Timperman, A.; Tracht, S. E. Sweedler, J. V. *Anal. Chem.* **1996**, *68*, 2693-2698.

[118] Zhao, F.; Harnisch, F.; Schröder, U.; Scholz, F.; Bogdanoff, P.; Herrmann, I. *Environ. Sci. Technol.* **2006**, *40*, 5193-5199

[119] Liu, G. *Chromatographia* **1989**, *28*, 493-496

[120] Cantú, R.; Evans, O.; Kawahara, R. K.; Wymer, L. J.; Dufour, A. P. *Anal. Chem.* **2001**, *73*, 3358-3364

[121] Rosés, M.; Canals, I; Allemann, H.; Siigur, K.; Bosch, E. *Anal. Chem.* **1996**, *68*, 4094-4100.

[122] Subirats, X.; Bosch, E.; Rosés. M. *J. Chromatogr. A* **2007**, *1138*, 203-215

[123] Espinosa, S.; Bosch, E.; Rosés, M. *Anal. Chem*. **2002**, *74*, 3809-3818

[124] Kaliszan, R.; Haber, P.; Baczek, T.; Siluk, D. *Pure Appl. Chem.*, **2001,** *73,* 1465–1475.

[125] Wiczling, P.; Markuszewski, M. J.; Kaliszan, M.; Galer, K.; Kaliszan, R. *J. Pharm. Biomed. Anal.* **2005,** *37*, 871-875.

[126] Kaliszan, R.; Wiczling, P.; Markuszewski, M. J. *J. Chromatogr.* A **2004,** *1060,* 165–175

[127] Kaliszan, R.; Wiczling, P. *Anal Bioanal Chem* **2005,** *382*, 718–727.

[128] Kaliszan, R.; Wiczling, P.; Markuszewski, M. J. *Anal. Chem.* **2004**, *76,* 749-760.

[129] Wiczling, P.; Markuszewski, M. J.; Kaliszan, R. *Anal. Chem.* **2004,** *76,* 3069-3077.

[130] (a) Sluyterman, L. A. A. E.; Elgersma, O. *J. Chromatogr.* **1978**, *150*, 17-30; (b) *ibid, idem,* **1978**, 150, 31-44.

[131] Andersen, T.; Pepaj, M.; Trones,R.; Lundanes, E.; Greibrokk, T. . *J. Chromatogr. A* **2004,** *1025*, 217–226.

[132] Kang, X.; Bates, R. C.; Frey, D. D. . *J. Chromatogr. A* **2000,** *890*, 37–43.

[133] (a) Liu, Y.; Anderson, D. J. *J. Chromatogr. A* **1997**, *762,* 207-217; (b) *idem, ibid,* **1997**, *762,* 47-54.

[134] Farnan, D.; Moreno, G. T. *Anal. Chem.* **2009**, *81*, 8846-8857.

[135] (a) Lian, S.; Anderson, D. J. *J. Chromatogr. A* **2001**, *909,* 191–205; (b) *idem, Anal. Chem.* **2002**, *74*, 5641-5649.

[136] Strong, D. L.; Dasgupta, P. K. *Anal. Chem.* **1989,** *61*, 939-945.

[137] Haddad, P. R.; Jackson, P. E.; Shaw, M. J. *J. Chromatogr. A* **2003**, *1000,* 725-742.

[138] Tian, Z. W.; Hu, R. Z.; Lin, H. S.; Hu, W. L. *J. Chromatogr.* **1988**, *439,* 151-157.

[139] Dimitrakopoulos, I. K.; Thomaidis, N. S.; Megoulas, N. C.; Koupparis, M. A. . *J. Chromatogr. A.* **2010,** *1217,* 3619-3627.

[140] Dasgupta, P. K.; McDowell, W. L.; Rhee, J.-S. *Analyst* **1986,** *111*, 87-90.

[141] Dong, S.; Dasgupta, P. K. *Environ. Sci. Technol.* **1987,** *21*, 581-588.

[142] Ullah, SM. R.; Adams, R. L.; Srinivasan, K.; Dasgupta, P. K. *Anal. Chem*. **2004,** *76,* 7084-7093.

[143] Dionex Corporation. CRD Carbonate Removal Device. http://www.dionex.com/en-us/products/accessories/reagents-accessories/crd/lp-73608.html

[144] Christian, G. D. *Analytical Chemistry.* Sixthe Ed., Wiley, New York. P213.

[145] Yeager, H. L. *ACS Symp. Ser.* **1982,** *180,* 41-64.

[146] Chen, Y.; Mori, M.; Pastusek, A. C.; Schug, K. A.; Dasgupta, P. K. *Anal. Chem.* **2011**, *83*, 1015-1021.

[147] Leithe, W. *Chem. Ing. Tech.* **1964,** *36,* 112-114.

[148] Johannson, G.; Backën, W. *Anal. Chim. Acta* **1974,** *69,* 415-424.

[149] Åström, O. *Anal. Chim. Acta* **1977,** *88,* 17-23.

[150] Righetti, P. G.; Fazio, M.; Tonani, C.; Gianazza, E.; Celentano, F. C. *J. Biochem. Biophys. Methods* **1988,** *16,* 129-140.

[151] GE Health care. Polybuffers. http://www.gelifesciences.com/aptrix/upp01077.nsf/content/Products?OpenDocument&parentid=555&moduleid=165538 Accessed February 21, 2011.

[152] Box, K.; Bevan, C.; Comer, J.; Hill, A.; Allen, R.; Reynolds, D. *Anal. Chem.* **2003,** *75,* 883-892.

[153] Hamer, W. J.; Wu, Y.-C. *J. Phys. Chem. Ref. Data* **192,** *1,* 1047-1100

[154] Tanaka, H.; Dasgupta, P. K.; Huang, J. *Anal. Chem.* **2000,** *72***,** 4713-4720.

[155] Dasgupta, P. K.; Jo, K. *Electroanalysis* **2002,** *14***,** 1383-1390.

[156] Small, D.; Dais, M.; Wong, M.; Tang-Liu, D. *Int. J. Pharm.* **1997**, *149*, 195-201.

[157] McCalley, D. V. *J. Chromatogr. A.* **2004**, *1038*, 77-84.

[158] Gritti, F.; Guiochon, G. *J. Chromatogr. A.* **2004**, *1038*, 53-66.

[159] Božek, P.; Hutta, M.; Hrivnáková, B. *J. Chromatogr. A.* **2005**, *1084*, 24-32.

[1 60] Kafkala, S.; Matthaiou, S.; Alexaki, P.; Abatzis, M.; Bartzeliotis, A.; Katsiabani, M. *J. Chromatogr. A.* **2008**, *1189*, 392-397.

[161] Buck, C. F.; Tomellini, S. A. *J. Chromatogr. Sci.* **1989**, *27*, 166-71.

[162] Little, E. L.; Jeansonne, M. S.; Foley, J. P. *Anal. Chem.* **1991**, *63*, 33-44.

[163] Wiczling, P.; Markuszewski, M. J.; Kaliszan, M.; Kaliszan, R. *Anal. Chem.* **2005**, *77*, 449-458.

[164] Ishihara, T.; Yamamoto, S. *J. Chromatogr. A* **2005**, *1069*, 99-106.

[165] Gallant, S. R.; Vunnum, S.; Cramer, S. M. *J. Chromatogr. A* **1996**, *725*, 295-314.

[166] Liu, S.; Chen, Z.; Xie, J.; Lin, J.; Chen, Z.; Rao, P. *Anal. Chem.* **2010**, *82*, 8544-8550.

[167] Shan, L.; Anderson, D. J.; *Anal. Chem.* **2002**, *74*, 5641-5649.

[168] Farnan, D.; Moreno, G. T. *Anal. Chem.* **2009**, *81*, 8846-8857.

[169] Ahamed, T.; Nfor, B. K.; Verhaert, P. D. E.M.; van Dedem, G. W. K.; van der Wielen, L. A. M.; Eppink, M. H. M.; van de Sandt, E. J. A. X.; Ottens, M. *J. Chromatogr. A* **2007**, *1164*, 181-188.

[170] Shan, L.; Anderson, D. J. *Anal. Chem.* **2002**, *74*, 5641-5649.

[171] Wiczling, P.; Kawczak, P.; Nasal, A.; Kaliszan, R. *Anal. Chem.* **2006**, *78*, 239-249.

[172] Strong, D. L.; Joung, C. U.; Dasgupta, P. K. *J. Chromatogr.* **1991**, *546*, 159-173.

[173] Haddad, P. R.; Jackson, P. E.; Shaw, M. J. *J. Chromatogr. A* **2003**, *1000,* 725-742.

[174] Chen, Y.; Dasgupta, P. K.; Srinivasan, K. *Anal. Chem.* Summitted.

[175] Strong, D. L.; Dasgupta, P. K.; Friedman, K.; Stillian, J. R. *Anal. Chem.* **1991**, *63*, 480-486.

[176] Dasgupta, P. K.; Strong, D. L.; Stillian, J. R.; Friedman, K. US Patent 5,045,204, September 3, 1991.

[177] Mishra, S. K.; Dasgupta, P. K. *Anal. Chem.* **2010,** *82,* 3981-3984.

[178] Henderson, L. J. *Am. J. Physiol.* **1098**, *21*, 173-179.

[179] Henderson, L. J. *Am. J. Physiol.* **1098**, *21*, 427-448.

[180] Righetti, P. G.; Fazio, M.; Tonani, C.; Gianazza, E.; Celentano, F. C. *J. Biochem. Biophys. Methods* **1988,** *16,* 129-140.

[181] Rabin, S.; Stillian, J.; Barreto, V., Friedman, K.; Toofan, M. *J. Chromatogr.,* **1993**, *640*, 97-109.

[182] Stillian, J. R.; Barreto, V. M.; Friedman, K. A.; Rabin, S. B.; Mahmood, T. US Patent 5,352,360. October 4, 1994.

[183] Haddad, P. R.; Jackson, P. E.; Shaw, M. J. *J. Chromatogr. A.* **2003,** *1000,* 725-742.

[184] Dasgupta, P. K. in *Ion Chromatography*, Tarter, J. G., Ed., Marcel Dekker, 1987. pp 220-224.

[185] Kielland, J. *J. Amer. Chem. Soc.* **1937,** *59,* 1675-1678.

BIOGRAPHICAL INFORMATION

Yongjing Chen got her BS in chemistry from Xiamen University in China in 2004. After that, she was recommended to Zhejiang University, where she studied ion chromatography with Dr. Yan Zhu and earned her MS in 2006. In spring 2007, she joined Dr. Purnendu K. Dasgupta's group at University of Texas at Arlington for her PhD study. Under Dr. Dasgupta's supervision, her PhD work was focusing on investigating the behavior and applications of ion exchanger based electrolytic devices. She developed Charge Detector (ChD) that responds to all analytes on a charge basis and Salt Remover (SR) that removes ionized salts from protein samples for ESI-MS, and Electrodialytic Buffer Generators (EBGs) that produce buffers of variable concentration and programmable pH gradient. The work on EBGs results in two patents: Membrane Suppressor Buffer Generator and Three-Electrode Buffer Generator and Method. She received 2011 American Chemical Society Division of Analytical Chemistry Summer Graduate Fellowship sponsored by Society for Analytical Chemists of Pittsburgh and Dean's Excellence Scholarship from UTA college of Science.